2014-09-15

The Surprising Photophysics of mOrange

Pearson, Dustin

UNIVERSITY OF CALGARY

The Surprising Photophysics of mOrange

by

Dustin D. Pearson

A THESIS

SUBMITTED TO THE FACULTY OF GRADUATE STUDIES

IN PARTIAL FULFILMENT OF THE REQUIREMENTS FOR THE

DEGREE OF MASTER OF SCIENCE

DEPARTMENT OF CHEMISTRY

CALGARY, ALBERTA

SEPTEMBER, 2014

Abstract

It is of little doubt that the discovery of fluorescent proteins (FPs) has dramatically advanced the fields of biology, medicine and chemistry. However, the inevitable loss of fluorescence through prolonged irradiation in a process known as photobleaching, is still not fully understood. Thus, through the investigation of one of the most well known photobleaching sensitive proteins, mOrange, further light has been shed on this topic. Unique to this investigation has been the photophysical approaches used in the elucidation of the loss of fluorescence kinetics, where the use of high-power light sources have revealed the contributions of the improperly folded green immature mOrange. Additionally, this green immature mOrange has shown to have a distinct link to the production of a red fluorescent by-product. Finally, it has been shown that the excitation of mOrange has the ability to produce modest amount of singlet oxygen ($^1O_2$), implicating $^1O_2$ as a cause of photobleaching.

Acknowledgements

First of all, this work is in no small part due to the efforts of my supervisor, Dr. Belinda Heyne. I cannot thank you enough for the guidance, motivation and challenges, without which I know that this would not have been possible. Thank you for your friendship and mentorship. Simply, thank you for everything, I know that these will be memories I cherish.

Second, I must thank my wife, Karla, you have supported me through my endeavours, encouraged and prayed alongside me. I cannot imagine my life without you and look forward to the new adventures we will have together.

Third, the Heyne group: Sara, Joel, Nicolas, Anita, Wyatt, Nicole and Chris. Thank you for the fun, laughs, amazing conversations both scientific and not. I will miss our time together but know that you will all move on to amazing things. Thank you.

For my family, you have shaped and moulded me in my youth, encouraged and directed me to bigger and better things. Thank you for all you have done. I am who I am because of you.

Finally, thank you to my committee, Drs. David Cramb, Marcus Samuel and David Schriemer. Thank you for your time and knowledge. The old idiom comes to mind “two heads are better than one”, how true this has shown, thank you.

Dedication

This is for Karla and Kaeden. As I finish this work, I am closing a chapter of my life, yet a new one begins, as we become parents. I look forward to what lay ahead.

Table of Contents

List of Tables

List of Figures and Illustrations

List of Symbols, Abbreviations and Nomenclature

Symbol	Definition
$^1O_2$	Singlet oxygen
$^1PS^*$	A photosensitizer in its singlet excited state
$^3O_2$	Ground state molecule oxygen
$^3PS^*$	A photosensitizer in its triplet excited state
ABDA	9,10-anthracenediyl-bis(methylene)dimalonate
BFP	Blue fluorescent protein
CALI	Chromophore assisted laser inactivation
CFP	Cyan fluorescent protein
Chi Sq	The Chi squared value
DSC	Dark state conversion
EGFP	Enhance green fluorescent protein
ESPT	Excited state proton transfer
Fluorophores	Molecules which can undergo fluorescence
FP(s)	Fluorescent protein(s)
FR mOrange	Far Red mOrange
FRAP	Fluorescence recovery after photobleaching
FRET	Förster resonance energy transfer
GFP	Green fluorescent protein
HOMO	Highest occupied molecular orbital
hν	A photon of light
IC	Internal conversion
IPTG	isopropyl β-D-thiogalactopyranoside
IR	Infrared
ISC	Intersystem crossing
$K_3Fe(CN)_6$	Potassium ferricyanide
LED	Light emitting diode
LUMO	Lowest unoccupied molecular orbital
Ni-NTA	Nickel-nitriloacetic acid
OD_{600}	Optical density at 600 nm
p-HOBDI	*p*-hydroxybenzylideneimidazolidinone
PAFP	Photoactivable fluorescent protein
PB	Photobleaching
PBS	Phosphate buffer saline
Photocycle	The cyclical excited state movement of a proton
PMSF	Phenylmethanesulfonyl fluoride
PTI	Photon technology international
ROS	Reactive oxygen species
S_0	Singlet ground state
S_1	Singlet excited state
SDS	Sodium dodecyl sulphate
SOB	Super optimal broth
t	Time

T_1	Excited triplet state
TTA	Triplet triplet annihilation
UV	Ultraviolet
YFP	Yellow fluorescent protein
ε	Extinction coefficient
λ_{max}	The maximum wavelength
ϕ_{1O2}	Singlet oxygen quantum yield
ϕ_{fl}	Fluorescent quantum yield
ϕ_{ISC}	Intersystem crossing quantum yield

Epigraph

"Neither do people light a lamp and put it under a bowl. Instead, they put it on its stand, and it gives light to everyone in the house."

Matthew 5:15, NIV

Chapter One: **Introduction**

1.1 The emergence of fluorescent proteins

Fluorescent microscopy has allowed huge advances within the medical and biological fields. Previous to fluorescent microscopy, optical examinations of live cells were rather ineffective, as imaging techniques could not correct for the light scattered by living matter.[1] Thus in order to better understand the inner workings of living matter, the specimens under study required chemical staining and fixation in order to achieve a useable image.[1] This process would invariably kill the specimens, leaving researchers to image only the dead matter. Without the ability to image live cells and tissues, researchers could only piece together what the living counterparts of their fixed specimens would do through a collection of their still images. However, upon the advent of fluorescent microscopy, the dynamic nature of life could be monitored in real time.[1]

All living matter has a certain level of fluorescence when exposed to a high intensity light source, called autofluorescence,[2] which did not allow researchers to differentiate between targets within the specimen. It was only with the introduction of fluorescent probes (fluorophores) that the ability to achieve temporal and spatial resolution of small molecules was made available.[3] The use of fluorophores within a specimen allowed researchers to track the fluorophore in the living matter, with a good signal to noise ratio; the mysteries of living specimens could be revealed.[1] These fluorophores were small molecules (for example, fluorescein) that could be attached to bio-molecules of interest, and then tracked within a cell to monitor the molecule's mobility due to their fluorescence.[4] Albeit a great advance, these fluorophores could not be genetically encoded into the cell, thus all the fluorescent constructs needed to be synthesized and added to the specimen, and by consequence the fluorophores could not be used as a real time

marker for gene expression.[5,6] These problems were eventually overcome with the 1994 edition of *Science* where Chalfie *et al.* showed the use of a small, green, biological fluorophore as the first visible marker for gene expression.[6]

The initial discovery of the Green Fluorescent Protein (GFP) in 1962[7] remained quiet and unassuming for several decades.[8] It was only after the work of Chalfie *et al.* that the true potential of this fluorescent protein (FP) began to be revealed.[6] Comprised of 238 amino acids, this protein (~27 kDa) was unique in its ability as a biological molecule to absorb light in the blue region and emit green light without the need for a chemical reaction to take place.[9,10] Consisting of a relatively rigid barrel structure created by 11 β-sheets, this barrel holds the 'key' to GFP's unique spectral properties (figure 1.1A).[9] This 'key', nestled within the center of the barrel, is the light absorbing and emitting chromophore, a *p*-hydroxybenzylideneimidazolidinone (*p*-HOBDI) moiety, held in place by an α-helix.[9-11] This chromophore is formed through the autocatalytic reaction of the tripeptide composed of the serine located in position 65, the tyrosine in position 66 and the glycine in position 67 (Ser65-Tyr66-Gly67), where the α and β carbons are oxidized via a molecule of oxygen on the methylene bridge. This joins the imidazole ring and the phenol ring in full π conjugation (see figure 1.1B and C).[10]

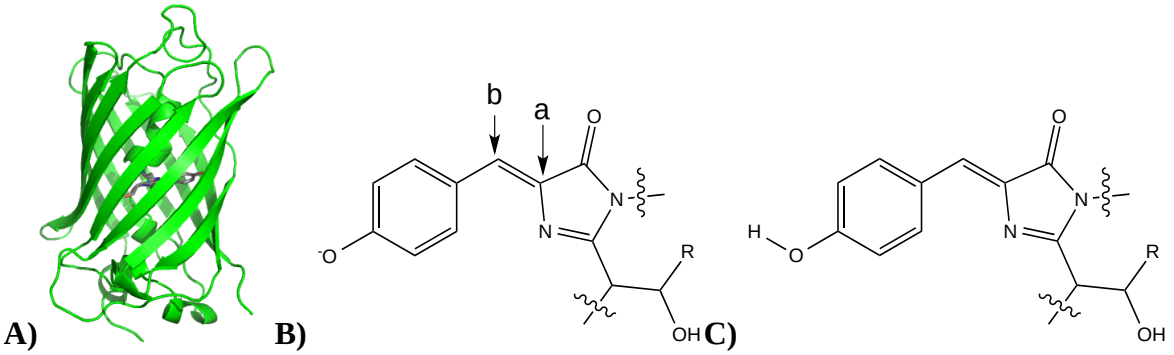

Figure 1.1: A) The 11-stranded β-barrel of GFP and its chromophore, coloured grey. B) The anionic *cis*-isomer of GFP's chromophore with the α and β carbons indicated by the arrows, and C) the neutral *cis*-isomer of GFP's chromophore.

The chromophore is primarily in the *cis*-isomer,[12] which exists in a 6:1 mixture of the protonated and deprotonated states with the main peaks of excitation at ~395 nm and ~475 nm respectively.[10] Since there are two separate excitation peaks for GFP, fluorescence can occur in two separate manners depending upon excitation wavelength. The first pathway occurs upon excitation of the ground electronic state (S_0) of the protonated form of the chromophore. Here, the excited state (S_1) becomes highly acidic causing the chromophore to act as a strong acid (figure 1.2). Once excited, the chromophore can undergo an Excited State Proton Transfer (ESPT), which happens on a very short time scale, within 20 ps. This allows the transfer of a proton through a proton wire to the glutamate anion in position 222 (figure 1.2),[13,14] and from here the chromophore can relax back to the S_0, releasing a photon of light at 508 nm.[10] The second pathway to fluorescence is by the excitation of the anionic form of the chromophore from S_0 to S_1, which can then emit light primarily at 503 nm upon relaxation back to S_0 (figure 1.2).[9] The main difference in emission between the protonated and deprotonated forms of the chromophore can be attributed to the ESPT event that takes place with the protonated form, lowering the energy of emission.[9]

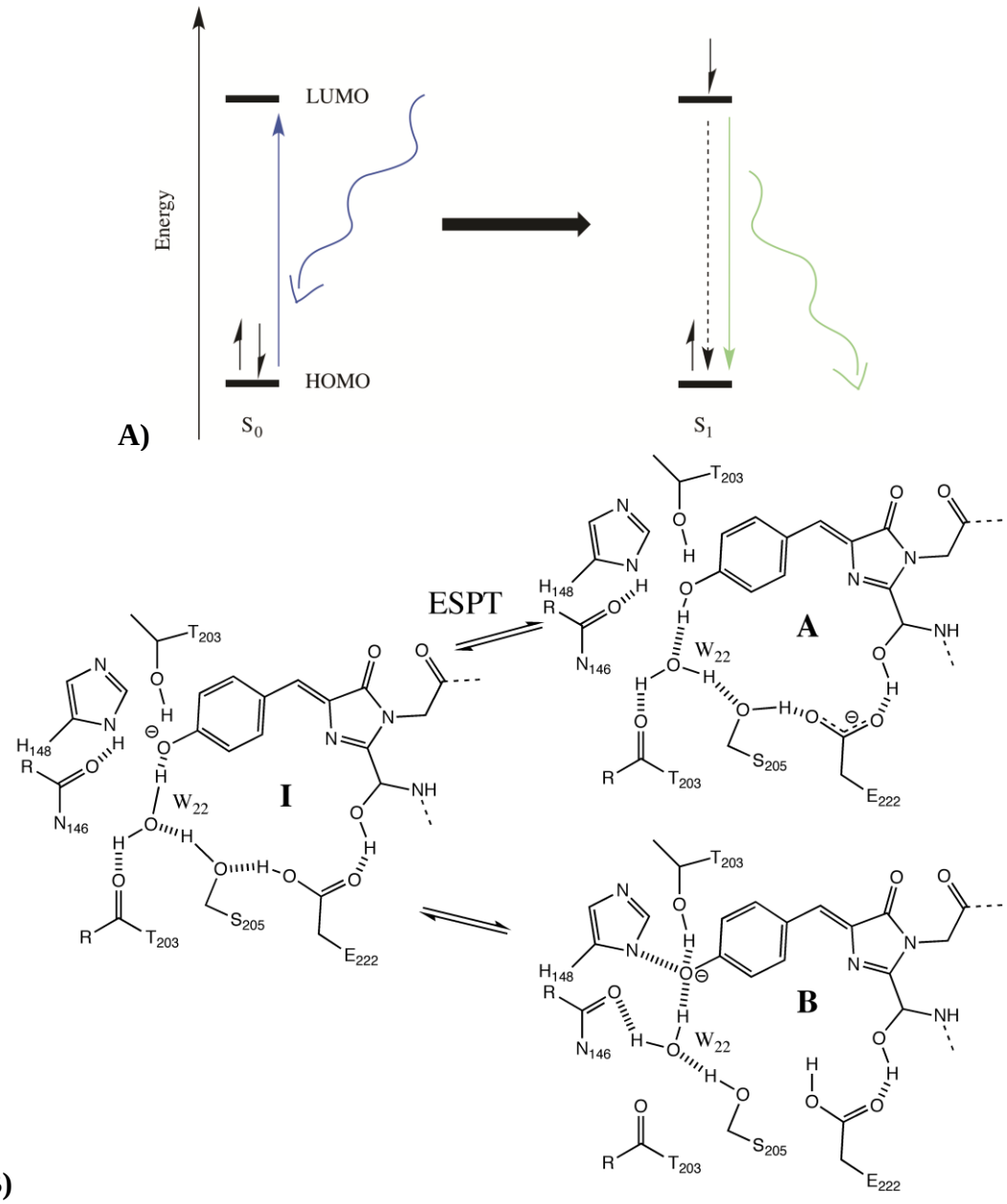

Figure 1.2: A) The simplified Jablonski diagram, depicting the S_0 ground state of a molecule, where the HOMO (highest occupied molecular orbital) can be excited via absorption (blue straight arrow) to the LUMO (lowest unoccupied molecular orbital) by a photon of light, represented by the curved blue arrow. The resulting excited state, S_1, can relax back to S_0 through internal conversion (dashed black line) or through fluorescence (solid green straight line) emitting a photon of light (curved green arrow). B) The hydrogen-bonding network of the neutral chromophore of GFP (A). Upon excitation, the chromophore undergoes the ESPT event, to the intermediate (I) where it can relax back to the ground state via fluorescence. In some instances, the chromophore can permanently lose its proton, resulting in the anionic chromophore (B). Adapted from Brejc *et al.*[15]

Although the *p*-HOBDI moiety of GFP is responsible for its unique spectral characteristics, on its own, the *p*-HOBDI moiety is barely fluorescent.[11,16] This is because the *p*-HOBDI moiety is maintained in a rigid, *cis*-coplanar configuration within the β-barrel due to an extensive hydrogen bonding network (figure 1.2).[17,18] Without the β-barrel, the excited *p*-HOBDI is free to relax back to S_0 primarily via ultrafast vibrational and rotational movement, known as internal conversion (IC).[11,19] Thus, it is only through the unique combination of the *p*-HOBDI moiety and the β-barrel that GFP is able to efficiently fluoresce, with an quantum yield of 0.79.[9,10]

As previously mentioned, with researchers striving to further understand the dynamics of living cells, the need for a genetically encoded marker was becoming prevalent. GFP was the perfect candidate for this, as GFP is a genetically encodable FP, which requires no external assistance in folding to achieve maturation, and is also relatively resistant to denaturation.[10] From this starting point, the uses of GFP have multiplied extensively, as it can be used in Förster Resonance Energy Transfer (FRET) experiments, single molecule detection, pH sensors, cell markers, and fusion tags to name a few.[8-10]

As further applications of GFP were explored, the creation and discovery of several variants and homologues of GFP were also being developed. One of the most prevalent variants, created by Zhang *et al.*, is the Enhanced GFP (EGFP) variant, which contains the point mutations F64L and S65T.[20] Compared to the wild type GFP, EGFP is 35 times brighter and also folds more efficiently.[20] As well as enhancing the brightness, several colour variants have been created, ranging from blue (BFP), to cyan (CFP), to yellow (YFP). Tsien has an excellent review article on the different colour variants of GFP and the mutations that helped to achieve them.[10] Through the combination of rational design and directed evolution, these mutants have provided

researchers brighter, longer lasting, and a greater range of coloured fluorescent tools. Even so, a full spectrum of FPs was not available, as a red emitting species could not be obtained through mutation. This limited potential applications considering light in the red spectrum provides greater signal to noise ratios when compared to the auto-fluorescence of living cells.

In an attempt to supplement the spectrum of FPs, Matz and co-workers argued that other brightly coloured marine species should have similar FPs.[21] As predicted, in other Cnidarians, specifically the Anthazoan, *Discosoma striata*, GFP homologues were found that displayed spectral characteristics in the red spectrum.[21,22] One FP of note, the tetrameric DsRed, contained an amino acid similarity to GFP of only 23%, yet still displayed the characteristic β-barrel and internal chromophore of GFP.[23] Along with the conserved barrel structure of DsRed, the chromophore also bears homology to the *p*-HOBDI moiety of GFP. The main difference in the DsRed chromophore is the extended π conjugation, due to an oxidation of the α carbon and nitrogen of the glutamine at position 66 (figure 1.3) to give an acylimine. This extended conjugation shifts the excitation and emission peaks to 558 and 583 nm respectively, giving the characteristic red fluorescence.[23] Just as GFP was utilized to create other coloured variants, DsRed was also capitalized on to produce a plethora of coloured mutants ranging from blue to deep red.[24-27] In addition, other mutants have been created such as photoswitchable FPs like mTFP0.7, where upon illumination at 453 nm there is a rapid loss in fluorescence followed by a thermal reversion to its fluorescent state.[28] As well there are photochromic FPs such as Dronpa, where excitation at 488 nm will convert the protein to a non-fluorescent state, which can then be excited at 405 nm to return its fluorescence.[13] Finally, there are other mutants called photoactivatable FPs (PAFPs), such as PAmCherry1, which have been developed to provide fluorescent microscopists with the ability to surpass the diffraction limit of light.[29] Indeed, Betzig

et al. was able to demonstrate a super resolution technique by compiling several images of PAmCherry1 being activated and subsequently bleached within a defined area (2 – 25 nm), achieving spatial resolutions of 1 nm.[30]

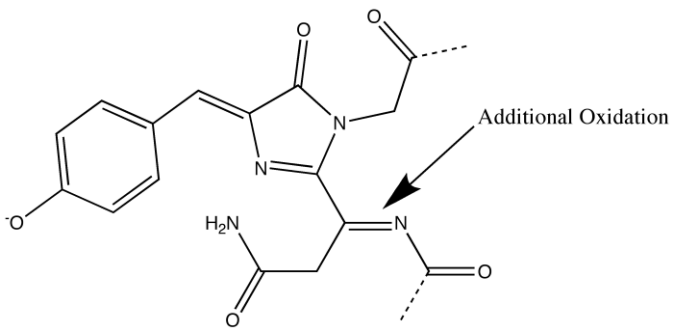

Figure 1.3: The chromophore of DsRed displaying the additional oxidation step required to extend the conjugation. Adapted from Yarbrough *et al.*[23]

Even with all the advances and mutations that FPs have undergone over the years, as with any fluorophore, they are still susceptible to a process known as photobleaching (PB). The process of PB is the overall destruction of the fluorophore due to light induced damage from each excitation event interacting with the surrounding molecules.[4,31] To quote Roger Tsien "Photobleaching is the simplest and most universal behavior of fluorophores", and FPs are no exception.[10] Most FPs that have not undergone mutations are fairly resistant to PB, as the chromophore is shielded from the bulk solvent within the β-barrel. Despite this, upon prolonged exposure to high intensity light, FPs will still lose their ability to fluoresce.[10,32] One reason postulated for this susceptibility to PB is due to the destructive effects that high intensity light can produce via the interaction of oxygen with excited fluorophores.[32] For example, the toxic quantities of reactive oxygen species (ROS) produced by the KillerRed protein derived from the jellyfish, Anthomedusa, efficiently kills their host cells upon excitation.[33] Considering the ability of ROS to induce oxidative stress on proteins,[34,35] the PB experienced by KillerRed is attributed

to the interaction of the ROS with the amino acids of KillerRed itself.[33,36] This suggests that ROS induced oxidative stress is one method of PB experienced in FPs.

Although most FPs do not possess the phototoxicity of KillerRed, they still undergo a loss of fluorescence upon high intensity excitation. This presents a problem as some long exposure techniques are complicated by the loss of fluorescence.[32] Despite this setback, some techniques have capitalized upon PB, such as Fluorescence Recovery After Photobleaching (FRAP) where a small area of fluorophores is bleached and the time taken to recover is monitored. Others such as FRET can use irreversible PB as a way to quantitatively determine FRET efficiency through acceptor bleaching.[37]

Currently, the methods of overcoming the issues of PB have rested in directed evolution. Through rational design, random mutagenesis and directed evolution, Shaner *et al.* have been able to screen libraries containing up to 100,000 clones, testing each clone for their photostability in intense light.[26] This has led to novel FPs such as mApple, which displays a red shifted fluorescence, greater photostability and brightness than that of its predecessor, mOrange.[26] Unfortunately, the rationale for the design was based upon the improvements made to mRFP1 in the variants mOrange and mCherry, and not from a mechanistic understanding of PB. Understanding the mechanism of PB will provide a consistent set of standards for PB across all FPs, however it is yet to be achieved.[31,37] In an attempt to elucidate the mechanism(s) of PB, it will be of benefit to understand FPs upon excitation, looking into the photophysics and photochemistry of the chromophore and its environment.

1.2 The photophysics of the *p*-HOBDI moiety

As outlined above, a commonality between all FPs is the presence of the light absorbing chromophore. Whether that is the *p*-HOBDI moiety that exists in GFP, or the more conjugated

versions of the chromophore within that of DsRed, there are some basic similarities between the excited state deactivation mechanisms of different FPs. These deactivation mechanisms, including PB, can be probed through the photophysical analysis of the common *p*-HOBDI moiety existing in most FPs.[38] Thus, gaining an understanding of FP photophysics, both computationally and experimentally, will endeavor to move researchers closer to understanding, designing and creating new, more photostable FPs. For the purpose of this introduction, we will be focusing on the *p*-HOBDI moiety as most of the current literature surrounding the photophysics of FPs pertains to this molecule.

1.2.1 Excited State p-HOBDI moiety

Before delving into the excited state (S_1) properties of the chromophore, first it will be of benefit to look at the model ground state (S_0) structure. As mentioned before, for most FPs the chromophore is situated as the *cis*-isomer (with some exceptions such as eqFP611 and TagRFP red FPs, having a *trans*-isomer), where the phenol ring is essentially coplanar to that of the imidazole ring (figure 1.4A).[8,12,17,19,38] This coplanarity is maintained through stabilizing effects such as the hydrogen bonding network of amino acids and internal water molecules as well as the steric effects of the amino acids of the β-barrel.[17,19,39] Without these stabilizing effects, it has been well documented that the *p*-HOBDI moiety readily undergoes non-radiative decay via IC from its excited state, rather than radiative decay.[17] One model for the IC pathway was proposed by Gepshtein *et al.* where IC occurred most readily via an intermediate involving rotation around the ϕ and ψ bond angles of the methylene bridge (figure 1.4), whose motions occurred in ground and excited states respectively. Where, in the ground state, the phenol ring of the *p*-HOBDI can twist relative to the imidazole ring in a paddle like motion along the ϕ bond angle (figure 1.4A). This paddle motion moves the phenol ring out of the plane of the *p*-HOBDI moiety, and once

excited, rotation along the ψ bond angle (figure 1.4B) results in the favorable intermediate, leading to deactivation primarily through IC.[17] Realizing the main non-radiative deactivation pathway is that IC, the need for a rigid, planar ground state becomes apparent.

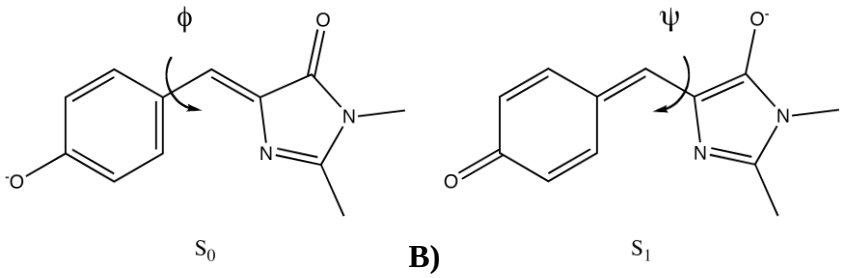

Figure 1.4: A) The ground state of the anionic deprotonated *p*-HOBDI moiety, where the phenol ring is free to move about the ϕ bond angle relative to the imidazole ring and B) the excited state of *p*-HOBDI moiety, where a keto-enol tautomerization has allowed the phenol ring to twist about the ψ bond angle, increasing the probability of deactivation through IC. Adapted from Gepshtein *et al.*[17]

Another factor to consider for the ground state is the probability of transition from S_0 to S_1. A good example of this is the comparison of GFP to EGFP. In the matter of chromophore excitation, the main difference between GFP and EGFP is the presence of both the protonated and deprotonated chromophore peaks at 395 and 475 nm respectively in GFP, while EGFP only has the deprotonated chromophore peak at 488 nm.[31] However, it should be noted that the ability for a molecule to absorb a photon of light and become excited, is associated with its molar extinction coefficient as this represents the absorption cross section of the molecule.[40,41] Therefore, when comparing the extinction coefficients ($\varepsilon(\lambda_{ex})$) of the deprotonated chromophores, EGFP is larger at ε_{488}= 53,000 $M^{-1}cm^{-1}$, where GFP is ε_{475}= 14,000 $M^{-1}cm^{-1}$.[10] This suggests that solutions of GFP and EGFP containing the same concentration of deprotonated chromophore, when irradiated, the EGFP solution will have a greater population of chromophores in the excited state compared to GFP. Although these deprotonated chromophores are both identical in structure, they have different extinction coefficients, which is indicative of

different protein environments. This suggests that one reason for the higher extinction coefficient of EGFP could rest in the ability of the β-barrel to maintain the deprotonated chromophore in a more planar structure, causing the transition from S_0 to S_1 to be more 'symmetrically allowed' for EGFP than that of GFP.[40]

The term 'brightness' in fluorescence, commonly refers to the product of a fluorophore's $\varepsilon(\lambda_{ex})$ and its ability to emit a photon of light, or fluorescence quantum yield (ϕ_{fl}).[42] Therefore, applying this to the FPs, with the similar ϕ_{fl} of EGFP (0.6) to that of GFP (0.79), EGFP's higher brightness relative to GFP can be primarily attributed to its extinction coefficient.[10] It may be argued that this is not a complete comparison as GFP's brightness is also contributed to by the protonated chromophore with ε_{395}= 30,000 $M^{-1}cm^{-1}$, which allows fluorescence due to ESPT.[31] Albeit true, the fluorescence due to excitation at 395 nm is quite low, with ϕ_f = 0.02 for the protonated chromophore, indicating that most of the fluorescence originated from the deprotonated chromophore.[43]

Knowing that for the *p*-HOBDI moiety, it is preferential that the molecule be rigid and planar for a S_0 to S_1 electronic transition to occur and not have it deactivate via IC, we can now examine some other structural aspects. As seen from figure 1.4, the *p*-HOBDI moiety is depicted as a phenolate anion as this is the state from which the molecule fluoresces. When protonated, the *p*-HOBDI moiety requires more energy to be excited and this can be seen in the excitation peaks for GFP where higher energy blue light is needed to excite the protonated chromophore at 395 nm verses the deprotonated at 475 nm. A simple explanation for this is when deprotonated, the extra electron density of the phenolate contributes to raising the overall highest occupied molecular orbital (HOMO) in energy, making the gap between the HOMO and the lowest unoccupied molecular orbital (LUMO) smaller (figure 1.5), thus resulting in a red shift.[31]

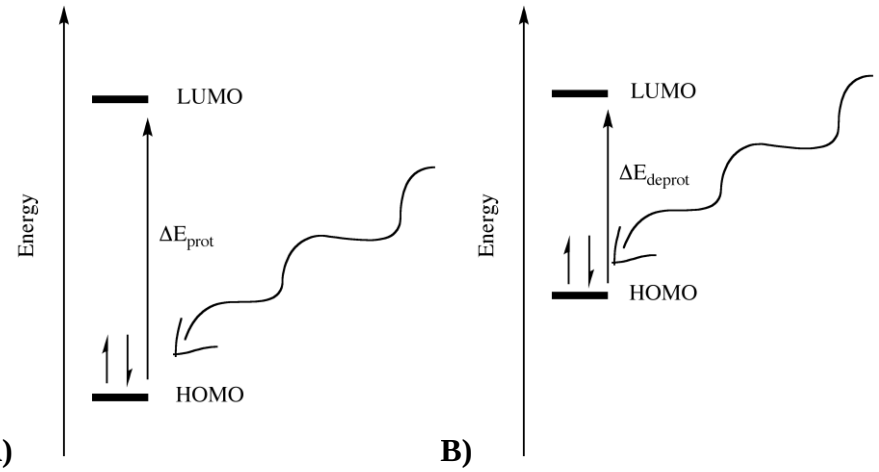

Figure 1.5: The cartoon energy diagrams representing the amount of energy needed to excite the A) protonated chromophore B) the deprotonated chromophore. $\Delta E_{prot} > \Delta E_{deprot}$. The curved arrows indicate a photon of light with energy of at least ΔE_{prot} or ΔE_{deprot}.

With the ground state of the *p*-HOBDI moiety modeled as an ideally anionic, planar and rigid molecule, to understand the photophysics of the *p*-HOBDI moiety, now we have to look at the molecule in its excited state (S_1). This excited state is achieved through the incident light on the chromophore of sufficient energy to excite an electron from the HOMO to the LUMO, resulting in a S_0 to S_1 transition. This transition is modeled in figure 1.4B, where a keto-enol tautomerization frees the phenol ring to move about the ψ bong angle.[17] If we are considering the excited chromophore within the FP, for most variants the primary mechanism of deactivation is through radiative decay. However, this does not free the *p*-HOBDI moiety from consideration of other deactivation pathways. From here, given the wide breadth of interaction that can occur with the excited *p*-HOBDI moiety, it will be of benefit to divide the interactions into two main categories in an attempt to understand the excited state dynamics of *p*-HOBDI. The first (section 1.2.1.1) will be structural effects focusing on the physical mechanism of excited state deactivation, including *cis-trans* isomerization and ESPT. The second (section 1.2.1.2) will be

non-structural, looking at pathways for excited state deactivation other than fluorescence such as Triplet-Triplet annihilation (TTA).

1.2.1.1 Structural photophysical effects of the excited p-HOBDI moiety

For the excited chromophore, there are two main structural changes that it can undergo. The first is the already discussed ESPT, and it should be noted that GFP is the first biological system to demonstrate a proton loss upon excitation.[8] Briefly, ESPT occurs due to the S_1 state being highly acidic as seen in the keto-enol tautomerization in figure 1.4B.[13,44,45] Upon relaxation, the chromophore loses its acidity and becomes susceptible to protonation, thus resulting in a light induced reversible proton transfer (photocycle).[8] Although ESPT describes a structural change to the excited chromophore, this process cannot account for the loss of fluorescence seen in PB. In light of this problem, Mizuno *et al.* suggests that one possible mechanism for the loss of fluorescence actually occurs through the protonation of the chromophore via the triple state (T_1) of the chromophore. It is generally accepted that T_1 is less acidic than S_1 in most cases where a phenol is present, and in addition the lifetime of T_1 is longer than S_1.[13] With a lower acidity and longer lifetime, the chromophore is more susceptible to protonation.[13] This idea holds merit as the irradiation of the deprotonated chromophore of monomeric photochromatic Dronpa at 488 nm, produced the non-fluorescent protonated form of the chromophore.[46]

The second structural effect of the excited *p*-HOBDI moiety is *cis*-*trans* isomerization. As stated before, most FPs have their chromophore in the *cis*-isomer, and it has been postulated that the isomerization process to the *trans*-isomer could contribute to the loss of fluorescence seen in photobleaching.[17,47,48] In the crystallographic study of Henderson *et al.*, they showed that

upon isomerization from the *cis* to *trans* isomer, the switchable mTFP0.7 lost its fluorescence. From their data, the *trans*-isomer disrupted fluorescence due to fewer hydrogen bonds available to stabilize the hydroxyl group of the phenol ring resulting in the formation of the protonated chromophore. Additionally, the crystallographic data showed the *trans*-isomer was significantly non-planar.[28] There are several other examples of the *cis-trans* isomerization leading to a loss in fluorescence (for some examples see references 13 and 40), but it will be of benefit to understand the possible mechanisms behind it.

From their ^{1}H-NMR studies, He *et al.* showed that in the ground state, *p*-HOBDI has a free energy barrier of 9.6 kJ/mol for *cis-trans* isomerization of the anionic chromophore.[49] This suggests a low barrier to rotation, and can easily be overcome upon excitation, leading to a lower bond order and thus resulting in isomerization.[47,50] Support for this structural change comes from the work of Usman *et al.* where using ultrafast polarization-sensitive infrared (IR) spectroscopy, they noticed a decrease in the imidazoline carbonyl stretching frequency with excitation. Upon matching the carbonyl bond vector to theoretical values of a twisted chromophore, Usman *et al.* found that the most likely configuration was a single twist of 120 ± 10° or a hula twist of 150 ± 30° between the phenol and the imidazole of *p*-HOBDI.[19] This isomerization can be seen in figure 1.6.

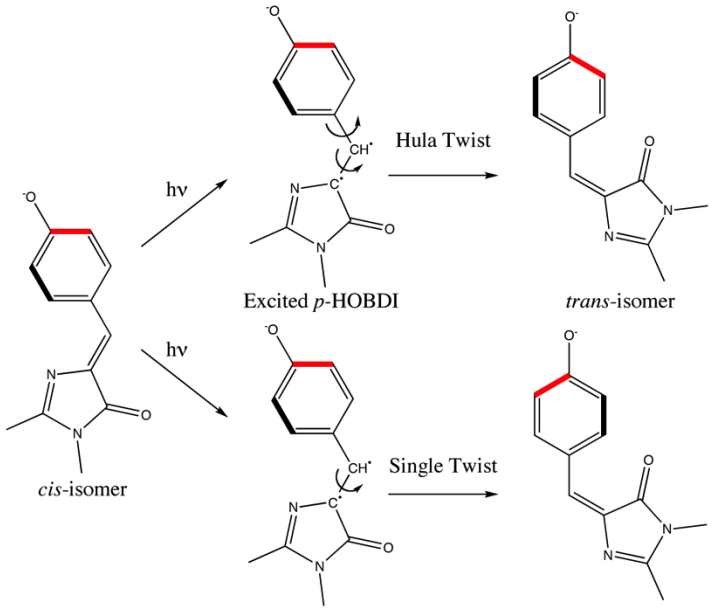

Figure 1.6: The isomerization pathways of the *p*-HOBDI moiety upon excitation via a Hula or Single twist. The resulting *trans*-isomers are structually identical, however, the bond colours indicate the different pathways for isomerization.

Although a promising method of excited state deactivation, the *cis-trans* isomerization had not been shown to conclusively lead to a permanent loss in fluorescence. For example, Dong *et al.* demonstrated that in the presence of a good nucleophile, the *trans p*-HOBDI reverts to its *cis*-isomer via an addition and elimination pathway involving the methylene bridge of the phenol and imidazole rings.[12] This pathway is further supported by the presence of a glutamate (148) and water molecule in close proximity to the methylene bridge within mTFP0.7, which repeatedly undergoes *cis-trans* photoinduced isomerizations.[12,28] Given that protonation and isomerization alone cannot produce the irreversible PB experienced by all FP, other areas have to be investigated.

1.2.1.2 Non-Structural photophysical effects of the excited p-HOBDI moiety

One of the more recent theories on loss of fluorescence focuses around the existence of a long lived dark state. This theory of Dark-State Conversion (DSC) suggests that upon excitation

the chromophore will undergo other interactions that do not lead to fluorescence such as conformational changes to undergo IC, protonation or triplet state (T_1) formation.[38] As the first two have already been discussed in the section above, the non-structural photophysical effect of DSC that will be focused on, is the T_1 formation. The T_1 of a molecule can be understood as an electronic isomer of S_1 where upon intersystem crossing (ISC) from S_1, an electron flips its spin (for example: from S_1 ↑↓ to T_1 ↑↑).[51] The lifetime of a molecule in T_1 is generally longer than that of S_1 and can decay to S_0 through phosphorescence, ISC and TTA.[35,51] Thus, examining the T_1 of *p*-HOBDI may provide clues towards irreversible PB.

It is Dean et al. who extensively studied the dark state of TagRFP and mKate, showed one possible link between PB and DSC. Within their work, they found that the dark state had three kinetic phases where the initial phase was monoexponential decay (<800 μs) followed by a steady state phase (800 μs to 5 ms) and finishing off with a gradual biexponential decay phase (>5 ms). They showed that if a FP were allowed to relax within the time scale of the first decay phase, the dark state was mostly reversible, however this was not the case of extended irradiation. Not surprisingly, they saw that with extended irradiation they found increased DSC, leading to higher levels of PB.[38] This result is supported by the basic fact of triplet state saturation, where even with a low quantum yield ($\phi_{DSC} = 1 \times 10^{-3}$)[38], the long life time of the dark state will enable a large percentage of the FPs to undergo DSC.[52] Thus, with extended irradiation a large population of FPs in the dark state will begin to form, allowing a greater number of FPs to become non-fluorescent through such pathways as protonation. Finally, Dean *et al*. looked at the role of DSC in several variants of TagRFP and mKate and noticed that in some cases the dark state was photoprotective (protecting from PB) while in others it was photoreactive (leading to PB). It should be noted, however, that Dean classified a 'dark state' as

any state that is non-fluorescent, less fluorescent, non-absorbing or less absorbing.[38] This suggests that the dark state could consist of protonated or isomerized chromophores, as well as those in the T_1 state. Therefore, although the model provides some insight into some mechanisms of PB, it is not comprehensive.

Albeit not a comprehensive model, Dean *et al.* demonstrated that some of the dark states could arise from T_1 of the excited chromophore, and one possible mechanism of T_1 to S_0 relaxation is TTA with molecular oxygen ($^3O_2$). One of the outcomes of this TTA pathway is the production of reactive oxygen species (ROS), as $^3O_2$ is in the triplet ground state.[35] As mentioned before, the production of these ROS is the manner in which KillerRed is able to efficiently kill its host cells. However, the production of ROS has other ramifications as seen in the work of Valencia-Perez and Heyne. Upon interaction of GFP with a photosensitizer such as Rose Bengal or Methylene Blue, there was an increased PB for GFP. With further inspection it was shown that the ROS, singlet oxygen ($^1O_2$), produced by the photosensitizers was interacting with the β-barrel such that the presence of covalent dimers of GFP could be detected in a western blot analysis only after irradiation.[53] This data suggests that FPs should change their PB characteristics upon the presence or absence of $^3O_2$. For such variants as mOrange and TagRFP-T, this observed change in the characteristics of PB holds true, where the lack of $^3O_2$ has a protective effect on the FPs. However, for others such as EGFP, this is not the case. Thus, although the T_1 state has provided further insight into the possible mechanisms of FP PB due to the creation of ROS, the understanding of PB is not complete. Considering up to now, only the chromophore has been examined in relation to PB, to garner a more complete picture the effects of the β-barrel on the chromophore will have to be investigated.

1.3 Effects of the β-Barrel on the *p*-HOBDI moiety

The effects of the β-barrel on the chromophore have already been discussed in some detail. However, it cannot be understated how the chromophore becomes nearly non-fluorescent without the presence of the β-barrel. Hydrogen bonding between the β-barrel and chromophore contributes significantly to the fluorescence of the chromophore, along with quadratic Stark effects, ESPT, and barrel mediated dynamic stokes shifts.[24,38] Without this β-barrel, the neutral chromophore of GFP is blue shifted in absorbance by 46 nm, from 395 nm to 349 nm.[54] In fact, the effects of the β-barrel are so pronounced that within the mFruit family of FPs, several mutations to the β-barrel, that do not affect the conjugation of the chromophore, can cause spectral changes by up to ~50 nm.[55] One of the main features of the β-barrel is its rigidity, locking the chromophore in place. This forces the primary mode of deactivation for the excited chromophore to be through radiative decay. It has been suggested that some β-barrels are in fact so rigid that they nearly inhibit the isomerization process despite the suggestion that *cis-trans* isomerizations have been indicated as a plausible mechanism for the PB of FPs.

For example, the monomeric photochromatic Dronpa easily isomerizes between the *trans* (off) and *cis* (on) states due to a flexible region of its β-barrel. Yet, this protein was developed from six mutations of its parental non-photochromatic protein, 22G. Upon further investigation it was shown that the dimer interfaces of the tight tetramer of 22G consisted of these flexible regions of Dronpa. This indicates that although flexible in the monomeric variant, when the β-barrel is rigidified by the tetramer, no photochromatic isomerization is observed.[13] Pletnev *et al.* provided further evidence that a rigid β-barrel can prevent isomerization, as they showed an expansion and contraction occurred during *cis-trans* isomerization in the photoswitchable

rsTagRFP.[56] Given that flexibility within the β-barrel leads to easily isomerizable proteins, it can be clearly seen for some FPs, photostability depends on β-barrel rigidity.

In addition to providing a rigid scaffold for the chromophore, the β-barrel also contributes to the unique internal protein environment. By introducing simple, well-planned point mutations, researchers have been able to drastically change various characteristics of FPs. For example, TagRFP is a bright monomeric red FP that is susceptible to PB. However, with the introduction of the Ser158Thr mutation, the photostability increases nine fold resulting in the most photostable FP currently known, TagRFP-T.[37,38] Even though the Ser158 is involved in the stabilization of the *trans*-chromophore, the mutation to Thr simply adds a small steric bulk (additional methyl group) that does not interrupt the hydrogen-bonding network as Thr also contains the necessary alcohol group to stabilize the chromophore.[57] In trying to rationalize the impact of this mutation, it is helpful to look at other point mutations done in crystallographic studies. One study of note carried out by Henderson *et al.* looked at the photoisomerization of mTFP0.7 in the crystal state, which provided excellent insights into the process of bright to dark conversions. In their work, the bright state of mTFP0.7 was a well-ordered cis-chromophore (indicating one primary conformer), but while in the dark state, the *trans*-chromophore was highly disordered. This high degree of disorder was postulated to be the reason for the ease of reversion from the dark to bright state. Upon further investigation, Henderson *et al.* noticed that the Ile 161 was destabilizing the *trans*-isomer. With mutation to a small, more polar amino acid such as Thr, the *trans*-chromophore was stabilized, thus increasing time of reversion significantly.[28] Based on this work, it can be postulated that for TagRFP-T, the mutation of the Ser to Thr provides additional steric bulk, helping to maintain the *cis*-isomer through prevention

of isomerization. However, until further studies on the crystal structure of TagRFP-T are done, the full impact of this methyl group can only be speculated.

The impact of an individual point mutation is difficult to gauge. Where critical amino acids can lead to an increased or decreased photostability, others may have no effect on the FP characteristics. With the more recent development of *in crystallo* absorption and fluorescence spectroscopy as well as PB, these key amino acids are slowing being revealed. For example, the mutation of Phe174Leu in several variants of TagRFP caused a decrease in the photostability, and concurrently the simple replacement of Met160 with Ala caused an increase in DSC.[28,38] Through the examination of the crystal structures, it can be seen that these are prominent in causing disorder within the structure as they prevent one single conformation of the chromophore from being found. This suggests that with a less stable environment, it is more likely that a FP will be able to undergo DSC and eventual PB. Additionally, carrying out PB *in crystallo* may provide some answers to the questions of PB through the understanding of protein structures after PB, and which amino acids within the β-barrel help to stabilize dark states. Despite the need of a deeper understanding of the β-barrel to further characterize PB mechanisms, it is still established that the unique internal environment provided by the β-barrel has a dramatic effect on the resistance of FPs to PB.

1.4 Pathways to Photobleaching

Considering the manners in which most FPs act upon excitation, it is plausible to produce two methods of irreversible PB. The rationale for this comes from the fact that FPs experience PB with and without the presence of $^3O_2$.[31] The first method of PB is oxygen-dependent, and would arise out of the creation of ROS. The destructive power of ROS is very well known and having a FP produce a toxic product would inevitably inhibit fluorescence due to oxidative stress

on the protein itself.[31] For example, $^1O_2$ once created through TTA has been shown to oxidatively react with the amino acids: His (3.2 X 10^7 $M^{-1}s^{-1}$), Trp (3 X 10^7 $M^{-1}s^{-1}$), Met (1.6 X 10^7 $M^{-1}s^{-1}$), Tyr (0.8 X 10^7 $M^{-1}s^{-1}$) and Cys (0.8 X 10^7 $M^{-1}s^{-1}$).[35,53] Given the short lifetime of $^1O_2$, this suggests that, if created, $^1O_2$ would primarily oxidize the amino acid within the vicinity of the ROS producing protein. With the wide breadth of interactions that could occur to the amino acids upon interaction with the ROS, it is not unimaginable that PB could occur due to these oxidizations, as was shown in the work of Valencia-Perez and Heyne.[53] Unfortunately, short of removing all traces of $^3O_2$ within the media (not something beneficial to living cells) the ability to regulate this pathway of PB is limited.

The second model for PB arises from the structural deactivation pathways of the excited *p*-HOBDI moiety. From the investigations of several photochromic, photoswitchable and photoactivatable FPs, it appears as though these proteins capitalize on the mechanism for PB. All of these types of photoconvertible proteins have in common, the activation (or deactivation) of the proteins fluorescence through a photoisomerized process, moving the chromophore from one isomer to another (for example, *cis* to *trans*). What is interesting however is only one of the states is fluorescent while the other is dark. This suggests that although these proteins show different characteristics, they all require the protein to have a dark state, just as PB ultimately leads the protein to a dark state. Thus, it could be considered that PB is simply a permanent version of the dark state within these FPs. Therefore, it follows that PB can result from a permanent stabilization of the non-fluorescent form of the chromophore. This most likely occurs do to the presence of a stabilizing pocket within the β-barrel for the non-fluorescent isomer. Thus by altering the amino acids around the area of potential isomerization to bulk, non-hydrogen bonding amino acids, the non-fluorescent isomer will be more likely to become destabilized,

preferentially returning to the fluorescent state. Of course this type of rational design requires 3D modeling as well as reliable crystallographic data of the parental FP, in order to be carried out. However, with the increasing number of structures being published, as well as the availability of affordable protein modeling, this task is quickly becoming achievable.

1.5 The motivation for the work presented within this thesis

With all the studies that have been carried out over the past few decades, none have achieved yet a plausible mechanism that can account for the PB of all FPs. Perhaps this is a mere fact of reality. With so many variants of FPs, all containing different internal protein environments from each other, there may not be one mechanism that can account for the PB of FPs as a whole. However, it has not been the intention to produce one grand unifying mechanism, rather it has been to highlight important commonalities that could lead to PB in a variety of FPs. Having highlighted these commonalities, the foundation has been laid, which is needed to better understand PB in FPs; allowing efficient research into the loss of fluorescence for FPs. Indeed, recognizing the available pathways of PB enables a deeper understanding of the results. Thus, in an attempt to add to the body of work on FP PB, the work presented in this thesis will focus on one of the most light sensitive FP available, mOrange. It is only through a detailed analysis of the loss of both the fluorescence and absorbance in chapter two, that an understanding for PB can be achieved in this protein.

Not only will this work illuminate the nature of the overall PB experienced in mOrange, it will endeavor to demonstrate the ramifications of the results. Hence the body of work presented in chapter three will examine the proposed photowitching of Subach *et al.*[58] It is in their work where it was shown that mOrange would oxidize to a far red emitting species in the presence of the external oxidant potassium ferricyanide.[58] However, given there are certain

photophysical aspects which were not addressed within the work, a detailed understanding of the processes involved is required to elucidate the mechanism responsible for the observed photoswitching. Finally, the work in chapter four will address the PB dependence of mOrange on the presence of molecular oxygen, and its ability to produce ROS.

Chapter Two: **On the interaction of mOrange with light.**

2.1 Introduction

As alluded to in the introduction, fluorescent proteins (FPs) have been of major interest for their use in *in vivo* imagining.[6,8,9] Of the FPs discovered and synthesized from the famous Green Fluorescent Protein (GFP) initially for this purpose, the spectrum of coloured FPs still lacked those that could fluoresce red.[10] This lack FP fluorescence capability did not go unnoticed, when in 1999, Matz *et al.* revealed the discovery of the tetrameric red homolog to GFP: DsRed.[21] The discovery of DsRed from the coral *Discosoma striata* enabled a plethora of red variants to be created, allowing advantages such as better signal to noise ratios in fluorescence studies or better contrast between fluorescence and background auto fluorescence to be realized.[2,36] Within the variants produced from DsRed, the family of FPs referred to as the 'mFruits' have been of particular interest due to their monomeric nature and the variety of colour resembling known fruits.[22,25] The brightest of these mFruits produces an orange coloured fluorescence and is appropriately named: mOrange.

As mentioned previously, DsRed and its variants are homologs of GFP sharing roughly 23% of the same amino acids,[23] yet still having fluorescent autocatalytic forming chromophores and protective β-barrels.[21] The red fluorescence comes from the extended conjugation within the chromophore, but unique to mOrange is the presence of a second cyclization which reduces conjugation, blue shifting the fluorescence from red to orange.[25] Figure 2.1 shows that the mOrange chromophore that is formed from the initial three amino acids of Threonine (Thr 66), Tyrosine (Tyr 67), and Glycine (Gly 68), when compared to the chromophore of DsRed which consists of Glutamine (Gln 66), Tyrosine (Try 67) and Glycine (Gly 68). As can be seen in figure 2.1, the second cyclization (oxazole ring) in mOrange disrupts the conjugation within the

chromophore compared to that of DsRed, supporting the observed blue shift.[24] Additionally, this chromophore assumes a relatively more planar conformation as compared to other mFruits, resulting in the observed high brightness and fluorescence quantum yield (Φ_{Fl} = 0.69).[24]

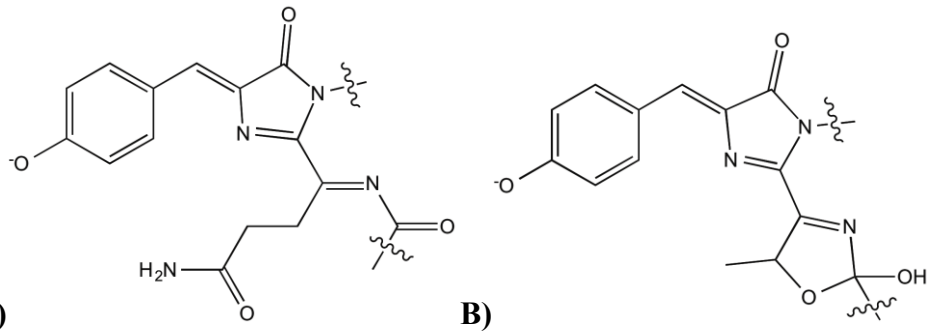

Figure 2.1: A) The chromophore of DsRed adapted from Yarbrough *et al.*[23] B) The chromophore of mOrange with the additional cyclization adapted from Shu *et al.*[24]

Interestingly, mOrange has spawned several different variants, some capable of photoswitching to far-red fluorescence while others are more stable or brighter versions of mOrange.[26,58] The impetus for the creation of these variants has been mOrange's desirable high quantum yield coupled with its innate susceptibility to photobleach. Known to be one of the most light sensitive FPs,[27] improvement of mOrange through directed mutation lead to the production of bright and more stable variants known as mApple and mOrange2.[26] Given that the purpose of this work was to investigate some of the mechanisms responsible for the photobleaching seen in FPs, and in doing so, provide the basis upon which improved FPs may be designed; mOrange situates itself as an ideal candidate for this study.

In order to best assess the photobleaching of mOrange, the use of purified protein is paramount as the cellular environment contains many components that could play a role in the photophysics of mOrange.[58] Thus, by using purified protein suspended within a PBS (pH 7.4) solution, any external influence on the photophysics of mOrange can be eliminated. Once in solution, the *in vitro* analysis of the photobleaching of mOrange can be investigated through the

exposure of mOrange to high intensity light sources such as LEDs and following the decay patterns via absorption and fluorescence spectroscopy.[26] From previous photobleaching studies carried out on other FPs, it was shown that photobleaching could lead to the production of a protonated by-product that is blue shifted compared to the FP.[59] Additionally, it has been shown that the decay patterns for FPs follow multi-exponential trends suggesting several mechanisms involved such as *cis-trans* isomerization of the chromophore, protonation and π-conjugation disruption.[36,38] Therefore, the primary investigation of mOrange photobleaching will focus on the interaction of light with mOrange, monitored via absorption and fluorescence spectroscopy, with attention being paid to production of by-products and decay patterns.

2.2 Material and Methods

2.2.1 Materials

For chemicals, Magnesium Chloride ($MgCl_2$), Calcium Chloride ($CaCl_2$), Glycerol, D-(+)-Glucose, Ampicillin, L-(+)-Arabinose, HEPES, Sodium Chloride (NaCl), β-Mercaptoethanol, Phenylmethanesulfonyl Fluoride (PMSF), Imidazole, Sodium Phosphate Monobasic (NaH_2PO_4) and Sodium Phosphate Dibasic (Na_2HPO_4) were purchased from Sigma-Aldrich Canada. The Lysogeny Broth and Yeast Extract were purchased from MP Biomedicals. Agar was purchase from Fischer Scientific.

The *E. coli.* cell lines, DH5α and Top10, were donated generously by Dr. Zaremberg and Dr. Ro respectively, of the Biological Sciences department of the University of Calgary. The pBAD-mOrange and pBAD-mApple plasmids were graciously gifted by Dr. Campbell of the University of Alberta.

2.2.2 Transformation of bacterial cells and mOrange expression and purification

To be able to obtain and purify the desired mOrange FP, two key *E. coli*. cell lines were used. The first being the DH5α cell line, used for amplification and storage of the plasmids and the second was the Top 10 cell line, used for expression of the proteins.

2.2.2.1 Generation of competent cells

The first step to obtaining purified protein is to have competent cells, able to be transfected with the desired plasmid. To make both the DH5α and Top 10 cell lines competent, first 100 μL of each cell line (obtained from a -80 °C stock), were thawed on ice for 30 minutes, then incubated in 2 mL of sterilized LB at 37 °C overnight at 240 rpm. From here, 100 mL of fresh sterilized LB was inoculated with one of the cell lines, and grown at 37 °C with shaking until the early log phase, as measured by optical density at 600 nm (OD_{600}), where $0.5 < OD_{600} < 0.7$, measured on a Varian Cary 50 single beam spectrophotometer. Once the early log phase was reached, the cells were split into two fractions, pelleted by centrifugation (Sorvall Legend RT, 4000 rpm, 10 minutes) and decanted of the supernatant. To each pellet of cells, 12.5 mL of sterile 0.1 M $MgCl_2$ was added and the cells were resuspended. Following this, the cells were repelleted, decanted and resuspended in 12.5 mL of sterile 0.1 M $CaCl_2$. The cells were then incubated on ice for 20 minutes. After incubation, the cells were repelleted and decanted, with the cells being resuspended in 2.5 mL per pellet of sterile 0.1 M $CaCl_2$ with 15 % glycerol. Finally, the now competent cells were proportioned into 100 μL aliquots and stored at -80 °C.

2.2.2.2 Transformation of DH5α cells, amplification of polyhistidine pBAD-mOrange plasmid and its extraction.

With the freshly competent cells, the mOrange plasmid could now be used to transform the DH5α cell line for amplification and storage using the heat shock technique. To do this, one aliquot of 100 μL of DH5α cells was thawed on ice. Once thawed, 150 - 200 ng, as determined by the Thermo Scientific Mircodrop 2000 UV-vis spectrophotometer, of the pBAD-mOrange was added to the cells and incubated on ice for 30 minutes. The cells were then heat shocked at 42 °C for 2 minutes in a water bath, then cooled on ice for an additional 2 minutes. From here 900 μL of Super Optimal Broth (SOB) with 0.01 M sterile $MgCl_2$, was added to the cells, which were then allowed to recover at 37 °C for 30 minutes while rocking. These cells were then pelleted (VWR Micro 2416, 13000 rpm, 2 minutes) and resuspended in 50 μL of the SOB broth, followed by plating on selective LB agar plates with 100 μg/mL of ampicillin. These plates were then incubated at 37 °C overnight. Finally, to ensure genetically identical DH5α cells, the now transformed DH5α cells were streaked onto another selective LB agar plate and grown at 37 °C overnight.

To extract the now amplified plasmids from the transformed DH5α cells, a GeneJET Plasmid Miniprep kit (Thermo Scientific) was used, following the procedure as outlined within the kit. The extracted plasmids were checked for their concentration using the Thermo Scientific Mircodrop 2000 UV-vis spectrophotometer and stored at -20 °C.

2.2.2.3 Expression and purification of mOrange

The expression and purification of mOrange follow a slightly modified version of the procedure reported by Ormö *et al.*[60] Competent Top 10 cells were transformed as outline in section 2.2.1.2. Using the streak plate of the transformed Top 10 cells, one colony was used to

inoculate 5 mL of LB containing 100 μg/mL of ampicillin, followed by growth at 37 °C overnight with 240 rpm shaking. To a 1 L wide mouth Erlenmeyer flask (VWR) with 200 mL of LB and 100 μg/mL of ampicillin, 2 mL of the overnight culture was added, followed by incubation at 37 °C with 240 rpm shaking until an OD_{600} of 0.6 was reached.

2.2.2.3.1 Optimization of protein maturation

According to the procedure outlined by Ormö *et al.*[60] expression of GFP from the pRSET plasmid vector requires 1 mM isopropyl β-D-thiogalactopyranoside (IPTG) to induce protein expression and 24 hours of 20 °C folding time, to allow proper folding of the protein. However, these conditions were not appropriate for expression of mOrange from the pBAD plasmid vector which requires L-(+)-Arabinose to activate the promoter to allow expression[61] in the Top 10 cell lines. Therefore, several iterations of L-(+)-arabinose amounts and different incubation temperature were assayed to obtain optimal protein expression and folding. Thus, to 200 mL cultures, 200, 400, or 600 μL of sterile 2% L-(+)-Arabinose was added to induce expression of the protein. From here, the temperature of incubation was increased by 5 °C increments from 20 °C, until 37 °C. It was determined via absorption spectroscopy that 400 mL of L-(+)-Arabinose and 37 °C provided the optimal conditions for protein folding.

2.2.2.3.2 Purification of mOrange

With these conditions determined, a 200 mL culture (OD_{600} = 0.6) was incubated for 24 hours, at this point the culture was visibly Orange-pink in colour and then centrifuged to pellet the cells. Once collected, the cells were weighed and resuspended in 3 mL/g of Resuspension Buffer A (0.05 M HEPES, pH 7.9, 0.3 M NaCl, 10 % glycerol, 0.002 M β-Mercaptoethanol, and 0.1 mM phenylmethanesulfonyl fluoride (PMSF)). The resultant suspension was sonicated

(Branson Sonifier) at 90% maximum power for 10 s intervals with 30 s rests, while on ice, for 12 minutes. This sonification process disrupted the bacterial cells, thus the resulting solutions were centrifuged (5000 rpm, 4400 X g, 2 hr., 4 °C) to separate the orange-pink soluble protein from the cellular remnants. The supernatant was then loaded onto a 1.5 mL nickel-nitriloacetic acid (Ni-NTA) column (Qiagen) that was previously equilibrated with Resuspension Buffer B (0.05 M HEPES, pH 7.9, 0.3 M NaCl), rendering the column orange-pink. Several washing steps, with the first being Resuspension Buffer B, then removed contaminant proteins until the absorbance at 280 nm was 0.001 (Mircodrop 2000). The second wash was Elution Buffer 1 (0.05 M HEPES, pH 7.9, 0.3 M NaCl, 0.02 M Imidazole) and was carried out until the absorbance at 280 nm was 0.001. mOrange was removed from the column using Elution Buffer 2 (0.05 M HEPES, pH 7.9, 0.3 M NaCl, 0.1 M Imidazole) until no further orange-pink colour could be seen on the column.

The resultant purified mOrange then underwent a buffer exchange with 0.05 M Phosphate Buffer Saline (PBS) with 0.3 M NaCl at a pH 7.4, through the use of a centrifugation filter (Millipore, Amicon Ultra Centrifugal Filters, Ultracel 10K, 10,000 MWCO) spun at 4500 rpm (3600 X g, 15 min, 4 °C). With mOrange now suspended in PBS, the protein was concentrated using the centrifugal filters at the same speed and duration for buffer exchange. The average protein yield using the above method was 1 mg of mOrange per 200 mL culture.

2.2.3 The photobleaching of mOrange with high power LED lights

To carry out the LED photobleaching experiments, three separate 3W LEDs, Ultraviolet-(UV), Blue and Green with their maximum peak wavelengths (power) at 405 nm (64.2 mW/cm^2), 450 nm (57.3 mW/cm^2) and 515 nm (18.3 mW/cm^2), respectively, were fabricated at the University of Calgary electronics shop. To ensure no overlap between the Blue and Green LEDs, a 488 nm shortwave cut-off filter was used on the Green LED (Optosigma). The solutions

used for photobleaching contained an average of 4.0 X 10^{-6} M mOrange in PBS (pH 7.4) for a total of 1 mL in a 0.4 cm width by 1 cm path length quartz cuvette (International Crystal Laboratories). Additionally, the cuvettes were placed at 1.3 cm from the centre of the cuvette to the front of the LED to ensure consistent irradiation. The experiments were followed by absorbance spectroscopy using a Varian Cary 50 single beam spectrophotometer and fluorescence spectroscopy with a Photon Technology International (PTI) Quanta Master 40 fluorimeter in CW mode with 2 nm slit-widths unless specified otherwise, and spectra were recorded at the time points of 0, 1, 2, 3, 5, 7, 10, 15, 20, 30, 40, 60, 90, 120, 180 and 240 minutes. Finally the power of the LEDs was measured using a Thorlabs PM100D meter with S120C photodiode power sensor at 1.3 cm from the front of the LED and the spectral profiles of each LED was determined using a Horiba FluoroMax-3 steady state spectrofluorimeter.

2.2.4 LASER light and mOrange

Using the same concentration of mOrange as the solutions used for the LED irradiations, mOrange was also irradiated using a Opotek Inc. Vibrant 355 tunable NIR-Vis pulsed laser (10 Hz). Using a Thorlabs PM100D meter with ES220C pyroelectric energy sensor, the power of the laser at each wavelength (497, 532, 548 and 560 nm) was measure for 100 shots before and after each photobleaching experiment. To ensure even exposure to the LASER, the solutions were continuously stirred during irradiation. Again, the experiments were followed by absorption and fluorescence spectroscopy, with the spectra being taken at intervals of 50 LASER shots.

2.2.5 Heat and mOrange

Using 3 mL solutions of mOrange (approximately 4.0 X 10^{-6} M) in a 1 cm X 1 cm sealed quartz cuvette (International Crystal Laboratories), the protein solutions were heated in the peltier temperature controlled cuvette holders of the Cary 50 absorbance spectrophotometer and

the PTI Quanta Master fluorimeter. Additionally, photobleaching experiments were carried out at 82 °C using a Cary dual cell peltier accessory temperature controlled cuvette holder, mounted in front of the Opotek Inc. Vibrant 355 LASER.

2.2.6 Data Analysis

For graphical analysis, KaleidaGraph 4.1 software was used to plot the data obtained from the absorbance and fluorescence spectrophotometers. Additionally, this software was used to fit the maxima of the growth and decay kinetics. For the absorbance maxima, the data were normalized, while for the fluorescence maxima the data were corrected for the inner filter effect following the procedure outline by Fery-Forgues *et al.*[62] and then normalized. For data analysis, a first order decay was fitted using the following equation:

$$y = Ae^{(-kx)}, \text{ Eq 2.1}$$

where A is a constant relating to the proportion of protein undergoing decay, and k is the rate constant for the decay. For a bi-exponential decay, the following equation was used:

$$y = Ae^{(-k_1 x)} + Be^{(-k_2 x)}, \text{ Eq 2.2a}$$

where A and B are constants relating to the proportion of protein undergoing decay by process 1 and 2, and k_1 and k_2 are the rate constants for the decays. Additionally, for a bi-exponential growth, the following equation was used to model the data:

$$y = A - Ae^{(-k_1 x)} + B - Be^{(-k_2 x)} \text{ . Eq 2.2b}$$

Peak deconvolution data were obtained by using the Origin 8.5 software.

2.3 Results

The first step in understanding the mechanisms of photobleaching was to obtain highly purified mOrange. Unfortunately, one of the issues related to variants of DsRed has been their

maturation and folding efficiencies.[25,27] Therefore, it was necessary to examine the methods of protein maturation, in order to ensure efficient production of mOrange.

2.3.1 Process of mOrange maturation

According to the work of Shaner *et al.*,[25] upon proper expression of mOrange the absorption maxima relating to the fully matured protein will be located at 548 nm, and should have an absorption spectra that matches that seen in figure 2.2A. In this spectrum, the main absorption peak seen between 475 nm and 575 nm relates to the mature mOrange protein, with a shoulder seen at 515 nm.[63] Achieving this mOrange spectrum is reliant upon the proper expression of the protein from the *E. coli.* host organism. Thus, in order to obtain expression of mOrange from the *E. coli.*, a well-established procedure for optimal expression of fluorescent proteins that requires lower temperatures to allow efficient folding of the proteins, was implemented.[6,10,60] This procedure relies on achieving lower than room temperatures (20 °C) for protein folding since it is known that higher temperatures tend to impede GFP folding.[10] Therefore, given that DsRed is a homologue of GFP,[64] and mOrange is a variant of DsRed, the use of this established procedure was logical.

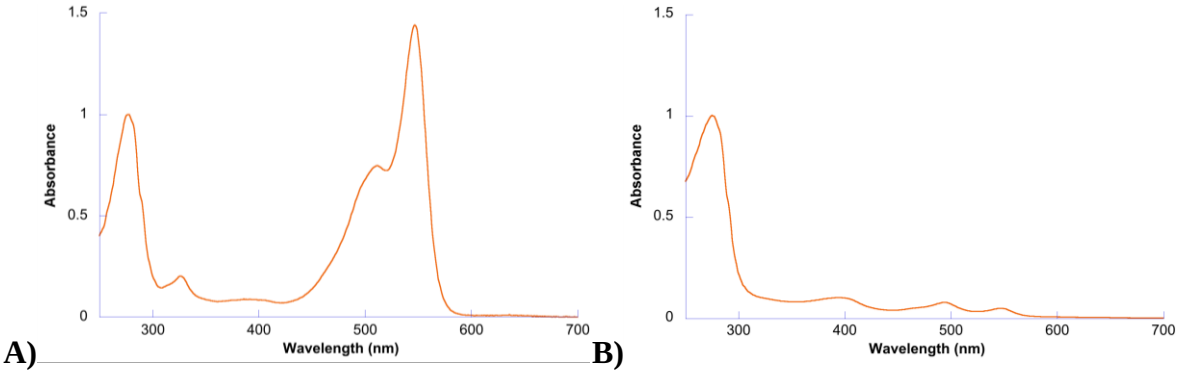

Figure 2.2: The comparison of the normalized absorbance of A) fully matured mOrange (3.51×10^{-6} M) with B) the immature version of mOrange grown 20 °C with L-(+)-arabinose (0.004 mg/mL), with the small peaks at ~400, 490 and 550 nm suggesting the presence of very dilute mature mOrange.

However, as seen in figure 2.2B, upon purification of the mOrange protein under this procedure, only a very small trace of the known mOrange peaks was visible, suggesting that the conditions for protein maturation were insufficient. Support for this is derived from the method of purification, where the use of a polyhistidine tag that was incorporated onto the mOrange, enables efficient purification using Ni^{2+}-nitrilotriacetic acid affinity chromatography columns (Ni^{2+} NTA columns).[65] Assuming that no other proteins within *E. coli.* contain the high affinity polyhistidine tag, the use of the Ni^{2+} NTA columns ensures the protein retrieved from the columns is primarily the desired mOrange (appendix B). Thus, given that figure 2.2B represents the absorption spectrum of the mOrange protein obtained from the purification process, the large tryptophan and tyrosine protein peak located at 277 nm suggests[66] the presence of unfolded, immature mOrange.

In order to rectify this issue, the procedure was modified by altering the amount of L-(+)-arabinose (protein expression initiator) and the temperature of incubation, with the resultant purified proteins examined for the presence of mOrange. The first variable examined was the amount of L-(+)-arabinose added, with the extraction and purification steps being performed at 4 °C immediately after the 24 hour folding time to ensure as little uncontrolled influence on protein folding as possible. As can be seen from figure 2.3A, little change was seen in the absorbance spectra of mOrange as the amount of L-(+)-arabinose was increased from 0.002 to 0.006 mg/mL. In fact, there appears to be a slight increase at ~490 nm with 0.002 mg/mL of L-(+)-arabinose, yet given that the maximum absorbance of mOrange is at 548 nm, this suggests that changing the concentration of L-(+)-arabinose is not the cause of the unfolded protein.

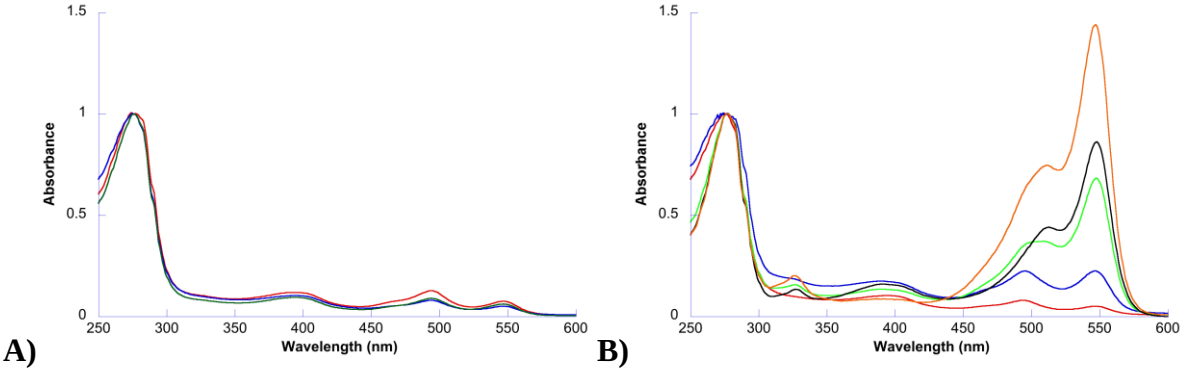

Figure 2.3: A) The absorbance of the immature version of mOrange grown 20 °C with varying L-(+)-arabinose concentrations (0.002, 0.004 and 0.006 mg/mL for the red, blue and green traces respectively). B) The comparison of the maturation of mOrange grown at 20 °C (red trace), 25 °C (blue trace), 30 °C (green trace), 35 °C (black trace), or 37 °C (orange trace), with L-(+)-arabinose (0.004 mg/mL).

The second variable examined was the change in temperature of incubation, which was increased from 20 °C to 37 °C. Again, the extraction and purification steps were performed at 4 °C immediately after the 24 hour folding time, ensuring as little uncontrolled influence on protein maturation as possible. Upon inspection of figure 2.3B, it can be clearly seen that as the temperature was increased to 37 °C, the presence of the desired mOrange peak increased. Although this need for higher temperatures is counter intuitive for variants of GFP[10], this could be explained through the mOrange chromophore maturation process as outlined in figure 2.4A. The process of chromophore maturation requires several steps to achieve the final matured chromophore (compound **9 Or**), to which it can be theorized that higher temperatures provide the needed energy to allow these steps to occur at faster rates. Concurrently, considering that the folding of fluorescent proteins is autocatalytic, requiring no external cofactors other than oxygen to achieve the final matured version,[10] this theory of the needed higher temperatures for proper mOrange folding, suggests that protein grown at 20 °C should be able to fold if sufficient energy were applied. Thus, mOrange was grown again at 20 °C, extracted, purified, and then incubated

in PBS at 37 °C for a further 16 hours while monitored using UV-vis absorption spectroscopy. As can be seen from the results in figure 2.5, the growth of the mOrange peak is clearly seen over the 16 hours, suggesting that indeed, the increased temperature provided the energy necessary to allow efficient protein folding.

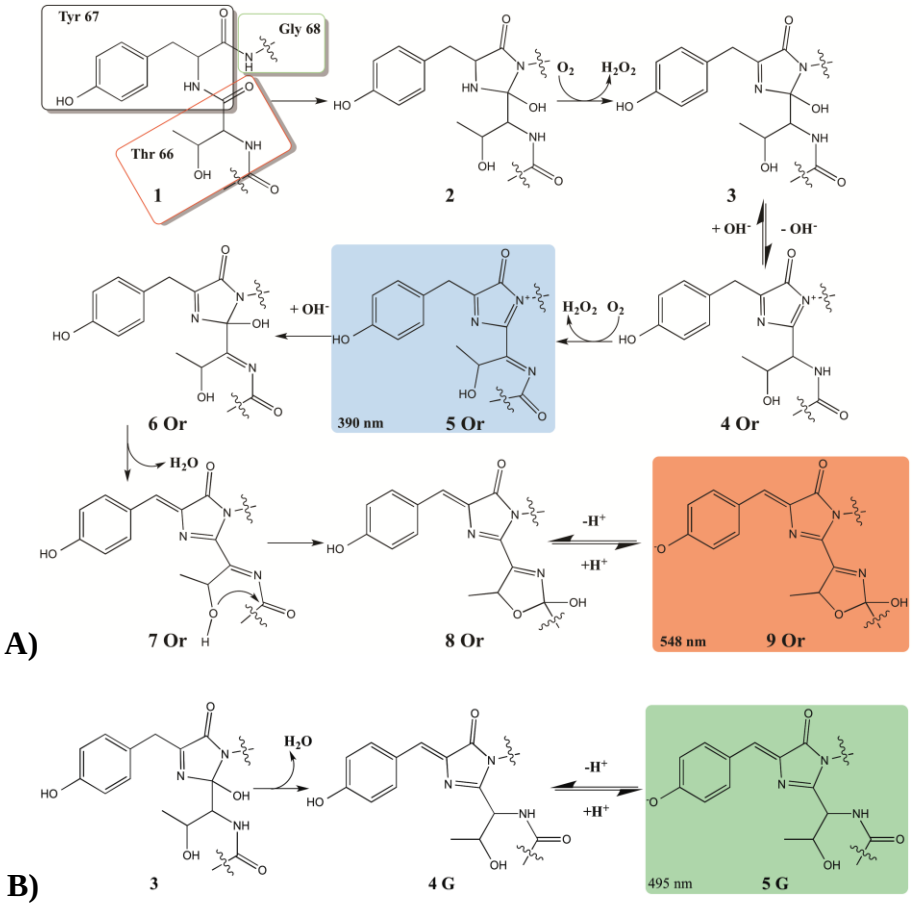

Figure 2.4: The branched maturation process of mOrange, adapted from Strack *et al.*[67] A) The path to the fully matured mOrange chromophore, starting with the three amino acids: Tyrosine (Tyr 67), Glycine (Gly 68) and Threonine (Thr 66). The branching point for this maturation process occurs at compound 3, where the protein can either produce the green immature (compound 5 G) or mature mOrange chromophores (compound 9 Or). B) The branched pathway to the green immature mOrange chromophore.

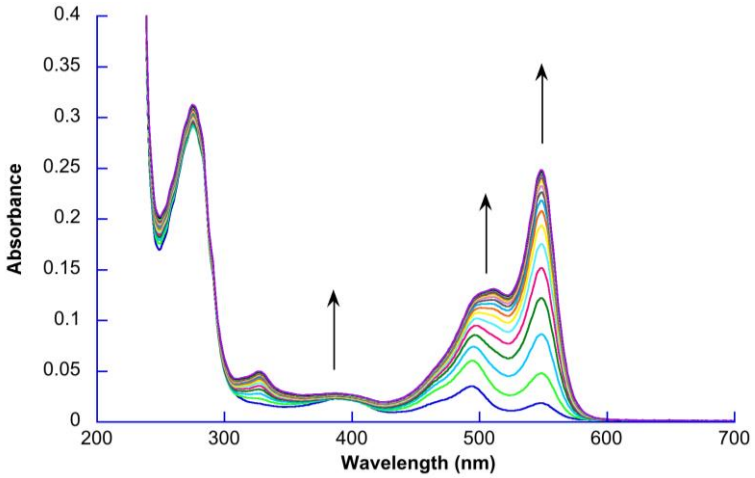

Figure 2.5: The absorbance of the of mOrange grown 20 °C with L-(+)-arabinose (0.004 mg/mL), then incubated at 37 °C for an additional 16 hours. The arrows indicate the direction of change.

Having established the conditions needed for proper protein production, it was necessary to identify the changes in absorbance seen during the maturation trials in order obtain a fundamental understanding of the constituents within the purified protein. This is a requirement for a complete understanding of the photobleaching dynamics of mOrange. Therefore, with a closer look at the proposed maturation process of mOrange, it can be seen from figure 2.6A that there are three different absorbing species present for the immature mOrange: blue (390 nm), green (495 nm), and orange (548 nm). Strack *et al.* suggested these three types of species for the maturation of DsRed (and its variants) could be used as identifiers for the progression of maturation.[67] Where the blue species was considered to be an intermediate on the pathway to forming the mature chromophore, although it is a non-fluorescent species. Conversely, the green absorbing species herein referred to as the 'green immature mOrange', is the result of a separate maturation pathway (figure 2.4B) that once formed, cannot convert to the desired matured mOrange protein and fluoresces in the green.[67] Given that two of the three absorbing species are

fluorescent, it is possible to identify the observed absorbing species seen in the spectrum of mOrange.

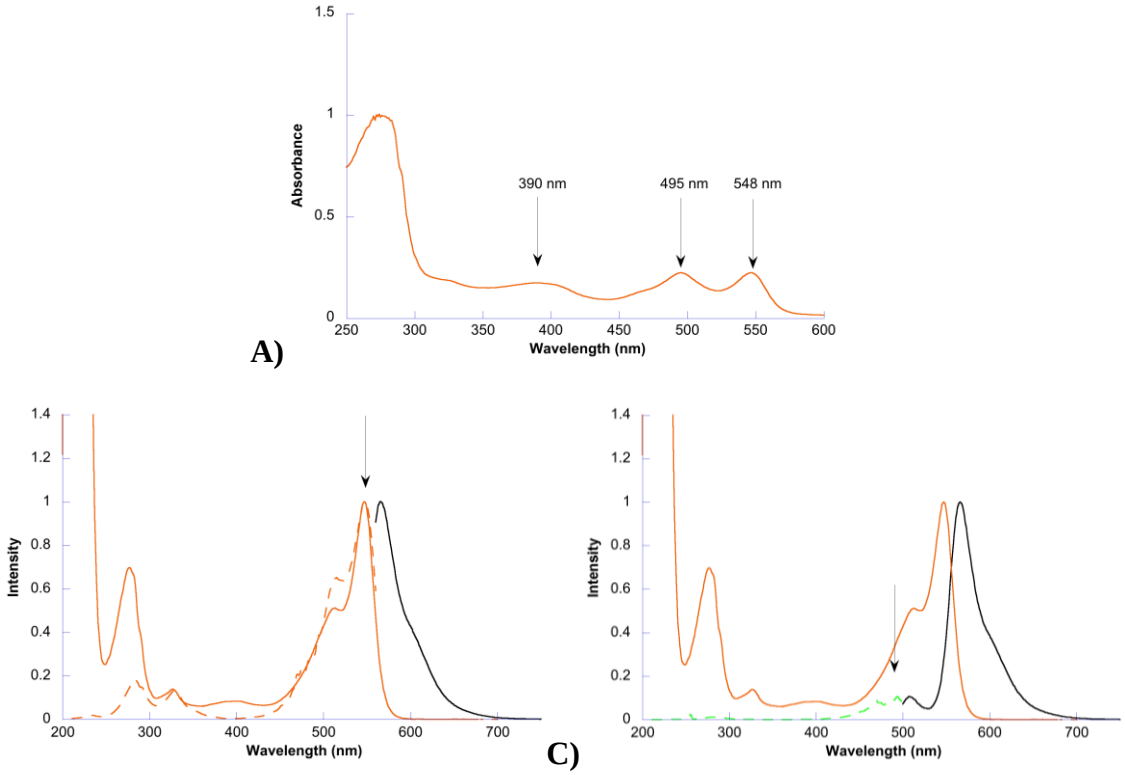

Figure 2.6: A) The absorbance of the immature version of mOrange grown 25 °C with L-(+)-arabinose (0.004 mg/mL). The arrows indicate the presence of the blue (390 nm), green (495 nm) and orange (548 nm) chromophore peaks. B) The fluorescence of a solution of mOrange to determine the presence of the mature mOrange. Where the absorbance spectrum of optimized mOrange is the orange solid line, the excitation spectrum of mOrange for emission at 562 nm is the orange dashed line, and the emission spectrum of mOrange when excited at 548 nm is the black solid line. C) The absorbance spectrum of optimized mOrange (orange solid line), the excitation spectrum of mOrange for emission at 510 nm (green dashed line) and the emission spectrum (black solid line) of mOrange when excited at 490 nm to investigate the presence of the green immature mOrange. The arrows represent the positions of excitation.

The identification of these species is achieved through the use of fluorescence spectroscopy and the results are shown in figure 2.6B and C. Considering the maximum absorbance for the mature mOrange is at 548 nm, when excited at this wavelength, this should

produce the desired orange fluorescence at 562 nm.[25] From figure 2.6B, when excited at 548 nm, the fluorescence of mOrange (black solid line) appears with its maxima at 562 nm. Performing an excitation scan, where the emission at 562 nm is monitored while the wavelength of excitation is scanned from 200 to 560 nm, the image of the absorbance peak for mOrange is observed. This suggests that the maximum wavelength needed to achieve the desired 562 nm fluorescence is 548 nm, confirming that the mature mOrange peak is indeed present in solution and is fluorescent. This excitation spectrum also indicates that the peak seen at 390 nm in figure 2.6A does not contribute to the orange fluorescence.

Repeating this experiment for the presence of the green immature mOrange, a solution of mOrange was monitored for green fluorescence. This solution was excited 495 nm since this is proposed to be the maximum of absorbance as seen from figure 2.6A. The results (figure 2.6C) suggest that there is both green and orange fluorescence. The presence of the green fluorescence with its maximum intensity at 507 nm suggests that indeed the green immature mOrange was present in solution. Again, the excitation spectrum (green dashed line) suggests the main peak needed to produce the green fluorescence is located at 495 nm, confirming the presence of the green immature mOrange. Additionally, with no peak seen at 390 nm in the excitation spectrum, the green fluorescence does not originate from the observed 390 nm peak. The fact that the orange fluorescence is seen when excited at 495 nm can be explain by the fact that both the green immature and mature mOrange overlap at 495 nm, this fact will be explained in more depth later in this chapter.

The third species to identify was the blue intermediate species at 390 nm (figure 2.6A). Support for the presence of the blue intermediate species was the excitation at 390 nm for both experiments shown in figure 2.6B and C, resulting in no observed fluorescence. Given that the

blue intermediate is known to be non-fluorescent,[67] the lack of fluorescence when excited implicates the 390 nm peak to be the blue intermediate species. Confirming this was the lack of 390 nm peaks present within the excitation spectra of figure 2.6B and C, where if the peak at 390 nm was contributing to either the observed green or orange fluorescence, known to come from the green immature or mature mOrange respectively, then by process of elimination the third peak must be the blue intermediate species.

Having identified the three main species in solution, by following the changes in absorbance intensity the progression of maturation can be followed. As suggested by Stack *et al.* and Moore *et al.*, a ramification of the branched maturation process is that the absorbance of the blue intermediate species should decreases as the presence of the matured DsRed variant increases.[67-69] In the case of mOrange, this is clearly seen in figure 2.7, as the ratio of 390 nm to 548 nm is plotted as a function of temperature. Where at 20 °C, the ratio is over 2, suggesting a prevalence of the blue intermediate species, while at 37 °C, the ratio is about 0.06, indicating most of the blue species has been converted into the mature mOrange protein. This conversion of the blue intermediate species is supported in literature, where in the work of Moore *et al.* mPlum, a DsRed variant, had its mature chromophore appear as the blue intermediate species disappeared.[68] Thus, this result supports the branched maturation mechanism for the chromophore formation.

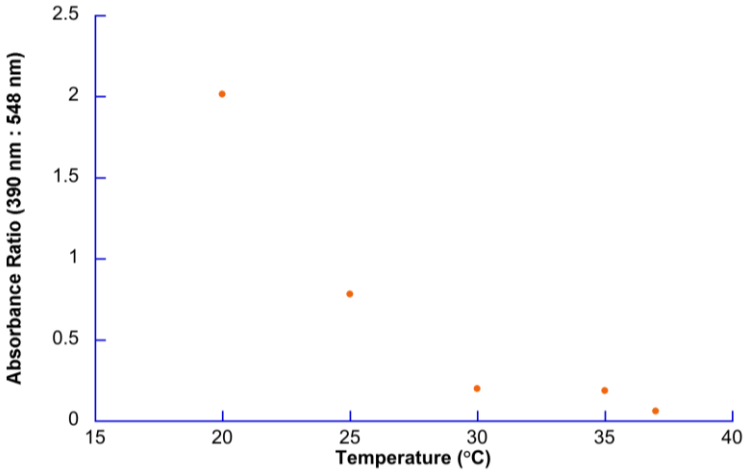

Figure 2.7: The ratio of absorbance of the blue intermediate species (390 nm) over the absorbance of mature mOrange (548 nm) as the folding temperature is increased from 20 °C to 37 °C, with L-(+)-arabinose (0.004 mg/mL).

With this support for the branched mechanism, another ramifications of this chromophore formation pathway is that any maturing protein undergoing the "green branch" of the pathway (figure 2.4B) should persist as a green immature within a solution of mOrange.[63] In fact, this was shown in figure 2.6C where supposedly mature mOrange displayed green fluorescence. Again this is well supported within the literature where Moore *et al*. proposed that contributing to the peak seen at 390 nm was the protonated form of the green immature DsRed variants, while Shu *et al*. found the presence of the anionic green immature mOrange in their crystal structure of mOrange.[24,68] Unfortunately, given that the difference between the mature mOrange and the green immature mOrange proteins is a matter of folding, it is nearly impossible to separate the proteins within a solution. This indicates that if any green immature mOrange is created, it may have an effect on the dynamics of photobleaching, as this will be a second absorbing species. Therefore, this green immature mOrange protein must be considered when trying to elucidate the mechanism of photobleaching.

2.3.2 Interaction of mOrange with high power LED lights

Establishing the methods of protein maturation provided the ability to produce the mature and highly pure protein necessary to carry out the photobleaching experiments. Yet before performing the experiments, it was necessary to examine the light sources available for spectral distribution and power. As seen before, there is the possibility of at least three separate absorbing species existing in a solution of purified mOrange. Thus the use of high power LEDs will enable the separation of the excitation wavelengths used in the photobleaching experiments to minimize multiple chromophore excitations. This is due to the narrow spectral distribution of LEDs,[70] allowing portions of the mOrange spectrum to be excited at separate intervals, enabling the effects of light on photobleaching at different wavelengths to be understood. The three LEDs chosen for the experiments were a UV LED with a maximum power intensity at 406nm, a Blue LED with a maximum power intensity at 447 nm, and a Green LED with its maximum intensity at 513 nm. The spectral distribution and power output of the LEDs is shown in figure 2.8A while the overlap between the LEDs and mOrange is shown in 2.8B, displaying the portion of the protein which will be excited with each LED.

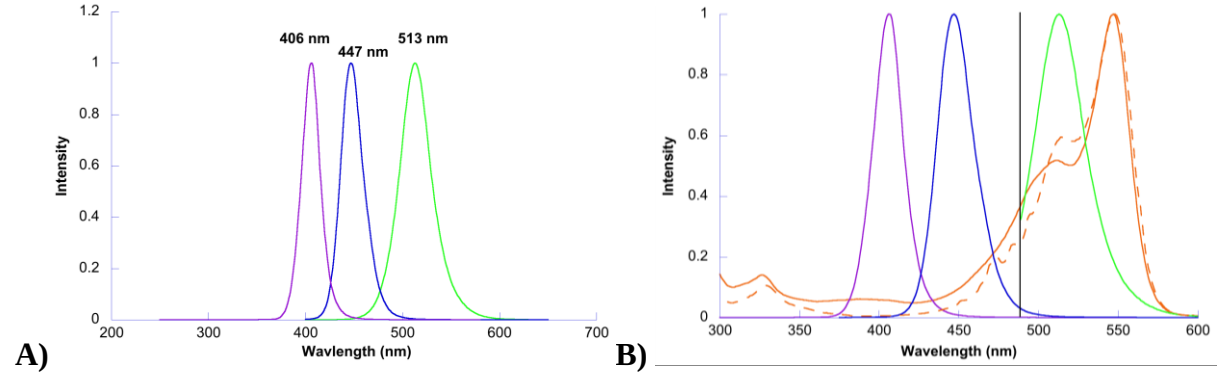

A) B)

Figure 2.8: A) The spectra of the available LED lights, where the powers of the lamps are 64.2, 57.3 and 18.3 mW/cm^2 for the UV, Blue (measured with a 380 nm shortwave cut off filter) and Green (measured with a 488 nm shortwave cut off filter) respectively. The value above each peak represents the maximum wavelength for each LED. B) The spectral overlap of mOrange where the absorbance is the orange solid line and the excitation spectrum for 562 nm emission is the orange dashed line, with the LED lights. To prevent the green light from exciting other portions of the protein, a 488 nm shortwave cut off filter was used to ensure mOrange chromophore excitation (represented by a black line). For each graph, the UV, Blue and Green LEDs are represented by their respective colour traces.

With the profile of each LED and their overlap with mOrange determined, spectroscopic analysis of the proteins absorbance and fluorescence stands as the most robust, versatile, and readily available methods to best assess the mechanisms of photobleaching.

2.3.2.1 Ultra Violet LED light

The first of the LEDs to be used in determining the photobleaching characteristics of mOrange, was the UV LED. This is because the spectral overlap between the UV LED and mOrange (figure 2.8B) is only between 372 nm and 450 nm, and with essentially no overlap with the mature excitation spectra, it can be assumed that the mature mOrange will not be excited. Thus, any loss in fluorescence or absorbance cannot be contributed to deactivation by excited chromophore of mOrange. To follow any resulting the loss from irradiation, the parameters that

will be examined to determine the photobleaching rates of mOrange come from Beer Lambert's law:

$$A = \varepsilon cl, \text{ Eq 2.3}$$

where A is the absorbance measured at a certain wavelength, ε is the extinction coefficient of an absorbing species ($M^{-1}cm^{-1}$) at a certain wavelength and l is the path length of the cell (cm). Thus, Beer Lambert's law indicates that the absorbance of a species in solution is proportional to its concentration. Given the reported extinction coefficient of mOrange is 71000 $M^{-1}cm^{-1}$ at 548 nm,[27] following the decay of the 548 nm peak should indicate the amount of mOrange undergoing photobleaching after a given amount of irradiation. Concurrently, as viable fluorescent mOrange proteins are photobleached, the fluorescence (λ_{Max} = 562 nm)[27] should decrease as well, allowing a second parameter to determine photobleaching rate.

Using these parameters as a guideline, the absorption and fluorescence of mOrange were followed to determine how they decayed due to the interaction of UV light as a function of time. From the results in figure 2.9A and 2.9B, it can be seen that for both the absorbance and fluorescence, there appears to be a steady decrease seen at the 548 nm and 565 nm respective maxima. Interestingly, when mOrange was excited at 548 nm, the fluorescence maximum is red shifted to 565 nm from the expected 562 nm. However, as mOrange is photobleached in the presence of the UV LED, there is an apparent blue shift in the fluorescence maxima to the expected 562 nm. This red shift from 562 nm can be explained based on the inner filter effect, where at higher concentrations, reabsorption of the emitted fluorescence can occur due to mOrange's absorption in the 550 nm – 570 nm region. Conversely at low concentrations, less reabsorption will occur at 562 nm allowing more of the fluorescence to be observed at this wavelength.[62] According to Fery-Forgues *et al.*, at absorption values of less than 0.05, the inner

filter effect will be negligible.[62] Therefore to confirm the present of the inner filter effect, a successive dilution of mOrange was performed and its fluorescence was monitored, with the maxima of mOrange blue shifting from 565 nm to 562 nm at absorbance values of less than 0.1 (data in appendix B).

One characteristic that has been well documented within the literature has been the permanency of photobleaching for FPs.[8,32,71-73] Essentially once bleached, the FPs should not regain their original absorption and fluorescent intensity. Thus, the solution that as irradiated with UV LED was left overnight without irradiation and no change was observed in absorption or fluorescence spectra, confirming the irreversibility of photobleaching.

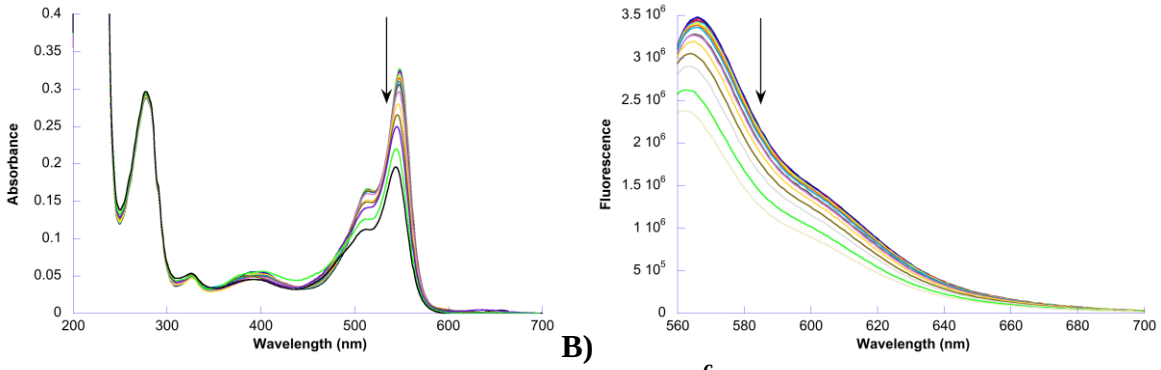

Figure 2.9: A) The absorbance of mOrange (4.61 X 10^{-6} M) while exposed to the UV LED (406 nm maximum) for 4 hours. B) The fluorescence of mOrange (4.61 X 10^{-6} M) while exposed to the UV LED (406 nm maximum) for 4 hours. The arrow indicates the direction of change.

With the decrease seen for both the absorbance and fluorescence spectra of figure 2.9, the manner in which mOrange is decaying is still not apparent. Thus the maxima for the absorbance and fluorescence were plotted as a function of time to determine if any trend in decay could be elucidated (figure 2.10). The data were relatively well fitted with a first order decay for both absorbance and fluorescence. This suggests that mOrange is interacting with the UV light in a

mOrange concentration dependent manner, where the interaction is leading to a unimolecular photobleaching process for mOrange.

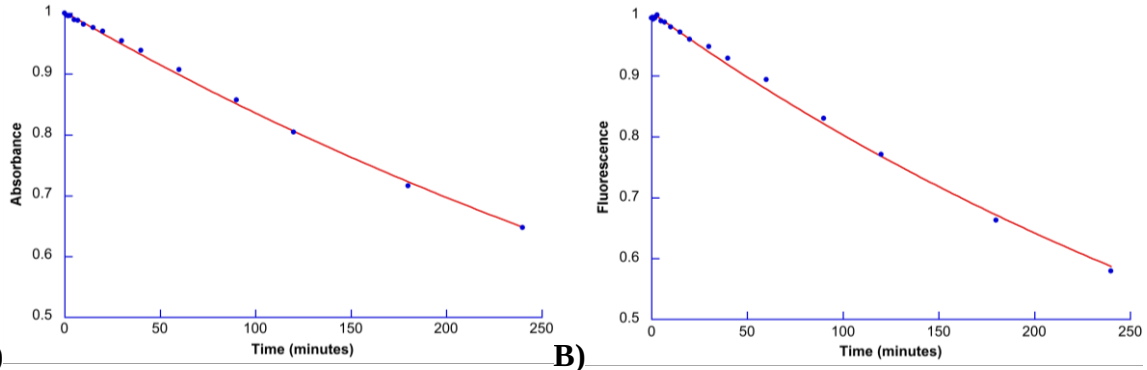

A) **B)**

Figure 2.10: The normalized absorbance of mOrange (4.61 X 10^{-6} M) at 548 nm while exposed to the UV LED (406 nm maximum) for 4 hours. B) The normalized and corrected fluorescence of mOrange (4.61 X 10^{-6} M) at 565 nm while exposed to the UV LED (406 nm maximum) for 4 hours. These experiments were performed once. The data was fitted with equation 2.1. The analysis of the data can be found in appendix A.

Specifically, this first order decay interaction can be thought of as the reaction scheme between light and mOrange:

$$[mO] + h\nu \xrightarrow{k_1} [mO]^*, \text{ Scheme 2.1}$$

where $[mO]$ is the concentration of mOrange, $h\nu$ is light, $[mO]^*$ is the concentration of photobleached mOrange, and k_1 is the forward rate constants for the reaction. Considering that $h\nu$ will be in excess due to the continuous and abundant LED source, the only species changing within solution will be the mOrange.[38] Thus the rate for mOrange disappearance can be represented as:

$$\frac{d[mO]_t}{dt} = -k[mO], \text{ Eq 2.4}$$

with $[mO]_t$ being the concentration of mOrange at time t, and k being the rate constant for the photobleaching process. The expression can be rearranged to achieve the integral:

$$\int \frac{d[mO]_t}{[mO]} = -\int kdt$$

Which is then integrated to give:

$$\ln[mO]_t = -kt + C.$$

To determine the constant C, the time (*t*) is set to 0 resulting in:

$$\ln[mO]_0 = C.$$

This constant can now be substituted in and the expression rearranged to give:

$$[mO]_t = [mO]_0 e^{-kT}. \text{ Eq 2.5}$$

Based on this rate constant for mOrange, it can be seen that the photobleaching of mOrange follows a unimolecular pathways that depends on its initial concentration, and the length of time it is irradiated.

Since it has been established that the irradiation of mOrange with the UV LED does not excite the mOrange chromophore, the loss of the 548 nm peak cannot be contributed to the established pathways of deactivation for fluorescent proteins (ex: chromophore protonation or *cis-trans* isomerization). Therefore there must be some other mechanism responsible for the decay seen. One possible explanation comes from the use of UV and Blue light that has been shown to interact with the β-barrel of fluorescent proteins resulting in enhanced structural flexibility.[13] Knowing that the mFruit FPs have an already flexible β-barrel,[36,74,75] it is possible that the UV light is interacting with the barrel of mOrange causing it to denature. Denaturation would lead to a dramatic change in the environment of mOrange's chromophore, resulting in the loss of absorbance and fluorescence seen, which is well supported in the literature[10,76-78]. Additionally, this process would be a unimolecular process since it is only dependent on the β-barrel of mOrange interacting with light. Thus, it is reasonable to conclude that the use of UV

light will result in the denaturation of the β-barrel of mOrange, ultimately leading to lower overall absorbance and fluorescence.

2.3.2.2 Blue LED light

With the fact that UV light does not excite mOrange's chromophore, the next step was to study the effects of Blue light on mOrange. From figure 2.8B, there appears to be a minimal overlap of the Blue LED with mOrange's chromophore from 450 nm to 470 nm. This would suggest that the Blue LED has the capability to interact with mOrange's chromophore. Therefore, carrying out the same experiments as in the previous section, it is possible to follow the photobleaching of mOrange and compare the effects of the two light sources. As depicted in figure 2.11, it can be seen that similar results were obtained as compared to the UV light (figure 2.9) where a decrease was seen in the absorbance (figure 2.11A) and fluorescence (figure 2.11B). Additionally, the decrease seen was less than that of the UV light, but this can be rationalized based on the power difference of the two LEDs, where the UV LED (64.2 mW/cm^2) is more powerful than the Blue LED (57.3 mW/cm^2).

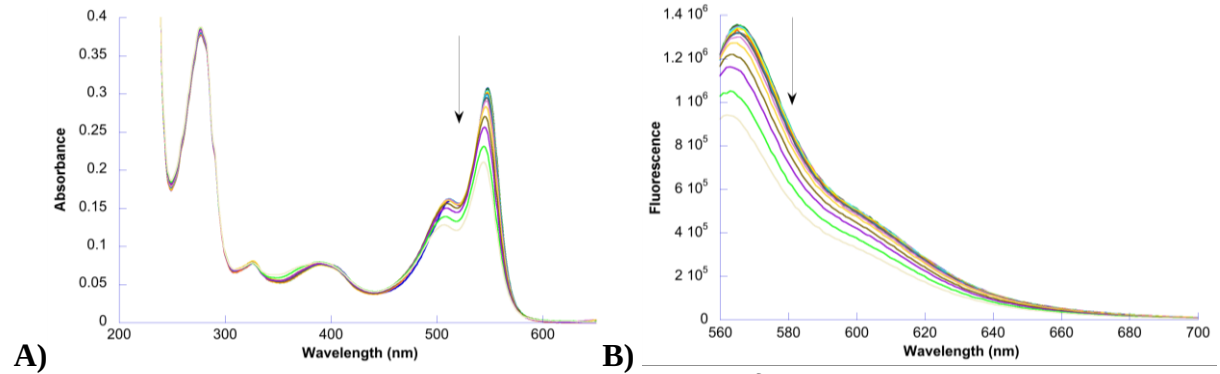

Figure 2.11: A) The absorbance of mOrange (4.34 X 10^{-6} M) while exposed to the Blue LED (447 nm maximum) for 4 hours. B) The fluorescence of mOrange (4.34 X 10^{-6} M) while exposed to the Blue LED (447 nm maximum) for 4 hours. The arrow indicates the direction of change.

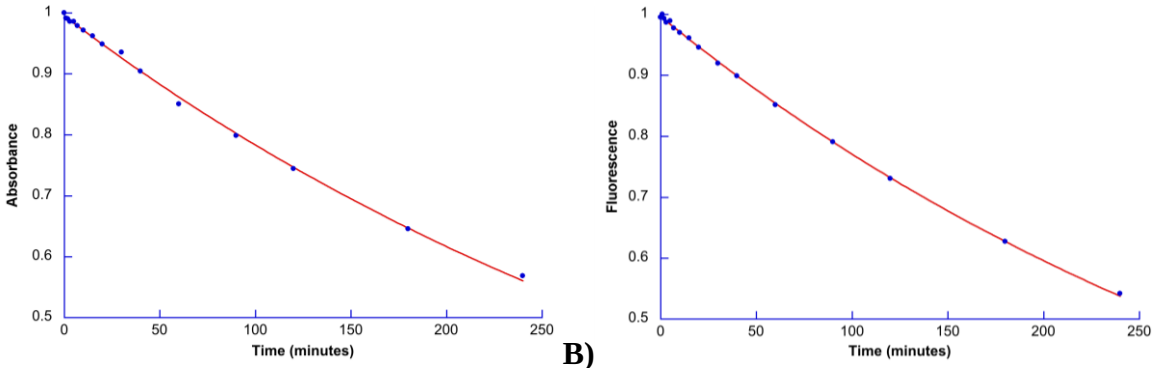

A) **B)**

Figure 2.12: A) The normalized absorbance of mOrange (4.34 X 10^{-6} M) at 548 nm while exposed to the Blue LED (447 nm maximum) for 4 hours. B) The normalized and corrected fluorescence of mOrange (4.34 X 10^{-6} M) at 565 nm while exposed to the Blue LED (447 nm maximum) for 4 hours. These experiments were performed once. The data were fitted with equation 2.1. The analysis of the data can be found in appendix A.

To better compare the results between the Blue and UV LEDs, the maxima for the absorbance and fluorescence were plotted as a function of time and fitted to first order decays (figure 2.12). As seen in table 2.1, the rate constants obtained with the Blue and UV light sources are very similar, suggesting that there is little effect from the small overlap of the Blue LED with the absorbance of the mOrange's chromophore. This indicates that the Blue light may be interacting with mOrange in a similar manner to that of the UV. Given the spectral distribution of the Blue light overlaps with that of the UV light, (figure 2.8B), this is not unimaginable. However, before this conclusion could be drawn, it is was necessary to examine the interaction of light with the chromophore of mOrange alone and compare the effects seen.

Table 2.1: The values of the first order decay rates as determined through the analysis of the maximum absorbance at 548 nm and fluorescence at 565 nm of mOrange during photobleaching with the indicated LEDs. Based on the use of equation 2.1.

LED of Irradiation	A	k_1 (min^{-1}) Absorbance	A	k_1 (min^{-1}) Fluorescence
Blue	1.002 (±0.002)	0.00182 (±0.00002)	1.005 (±0.003)	0.00224 (±0.00004)
UV	0.995 (±0.002)	0.00239 (±0.00003)	0.997 (±0.001)	0.00257 (±0.00016)

2.3.2.3 Green LED light

With the examination of the effects of both UV and Blue light on mOrange, the next logical step was to determine the effects of Green light on mOrange and understand how the excitation of the mature chromophore leads to its photobleaching. As a note, to ensure that only the mature mOrange was excited, a 488 nm shortwave cutoff filter was used to prevent light with wavelengths shorter that 488 nm from interacting with mOrange. From the results (figure 2.13) it is immediately clear that the excitation of mOrange due to Green light has dramatically different results than that of either UV or Blue light. First of all, the decrease seen in the absorbance (figure 2.13A) and fluorescence (figure 2.13B) for the mature mOrange peak is significantly larger than that of either the Blue or UV LEDs even though the power of the Green LED light is about three times less than either the Blue or UV LED. Looking at figure 2.13, the most noticeable difference with the use of the Green LEDs, is that there appears to be the growth of a second peak at about 410 nm in the absorbance spectrum, red-shifted from the blue intermediate species peak at 390 nm. The appearance of this peak and the presence of an isobestic point at 467 nm suggests the production of an absorbing by-product.

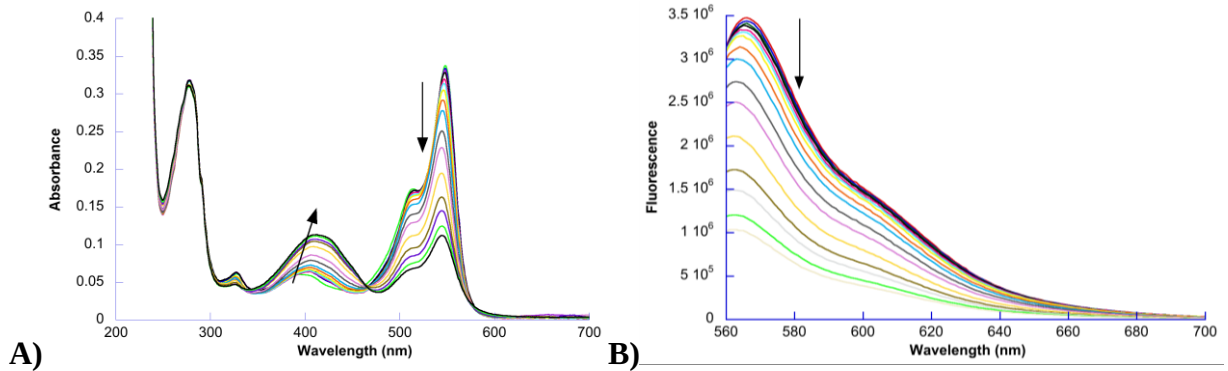

Figure 2.13: A) The absorbance of mOrange (4.72 X 10^{-6} M) while exposed to the Green LED (513 nm maximum) for 4 hours. B) The fluorescence of mOrange (4.72 X 10^{-6} M) while exposed to the Green LED (513 nm maximum) for 4 hours. The arrows indicate the direction of change.

As suggested in the literature for GFP, the appearance of a blue shifted peak was due to the photochemically induced protonation of GFP's chromophore.[9,45,79] Given the similarity between the chromophores of GFP and mOrange,[24] it is not unimaginable that mOrange could undergo a photochemical protonation of its chromophore. Thus in order to test this hypothesis, mOrange was photobleached again, and then small volumes of NaOH were added to the solution to determine if the by-product was indeed a protonated version of mOrange. From the results in figure 2.14A, it is apparent that the addition of NaOH decreases the peak at 420 nm and causes an increase of the mature mOrange peak. It should be noted that the shoulder of mOrange, usually located at 515 nm, is blue shifted to 500 nm, while the main peak is blue shift from 548 nm to 543 nm (figure 2.14A). This suggests the deprotonation due to NaOH does not completely return the mOrange to its original state. However, this can be explained based on the fact that the addition of NaOH will deprotonate the amino acids immediately adjacent to the chromophore, as well as the chromophore itself, altering the stabilizing amino acids of the chromophore's environment. This increase in pH has already been shown to cause a blue shift in the absorbance of mOrange by Shu *et al.*, supporting the observed trends.[24] Given this information, it can be

assumed that the by-product is linked to the photobleaching of mOrange, suggesting photochemical protonation to be a possible mechanism of photobleaching. Importantly, it should be noted that the increase seen for the mature mOrange peak upon NaOH addition to photobleached mOrange, does not return the spectrum to its original intensity. This suggests that there exist some other pathways of photobleaching that cannot be reversed through the simple addition of NaOH.

To test if the by-product could be the result of protonation, non-irradiated mOrange was subjected to changes in pH, since it is known that mOrange is sensitive to pH (pKa = 6.5).[27] From figure 2.14C it can be readily seen that when the pH was lowered to 4 with the addition of HCl, all of the mature mOrange peak is removed, and in its stead is a peak at 406 nm resembling that of the peak seen in figure 2.14A. This supports the protonation pathway for the appearance of the by-product.

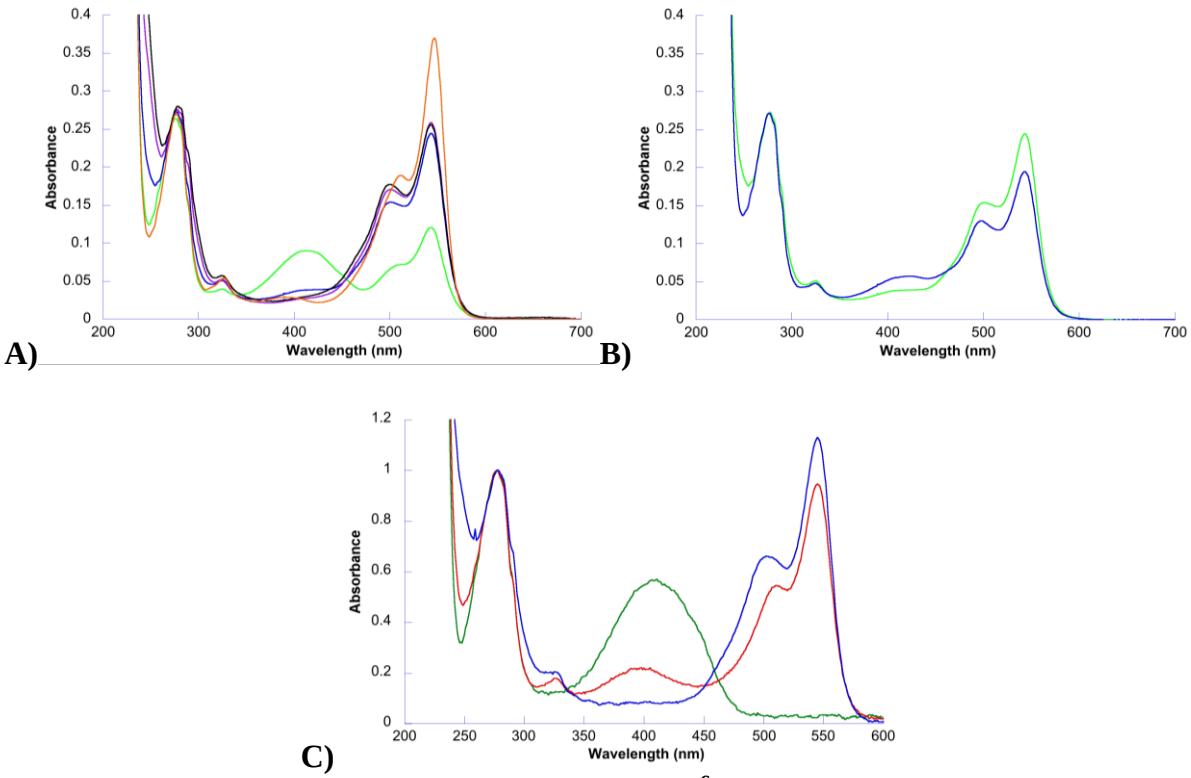

Figure 2.14: The absorbance of mOrange (5.18 X 10^{-6} M) after exposure to the Green LED (513 maximum) for 4 hours, followed by successive additions of NaOH (1 M) to increase the pH. The traces are: green (pH 7.4, 4 hours irradiation), blue (pH 8.5), purple (pH 10), black (pH 11) and orange (pH 7.4 no irradiation). B) The demonstration of the ability to reverse the deprotonation from the use of 1 M NaOH (2 µL), with the addition of 1 M HCl (2 µL) in a 1 mL total volume. The traces are: blue (pH 8) and green (pH 8.5). C) The normalized absorbance of mOrange at pH 7.4 (red trace), pH 4 (green trace), and pH 9 (blue trace). The pH data was kindly provided by Anita Ludwar.

Although the deprotonation of the by-product by NaOH and the protonation of mOrange do indicate a link between the by-product and mature mOrange, another method of determining the relationship is to look at the kinetics. By looking at the formation kinetics of the by-product, if they were to follow the same rate as that of mOrange disappearance, this will add further weight to the connection between the by-product and mOrange. However, looking back to the appearance of the by-product, there seems to be a distinct red-shift in the peak from 390 nm to 414 nm (figure 2.13A). The basic scheme of photobleaching would suggest that the appearance of the by-product, assuming that it is only one species, should have an increase in absorbance

that is not shifted. This is because if it is assumed that the mature mOrange proteins are all conserved (containing the same amino acids), for every bleaching event, the same product should be produced, as well as the consistent method in which the chromophore undergoes excitation.[80,81] Therefore, this suggests that there is an additional species present that is affecting the absorption spectra of the by-product, which could simply be contributed to the known intermediate blue species seen at 390 nm before irradiation (see figure 2.2A for the absorbance of mOrange before irradiation). Thus, by subtracting the initial spectrum from all subsequent spectra obtained after Green LED irradiation, the growth of the actual by-product can be seen, non-shifted with a maximum at 420 nm (figure 2.14A). Plotting the maxima of the by-product at 420 nm, reveals that the kinetic rate constants of appearance follows a bi-exponential growth (see table 2.2). Having determined this, the absorbance and fluorescence maxima of mOrange were examined to see if they also follow the same pattern.

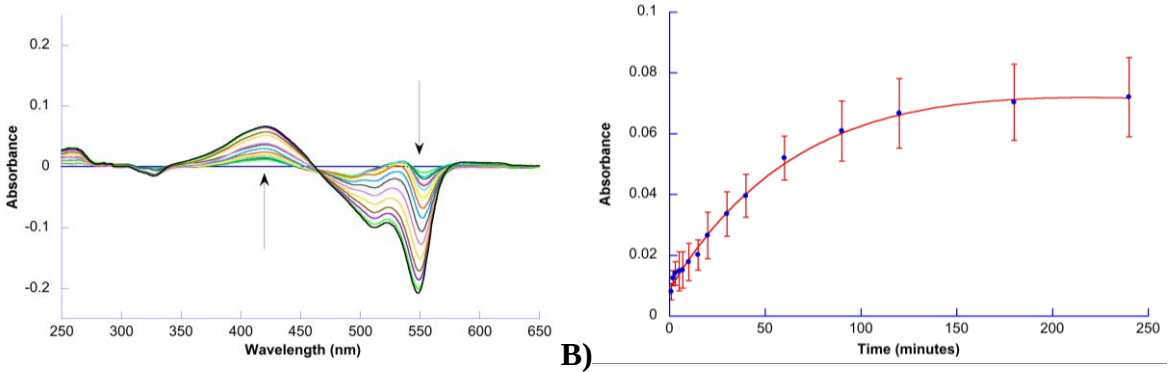

Figure 2.15: A) The absorbance of mOrange (4.53 X 10^{-6} M) with the initial spectrum (t = 0) removed to display growth and decay occurring within the absorbance spectra. The sample was exposed to the Green LED (513 nm maximum) for 4 hours. B) The absorption spectrum of mOrange at 420 nm, with the time = 0 min removed from all subsequence spectra (displays peak growth kinetics) while irradiated with a green LED for 4 hours. The data was modeled using equation 2.2a and the analysis is in appendix A.

From figure 2.15A and 2.15B, it can be seen that a bi-exponential decay were fit to both the absorbance and fluorescence, resulting in rate constants that differ by two orders of

magnitude, similar to that seen with the appearance of the by-product (see table 2.2). This similarity in magnitude difference of rate constants indicates that the appearance of the protonated by-product may be linked to the direct excitation and decay of mOrange. Confirming this link is the previously discussed NaOH addition data, suggesting that the by-product is primarily the protonated form of the mature mOrange. Thus it can be concluded that upon irradiation of mOrange with the Green LED, the chromophore undergoes a photochemical induced protonation, in a bi-exponential fashion. As mentioned in the first chapter, GFP can undergo a photochemical deprotonation known as excited state proton transfer (ESPT).[82] Given the homology to GFP, it is possible that mOrange could also undergo an excited state deprotonation from the protonated by-product. However, when the protonated by-product of mOrange was irradiated with the UV light (data in appendix B), no retrieval of the mature mOrange peak was seen. This confirms that the protonated by-product is a permanent photobleached state for mOrange.

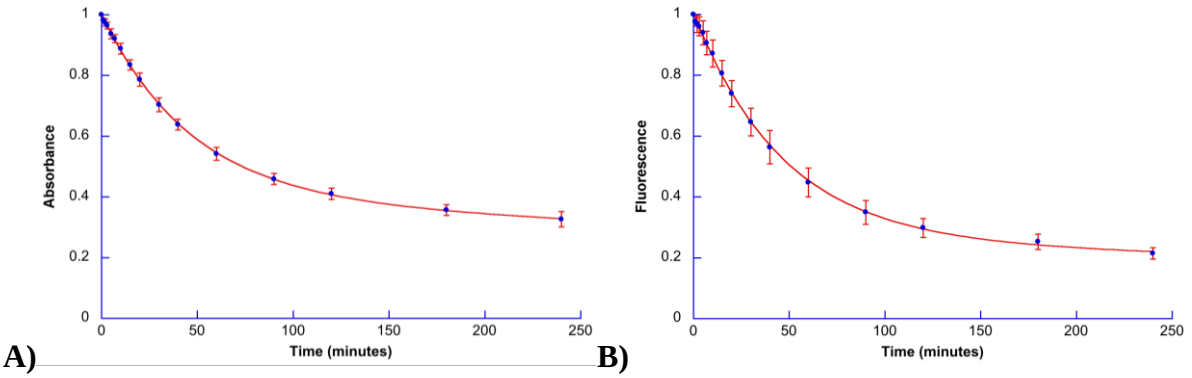

Figure 2.16: The normalized absorbance of mOrange at 548 nm while exposed to the Green LED (513 nm maximum) for 4 hours. This was experiment was performed 4 times. B) The normalized and corrected fluorescence of mOrange at 565 nm while exposed to the Green LED (513 nm maximum) for 4 hours. This experiment was performed 3 times. The data was modeled using equation 2.2a and the analysis is in appendix A.

Table 2.2: The values of the rate constants of mOrange as determined through the analysis of the decay for the maximum absorbance at 548 nm and fluorescence at 565 nm of mOrange during photobleaching with the Green LED. The rate constant for the appearance of the protonated by-product at 420 nm is shown in comparison. The values are based on the use of equation 2.2a for the decay and equation 2.2b for the growth.

λ_{max} (type of measurement)	A	k_1 (min^{-1})	B	k_2 (min^{-1})
548 nm (absorbance)	0.404 (±0.019)	0.000907 (±0.000216)	0.598 (±0.018)	0.0216 (±0.0008)
565 nm (fluorescence)	0.262 (±0.038)	0.000804 (±0.000669)	0.744 (±0.037)	0.0215 (±0.0013)
420 nm (absorbance)	0.0657 (±0.0015)	0.0166 (±0.0011)	0.00867 (±0.00098)	2.00 (±1.61)

From these data, when compared to the previous Blue and UV LED lights, the difference is striking for the interaction of Green LED light with mOrange. Whereas the Blue and UV LEDs lead to the disappearance of mOrange via a first order decay, the Green LED results in a bi-exponential decay with the concomitant appearance of a protonated by-product. This suggests that the photobleaching that arises from the direct excitation of the chromophore, leads to significantly different results than when the chromophore is not excited, as was seen with the UV and Blue lights, reinforcing the hypothesis that the Blue and UV LEDs are acting in the same fashion. Given that the data for the Green LED irradiation were fitted to bi-exponential decays, it is necessary to explore what could be happening to mOrange during chromophore excitation.

In order to account for the bi-exponential disappearance of mOrange, the prominent scenario is based on the idea that two separate chromophores are present in solution and interact with light emitted by the Green LED. Support for this idea stems from the maturation of the protein, where in section 2.3.1, the presence of green immature mOrange was seen at 495 nm. Based on the branched maturation pathway proposed by Strack *el al.* the green immature

mOrange should persist once achieved.[67] Therefore, if the immature spectra were to overlap with that of mature mOrange at 548 nm, then the decay at 548 nm will include both the loss of the green immature and mature mOrange proteins. This comes from Beer's Law, where the absorbance at 548 nm can be described as:

$$A^{548} = \varepsilon^{548}_{Mature} l[mO]_{Mature} + \varepsilon^{548}_{Green} l[mO]_{Green}, \text{ Eq 2.6}$$

where $[mO]_{Mature}$ and $[mO]_{Green}$ are the respective concentrations of mature mOrange and green immature mOrange, and $\varepsilon_{Mature}(548)$ and $\varepsilon_{Green}(548)$ represent the molar extinction coefficient of the mature mOrange and the green immature mOrange. Given that each species will undergo its own photobleaching at 548 nm, this can be modelled as:

$$[mO]_{Mature} + h\nu \xrightarrow{k_1} [mO]^*_{Mature} \text{ Scheme 2.2, and}$$

$$[mO]_{Green} + h\nu \xrightarrow{k_2} [mO]^*_{Green} \text{ Scheme 2.3}$$

where k_1 and k_2 are the rate constants for decay of the mature and green immature mOrange respectively. Unfortunately, a caveat for determining the rate of decay is that the ε^{548} are not known for either the green immature or mature mOrange alone;[27] thus it is not possible to determine the individual contributions to the total mOrange concentration from each species. This indicates that the rate of decay cannot be expressed in terms of concentration. However, it was shown in equation 2.6 that the total concentration of mOrange species in solution can be described by the total absorbance at 548 nm (A^{548}) which consists of the absorbance for the green immature mOrange and the mature mOrange. Thus the rate of decay for the green immature and mature mOrange is best described through their absorbance at 548 nm:

$$\frac{d(A^{548}_{Mature})}{dt} = -k_1(A^{548}_{Mature@t}) \text{ Eq 2.7}$$

$$\frac{d(A_{Green}^{548})}{dt} = - k_2(A_{Green@t}^{548}), \text{ Eq 2.8}$$

where (A_{Mature}^{548}) and (A_{Green}^{548}) are the absorbance at 548 nm for the mature and green immature mOrange respectively. Also, $(A_{Mature@t}^{548})$ and $(A_{Green@t}^{548})$ are the absorbance at 548 nm of the mature and green immature mOrange at time = *t* respectively. Now equations 2.7 and 2.8 can be rearranged and solved following the same logic set out for equation 2.4, then substituted into equation 2.6, resulting in:

$$(A_t^{548}) = (A_{Mature}^{548})_0 e^{- k_1 t} + (A_{Green}^{548})_0 e^{- k_2 t}. \text{ Eq 2.9}$$

Here, (A_t^{548}) relates to the total absorbance at some time (t), since it has been established that the total absorbance of mOrange at 548 nm is the sum of the absorbance values for the green immature and mature mOrange. From equation 2.9, it can be shown that if the green immature protein overlaps with the mature mOrange, then upon excitation and assuming that one excitation event leads to a unimolecular process, the absorbance at 548 nm should follow a bi-exponential decay, to which it does. Again, since this scenario takes into account two different chromophores that will undergo photobleaching, the end results should be the presence of two different photobleached by-products. It should be noted that the presence of only one peak at 406 nm suggests one species, yet, if there were overlap in the spectra between the by-products, then the two by-products will appear as one.

To reiterate, with the evidence provided from the exploration of mOrange using high power LED lights, it has been demonstrated that the excitation of the chromophore using green light produces dramatically different results than that of either Blue or UV light. Where the Blue and UV lights demonstrated primarily first order decay through β-barrel interactions, the use of

the Green light caused excitation of mOrange's chromophore, which leads to a significant loss of the protein maximum of fluorescence and absorbance via a bi-exponential decay. Ideally, from the analysis of the data, it should be possible to assign rate constants to the individual aspects contributing to the loss of fluorescence and absorbance. However, further evidence is required in order to determine distinguish the green immature mOrange decay from that of the mature mOrange. To achieve this, it was determined that the most likely experiment that will elucidate the mechanism of decay will be the use of a high power, tuneable laser. Indeed, using a highly specific (a single wavelength) light source such as a laser, if two slightly overlapping and absorbing chromophores were present in solution, it may be possible to preferentially excite one over the other.

2.3.3 Interaction of mOrange with LASER light

As was seen in section 2.3.2, the use of LED lights provided the basis upon which the kinetics of photobleaching could be understood. Yet given the proximity of the green immature mOrange (λ_{max} = 495 nm) to the mature mOrange (λ_{max} = 548 nm), even though the LEDs used are considered to have a narrow spectral bandwidth (λ_{max} ± 30 - 50 nm), simultaneous irradiation could have occurred for these two populations of mOrange using the Green LED (513 nm ± ~50 nm). Thus, to prevent simultaneous excitation of the green immature and mature mOrange, the use of a tuneable laser was employed, allowing a single wavelength to carryout the photobleaching experiments. Thus, following the same experimental setup from the photobleaching experiments with the high power LEDs, the irradiation source was changed to the use of an Opotek Inc. Vibrant 355 tunable NIR-Vis pulsed laser (10 Hz), where 532 nm was used to irradiate mOrange initially.

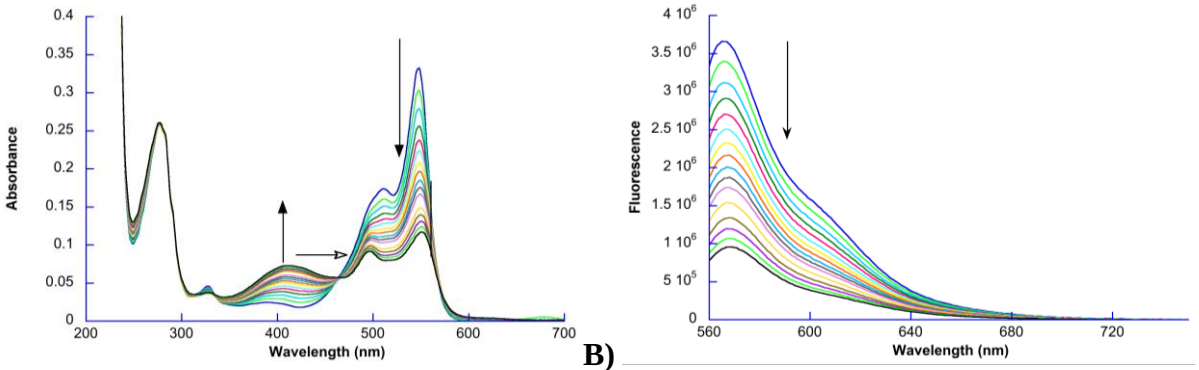

Figure 2.17: A) The absorbance of mOrange (4.69 X 10^{-6} M) while exposed to the pulsed laser (532 nm, 10 mJ, 10 Hz) for 1000 shots. The hollow arrow is indicating the presence of the revealed peak at 496 nm. B) The fluorescence of mOrange (4.69 X 10^{-6} M) while exposed to the pulsed laser (532 nm, 10 mJ, 10 Hz) for 1000 shots. The black arrows indicate the direction of change.

Upon initial inspection, the photobleaching trends of mOrange absorbance and fluorescence follow those seen with the high power LEDs, with an increase in absorbance seen at 414 nm (protonated by-product) and decreases seen at 548 nm and 565 nm for the absorbance and fluorescence respectively. Fascinatingly, the use of the 532 nm pulsed laser revealed the presence of a peak in the mOrange spectra with a maxima at 496 nm (arrow in figure 2.17A). Knowing that the green immature mOrange has its absorption maxima at 495 nm (see section 2.3.1), this seems to suggest that the peak revealed through laser irradiation is the green immature mOrange. Since it is known that the green immature mOrange fluoresces at 510 nm (figure 2.6C),[24] in an effort to confirm the 496 nm peak's identity, the peak was excited at 495 nm and found to fluoresce at 510 nm (appendix B). With this strong evidence, the revealed peak at 496 nm is supported to be the green immature mOrange.

With the presence of the green immature mOrange determined, the next step was to elucidate the extent of overlap between the green immature and the mature mOrange. In order to estimate the extent of overlap between the two mOrange populations, peak deconvolution was carried out on the spectra of mOrange before irradiation using the Origin 8.5 software suite.

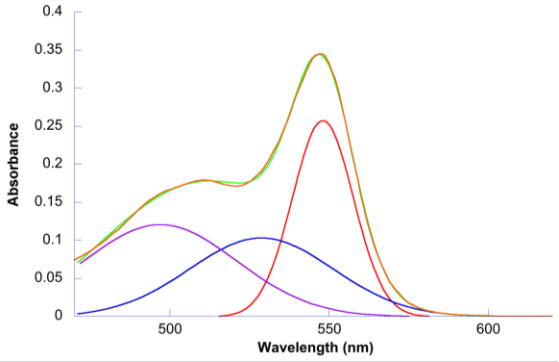

Figure 2.18: The peak deconvolution of mOrange fitted to the absorbance spectrum of mOrange (4.85 X 10^{-6} M) before irradiation. The data were deconvoluted using the Origin 8.5 software suite. Where the traces are orange (mOrange before irradiation), green (cumulative peak fit), purple (green immature mOrange representation), blue (mOrange shoulder representation), and red (mOrange main representation).

With the deconvolution, three peaks appeared and gave a relatively good fit to the experimental data (fit data can be found in appendix A). These three peaks are the main mature mOrange representation (red trace), the expected vibronic shoulder of mature mOrange representation (blue trace)[63] and the green immature mOrange representation (purple trace). Examining the green immature mOrange representation (figure 2.18 purple trace), it appears to extend to 548 nm. This indicates that the green immature mOrange should photobleach if excited by the relatively broad, compared to the laser, Green LED light, so the bi-exponential decay depending on the decay of both the green immature and mature mOrange holds weight. Using this approximation to determine the amount of overlap of the green immature mOrange, it can be seen that if the excitation of mOrange is moved to 560 nm, the mature mOrange will be primarily excited. On the other hand, if the excitation were to be moved to 497 nm, a large majority of the green immature peak will be excited. This suggests a large majority of the bi-exponential rate, will be dominated by the green immature rate during excitation at 497 nm. Alternatively, as the excitation of mOrange is moved to 560 nm, the contribution of the green immature mOrange in the bi-exponential decay should decrease until the data fits a first order decay, relating to the sole

photobleaching of the mature mOrange. Therefore, in order to determine if this is the case, three additional photobleaching experiments were carried out with the tuneable laser using the wavelengths of: 497 nm, 548 nm and 560 nm. The results are shown in figure 2.19.

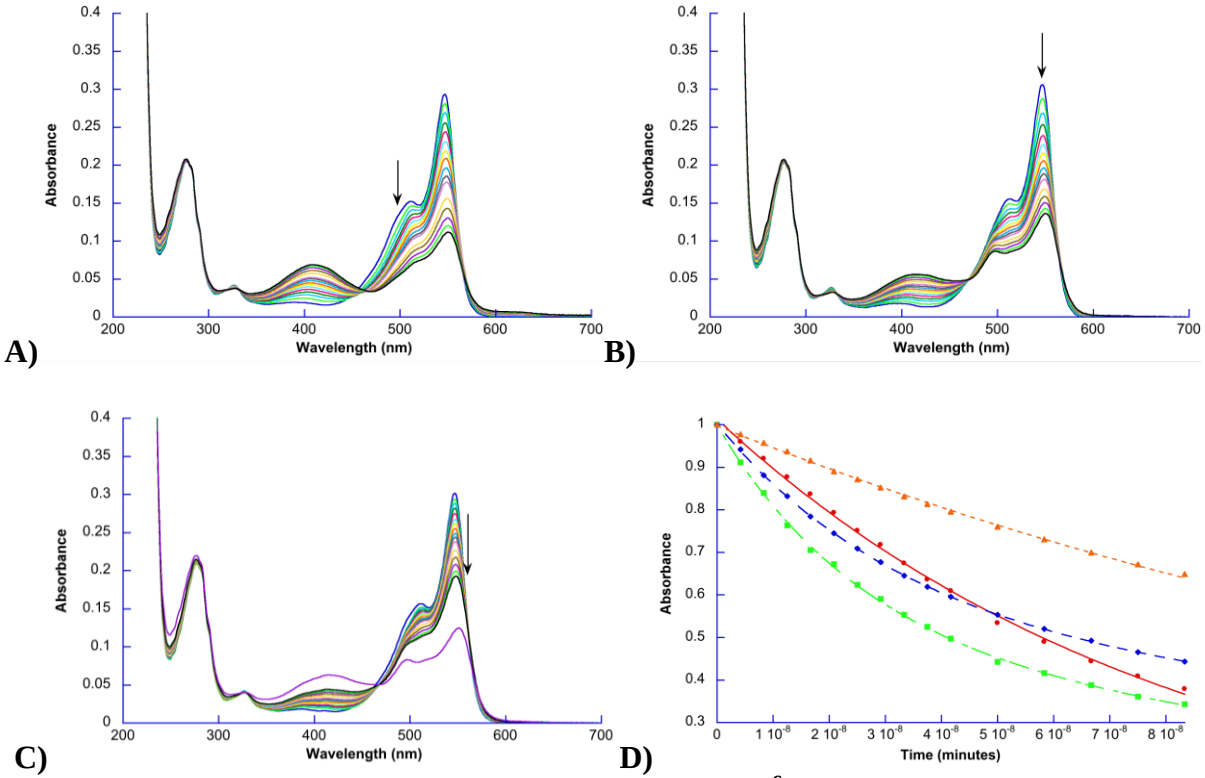

Figure 2.19: The absorbance of A) mOrange (4.11 X 10^{-6} M) exposed to the pulsed laser (497 nm, 31.66 ± 12.59 mJ, 10 Hz) for 1000 shots, B) mOrange (4.29 X 10^{-6} M) exposed to the pulsed laser (548 nm, 10.20 ± 1.79 mJ, 10 Hz) for 1000 shots, and C) mOrange (4.23 X 10^{-6} M) exposed to the pulsed laser (560 nm, 8.82 ± 2.50 mJ, 10 Hz) for 1000 shots (purple trace is 3000 shots). The arrows indicate the position of the laser irradiation wavelength. D) The normalized decay at 548 nm for mOrange due to pulsed laser irradiation at 497 nm (red trace), 532 nm (green trace), 548 nm (blue trace) and 560 nm (orange trace). For 497 and 560 nm laser irradiation, the decays were modeled by equation 2.1 while the 532 and 548 nm laser irradiation decays were modeled by equation 2.2a. The analysis can be found in appendix A.

Upon examination of figures 2.19A-C, the trends of photobleaching are similar to what is seen for irradiation at 532 nm, with a few noticeable differences. First of all, irradiation of mOrange with the 497 nm laser does not lead to the appearance of a peak at 496 nm (figure 2.19A), as it can be seen for the 532 nm irradiation (figure 2.17A). Conversely, as the excitation

wavelength moved to either 548 nm (figure 2.19B) or 560 nm (figure 2.19C), the peak is clearly perceived. It should be noted, that when mOrange was irradiated at 560 nm, due to its low absorbance at that wavelength, the protein did not bleach to the same extent when compared to the 497 nm – 548 nm irradiations. In order to see the presence of the 496 nm peak when mOrange was irradiated at 560 nm, it was necessary to carry out the irradiation for 3000 shots, which was three times greater than the other laser experiments (figure 2.19C purple trace). Secondly, all three additional irradiations display the growth of the protonated by-product. Interestingly with the 497 nm irradiation, the protonated by-product has a maximum at 406 nm, while the 560 nm irradiation placed the protonated by-product at a maximum of 418 nm.

Considering that the bi-exponential decay predicts the presence of two separate, yet overlapping by-products, this apparent shift in the protonated by-product peak depending on the wavelength of irradiation, helps support this hypothesis. Specifically, when irradiated at 497 nm the by-product present is primarily due to the protonation of the green immature peak, as confirmed through the first order decay seen in the absorbance. While conversely, the by-product seen at 418 nm due to the 560 nm irradiation relates it to the protonation of the mature mOrange. Unfortunately, the growths of the protonated by-products do not fit either a first order or bi-exponential growth, thus a complete analysis cannot be carried out.

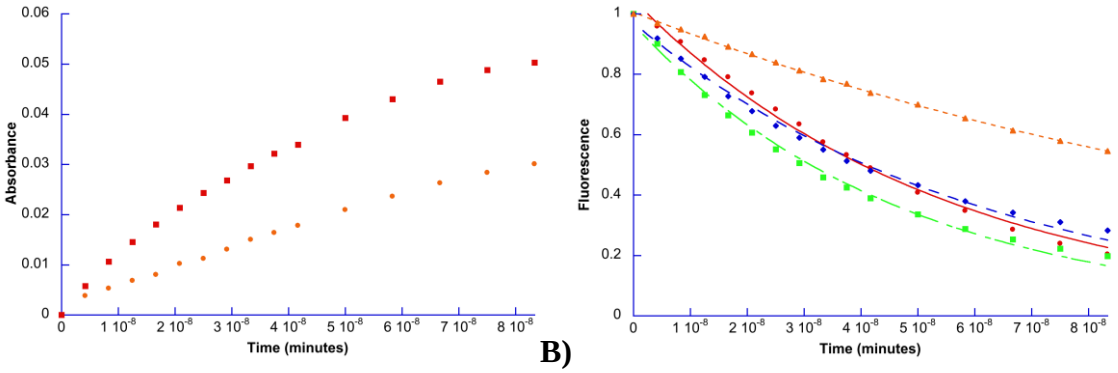

A) **B)**

Figure 2.20: A) The absorption spectrum of mOrange at 406 nm (red trace, 497 nm irradiation) and 418 nm (orange trace, 560 nm irradiation) to represent the growth of the protonated by-product, with the initial spectrum (no shots) removed from all subsequence spectra while irradiated with the laser for 1000 shots. B) The normalized and corrected fluorescence decay at 565 nm for mOrange while irradiated with either 497 nm (red trace), 532 nm (green trace), 548 nm (blue trace) or 560 nm (orange trace). For 497 and 560 nm laser irradiation data were modeled with equation 2.1, while the 532 and 548 nm laser irradiation data were modeled with equation 2.2a. The analysis can be found in appendix A.

From the peak deconvolution it was predicted that as the wavelength of irradiation moved from 497 nm to 560 nm, the rates of decay will tend to change from a bi-exponential dominated by the decay of the green immature mOrange, to that of a bi-exponential (or first order decay) dominated by the mature mOrange. This can be seen in figures 2.19D and 2.20B, where for the 497 nm and 560 nm irradiation, the data were best modeled with first order decays, while the decays from the irradiation at 532 nm and 548 nm were best modeled with a bi-exponential (appendix A). However, to better demonstrate the shift in contribution to the decays, the values of the pre-exponential factors, *A* (contribution of the mature mOrange) and *B* (contribution of the green immature mOrange), from equations 2.1 and 2.2 as found through the analysis of the laser irradiation data are displayed in tables 2.3 and 2.4. Here, it can be seen that as the wavelength of irradiation increased to 560 nm, the contribution to the decays from the green immature mOrange decreases from complete contribution at 497 nm, to no contribution at 560 nm. On the other hand, the contribution of the mature mOrange increases from nothing at 497 nm to

complete contribution at 560 nm. Based on this data, it is now possible to assign the values of decay for the green immature and mature mOrange.

Table 2.3: The contributions to the overall decay as determined through the analysis of the loss of absorbance at 548 nm of mOrange during photobleaching at the indicated wavelengths, as well as the associated rate constants. Where *A* and *B* represent the contributions of the mature and the green immature mOrange respectively.

Wavelength of Irradiation	*A*	k_1 (min^{-1})	*B*	k_2 (min^{-1})
497 nm	-	-	1.014 (±0.005)	1.22 X 10^7 (±2 X 10^5)
532 nm	0.501 (±0.074)	5.27 X 10^6 (±1.52 X 10^6)	0.498 (±0.072)	4.00 X 10^7 (±4.9 X 10^6)
548 nm	0.520 (±0.035)	2.99 X 10^6 (±5.9 X 10^5)	0.482 (±0.035)	3.03 X 10^7 (±1.7 X 10^6)
560 nm	0.998 (±0.002)	5.33 X 10^6 (±5 X 10^4)	-	-

Table 2.4: The contributions to the overall decay as determined through the analysis of the loss of fluorescence at 565 nm of mOrange during photobleaching at the indicated wavelengths, as well as the associated rate constants. Where *A* and *B* represent the contributions of the mature and the green immature mOrange respectively.

Wavelength of Irradiation	*A*	k_1 (min^{-1})	*B*	k_2 (min^{-1})
497 nm	-	-	1.048 (±0.013)	1.84 X 10^7 (±5 X 10^5)
532 nm	0.354 (±0.076)	9.41 X 10^6 (±1.84 X 10^6)	0.646 (±0.076)	3.47 X 10^7 (±2.4 X 10^6)
548 nm	0.338 (±0.119)	5.55 X 10^6 (±2.66 X 10^6)	0.661 (±0.118)	2.70 X 10^7 (±2.9 X 10^6)
560 nm	1.006 (±0.002)	7.34 X 10^6 (±6 X 10^4)	-	-

Before further analysis can be carried out, it needs to be noted that the apparent rate constants found from the laser irradiation are much greater than that of the LEDs. However, the power of the irradiation source has been shown to be linked linearly to the bleaching experienced by fluorescent proteins.[83] Considering the laser power per shot has an average power of 10 mJ/cm^2 and each shot lasts for about 5 ns, the average watts received per shot is 2000000 W/cm^2. Comparing the laser power to the Green LED power at 18.3 mW/cm^2, the difference in magnitude about 10^8. This suggests that the pulsed laser should be produce rate constants about 10^8 times larger than the LED. Looking at the rate constants for the Green LED and the pulsed laser this appears to be the case, with the Green LED producing a k_1 for the decay at 548 nm of 1 X 10^{-3} min^{-1}, while the k_1 for the pulsed laser was found to be 5.33 X 10^6 min^{-1}, which is about 10^9 times greater than the LED rate. Although this is not exact, it allows the differences in rate constants between the two irradiation sources to be understood.

To reiterate, it was found through the peak deconvolution that the irradiation at 560 nm should preferentially excite the mature mOrange. With the fact that the decay at 548 nm for the 560 nm irradiation produced a first order rate, this confirms that only one species is undergoing photobleaching. Combining this information together it is possible to assign a value of decay for the mature mOrange. From the analysis of figure 2.19D (orange trace), the rate constant of decay for mature mOrange is found to be 5.33 X 10^6 ± 5 X 10^4 min^{-1}. On the other hand, considering that the irradiation at 497 nm should preferentially excite the green immature mOrange, from the analysis of the decay at 497 nm (figure 2.19D, red trace) the rate constant of photobleaching for the green immature mOrange is found to be: 1.22 X 10^7 ± 2 X 10^5 min^{-1}. The ramifications of these rates are that the mature mOrange is less sensitive to light when compared to the green immature mOrange.

What can be summarized from this data is that the photobleaching of mOrange has been shown to be a combination of both the green immature and mature mOrange proteins. Using relatively broad LED lamps led to the photobleaching of both the populations of mOrange. However, using a tuneable LASER to probe the characteristics of photobleaching led to the distinct separation of the photophysical properties for the two mOrange populations, enabling the respective contributions of photobleaching to be elucidated. From the data collected, the rates of decay indicate that for the mature mOrange, photobleaching is slower than that of the green immature mOrange, suggesting that the fully matured mOrange is more resilient to photobleaching than its immature counterpart. Unfortunately, these rates are still determined with both populations present in the sample. If it were able to separate the two mOrange populations, it may be possible to confirm the rate constants found in the kinetic analysis. Yet, with the conserved nature of the protein β-barrel and the fact that the only difference between the two populations of mOrange is a matter of folding within the barrel of the protein, standard protein separation method are of no use. Therefore, the green immature mOrange cannot be separated from the mature mOrange, unless heat is added, as developed below.

2.3.4 Separation of the immature mOrange from the mature

From the laser irradiation kinetic study, it was found that the mature mOrange was more resilient to photobleaching compared to the green immature mOrange. Given that the folding is incomplete in the green immature mOrange,[67] perhaps the addition of heat will denature the green immature mOrange at a lower temperature than that of the mature mOrange. Therefore, through the incremental increase of heat it was seen that at 80°C, the shoulder of mOrange located at 515 nm decreases dramatically (figure 2.21A). Additionally, the blue intermediate species present at 390 nm denatures completely suggesting that the incomplete maturation leads

to less heat resilient proteins. To ensure the complete denaturation of the green immature mOrange, its fluorescence was followed at 510 nm (figure 2.21B) where upon 82°C, no fluorescence was seen. As discussed above, the fluorescence seen at 82°C (λ_{max} = 565 nm) is the fluorescence that originates form the mature mOrange in solution. This last result confirms that the green immature mOrange was denatured. Although this denaturation process is not a removal of the physical protein from solution, it is a removal of the green immature mOrange's photophysical properties from solution. This suggests that the green immature mOrange will no longer interact with light and only the mature mOrange will remain to be excited. Interestingly, the loss of the green immature mOrange has led to the red-shift of the absorption spectra for mOrange, such that the maxima is now at 550 nm.

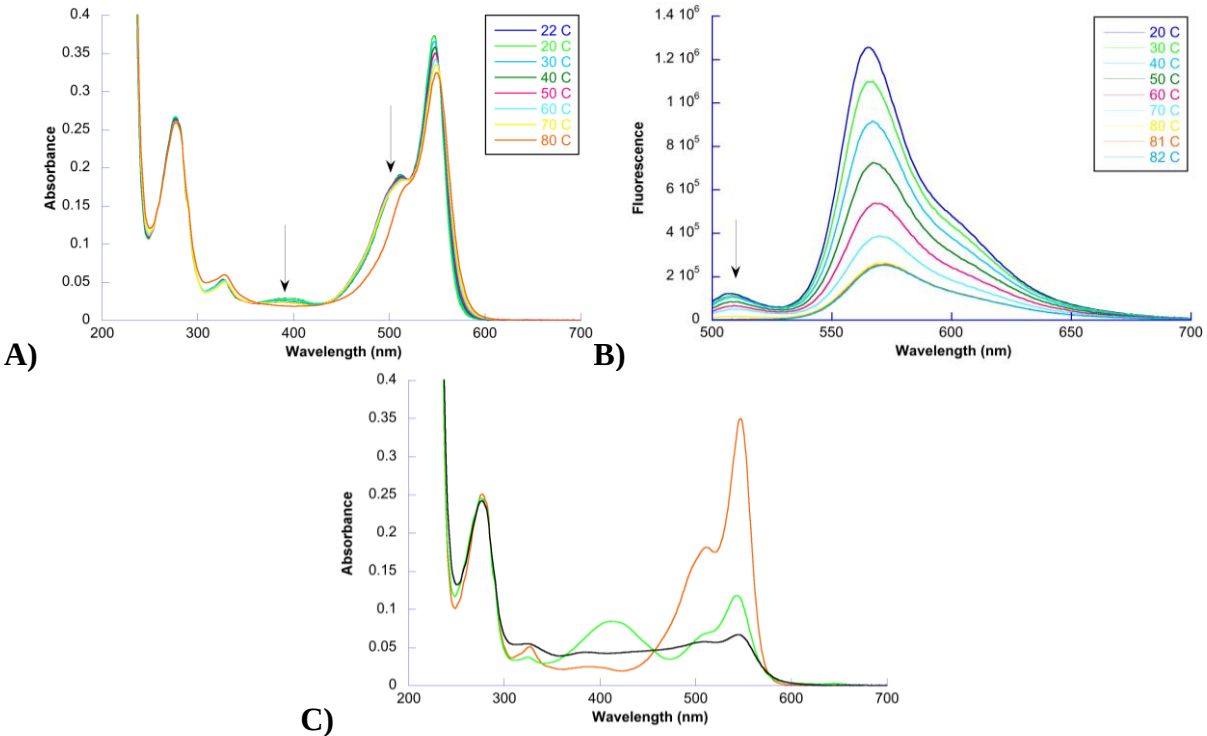

Figure 2.21: A) The absorbance of mOrange (5.23 X 10^{-6} M) during heating using a Cary 50 Peltier accessory. B) The fluorescence of the immature green mOrange (excited at 490 nm) during heating, with its complete absence at 82 °C. The arrows indicate the peak loss achieved with heating. C) The room temperature absorbance of mOrange (4.91 X 10^{-6} M) before irradiation (orange trace) and after 4 hours of irradiation with the Green LED (green trace). Once photobleached, the sample was heated to 82 °C and the absorbance was taken (black trace).

Having the ability to remove the photophysical presence of the green immature mOrange enables the sole focus on the bleaching of mature mOrange. Thus to determine the effects of light on mature mOrange, a sample was heated to 82°C then irradiated with a tuneable laser at 532 nm for 1000 shots. As shown in Figure 2.22A, the results display a distinct loss of the mature mOrange between 470-580 nm, similar to the loss seen in the previous photobleaching experiments. Albeit the main peak of mOrange at 82°C follows a similar photobleaching trend when at room temperature, the appearance of the protonated by-product is not seen; instead a steady increase is seen in the absorbance from about 250 nm to 470 nm. Given that it has been shown that irradiation produces the protonated by-product, the overall increase seen in the

absorption spectra could indicate that the by-product is unstable at 82°C, leading to its denaturation causing Rayleigh scattering, resulting in the increased absorption.[66,84] Indeed this was confirmed through the control experiment as seen in figure 2.21C.

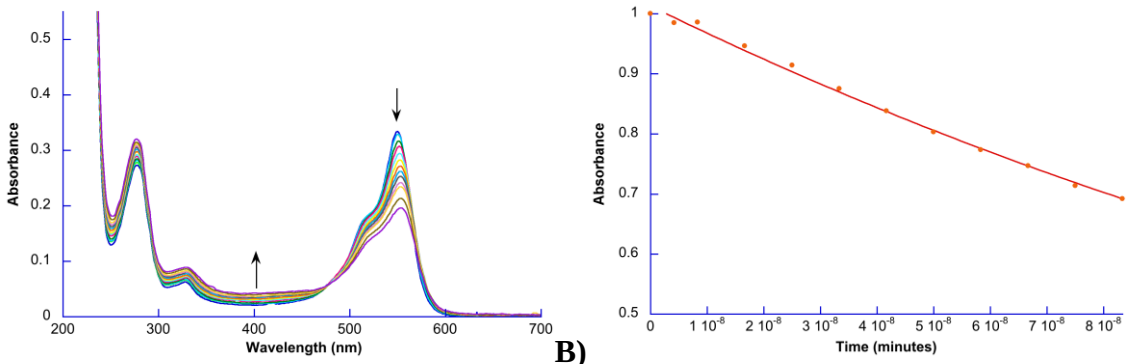

A) **B)**

Figure 2.22: A) The absorbance of mOrange (5.39 X 10^{-6} M) while exposed to the pulsed laser (532 nm, 10.17 ± 1.72 mJ, 10 Hz) for 3000 shots while the solution was maintained at 82 °C using Cary peltier cuvette temperature regulating accessories. B) The normalized absorbance of mOrange at 550 nm during irradiation by the pulsed laser (532 nm, 10.17 ± 1.72 mJ, 10 Hz) for 1500 shots while the solution was maintained at 82 °C using Cary peltier cuvette temperature regulating accessories. The data were modeled with equation 2.1 (fit analysis in appendix A).

The maximum absorbance at 550 nm for mOrange can be plotted and fitted to assess the rate constant for the decay. Form figure 2.22B, the decay was best modeled by a first order, with a rate constant of 4.57 X 10^6 ± 1.0 X 10^5 min^{-1}. Comparing this rate constant with that found with the 560 nm LASER irradiation at room temperature (5.33 X 10^6 ± 5 X 10^4 min^{-1}), they are remarkably similar. The small difference between these two rates could be attributed to the fact that they were performed under slightly different conditions. It should not be overlooked that this result is significant due to the 532 nm laser producing a first order decay at 82°C, where before with the photophysical presence of the green immature mOrange, the decay seen was bi-exponential. Thus, considering the relatively high similarity between these two rates, the removal of the green immature mOrange suggests that the mature mOrange photobleaches at a rate constant of 5.33 X 10^6 ± 5 X 10^4 min^{-1} at room temperature. Conversely, the rate constant for the

green immature mOrange photobleaching, can be consider to be $1.22 \times 10^7 \pm 2 \times 10^5$ min^{-1}. Unfortunately, with the presence of mature mOrange fluorescence during green immature mOrange excitation at 490 nm (figure 2.21B), as well as the bi-exponential growth for the 406 nm protonated by-product (figure 2.20A, red trace), the rate determined for the green immature mOrange contains some uncertainty as it has not been fully separated from the mature mOrange.

2.4 Conclusions

In the effort to better understand the mechanisms of photobleaching for fluorescent proteins, the photobleaching sensitive variant of DsRed, mOrange, was chosen as the ideal candidate. Given that the chromophore formation of DsRed has been shown to follow a branched pathway[24,67] it was determined through the study of the maturation of mOrange, that this protein does indeed possess the ability to form both the mature (orange) and immature (green) versions. Having established the processes of maturation for mOrange, exposing purified samples of mOrange to high-powered LED lights that do not excite the mOrange chromophore (UV and Blue LEDs), demonstrated first order decays of the 548 nm peak of mOrange due to β-barrel interactions. However, the exposure of mOrange to a Green LED capable of exciting the chromophore produced a bi-exponential decay at 548 nm, with the presence of a protonated by-product at 406 nm. Unable to explain this rate of decay, the use of a more specific, single wavelength laser was employed.

It is to the best of our knowledge that the study of photobleaching in fluorescent proteins using a tuneable laser at several wavelengths has never been previously carried out. The novelty of this study revealed the presence of the green immature mOrange present within a solution of supposedly fully mature mOrange, providing an explanation of the observed bi-exponential decay rate. By changing the wavelengths of irradiation to target specifically the green immature

mOrange or the mature mOrange alone, the contributions to the rate constant of photobleaching were determined. From this data it was shown that the green immature mOrange photobleaches at a rate constant in the order of $1.22 \times 10^{7} \pm 2 \times 10^{5}$ min^{-1}, while the mature mOrange follows a rate constant of $5.33 \times 10^{6} \pm 5 \times 10^{4}$ min^{-1}. This suggests that the mature mOrange is more resilient to photobleaching than that of its immature counterpart. To confirm this, heat was used to remove the photophysical presence of the green immature mOrange. From here, the novel study of photobleaching at 82 °C was carried out to confirm the decay rate for the mature mOrange alone.

The ramifications of this study suggest that it is possible for variants of DsRed to contain improperly formed chromophores. More importantly, this study suggests that the presence of the immature variants can lead to rates of decay not representative of the fully formed chromophores. Yet this study has not been able to determine the effects, if any, that the green immature mOrange has on the decay of mature mOrange. This question will be part of the focus for the subsequent chapters.

Chapter Three: **On the photoconversion of mOrange with Potassium Ferricyanide**

3.1 Introduction

Of the improvements and modifications carried out on fluorescent proteins (FP) over the years, one of the most interesting has been the development of photochromic and photoswitchable FPs. The development of photochromic proteins, for example, Eos has enabled one FP to produce two distinct colours of fluorescence (green or orange for Eos) depending upon the wavelength of light used for activation.[85] Conversely, photoswitchable proteins have enabled the temporal and spatial activation or deactivation of FPs using light, for example: Dronpa, enabling fluorescent emission only where light was used to activate Dronpa within the imaging experiment at hand.[43,85] In both cases, these types of FPs require the use of light to produce the desired conversion seen in their fluorescence capability, allowing different aspects within a specimen to be highlighted from the bulk background fluorescence. Thus these photoconversions, hold high potential in super-resolution imaging.[46,86] Therefore, the search for more photoconvertible proteins has been ever expanding.

One of the fruits from the search for more photoconvertible FPs, has been found in mOrange where Kremers *et al.* first reported the formation of highly red-shifted fluorescence.[85] However, the far-red fluorescence observed in mOrange was unstable and relatively dim.[58] Therefore to improve the photoconversion observed in mOrange, Subach *et al.* suggested that the presence of intracellular oxidizers may be necessary to obtain more stable far-red fluorescence.[26,58] Thus, through the exposure of mOrange to a variety of oxidants and a 489 nm centered LED array, Subach *et al.* were able to show the presence of the photoconverted far-red (FR) species of mOrange when the oxidant potassium ferricyanide ($K_3Fe(CN)_6$) was used. The spectral characteristics of this FR mOrange species are that the absorbance has a maximum at

631 nm, with a low molar extinction coefficient of 17200 $M^{-1}cm^{-1}$ compared to other FPs and the fluorescence has a maximum at 662 nm with a small fluorescence quantum yield (ϕ_{Fl} = 0.19).[58]

Interestingly, it was suggested that the FR mOrange was produced through the excited state chromophore interacting with $K_3Fe(CN)_6$, leading to an oxidative reddening by extending the conjugation of the chromophore. However, there are two factors that dispute the possibility of the excited chromophore of mOrange interacting with $K_3Fe(CN)_6$. The first is that in my opinion, the possibility of this occurring is small since $K_3Fe(CN)_6$ would need to be able to diffuse through the β-barrel of mOrange and come in contact with the chromophore during excitation for the proposed oxidization to occur. In agreement with my objection would be the idea that the chromophore of FPs is relatively shielded from the external environment.[10] Indeed, even until recently[74,75] the pathway for molecular oxygen ($^3O_2$) access has been not well understood, suggesting that only very small molecules, if any, would interact with the central chromophore of most FPs. Concurrently, comparing the Van der Waals solid state radii of the spherical ferricyanide anion (5.6 Å)[87] and cylindrical $^3O_2$ (longest axis is 1.67 Å),[88] along with the fact that the center of the β-barrel is largely hydrophobic,[10] it can be debated as to whether the ferricyanide anion could actually enter into the β-barrel of the chromophore. The second factor to consider is that a key aspect was not addressed within the work of Subach *et al.* which was the fact that $K_3Fe(CN)_6$ absorbs light. If the $K_3Fe(CN)_6$ were to be excited via the 489 nm LED arrayed used by Subach *et al.*, it is possible that the mechanism responsible for the oxidative reddening could be due to the excited $K_3Fe(CN)_6$ acting on mOrange.

Realizing some of the potential pitfalls of the observed photoconversion for the FR mOrange, the need for further exploration of this topic was apparent. Having investigated some of the aspects contributing to the photobleaching of mOrange, the foundation needed was already

laid. Therefore, to better understand the mechanisms of oxidative reddening, the photobleaching of mOrange was required while in the presence of $K_3Fe(CN)_6$. As seen in chapter two, the use of LED and laser irradiation enabled the separation of excitable chromophores. Additionally, since the product of oxidation is a species that absorbs and fluoresces in the red, it is possible to follow the experiments using absorption and fluorescence spectroscopy. Finally, by using western blot techniques, it will be possible to determine if there are any adverse effects on mOrange due to the presence of $K_3Fe(CN)_6$.

3.2 Methods

3.2.1 Materials

In addition to the materials used in chapter two, the study of $K_3Fe(CN)_6$ required further chemical and instruments to complete an in-depth analysis of the FR mOrange production. Specific to this investigation, Imidazole, $K_3Fe(CN)_6$, Gylcine, Trizma pH 7.0 buffer, and Tris-Base were obtained from Sigma Aldrich Canada. Sodium Dodecyl Sulfate (SDS), Ammonium Persulfate, TEMED, 40% Acrylamide/Bis solution 19:1, and Tween 20 surfactant were obtained from BioRad Canada. The x-ray developer (V-307) and fixer (V-306) were obtained form Christie InnoMed. The reagents used for the development for the western blots were Amersham ECL Western Blotting Detection Reagents from GE Healthcare Limited. Additionally, the western blots required the use of EZ-Run Pre-stained Rec Protein Ladder (BP3603-500) from Fisher Scientific, Living Colors® mCherry monoclonal antibody and Goat anti Mouse Horseradish peroxidase conjugate antibody from Clontech Laboratories Inc. Finally to carry out the western blot electrophoresis and transfer, a C.B.S. Scientific Company Quadra Mini-Vertical PAGE and Blotting System with cooling labyrinth was used. The membrane used for the transfer of the protein from the electrophoresis gel was Millipore Immobilon-P PVDF Transfer

Membranes with a pore size of 0.45 μm from EMD Millipore USA and the film used to capture the chemiluminescence was Amersham Hyperfilm™ ECL high performance chemiluminescence film from GE Healthcare Limited.

3.2.2 Experimental Setup

The methods and materials required for the production of mOrange are in section 1.2 of chapter one. A 0.01 M stock solution of $K_3Fe(CN)_6$ was created with 32.92 mg of $K_3Fe(CN)_6$ that was dissolved in 10 mL of MilliQ water (18.2 MΩ.cm mL). With this stock solution, 25 μL was added to a solution of mOrange (containing an average of 4.0 X 10^{-6} M) in 975 μL of phosphate buffer saline (PBS, pH 7.4), for a total of 1 mL with a final $K_3Fe(CN)_6$ of 0.25 mM, in a 0.4 cm width by 1 cm path length quartz cuvette (International Crystal Laboratories). This cuvette was then irradiated with a light source, once finished the samples were stored at 4 °C until western blot analysis.

3.2.3 High Powered LED and LASER Irradiation

With the prepared mOrange and $K_3Fe(CN)_6$ solution, to model the experimental setup of Subach *et al.* high powered LEDs were used to irradiate the mOrange solutions.[58] For the LEDs, the UV, Blue or Green LEDs with peak wavelengths (power) of 405 nm (64.2 mW/cm^2), 450 nm (57.3 mW/cm^2) and 515 nm (18.3 mW/cm^2) respectively (fabricated at the University of Calgary electronics shop), were used to irradiate the solutions. Irradiation time was for a total of 4 hours, with the absorption spectroscopy (Varian Cary 50 single beam spectrophotometer) and fluorescence spectroscopy Photon Technology International (PTI, Quanta Master 40 fluorimeter in CW mode) being check at 0, 1, 2, 3, 5, 7, 10, 15, 20, 30, 40, 60, 90, 120, 180 and 240 minutes. To ensure no overlap between the Blue and Green LEDs, a 488 nm shortwave cutoff filter was used on the Green LED (Optosigma). For fluorescence, the solution was excited at 548 nm to

follow mOrange fluorescence with 2 nm slits for excitation and detector slit widths, but to follow far-red emission from photoconversion of mOrange, excitation at 620 nm was carried out with 4 nm excitations slit widths and 6 nm detector slit widths.

As in chapter one, to examine if the relatively broad LEDs affected the interaction of mOrange, the Opotek Inc. Vibrant 355 tunable NIR-Vis pulsed laser (10 Hz) was used. Using a Thorlabs PM100D meter with ES220C pyroelectric energy sensor, the power of the laser at each wavelength (497, 532, 548 and 560 nm) was measured for 100 shots before and after each photobleaching experiment. Again the experiments were followed using absorbance and fluorescence spectroscopy.

3.2.3.1 Use of Imidazole

Considering $K_3Fe(CN)_6$ is a known oxidant,[36] the use if imidazole was employed to possibly mitigate the mOrange's oxidation. Following the same experimental setup as outlined in section 3.2.3, imidazole was added to final concentration of 10 mM in a total of 1 mL (50 μL of a 0.2 M stock solution of imidazole dissolved in MilliQ water) before irradiation. The irradiations were carried out using the LED lamps. Additionally, to determine if the addition of imidazole could mitigate the effects of $K_3Fe(CN)_6$ during irradiation, the solutions of mOrange and $K_3Fe(CN)_6$ were irradiated for 10 minutes, at which point imidazole (final concentration of 10 mM) was added and the irradiation was continued.

3.2.3.2 Use of Heat

The same setup and procedure was followed as outlined in chapter two.

3.2.4 Western Blot Analysis

To determine if any physical effects were done to mOrange due to the $K_3Fe(CN)_6$ during irradiation, western blot analysis was carried out for the samples of irradiation. This was done through the successive dilution of the mOrange samples until a final concentration of 1 ng/μL was achieved. From here, the samples along with the EZ Run Protein Ladder were loaded into a 5% Acrylamide/Bis stacking with 15 wells, on top of a 12% Acrylamide/Bis resolving gel. The samples were run at 140 V, 3A for 1.66 hours with stirring, using 1X Running Buffer (25 mM Tris-Base, 0.25 M Gylcine and 0.1% SDS). Once completed, the protein samples were transferred from the 12% resolving gel to a methanol activated the Immobilon-P membrane using the cooled (ran in a 4 °C refrigerator) C.B.S. blotting system and 1X transfer buffer (consisting of a 1:1:3 ratio of 5X transfer buffer, 100% methanol and MilliQ H_2O) where the 5X transfer buffer is composed of 125 mM Tris-Base and 1.25 M Glycine. The transfer was carried out at 100V, 3A for 1.25 hours. From here the membrane was fixed in methanol for five seconds, then washed in a PBS and 0.05% Tween 20 (PBS/Tween) solution three times. The membrane was blocked using a 5% skim milk PBS/Tween solution, then incubated with the primary mouse anti mCherry (1:1000 dilution) monoclonal antibody in 5% skim milk PBS/Tween for one hour at room temperature. This membrane was washed and reblocked, then incubated with secondary goat anti mouse antibody (with horse radish peroxidase attached) for and an additional hour at room temperature. After a final washing, the membrane was then developed using the Amersham ECL reagents in a 1:1 ratio using Amersham Hyperfilm™ ECL high performance chemiluminescence film. Finally the chemiluminescence film was developed and fixed using the Christie Immomed x-ray developer and fixer solutions.

3.3 Results

The work of Subach *et al.* made use of a high power LED with its maximum centered at 489 nm.[58] With the use of this LED, they were able to demonstrate that in the presence of the external oxidant, $K_3Fe(CN)_6$, mOrange would undergo a photoconversion to a far-red emitting variant. The reasoning provided for this photoconversion rested in the fact that during excitation, the chromophore of mOrange would become susceptible to oxidation due to its propensity to donate an electron, becoming oxidized.[58,89] For Subach *et al*. the electron acceptor was $K_3Fe(CN)_6$. However, having carried out the work in chapter two, it was shown that the relatively broad spectral distribution of LEDs (compared to a laser) could lead to multiple excitations if two chromophores were residing within the spectrum of the LED lamp. Given this fact and that it is known that $K_3Fe(CN)_6$ absorbs in the 360 nm to 460 nm region (figure 3.1), it is possible that the far-red conversion may be due to the interaction of excited $K_3Fe(CN)_6$ and mOrange with a 489 nm centered LED lamp. To test the possibility for $K_3Fe(CN)_6$ to be excited, we extrapolated the profile of a 489 nm LED lamp from the spectrum of the Blue LED lamp (λ_{max} = 447 nm) used in chapter two by artificially moving its center from 447nm to 489 nm and overlapping it with the spectra of mOrange and $K_3Fe(CN)_6$ (figure 3.1).

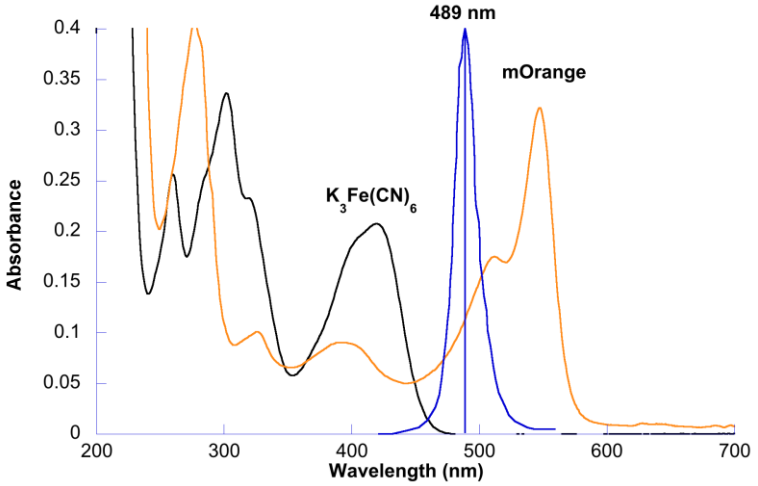

Figure 3.1: The overlap between mOrange (4.53 X 10^{-6} M), $K_3Fe(CN)_6$ (0.25 mM) and an artificial 489 nm LED spectrum. The spectrum of the 489 nm LED was created from the spectrum of a Blue LED centered at 447 nm, which was then artificially shifted to 489 nm. This was carried out to indicate the possibility of exciting both mOrange and $K_3Fe(CN)_6$ simultaneously.

The extrapolation made in figure 3.1 suggests that the use of the 489 nm centered LED has the possibility of exciting both mOrange and $K_3Fe(CN)_6$. Additionally, it was shown in chapter two that a solution of mOrange is actually composed of both the green immature mOrange and the mature mOrange. Therefore, the use of a 489 nm centered LED with mOrange would primarily excite the green immature mOrange (λ_{Max} = 495 nm), and given the effects of the green immature mOrange during excitation have not been studied previously, further investigation is necessary. Thus, to further study the photoconversion of mOrange with $K_3Fe(CN)_6$, it was necessary to separate the excitation of $K_3Fe(CN)_6$ and mOrange and examine the individual components contributing to the far-red variants.

3.3.1 mOrange and $K_3Fe(CN)_6$ with high-powered LEDs

As seen in chapter two, three separate high-powered LEDs were available for use. Needing to determine the areas of excitation, figure 3.2 displays the overlap between the spectra for these LEDs with the spectra of $K_3Fe(CN)_6$ and mOrange. It is clear from figure 3.2 that for

the UV LED, there is significant overlap between $K_3Fe(CN)_6$, while for the Green LED (with the 488 nm filter), only mOrange is within the lamp spectrum. Finally, with the Blue LED it can be seen that both $K_3Fe(CN)_6$ and mOrange overlap with the lamp spectrum, suggesting that both species are able to become excited. Given these overlaps, the use of these three LEDs enables the separation of excitement for mOrange and $K_3Fe(CN)_6$. Thus, to determine if the oxidative reddening seen for mOrange is due to the excitement of $K_3Fe(CN)_6$, the first LED used to photobleach a solution of mOrange and $K_3Fe(CN)_6$ was the UV LED.

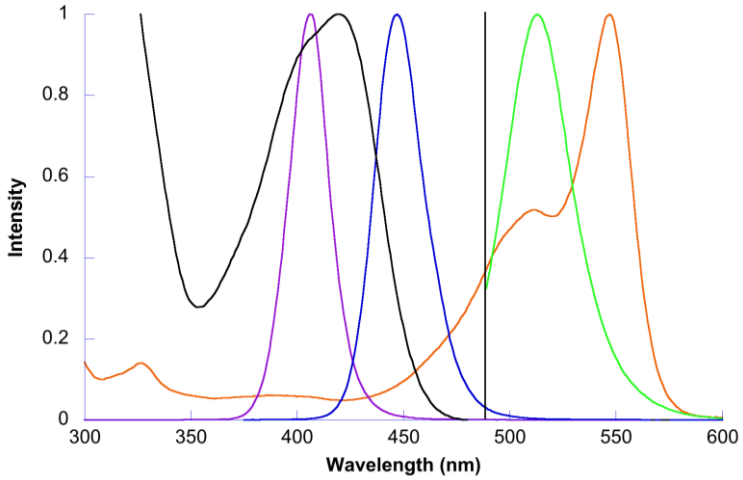

Figure 3.2: The normalized absorbance spectra of mOrange (orange trace) and $K_3Fe(CN)_6$ (black trace), overlapped with the normalized UV (purple trace), Blue (blue trace) and Green (green trace) LED spectra to indicate the areas of excitation. The black vertical line indicates the 488 nm shortwave cutoff filter.

3.3.1.1 mOrange and $K_3Fe(CN)_6$ with the UV LED

Having determined the primary areas of excitation for each LED, figure 3.2 clearly shows a significant overlap between the UV LED and $K_3Fe(CN)_6$, while as discussed in chapter two, the UV LED does not excite mOrange. This overlap of the UV LED and $K_3Fe(CN)_6$ suggests that the UV LED could excite the $K_3Fe(CN)_6$, creating an excited species that may interact with and subsequently affect the photophysical properties of mOrange. According to Arellano *et al.* the exposure of $K_3Fe(CN)_6$ to UV light leads to its photolytic degradation, releasing cyanide ions

into solution.[90] Therefore, it is critical to understand the photolytic degradation of $K_3Fe(CN)_6$ in the presence of UV light under the experimental conditions in order to define the $K_3Fe(CN)_6$ interaction with mOrange. Using the same concentration of $K_3Fe(CN)_6$ for photoconversion as Subach *et al.*,[58] a solution of PBS (pH 7.4) and $K_3Fe(CN)_6$ (0.25 mM) was irradiated in front of the UV LED for a total of four hours in the absence of protein. From the results in figure 3.3A, it can be seen that exposure to the UV LED leads to a significant decrease in the main absorption intensity of $K_3Fe(CN)_6$ (λ_{max} = 419 nm), and as seen previously in the literature for $K_3Fe(CN)_6$, this decay can be attributed to photolytically induced degradation.[90]

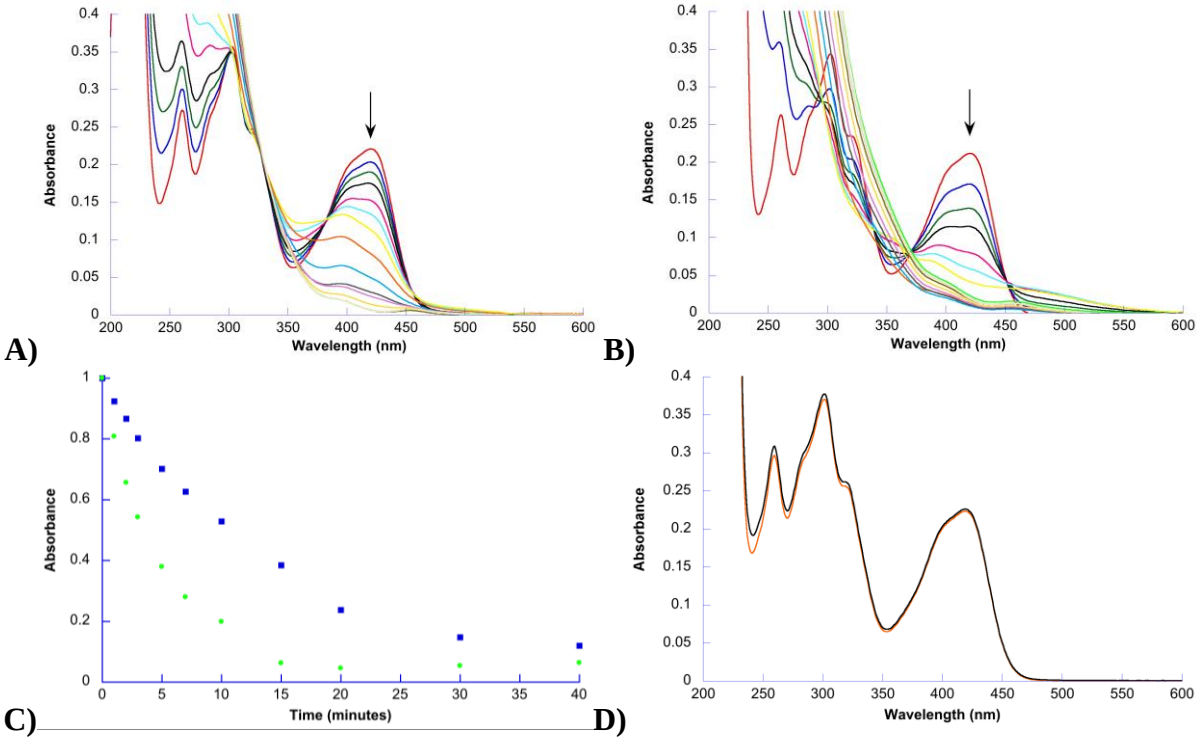

Figure 3.3: A) The absorbance of $K_3Fe(CN)_6$ (0.25 mM) while exposed to the UV LED for 4 hours. B) The absorbance of $K_3Fe(CN)_6$ (0.25 mM) and imidazole (10 mM) while exposed to the UV LED for 4 hours. The arrows indicate the major decrease in absorption seen. C) The comparison of the absorption maxima at 419 nm for $K_3Fe(CN)_6$ (0.25 mM, blue squares) and $K_3Fe(CN)_6$ (0.25 mM) with imidazole (10 mM, green circles) for the first 40 minutes of UV irradiation. D) The absorbance spectrum of $K_3Fe(CN)_6$ (0.25 mM) with imidazole (10 mM) initially (orange trace) and after resting in the dark for 18 hours (black trace).

$K_3Fe(CN)_6$ is also know to act as an oxidant,[58,91,92] and as such this raises the question of whether its oxidative capabilities will have an additional effect on the observed decay in absorption intensity. In order to answer this question, an antioxidant can be used to elicit its oxidant capabilities. One candidate was the side chain of L-histidine, imidazole, since the oxidation of L-histidine by $K_3Fe(CN)_6$ is known in the literature.[93,94] Therefore, in order to correlate a possible dependence of absorption intensity on to the oxidative capabilities of $K_3Fe(CN)_6$, $K_3Fe(CN)_6$ was irradiated in the presence of imidazole. Additionally, as imidazole does not absorb UV light in the same region as the main peak of $K_3Fe(CN)_6$ (appendix B), it is an ideal antioxidant to study in our system.

Indeed, evidence of oxidation by $K_3Fe(CN)_6$ can be seen in figure 3.3. The decrease in the absorption intensity of $K_3Fe(CN)_6$ at 419 nm is greater when in the presence of imidazole (figure 3.3C), and an increase in absorption between 475 – 570 nnn can also be seen (figure 3.3B). As very little change in absorption intensity for $K_3Fe(CN)_6$ in the presence of imidazole without irradiation was observed (figure 3.3D), it can be concluded that oxidation of imidazole by $K_3Fe(CN)_6$ is a photoinduced process that occurs under the UV LED irradiation. As our FP may also be susceptible to oxidation by $K_3Fe(CN)_6$, we must take this process into account.

With the photobleaching characteristics of $K_3Fe(CN)_6$ determined, the next step was to investigate the effects of the addition of mOrange. First of all, to determine if mOrange would interact with $K_3Fe(CN)_6$ without irradiation, a solution of mOrange (4.61×10^{-6} M) and $K_3Fe(CN)_6$ (0.25 mM) was incubated at room temperature and left overnight in the dark. From figure 3.4A, it can be seen that there is no loss of either the main $K_3Fe(CN)_6$ peak at 419 nm, or the main absorbance peak of mOrange at 548 nm. This suggests that the presence of $K_3Fe(CN)_6$ alone has no effect on mOrange.

Before examining the effects of excited $K_3Fe(CN)_6$ on mOrange, it is important to first recall chapter two. It was shown in chapter two that when mOrange was irradiated with UV light, there was a first order decay seen for both the absorbance and fluorescence with the following decay rate constants of: $k_{abs} = 2.39 \text{ X } 10^{-3} \pm 3 \text{ X } 10^{-5} \text{ min}^{-1}$ and $k_{fl} = 2.57 \text{ X } 10^{-3} \pm 2 \text{ X } 10^{-5} \text{ min}^{-1}$. This result was attributed to UV light induced β-barrel excitations. In addition, it was shown in chapter two that if two species overlap in absorbance, the total absorbance is additive suggesting that in a solution of $K_3Fe(CN)_6$ and mOrange, both species should interact with the incident UV light. Therefore, three scenarios can be predicted for the decay of mOrange in the presence of $K_3Fe(CN)_6$. The first scenario would be that excited $K_3Fe(CN)_6$ (or a by-product of its excitation) will interact with mOrange, altering the rate of decay. To determine if this scenario was occurring, a simple comparison of the rates of decay to that found in chapter two could be performed. Unfortunately, the second and third scenarios are more difficult to separate. The second scenario consists of excited $K_3Fe(CN)_6$ not interacting with mOrange, leading to the decay of mOrange following a first order decay as seen previously. Likewise, the third scenario will follow the same first order decay as seen in chapter two, yet the excited $K_3Fe(CN)_6$ would interact with the mOrange (for example with the β-barrel) but in such a manner as the rates of decay will be unaffected. Recognizing the multiple possibilities for interaction, it is imperative to closely examine the rates of decay of absorbance and fluorescence for mOrange in the presence of $K_3Fe(CN)_6$.

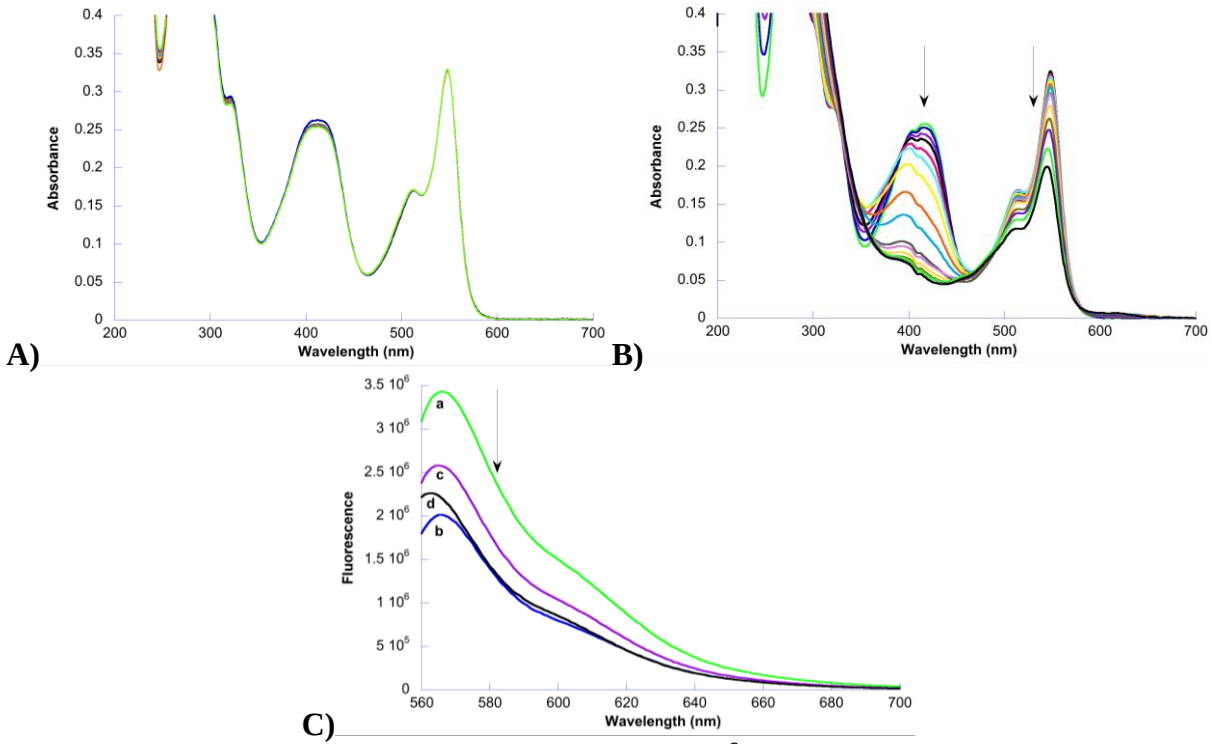

Figure 3.4: A) The absorbance of mOrange (4.61 X 10^{-6} M) and $K_3Fe(CN)_6$ (0.25 mM) while incubated overnight in the dark. B) The absorbance of mOrange (4.57 X 10^{-6} M) and $K_3Fe(CN)_6$ (0.25 mM) while exposed to the UV LED for 4 hours. C) The fluorescent emission spectra of mOrange (4.57 X 10^{-6} M) with $K_3Fe(CN)_6$ (0.25 mM) while exposed to a UV LED for 4 hours where the time points are 0 (a), 15 (b), 60 (c) and 240 (d) minutes.

To reiterate, one of the goals of this investigation is to determine the conditions leading to the formation of the FR mOrange product. As mentioned in section 3.1, the main peaks of absorbance for the FR mOrange were at 631 nm and 662 nm for absorbance and fluorescence respectively.[58] Thus in addition to examining the main fluorescence of mOrange (through excitation at 548 nm), the emission at 661 nm (through excitation at 631 nm) was monitored before and after irradiation. Concurrently, the absorbance spectra were monitored at 631 nm for any additional peak formation. From the results obtained from UV irradiation of mOrange and $K_3Fe(CN)_6$ (figure 3.4B) it can be seen that there is a definite decrease in the main absorption peaks of mOrange and $K_3Fe(CN)_6$ at 548 and 419 nm respectively. When looking at the 631 nm

region of the spectra, there appears to be a slight increase seen, however this peak was not fluorescent. Moving to the main fluorescence of mOrange when excited at 548 nm (figure 3.4C), there also appears to be a decrease as was seen for the 548 nm absorbance peak.

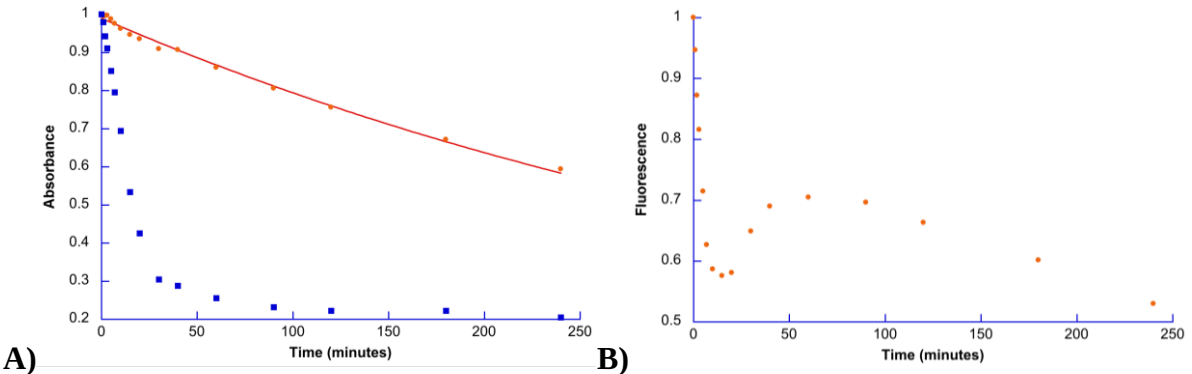

A) **B)**

Figure 3.5: A) The absorbance decay of mOrange (4.57 X 10^{-6} M) at 548 nm (orange circles, modeled with equation 2.1) and 419 nm (blue squares), in the presence of $K_3Fe(CN)_6$ (0.25 mM) while exposed to the UV LED for 4 hours. B) The fluorescent emission maxima of mOrange (4.57 X 10^{-6} M) at 565 nm in the presence of $K_3Fe(CN)_6$ (0.25 mM) while exposed to the UV LED for 4 hours. Fit analysis in appendix A.

Even with the decreases seen in the absorbance and fluorescence spectra, the trends of decay are still not apparent. Therefore, to determine if the excited $K_3Fe(CN)_6$ was interacting with mOrange, the maxima of absorbance (548 nm) and fluorescence (565 nm) were plotted as a function of time. From figure 3.5A (orange circles), the absorbance decay appears to follow a first order trend with a rate of 2.20 X 10^{-3} ± 5 X 10^{-5} min^{-1}. This rate is remarkably close to the rate of mOrange and UV light alone (2.39 X 10^{-3} ± 3 X 10^{-5} min^{-1}) suggesting that perhaps the excited $K_3Fe(CN)_6$ is not affecting the rate of decay. However, when the decay of fluorescence is examined (figure 3.5B), a massive change is seen from the expected first order rate. In fact a significant proportion of the fluorescence is lost (decreases to 57.5 %) within the first 15 minutes of irradiation, followed by a recovery to 70% at one hour, which then decrease to almost 53%

after 4 hours of irradiation. This dramatic alteration of the expected results suggests that there must be some additional mechanisms acting on the fluorescence decay seen.

These results present an intriguing situation. On the one hand, the rate of absorbance decay fits that of the UV irradiation of mOrange alone, while on the other hand the rate of fluorescence decay does not. To better understand these results, it is essential to understand what contributes to absorption and fluorescence in FPs. To start, for the absorbance spectrum of mOrange, the main peak at 548 nm represents the transition from the ground state of the chromophore to its excited state.[25,40] Conversely, fluorescence spectroscopy represents only the number of excited mOrange chromophores emitting a photon of light.[40] What is important to note about fluorescence is that not all of the excited molecules will necessarily emit light. In fact a parameter that indicates the number of chromophores undergoing fluorescent decay is known as the fluorescence quantum yield (Φ_{fl}). To clarify, Φ_{fl} is the ratio that represents the number of excited chromophores undergoing emissive decay (emission of light) over the total number of excited molecules, which for mOrange is 0.69.[25,40] This means that for a given population of unaltered excited mOrange molecules, only 69% will undergo fluorescence and emit a photon of light.

Interestingly, the fluorescence of FPs is highly dependent on the environment of the chromophore.[95] Once excited, the environment of the chromophore which is formed from the β-barrel, protects the excited chromophore from external quenching as well as from vibrational and rotational relaxing (known collectively as non-radiative decay) in order to preferentially undergo emissive decay.[73,96] In fact where most fluorescent chromophores (fluorophores) will preferentially undergo vibrational relaxation at higher temperatures, the β-barrel of FPs enable the stabilization of the excited chromophore such that fluorescence occurs even at 82 °C (as seen

in chapter two).[73] Given the necessity for a stabilizing environment to have fluorescence from the excited chromophore, if there were to be a change in the environment such that the excited chromophore was not as readily stabilized, then the number of excited chromophores undergoing emissive decay would decrease.[97] However, this would not affect the chromophore's absorbance to the same degree.[97] Specifically, excitation is a change in the orientation of a chromophore's dipole, forming a transition dipole that in FPs, the β-barrel acts to stabilize this change in orientation.[98] It is this resulting transition dipole that requires stabilization to favour emissive decay.[97,98] Thus by changing the β-barrel of mOrange, the fluorescence will be affected to a much greater degree than the absorbance. In summary, if there were to be a change to the environment of mOrange's chromophore such that the excited state would preferentially undergo non-radiative decay, then the observed absorbance would only decrease slightly, while the apparent fluorescence would decrease significantly. From the results of figure 3.5, this is suggested to be the case for the large initial decrease in the observed fluorescence of mOrange.

Specifically for the case of mOrange and $K_3Fe(CN)_6$, upon excitation with the UV LED lamp it is possible that the excited $K_3Fe(CN)_6$ could interact with the amino acids of the β-barrel of mOrange, causing the environment of the excited chromophore to be altered. The support for this interaction can be found in figure 3.3B where it was shown that excited $K_3Fe(CN)_6$ readily interacts with imidazole, leading to significantly quicker decay for its main absorption peak 419 nm. Additionally, by comparing the loss of the $K_3Fe(CN)_6$ peak at 419 nm (figure 3.5A, blue squares) with the fluorescence decay of mOrange (figure 3.5B, orange circles) it appears that the initial sharp decrease in mOrange fluorescence matches the $K_3Fe(CN)_6$ absorbance decay trend. Here it can be seen that once the $K_3Fe(CN)_6$ absorption maximum at 419 nm ceases its decrease, mOrange fluorescence undergoes its slight recovery. Thus by combining $K_3Fe(CN)_6$'s propensity

to interact with imidazole (side chain of histidine), along with its known interaction with other amino acid side chains such as phenol (tyrosine) and indole (tryptophan),[91] the interaction of excited $K_3Fe(CN)_6$ with the β-barrel of mOrange is highly likely. Considering the well known flexibility of the mFruit β-barrel,[36,75] this interaction with excited $K_3Fe(CN)_6$ could lead to a 'breathing' or stretching of the β-barrel. This expansion of the β-barrel would ultimately cause less stabilization for the excited chromophore, allowing non-radiative decay pathways to compete, resulting in the observed significant decrease in the fluorescence.

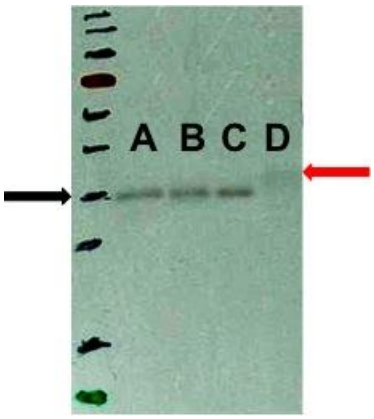

Figure 3.6: The western blot of mOrange samples where column A is purified mOrange, column B is mOrange after 4 hours exposure to UV light, column C is mOrange and $K_3Fe(CN)_6$ no irradiation, and column D is mOrange and $K_3Fe(CN)_6$ after 4 hours of UV light irradiation. The black arrow is pointing to the position of the mOrange protein band at about 34 KDa, while the red arrow is pointing to a faint but heavier band with a weight of approximately 36 KDa.

One method to determine if the excited $K_3Fe(CN)_6$ was interacting with the β-barrel of mOrange is to use western blot analysis, which utilizes antibodies specific to the β-barrel of mOrange in order to identify the protein. If the excited $K_3Fe(CN)_6$ was interacting with mOrange, it is possible that the β-barrel could be altered to such an extent that the western blot analysis would not readily recognize the protein. Following this line of thought, figure 3.6 shows the western blot of mOrange with $K_3Fe(CN)_6$, with and without UV irradiation (columns D and

C respectively). Additionally, mOrange with and without UV irradiation are shown for comparison (columns B and A respectively). From the results, the prominent mOrange band seen at 34 KDa for columns A – C, is no longer present in column D. In fact there appears to be a very faint and slightly heavier band present when mOrange is irradiated with UV light in the presence of $K_3Fe(CN)_6$ (red arrow). Given the column A of figure 3.6 is the purified mOrange protein, and the same batch of purified mOrange has been used for the subsequent columns, it can be assumed that no other proteins were present to interact with the antibodies. On top of this, column B and C demonstrated that the respective presence of UV LED irradiation and $K_3Fe(CN)_6$ alone without irradiation have no effect on the western blot analysis. These results indicate that excited $K_3Fe(CN)_6$ was interacting with the β-barrel of mOrange, providing support for the β-barrel mechanism explaining the observed fluorescence decrease.

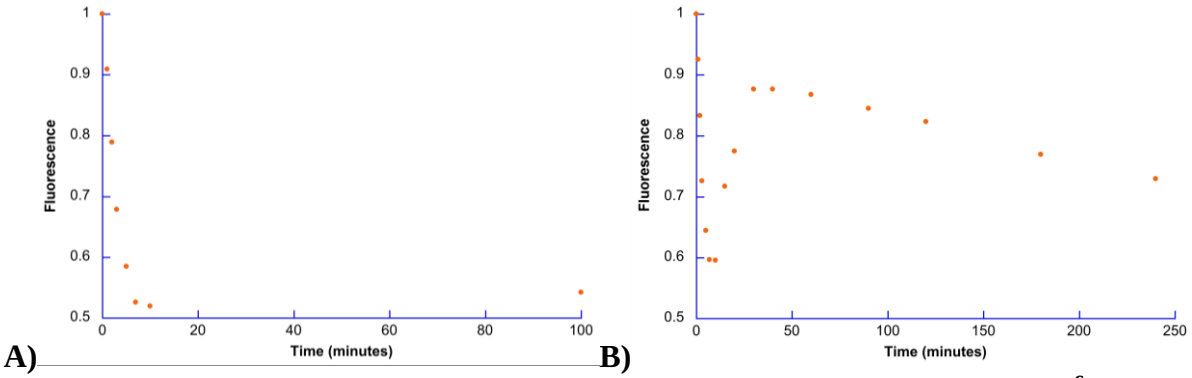

Figure 3.7: A) The fluorescence decay at 566 nm of mOrange (4.13 X 10^{-6} M) with $K_3Fe(CN)_6$ (0.25 mM) irradiated for 10 minutes with the UV LED, then stored in the dark for 90 minutes at room temperature. B) The fluorescence decay at 566 nm of mOrange (4.71 X 10^{-6} M) with $K_3Fe(CN)_6$ (0.25 mM) irradiated for 10 minutes with the UV LED, followed by the addition of imidazole (10 mM) and subsequent exposure to the UV LED for a total of 4 hours.

Based on the evidence provided, it is highly likely that the excited $K_3Fe(CN)_6$ is interacting with the β-barrel of mOrange to cause its significant fluorescence decay. Unfortunately the slight return of fluorescence is not well understood. In an effort to study the

slight return in fluorescence, two experiments were performed. In the first experiment (figure 3.7A), it was reasoned that with the disappearance of $K_3Fe(CN)_6$ correlating to the loss in fluorescence, perhaps the lack of excited species interacting with the β-barrel of mOrange could allow a slight return of the β-barrel to a more stabilizing environment for the chromophore. Thus mOrange was irradiated with the UV LED in the presence of $K_3Fe(CN)_6$ for 10 minutes, at which point the solution was stored in the dark to prevent the formation of further excited $K_3Fe(CN)_6$. From the results (figure 3.7A), there is a slight retrieval of fluorescence after 90 minutes in the dark, however it is not as significant when compared to figure 3.5B (orange circles). This suggests that the return of fluorescence is not an innate process of the $K_3Fe(CN)_6$ oxidized mOrange.

The second experiment made use of the antioxidant imidazole. The reason for the use of imidazole was that since it has been shown that $K_3Fe(CN)_6$ interacts readily with this antioxidant (figure 3.3) perhaps the addition of imidazole could mitigate the effects of any excited species created in solution. From figure 3.7B, after mOrange and $K_3Fe(CN)_6$ were irradiated for 10 minutes, the addition of imidazole resulted in a much more significant return of fluorescence (~87.5 %) when compared to mOrange and $K_3Fe(CN)_6$ alone (~70 %). These results suggest that the presence of the UV LED light is needed to achieve the return of fluorescence seen, as well as the presence of imidazole helps to mitigate further adverse effects of excited $K_3Fe(CN)_6$. Unfortunately, the mechanism of the photoinduced return is as of yet, still unclear and thus further experiments are required. However, this is beyond the scope of the current work.

Finally, to conclude the discussion of the alteration in the decay seen for fluorescence of mOrange due to excited $K_3Fe(CN)_6$, the last portion of the fluorescence decay must be addressed. As seen for the fluorescence, after the initial decrease and slight retrieval of

fluorescence, the fluorescence continues to decrease (figure 3.5B). Even with the addition of imidazole after 10 minutes, the decrease can still be seen (figure 3.7B). Unlike the retrieval of fluorescence, this result can easily be explained, since it is known that the presence of the UV light will lead to fluorescence decay in mOrange. Support for this is derived from the disappearance of the $K_3Fe(CN)_6$ peak in figure 3.5A (blue squares) where after 60 minutes little change was observed. It should be noted that the complete removal of the 419 nm peak is not expected since the initial spectra of mOrange has a non-zero value at 419 nm (see chapter two, figure 2.2A). Knowing that the absorbance at 419 will not be completely removed, with no change observed in figure 3.5A, it can be assumed that there is no further $K_3Fe(CN)_6$ to interact with mOrange. These data indicate that after 60 minutes of irradiation, only mOrange will remain to interact with the UV LED. As outlined in chapter two, this interaction with the UV LED will lead to the observed, continued fluorescence decay.

Given the data presented in this section, it is highly likely that the excited $K_3Fe(CN)_6$ interacts with mOrange to cause its loss in fluorescence. In an effort to further confirm this data, the same photobleaching experiments were carried out with the presence of imidazole (10 mM). As discussed earlier, it was shown that $K_3Fe(CN)_6$ interacts with imidazole, and from figure 3.7B the protective effects of imidazole for mOrange can be observed. Based on these observations, if imidazole did have a protective ability against excited $K_3Fe(CN)_6$ for mOrange, then the presence of imidazole should prevent the observed changes in fluorescence. The results of this experiment are shown in figure 3.8.

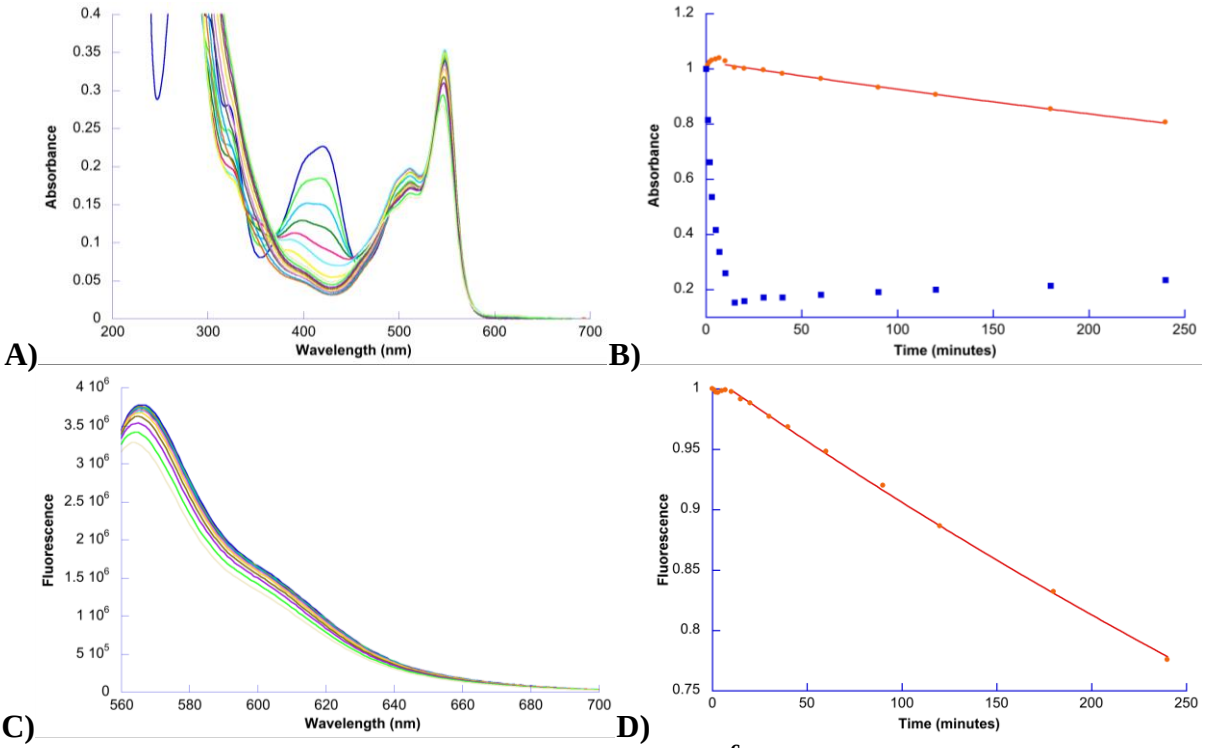

Figure 3.8: A) The absorbance of mOrange (4.79 X 10^{-6} M) and $K_3Fe(CN)_6$ (0.25 mM) with imidazole (10 mM), while exposed to the UV LED for 4 hours. B) The maximum absorbance of mOrange at 548 nm (orange circles) and 419 nm (blue squares), while in the presence of $K_3Fe(CN)_6$ (0.25 mM) and imidazole (10 mM) during exposure to the UV LED for 4 hours. C) The fluorescence of mOrange (4.79 X 10^{-6} M) and $K_3Fe(CN)_6$ (0.25 mM) with imidazole (10 mM), while exposed to the UV LED for 4 hours. D) The maximum normalized and corrected fluorescence of mOrange at 565 nm, while in the presence of $K_3Fe(CN)_6$ (0.25 mM) and imidazole (10 mM) during exposure to the UV LED for 4 hours. The data after 10 minutes, were modeled to equation 2.1 the analysis can be found in appendix A.

Looking at the results, the effects of imidazole are dramatic as the decay observed for mOrange's absorbance and fluorescence (figure 3.8A and C) is less than without imidazole. Interestingly, the maxima of absorbance (figure 3.8B) displays a slight increase in absorbance, followed by a steady decrease after 10 minutes that follows a first order decay. The delay in the decrease of absorbance until 10 minutes can be attributed to the fact that there are two absorbing species in the original solution. Briefly, since it was established that the $K_3Fe(CN)_6$ will be primarily excited by the UV LED, as long as $K_3Fe(CN)_6$ predominates in solution, then it will be

the species to primarily interact with the UV light. This indicates that until most of the $K_3Fe(CN)_6$ is degraded, mOrange will only be excited to a lesser extent. This is supported by the decrease seen for $K_3Fe(CN)_6$ at 419 nm (figure 3.8B, blue squares), where at 10 minutes most of the $K_3Fe(CN)_6$ had degraded with only a about a quarter of the peak's original intensity. The increase seen in absorbance during this 10 minute delay is unexpected, but may be explained upon inspection of figure 3.3B when $K_3Fe(CN)_6$ was irradiated with the UV LED in the presence of imidazole, as there appears to be an absorbing by-product formed within the 450 – 570 nm region. Considering the appearance of by-product overlaps with the mOrange spectra at 548 nm, the absorbance of the by-product would create an increase in absorbance that could not be attributed to mOrange. An unfortunate consequence of this absorbing by-product is that the rate of decay for mOrange is affected, resulting in a rate constant of $1.01 \times 10^{-3} \pm 3 \times 10^{-5}$ min^{-1} which is roughly half that for mOrange and UV LED ($2.39 \times 10^{-3} \pm 3 \times 10^{-5}$ min^{-1}).

Moving to the maxima of fluorescence, the protective effects of imidazole are immediately apparent with no loss of fluorescence seen for the first 7 minutes. As with the absorbance, this delay in fluorescence decay can be attributed to the fact that mOrange is not excited to the same extent until most of the $K_3Fe(CN)_6$ has been degraded. The subsequent loss in fluorescence after 10 minutes fits a first order decay with a rate constant of $1.09 \times 10^{-3} \pm 1 \times 10^{-5}$ min^{-1}. Again the rate is roughly half that seen for the UV LED and mOrange alone ($2.57 \times 10^{-3} \pm 2 \times 10^{-5}$ min^{-1}) but this is not an appropriate comparison given the presence of the absorbing by-product. Based on these results, it can be concluded that imidazole prevents the interaction of excited $K_3Fe(CN)_6$ with mOrange, confirming that it is excited $K_3Fe(CN)_6$ causing the observed decrease in fluorescence.

The study of mOrange and $K_3Fe(CN)_6$ during UV LED irradiation has enabled the investigation of the effects of excited $K_3Fe(CN)_6$. It was determined that presence of excited $K_3Fe(CN)_6$ interacts with the β-barrel of mOrange, causing the loss of β-barrel stabilization for the excited chromophore of mOrange, ultimately leading to a loss of fluorescence. However, with the lack of far-red fluorescence, it can be assumed that the sole excitation of $K_3Fe(CN)_6$ is not responsible for the FR mOrange seen by Subach *et al.*[58] Thus, the next step in the study of the FR mOrange was to look at the affects the Blue LED lamp has on the same mOrange and $K_3Fe(CN)_6$ solution.

3.3.1.2 mOrange and $K_3Fe(CN)_6$ with the Blue LED

As established in figure 3.2, the Blue LED overlaps with the absorbance spectra of mOrange and $K_3Fe(CN)_6$. Comparing the extent of overlap with that of the UV LED, there appears to be significantly less overlap for the Blue LED and $K_3Fe(CN)_6$, suggesting that the $K_3Fe(CN)_6$ will be excited to a lesser degree. Given the possibility of less excitation for $K_3Fe(CN)_6$, it is essential to first establish the interaction of $K_3Fe(CN)_6$ with the Blue LED. Additionally since imidazole demonstrated itself to be vital tool in the UV LED investigation, the effects of $K_3Fe(CN)_6$ with imidazole during Blue LED irradiation are needed to be determined. From figure 3.9 the interaction of $K_3Fe(CN)_6$ with the Blue LED can be seen.

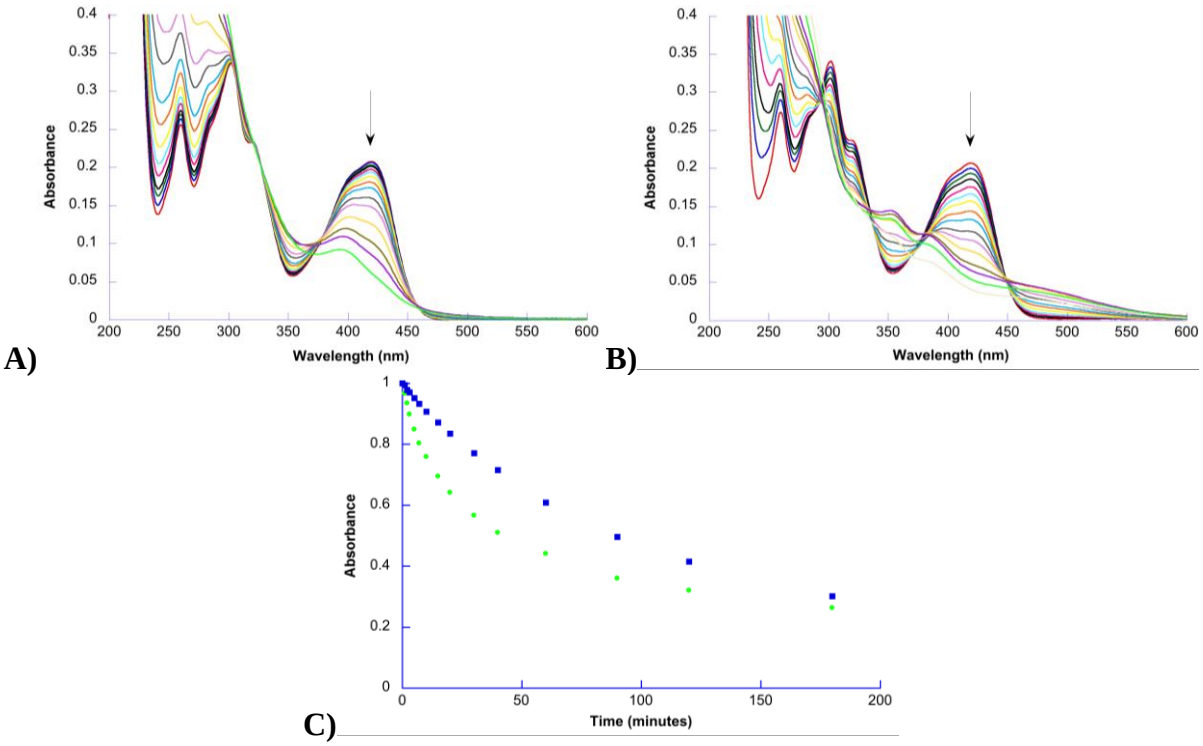

Figure 3.9: A) The absorbance of $K_3Fe(CN)_6$ (0.25 mM) while exposed to the Blue LED for 4 hours. B) The absorbance of $K_3Fe(CN)_6$ (0.25 mM) and imidazole (10 mM) while exposed to the Blue LED for 4 hours. The arrows indicate the major decrease in absorption seen. C) The 419 nm maxima decay from experiments A) (blue squares) and B) (green circles) plotted over time.

Similar to the results seen in figure 3.3, the irradiation of the $K_3Fe(CN)_6$ in the absence of protein with the Blue LED (figure 3.9A) leads to a decrease at the main 419 nm peak. This indicates that the $K_3Fe(CN)_6$ is being excited by the Blue LED, leading to its photolytic degradation. Upon addition of imidazole (figure 3.9B), the decrease seen at the main 419 nm peak appears to be enhanced, mirroring the results of the UV LED lamp, even having the appearance of the by-product between the 450 – 570 nm region. However, when the maxima at 419 nm are plotted over time (figure 3.9C), the rates of decay for both $K_3Fe(CN)_6$ and $K_3Fe(CN)_6$ with imidazole are slower than that of the UV LED. Most significantly, the main 419 nm peak was essentially removed within the first 40 minutes of UV LED irradiation (figure

3.3C) whereas the Blue LED still has some of the main peak remaining (~30%) even after three hours of irradiation. Yet, these results are not unexpected as was previously mentioned, the overlap between the Blue LED and $K_3Fe(CN)_6$ is less when compared to the UV LED. Therefore, from figure 3.9 it can be concluded that the Blue LED does lead to the excitation and subsequent photolytic degradation of $K_3Fe(CN)_6$, albeit less than seen previously.

Establishing that the Blue LED interacts with $K_3Fe(CN)_6$, as mentioned in figure 3.2 the Blue LED also overlaps with mOrange. This indicates that manner of interaction for a solution of $K_3Fe(CN)_6$ and mOrange may be different than previously described for the UV light. To get a better idea of what may happen, the results of mOrange and the Blue LED from previous chapter must be discussed. In chapter two, it was shown that the Blue LED lamp interacted with mOrange in a similar manner to the UV light. Even though the Blue LED had a slight overlap with the main peak of mOrange, the protein still photobleached in a first order manner (k_{abs} = 1.81 X 10^{-3} ± 2 X 10^{-5} min^{-1} and k_{fl} = 2.24 X 10^{-3} ± 4 X 10^{-5} min^{-1}) with similar rates to the UV LED, suggesting that mOrange was primarily interacting with the Blue LED through the excitation and subsequent alteration of its β-barrel. From this data, it is proposed that due to the small overlap between the Blue LED and mOrange, the amount of mOrange chromophores undergoing excitation during irradiation will be minute. Thus, the interaction that will be seen from the excitation of mOrange and $K_3Fe(CN)_6$ should follow the trend set out by the UV LED, suggesting that there should be little to no FR mOrange production.

With this assumption in mind, the next step in the investigation was to irradiate mOrange and $K_3Fe(CN)_6$ with the Blue LED. From the results for this experiment in figure 3.10A, it is clear that the Blue LED lamp irradiation leads to the decrease of the main 419 nm $K_3Fe(CN)_6$ peak, followed by the slight decrease in the 548 nm mOrange peak. Additionally, the shoulder of

mOrange at 515 nm appears to increase as well as the 600 – 700 nm region of the spectra. Given that the FR mOrange is expected to have a maximum absorbance at 631 nm for mOrange[58] the increase within the 600 – 700 nm region suggests the possible presence of FR mOrange. Unfortunately, when this solution was excited at 631 nm, no FR fluorescence was seen under our experimental conditions. This suggests that the increase seen is a non-fluorescent by-product similar to the results obtained with the UV LED. Moving to the fluorescence of mOrange when excited at 548 nm (figure 3.10B), the solution appears to decay as irradiation progresses. However, in order to better compare the decays seen for the Blue LED to that of the UV LED, the trends of decay need to be determined.

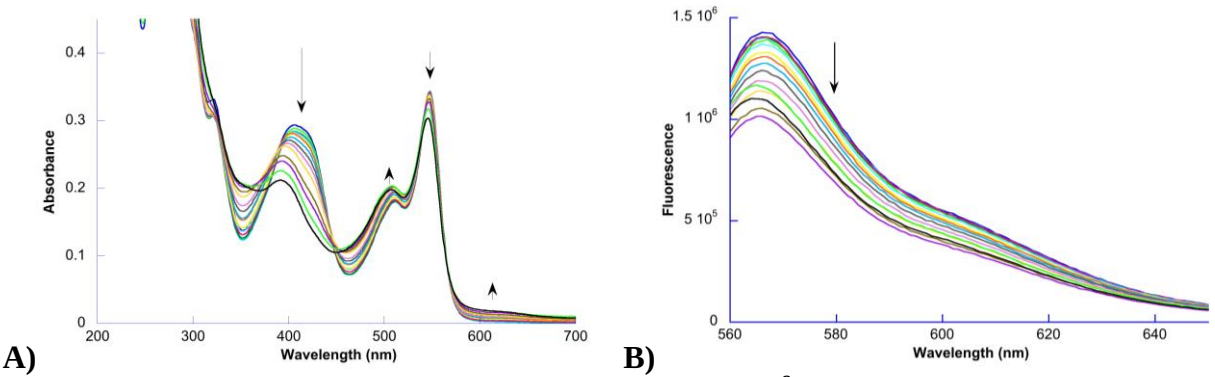

A) **B)**

Figure 3.10: A) The absorbance of mOrange (4.80 X 10^{-6} M) and $K_3Fe(CN)_6$ (0.25 mM) while exposed to the Blue LED for 4 hours. B) The fluorescent emission spectra of mOrange (4.80 X 10^{-6} M) with $K_3Fe(CN)_6$ (0.25 mM) while exposed to a Blue LED for 4 hours.

Plotting the maxima of mOrange at 548 nm (figure 3.11A, orange circles) it can be seen that mOrange starts to undergo photobleaching after 30 minutes of irradiation. This is significantly slower than that seen for the UV LED, where the absorbance decayed in a first order fashion from initial irradiation. In order to explain this delay in absorbance two factors have to be recalled. First of all, as was mentioned for the 419 nm decay when $K_3Fe(CN)_6$ was irradiated alone with the Blue LED, due to the smaller overlap of the $K_3Fe(CN)_6$ and the LED,

less $K_3Fe(CN)_6$ is excited within a given time frame. Secondly, it was seen within the UV LED irradiation of mOrange, $K_3Fe(CN)_6$ and imidazole (figure 3.8), that the predominance of $K_3Fe(CN)_6$ in solution competes with mOrange for exposure to the light. These two factors indicate that with a smaller amount of $K_3Fe(CN)_6$ undergoing decay within a given time frame, there will remain a large portion of $K_3Fe(CN)_6$ to interact with the Blue light. This suggests that the blue light will not interact with the β-barrel as readily, delaying the decay of mOrange until sufficient $K_3Fe(CN)_6$ has been degraded. This fact is supported by the slower decay of $K_3Fe(CN)_6$ (figure 3.11A, blue squares). Unfortunately, the decay of mOrange did not fit a first order decay, necessitating the fluorescence to be investigated.

Moving to the maxima of fluorescence (figure 3.11B), the first two hours of irradiation caused the fluorescence to decrease to nearly 70%. After an additional hour of irradiation, the fluorescence recovered to 80%, then decreased again to 75% after a further hour irradiation, following the same retrieval and decay seen for the UV LED. However, the extent of decay was much less than the UV LED, where the UV LED led to a 50% loss of fluorescence within the first 15 minutes. Yet given the low excitation of $K_3Fe(CN)_6$ by the Blue LED, this lower decay can be attributed to the presence of less excited $K_3Fe(CN)_6$ in solution. Considering the pattern of decay for the Blue LED is consistent with that produced by the UV LED, albeit delayed and to a lesser extent, it is plausible that these two LEDs are acting in the same manner.

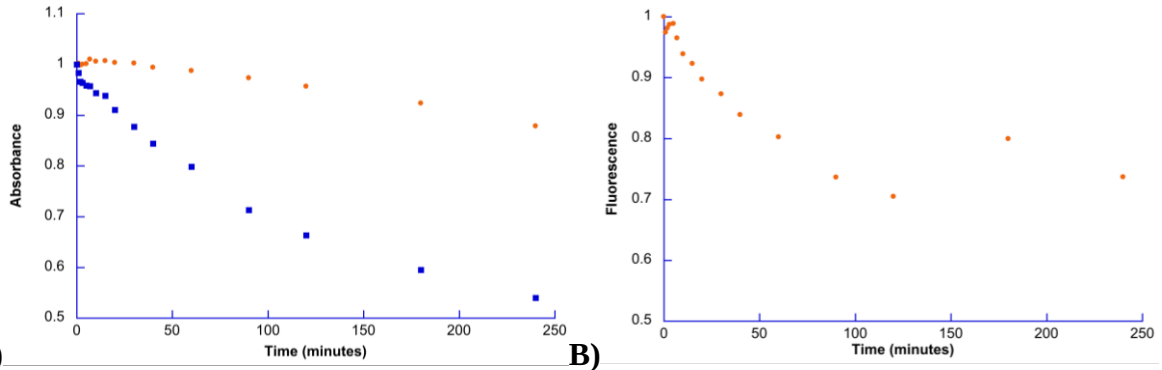

A) **B)**

Figure 3.11 A) The absorbance decay of mOrange (4.80 X 10^{-6} M) at 548 nm, in the presence of $K_3Fe(CN)_6$ (0.25 mM) while exposed to the Blue LED for 4 hours. B) The fluorescent emission maxima of mOrange (4.80 X 10^{-6} M) at 566 nm in the presence of $K_3Fe(CN)_6$ (0.25 mM) while exposed to the Blue LED for 4 hours.

To ensure that the Blue LED was indeed exciting $K_3Fe(CN)_6$ allowing it to interact with the β-barrel of mOrange, a western blot analysis was performed. From figure 3.12 the western blot of mOrange can be seen, where mOrange and mOrange after four hours of Blue LED irradiation (columns A and B) are shown. For comparison, mOrange with $K_3Fe(CN)_6$ before irradiation (column C) and after four hours of Blue light irradiation (column D) are shown. As was seen for the UV light irradiation, when $K_3Fe(CN)_6$ was excited in the presence of mOrange, it lead to the alteration of the visible protein band. These results are similar to the UV LED results, indicating that the β-barrel of mOrange is being altered by the Blue light excited $K_3Fe(CN)_6$ such that the protein is less recognized by the antibodies. Therefore, it can be concluded that the Blue LED is preferentially exciting $K_3Fe(CN)_6$ leading to the alteration of mOrange's β-barrel, resulting in the observed absorption and fluorescent trends.

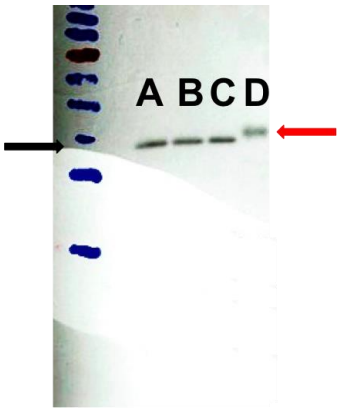

Figure 3.12: The western blot of mOrange samples where column A is purified mOrange, column B is mOrange after 4 hours exposure to the Blue LED, column C is mOrange and $K_3Fe(CN)_6$ no irradiation, and column D is mOrange and $K_3Fe(CN)_6$ after 4 hours of Blue LED irradiation. The black arrow is pointing to the position of the mOrange protein band at about 34 KDa, while the red arrow is pointing to a faint but heavier band with a weight of approximately 36 KDa.

Even with the western blot analysis, similar trend in absorption and fluorescence and lack of FR mOrange, to be certain of the method of interaction for $K_3Fe(CN)_6$ and mOrange it remains to be determined if the observed interactions can be mitigated through the addition of imidazole. Having demonstrated in figure 3.8 that the addition of imidazole prevented the interaction of excited $K_3Fe(CN)_6$ with mOrange during UV LED irradiation, this experiment was repeated for the irradiation with the Blue LED. Upon inspection of the absorbance spectra (figure 3.13A) the interaction of imidazole is not immediately clear, as the 548 nm peak of mOrange and the 419 nm peak of $K_3Fe(CN)_6$ still decay. In addition, the maxima of absorbance for mOrange (figure 3.13B, orange circles) does not display any significant changes compared to mOrange and $K_3Fe(CN)_6$ alone. The only noticeable difference is that the decay for the 548 nm peak is slightly larger in the presence of imidazole, since the decay for the 548 nm peak reached about 80% of the original intensity. Whereas for mOrange and $K_3Fe(CN)_6$ alone, the 548 nm peak only decreased to 90% of the original intensity. This suggests a quicker decay for mOrange with the

presence of imidazole. This intriguing result is counterintuitive as it was shown that the presence of imidazole mitigates the interaction of excited $K_3Fe(CN)_6$, yet the key to this difference lies in the 419 nm decay of $K_3Fe(CN)_6$. From figure 3.13B (blue squares) the decay for $K_3Fe(CN)_6$ with imidazole present is occurring at a quicker rate than that of mOrange and $K_3Fe(CN)_6$ alone (figure 3.11A, blue squares). As was seen for the UV LED, once enough $K_3Fe(CN)_6$ has been degraded in solution, a greater portion of mOrange can interact with the incoming light, leading to a greater decay. This suggests that since the $K_3Fe(CN)_6$ is decaying faster with imidazole present, a greater amount of mOrange will interact with the Blue LED, leading to more mOrange proteins undergoing decay. However, the effects of imidazole are best described through the fluorescent decay.

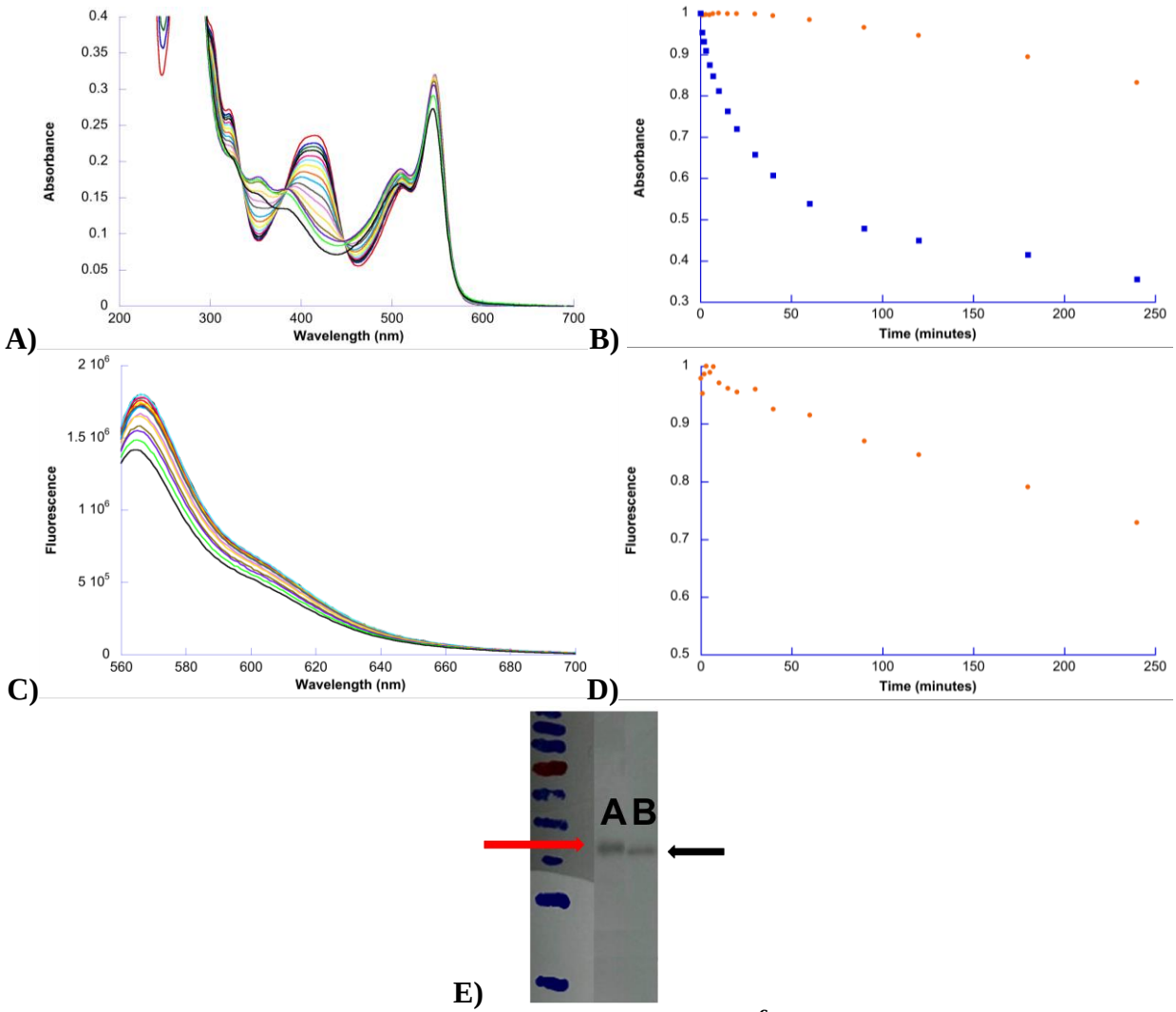

Figure 3.13: A) The absorbance of mOrange (4.51 X 10^{-6} M) and $K_3Fe(CN)_6$ (0.25 mM) with imidazole (10 mM), while exposed to the Blue LED for 4 hours. B) The maximum absorbance of mOrange at 548 nm (orange circle) and 419 nm (blue squares), while in the presence of $K_3Fe(CN)_6$ (0.25 mM) and imidazole (10 mM) during exposure to the Blue LED for 4 hours. C) The fluorescence of mOrange (4.51 X 10^{-6} M) and $K_3Fe(CN)_6$ (0.25 mM) with imidazole (10 mM), while exposed to the Blue LED for 4 hours. D) The maximum normalized and corrected fluorescence of mOrange at 565 nm, while in the presence of $K_3Fe(CN)_6$ (0.25 mM) and imidazole (10 mM) during exposure to the Blue LED for 4 hours. These experiments were performed once. E) The western blot of mOrange and $K_3Fe(CN)_6$ (column A) and mOrange, $K_3Fe(CN)_6$ and imidazole (column B) after 4 hours irradiation with the Blue LED. The ready arrow points to the heavier and faint band while the black arrow points to the expected mOrange band.

Similar to the results of the UV LED, the trend of fluorescence decay (figure 3.13D) loses the prominent decay within the first two hours of irradiation, as well as the retrieval,

instead assuming a consistent decay pattern. This suggests that the addition of imidazole is indeed mitigating the effects of the excited $K_3Fe(CN)_6$ on mOrange. In support of this conclusion is the western blot of mOrange, $K_3Fe(CN)_6$ and imidazole (figure 3.13E) where with imidazole present (column B), mOrange resumes the solid, protein band around 34 kDa, compared to the 36 kDa mOrange band with only $K_3Fe(CN)_6$ (column A).

In summary, the use of the Blue LED caused the excitation of $K_3Fe(CN)_6$, albeit to a lesser extent than the UV LED, ultimately resulting in the loss of fluorescence and absorbance for mOrange. These observed decays were due to the interaction of excited $K_3Fe(CN)_6$ with the β-barrel of mOrange, as shown by the western blot analysis, and were mitigated through the addition of imidazole. However, given that the excitation of a solution of mOrange and $K_3Fe(CN)_6$ did not result in the desired FR mOrange, the next step in this investigation was to excite this solution using the Green LED.

3.3.1.3 mOrange and $K_3Fe(CN)_6$ with the Green LED

With the UV and Blue LEDs failing to produce the desired FR mOrange in the presence of $K_3Fe(CN)_6$, it can be assumed that the excitation of $K_3Fe(CN)_6$ is not responsible for the FR mOrange. This leaves the investigation to focus on the excitation of mOrange in the presence of $K_3Fe(CN)_6$. As mentioned previously, it was essential that only mOrange was excited, thus the Green LED was used in combination with a 488 nm shortwave cut-off filter. This ensured that only wavelengths longer than 488 nm would be incident upon the mOrange and $K_3Fe(CN)_6$ solution. Looking back to figure 3.2, the lack of significant overlap between $K_3Fe(CN)_6$ and the Green LED spectrum supports this prediction. However, to ensure that $K_3Fe(CN)_6$ was not excited during irradiation with the Green LED, a solution of $K_3Fe(CN)_6$ was exposed to the

Green LED for 4 hours (figure 3.14A). From the results, there is no significant observable change at the characteristic 419 nm peak of $K_3Fe(CN)_6$. This indicates that indeed, the Green LED is not interacting with $K_3Fe(CN)_6$ to cause its photolytic degradation.

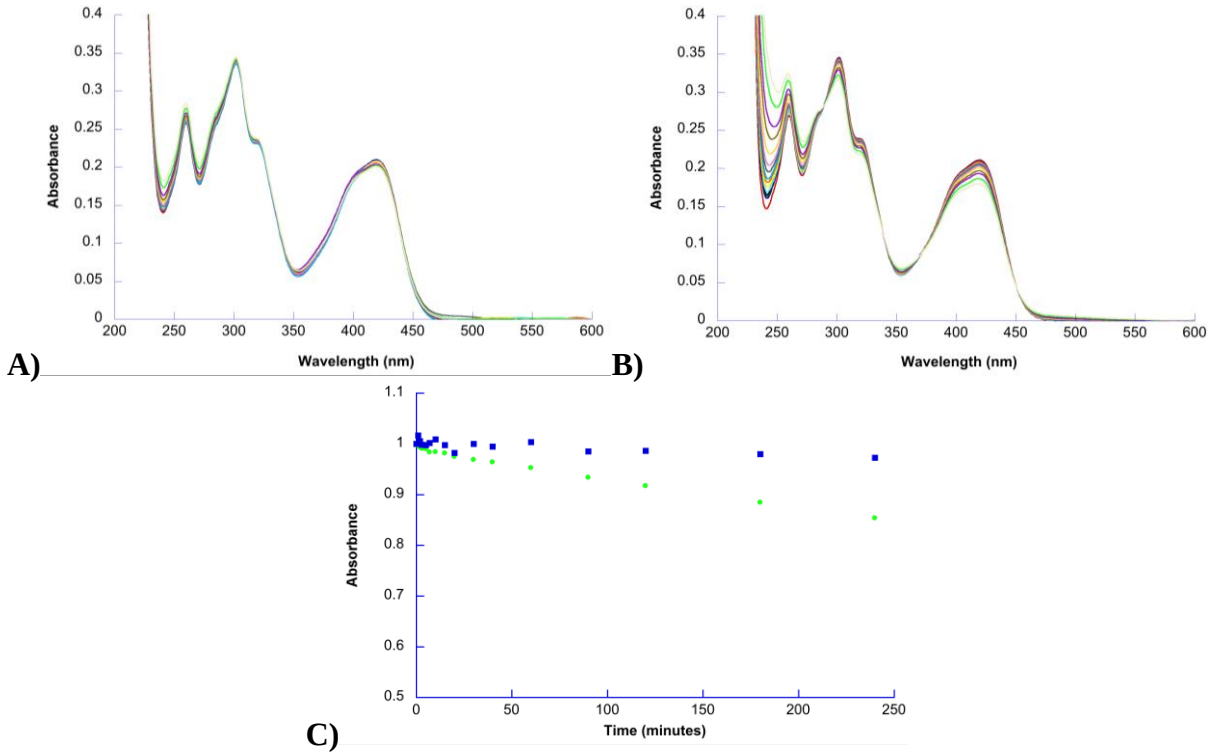

Figure 3.14: A) The absorbance of $K_3Fe(CN)_6$ (0.25 mM) while exposed to the Green LED for 4 hours. B) The absorbance of $K_3Fe(CN)_6$ (0.25 mM) and imidazole (10 mM) while exposed to the Green LED for 4 hours. C) The absorbance at 419 nm for $K_3Fe(CN)_6$ (blue squares) and $K_3Fe(CN)_6$ with imidazole (green circles) while exposed to the Green LED for 4 hours.

Moving to the addition of imidazole in figure 3.14B, there appears to be a slight decrease at the 419 nm peak. From the previous experiments of $K_3Fe(CN)_6$ and imidazole using the Blue and UV LEDs, it was shown that when imidazole was present there was an enhanced decay for the $K_3Fe(CN)_6$ peak. This suggests that with the antioxidant present, there is a slight decay induced by the Green LED. However, given the relatively small amount of decrease seen for the 419 nm peak (figure 3.14C, green circles) where after four hours only 10% of the original

intensity was lost, the photolytic induce degradation is very low for the Green LED. Unfortunately this suggests that even with the cut-off filter, there is a small overlap between the $K_3Fe(CN)_6$ and the Green LED. Thus, this excitation of $K_3Fe(CN)_6$ will have to be taken into consideration during the investigation of mOrange, $K_3Fe(CN)_6$ and the Green LED lamp.

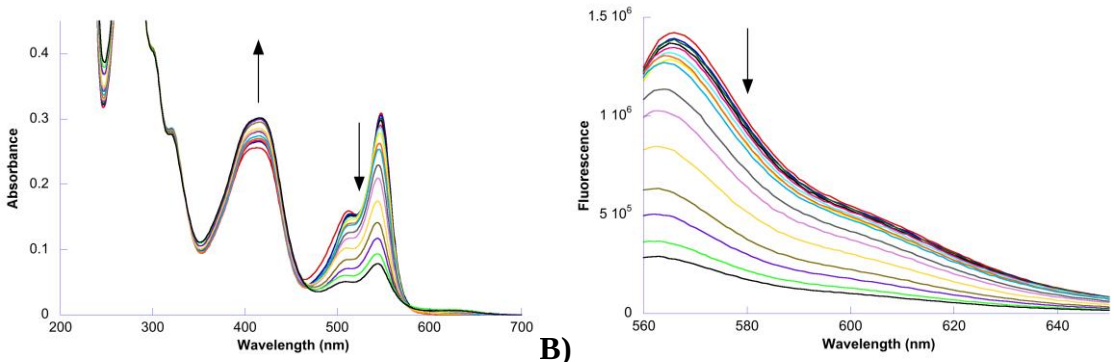

A) **B)**

Figure 3.15: A) The absorbance of mOrange (4.36 X 10^{-6} M) and $K_3Fe(CN)_6$ (0.25 mM) while exposed to the Green LED for 4 hours. B) The fluorescent emission spectra of mOrange (4.36 X 10^{-6} M) with $K_3Fe(CN)_6$ (0.25 mM) while exposed to the Green LED for 4 hours.

After having established the slight interaction of the Green LED and $K_3Fe(CN)_6$, the next step was to determine mOrange's interaction with $K_3Fe(CN)_6$ upon excitation. Thus, a solution of mOrange and $K_3Fe(CN)_6$ was irradiated with the Green LED for four hours. From the results in figure 3.15A, it can be seen that the main peak of mOrange at 548 nm decreases significantly, whereas the peak at 419 nm increased in intensity. Recalling the results from chapter two, upon irradiation of mOrange with the Green LED, the main peak at 548 nm decreased via a bi-exponential decay due to the presence of both the green immature and mature mOrange. Concurrently, there was an increase at 406 nm due to the appearance of the by-products of photobleaching. This protonated by-product appearance when mOrange was irradiated alone with the Green LED, would suggest that the $K_3Fe(CN)_6$ peak at 419 nm should increase when in the presence of mOrange and the Green LED. The reason for this is due to the lack of change

seen for $K_3Fe(CN)_6$ and the Green LED alone (figure 3.14C blue squares) and the fact that absorbance is additive. Thus if the there is no interaction between $K_3Fe(CN)_6$ and mOrange during the Green LED excitation, then by removing the spectra of $K_3Fe(CN)_6$ (figure 3.14A) from the spectra of mOrange and $K_3Fe(CN)_6$ (figure 3.15A), the resulting spectra should resemble mOrange's interaction with the Green LED alone, as can be seen in figure 3.16A.

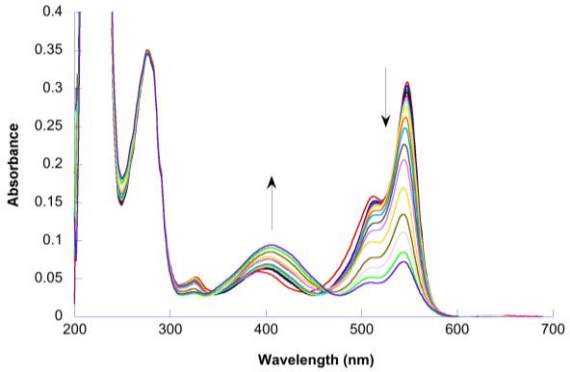

Figure 3.16: The resulting absorbance spectrum of mOrange (4.36 X 10^{-6} M) after having the absorbance spectrum of $K_3Fe(CN)_6$ (0.25 mM) while exposed to the Green LED for 4 hours, removed from the absorbance spectrum of mOrange (4.36 X 10^{-6} M) and $K_3Fe(CN)_6$ (0.25 mM) while exposed to the Green LED for 4 hours.

On top of having the differential spectra that resembles mOrange and the Green LED alone, the significant loss of fluorescence (figure 3.15B) indicates that the presence of $K_3Fe(CN)_6$ has no effect on mOrange during photobleaching. However, before any conclusions can be drawn, the trends of decay have to be examined for mOrange's loss in absorbance and fluorescence. Upon inspection of figures 3.17, the loss in absorbance at 548 nm and fluorescence intensity at 565nm were best fitted by a bi-exponential decay. The rate constants obtained under these experimental conditions were compared to those obtained from mOrange and the Green LED alone (table 3.1).

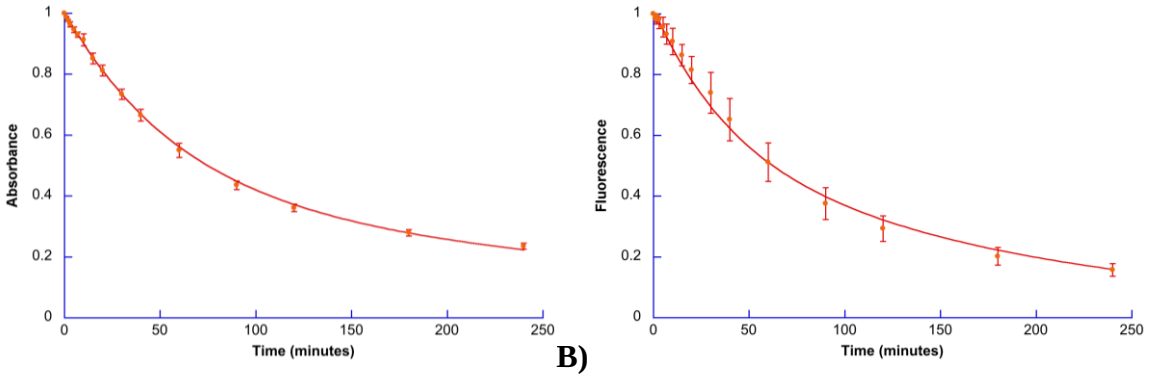

A) **B)**

Figure 3.17: A) The absorbance decay of mOrange (at 548 nm, in the presence of $K_3Fe(CN)_6$ (0.25 mM) while exposed to the Green LED for 4 hours. This experiment was repeated three times. B) The fluorescent emission maxima of mOrange at 565 nm in the presence of $K_3Fe(CN)_6$ (0.25 mM) while exposed to the Green LED for 4 hours. This experiment was repeated three times. The data was modeled with equation 2.2a and the analysis is in appendix A.

Table 3.1: The comparison of the rates of decay at 548 nm (absorbance) and 565 nm (fluorescence) for mOrange and $K_3Fe(CN)_6$ irradiated with the Green LED (+) to that of mOrange irradiated with the Green LED alone (-). The experimental results of mOrange alone (-) were directly taken from chapter two. *A* and *B* represent the contributions of the mature and the green immature mOrange respectively.

λ_{max} ($K_3Fe(CN)_6$)	*A*	k_1 (min^{-1})	*B*	k_2 (min^{-1})
548 nm (+)	0.397 (±0.104)	0.00259 (±0.00104)	0.607 (±0.102)	0.0167 (±0.00231)
548 nm (-)	0.404 (±0.019)	0.000907 (±0.000216)	0.598 (±0.018)	0.0216 (±0.000803)
565 nm (+)	0.575 (±0.226)	0.00548 (±0.00202)	0.440 (±0.221)	0.0256 (±0.0109)
565 nm (-)	0.262 (±0.038)	0.000804 (±0.000669)	0.744 (±0.037)	0.0215 (±0.00131)

In chapter two, it was determined through the use of laser irradiation that k_2 was linked to the decay of the green immature mOrange while k_1 was linked to the decay of the mature mOrange. Upon inspection of the k_2 rate constants in table 3.1, the rate of decay for the green immature mOrange is actually slightly slowed for the absorbance in the presence of $K_3Fe(CN)_6$.

However, the rate constant for the decay in fluorescence suggests that there is no observable change from the contribution of the green immature mOrange. Thus it appears from the data that $K_3Fe(CN)_6$ has no significant impact on the disappearance of the immature form of mOrange. Conversely, the k_1 rate constants both for the absorbance and fluorescence suggest that there is an order of magnitude faster decay for mature mOrange when $K_3Fe(CN)_6$ is present. In order to explain the impact of $K_3Fe(CN)_6$ on the rate constant for the mature protein disappearance, two different scenarios can be imagined. Although it needs to be noted, that caution is to be exercised for the interpretation of these results, as there is significant error for the observed rate constants. Thus, the following discussion is speculative on the observed changes in the rate constants. The first scenario comes from the interaction of excited $K_3Fe(CN)_6$ with imidazole (figures 3.3B and 3.9B), where an absorbing by-product was created in the 450 – 570 nm region. Given that imidazole is the side chain of L-histidine, which is an amino acid of mOrange,[25] it is possible that the slight excitation of $K_3Fe(CN)_6$ by the Green LED has led to the appearance an absorbing by-product. This by-product would then slightly alter the observed decay rate for the absorbance and fluorescence. Unfortunately, without a way to quantify the amount of this absorbing by-product, it is not possible to remove the effects of this by-product from the spectra. However, western blot analysis provides important information. Indeed, the western blot of mOrange in the presence of $K_3Fe(CN)_6$ after four hours of irradiation with the Green LED (figure 3.18) indicates no change to the β-barrel of mOrange. This means that if there is any excited $K_3Fe(CN)_6$, it is not interacting with the β-barrel of mOrange to any significant extent, making the first scenario involving a by-product of $K_3Fe(CN)_6$ unlikely.

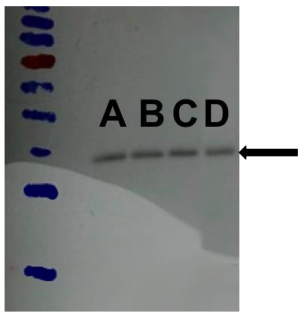

Figure 3.18: The western blot of mOrange (column A), mOrange after 4 hours Green LED irradiation (column B), mOrange and $K_3Fe(CN)_6$ no irradiation (column C) and mOrange and and $K_3Fe(CN)_6$ after 4 hours irradiation with the Green LED (column D). The black arrow points to the expected mOrange band at 34 kDa.

The second scenario that may be contributing to this fluctuation in the rate constants could be that the excited mOrange chromophores are indeed interacting with the $K_3Fe(CN)_6$ in solution, creating the desired FR mOrange. With a greater number of excited mOrange molecules being acted on, it is possible that the rates of decay will be affected. Support for this idea comes from the proposed mechanism of Subach *et al.* where it was proposed that the excited mature mOrange chromophore was interacting with the $K_3Fe(CN)_6$.[58] Thus with more excited mOrange undergoing decay, the rate for the decay of mature mOrange would be altered in the presence of $K_3Fe(CN)_6$. Therefore, with the observed alterations in the decay rate constant for mature mOrange, there should be the appearance of FR mOrange in the absorbance spectra.

To determine if there was the photoconversion of mOrange to the FR mOrange during irradiation, the absorbance at 631 nm from figure 3.15A was plotted. From the trend at 631 nm (figure 3.19A), there appears to be the presence of a FR product after four hours of irradiation. Indeed, when this solution was excited at 631 nm, fluorescence at 661 nm was observed (figure 3.19B, black trace). However, this fluorescence was so weak in comparison to the main fluorescence at 565 nm (figure 3.19B, orange trace), the experimental parameters had to be altered to better follow the appearance of the FR fluorescence. Thus, the slits on the PTI

fluorimeter were doubled to 4 nm for excitation light and tripled to 6 nm for the detector. Repeating the exposure of mOrange and $K_3Fe(CN)_6$ to the Green LED, the FR mOrange fluorescence was monitored. It can be seen from figure 3.19C and D that with the optimized parameters, the presence of the FR mOrange could be readily observed and has its maximum at the expected 661 nm. With the presence of the FR mOrange and the concurrent change to the mature mOrange rate constants, the data indicates that an excitation event of the mature mOrange is the initiating factor that leads to the formation of the FR mOrange. However, to better corroborate this link, as was shown in chapter two for the growth of the protonated by-product and the decay of mOrange, by matching the rate constants for the growth of the FR mOrange and the decay of the mature mOrange, a link between the species can be drawn. Unfortunately, the growth of the 631 nm absorbance (figure 3.19A) or the 661 nm fluorescence peak (figure 3.19D) could not be fit to either a first order or bi-exponential growth. Thus, without a proper analysis, the growth of the FR mOrange cannot be linked to mature mOrange.

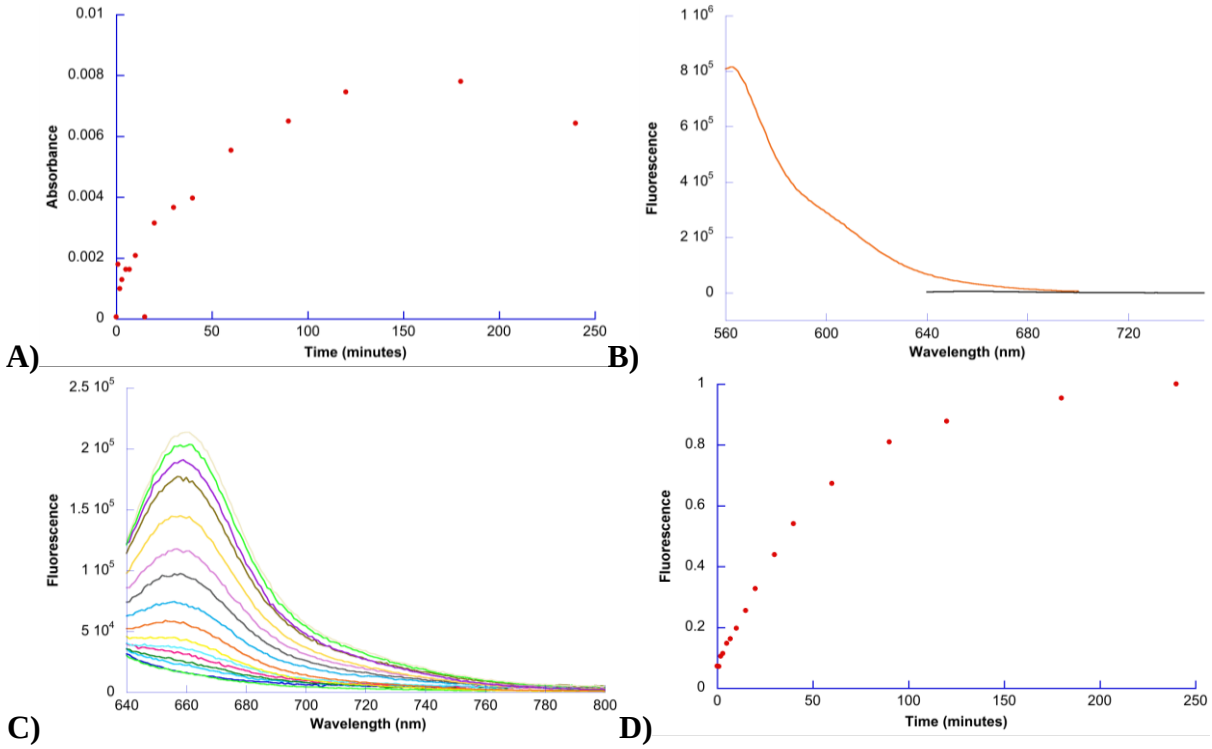

Figure 3.19: A) The absorbance of mOrange (4.36 X 10^{-6} M) at 631 nm in the presence of $K_3Fe(CN)_6$ (0.25 mM) while exposed to the Green LED for 4 hours. B) The fluorescent emission of mOrange when excited at 548 nm (orange trace) and 631 nm (black trace), while in the presence of $K_3Fe(CN)_6$ (0.25 mM) after exposure to the Green LED for 4 hours. C) The fluorescence of mOrange (4.54 X 10^{-6} M) when excited at 631 nm, while in the presence of $K_3Fe(CN)_6$ (0.25 mM) during exposure to the Green LED for 4 hours. D) The maximum normalized and corrected fluorescence of mOrange (4.54 X 10^{-6} M) at 661 nm, while in the presence of $K_3Fe(CN)_6$ (0.25 mM) during exposure to the Green LED for 4 hours.

Before any further conclusions can be drawn on the observed alterations to the decay rate constants for mOrange, one final option must be explored which arises out of the combination of exciting both $K_3Fe(CN)_6$ and mOrange simultaneously to produce the FR mOrange. In agreement with this option is the very low amount of FR mOrange (4.65 X 10^{-7} M) produced, at about 10% of the original mOrange concentration, based on the reported[58] extinction coefficient of 17,200 cm^{-1} M^{-1} and an absorbance value of 0.008. With less than 10% of the $K_3Fe(CN)_6$ lost through excitation during the Green LED irradiation, this low percentile of excited $K_3Fe(CN)_6$

could account for the small conversion of mOrange. Therefore to test this theory, if imidazole were to be added, the excited $K_3Fe(CN)_6$ should preferentially interact with the imidazole preventing the formation of the FR mOrange. Carrying out this thought process, mOrange, $K_3Fe(CN)_6$ and imidazole were irradiated with the Green LED for four hours. Afterwards the solution was excited at 631 nm, and from figure 3.20 the FR fluorescence is apparent. This result indicates that it is not the combination of excited $K_3Fe(CN)_6$ and mOrange that leads to the production of the FR mOrange.

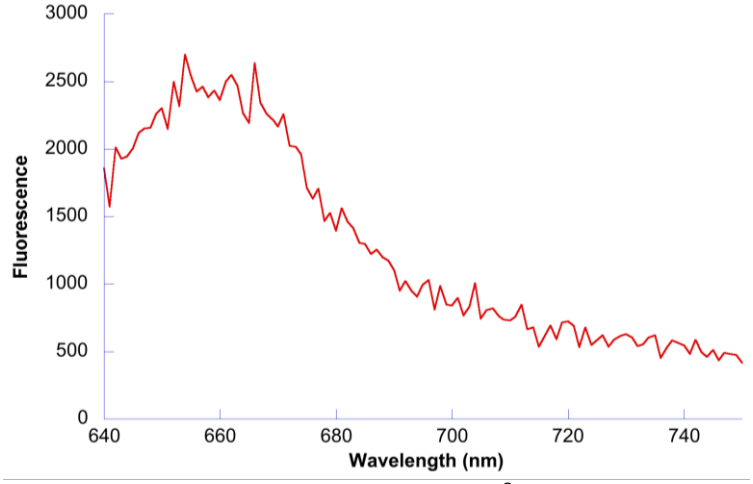

Figure 3.20: The fluorescence of mOrange (4.70 X 10^{-6} M) when excited at 631 nm, in the presence of $K_3Fe(CN)_6$ (0.25 mM) and imidazole (10 mM) after being exposed to the Green LED for 4 hours. The fluorimeter had 2 nm slits for excitation and detection.

In summary, having explored the use of the UV and Blue LED on solutions of mOrange and $K_3Fe(CN)_6$, it was determined through the use of absorbance and fluorescence spectroscopy, that excited $K_3Fe(CN)_6$ alone is not responsible for the production of the FR mOrange. Instead it was shown that excited $K_3Fe(CN)_6$ leads to the dramatic decrease in mOrange fluorescence, which can be mitigated through the addition of imidazole. Therefore, moving to the Green LED allowed the exploration of the excitation of mOrange in the presence of $K_3Fe(CN)_6$. As predicted by Subach *et al.*, our results indicates that it is the sole excitation of mOrange that can initialize

an interaction with unexcited $K_3Fe(CN)_6$, leading to the desired FR mOrange. Unfortunately, the growth kinetics of the FR mOrange could not be fit to either a first order or bi-exponential decay, preventing a connection from being formed between the mature mOrange decay. However, from the experiments carried out in chapter two, it was shown that a link between produced by-products of photobleaching could be elucidated using a tuneable laser. Thus, to determine from which species (if not both) the FR mOrange was being converted, the solution of mOrange and $K_3Fe(CN)_6$ was excited using the Opotek Inc. Vibrant 355 tunable NIR-Vis pulsed laser (10 Hz).

3.3.2 mOrange and $K_3Fe(CN)_6$ with LASER light

Chapter two saw the separation of the individual components responsible for the decay of mOrange through the use of four distinct wavelengths of excitation: 497, 532, 548 and 560 nm. It was shown that at 497 nm, primarily the green immature mOrange was being excited. As the wavelength of excitation was moved to the red, a greater contribution of the mature mOrange was seen until 560 nm where the mature mOrange was primarily excited. Considering the high power LED investigation has demonstrated that it is an excitation event of mOrange in the presence of $K_3Fe(CN)_6$ which leads to the formation of the FR mOrange, it is necessary to determine from which species, if not both, the FR mOrange is originating. Therefore, solutions of mOrange and $K_3Fe(CN)_6$ were excited with the same setup described in chapter two, using each excitation wavelength, monitoring the resultant absorbance and fluorescence. Yet, before these experiments could be carried out, the interaction of $K_3Fe(CN)_6$ with the laser was required. Unlike the previous sections, the use of imidazole will not be employed as it was shown in the Green LED section (section 3.3.1.3) that upon addition of imidazole to the solution of mOrange and $K_3Fe(CN)_6$, no difference in amount of FR mOrange was seen. Moving to the results, from figure 3.21 it can be seen that with the 497 nm laser excitation no change occurred to the

$K_3Fe(CN)_6$ spectra, indicating no $K_3Fe(CN)_6$ was excited by the 497 nm laser. Given that the 497 nm laser is the only wavelength that is close in proximity to the $K_3Fe(CN)_6$ (absorbance from 200 – 475 nm, figure 3.21) is can be assumed that the three other red shifted wavelengths of excitation will not interact with $K_3Fe(CN)_6$.

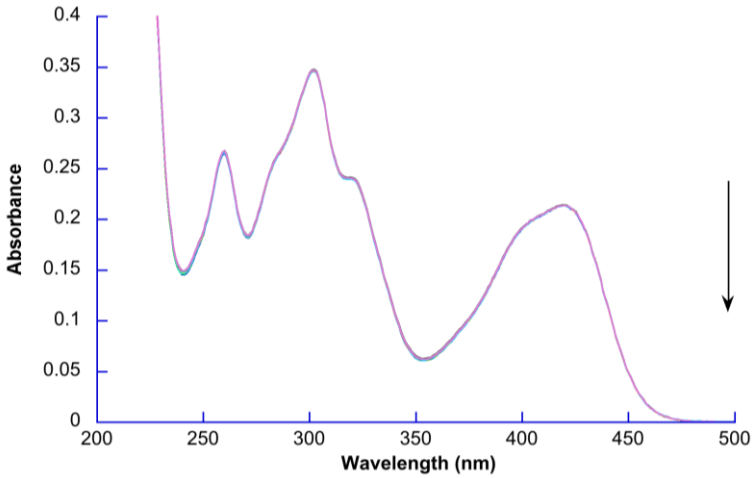

Figure 3.21: The absorbance of $K_3Fe(CN)_6$ (0.25 mM) while exposed to a pulsed laser (497 nm, 9.12 ± 0.44 mJ, 10Hz) for 1000 shots. The arrow indicates the wavelength of excitation relative to the absorbance spectrum.

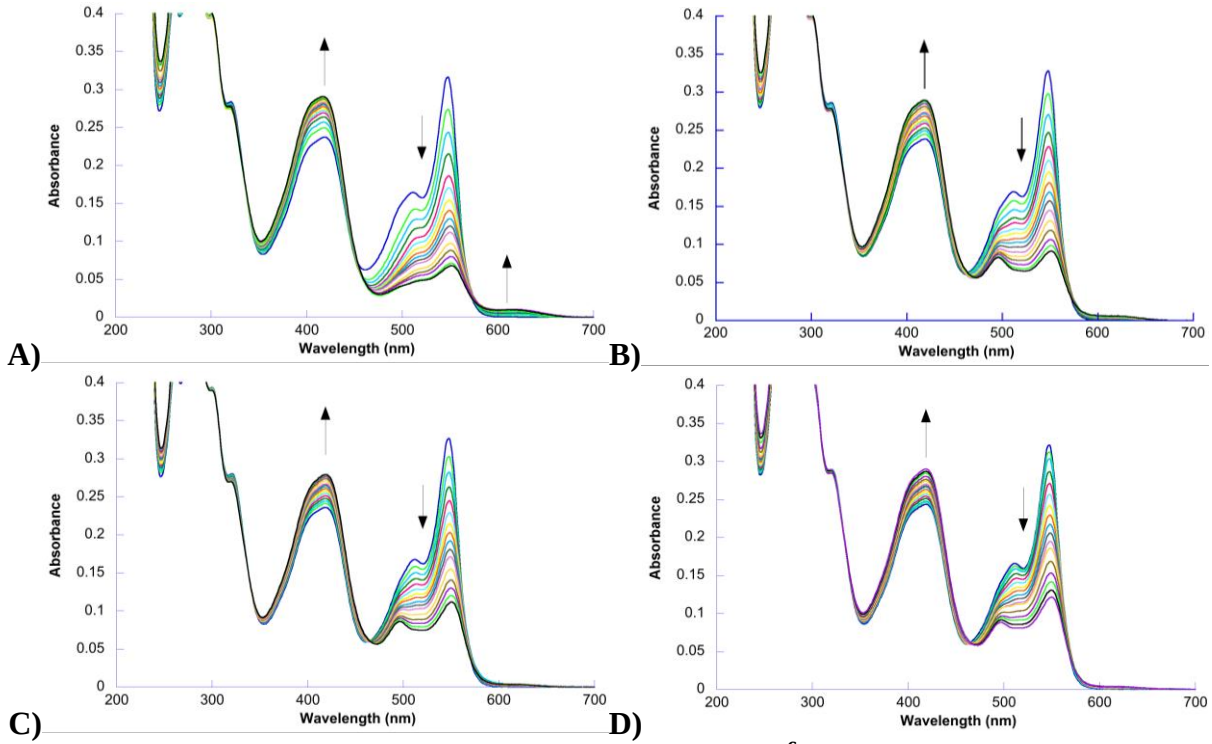

Figure 3.22: A) The absorbance of mOrange (4.46 X 10^{-6}M) with $K_3Fe(CN)_6$ (0.25 mM) while exposed to a pulsed laser (497 nm, 10.78 ± 0.61 mJ, 10Hz) for 1000 shots. B) The absorbance of mOrange (4.62 X 10^{-6} M) with $K_3Fe(CN)_6$ (0.25 mM) in PBS while exposed to a laser (532 nm, 10 ± 2.50 mJ, 10Hz) for 1000 shots. C) The absorbance of mOrange (4.60 X 10^{-6} M) with $K_3Fe(CN)_6$ (0.25 mM) while exposed to a pulsed laser (548 nm, 10 ± 2.50 mJ, 10Hz) for 1000 shots. D) The absorbance of mOrange (4.52 X 10^{-6} M) with $K_3Fe(CN)_6$ (0.25 mM) while exposed to a pulsed laser (560 nm, 19.51 ± 7.45 mJ, 10Hz) for 1000 shots. The arrows indicate the direction of change observed in the absorption spectra.

In figure 3.22, the laser excitation of mOrange in the presence of $K_3Fe(CN)_6$ is shown for all four wavelengths of excitation. Common to each wavelength of excitation is the decrease of the mOrange 548 nm peak, and increase of the 419 nm $K_3Fe(CN)_6$ peak. As was suggested in the Green LED section (section 3.3.1.3), this increase at the 419 nm peak is due to the presence of the protonated by-product of mOrange and the decrease at 548 nm is associated to the photobleaching of mOrange. Therefore, our experiment indicate that mOrange in the presence of $K_3Fe(CN)_6$ is behaving in a similar manner to that seen for the laser excitation of mOrange alone. In addition to this, mirroring the results of chapter two is the observation of the green

immature mOrange peak upon irradiation using the 532, 548 and 560 nm laser excitation wavelengths (figure 3.22B – D), as well as its absence with the use of 497 nm laser excitation (figure 3.22A). However, where the results deviate from those of chapter two is seen after 1000 shots of the pulsed laser. Upon inspection of the FR mOrange region at 631 nm, there appears to be an increased presence of an absorbing species with the 497 nm laser excitation (3.23A, red circles), while it is almost non-existent with the 560 nm laser excitation (figure 3.23A orange triangles). As was mentioned previously, it was shown that the 497 nm laser excitation was primarily interacting with the green immature mOrange. Thus, with the increased presence of the FR mOrange with 497 nm laser excitation, this data appears to suggest a link between the FR mOrange and the green immature mOrange. To confirm this, the rates of decay for mOrange were examined (figure 3.23B and table 3.2).

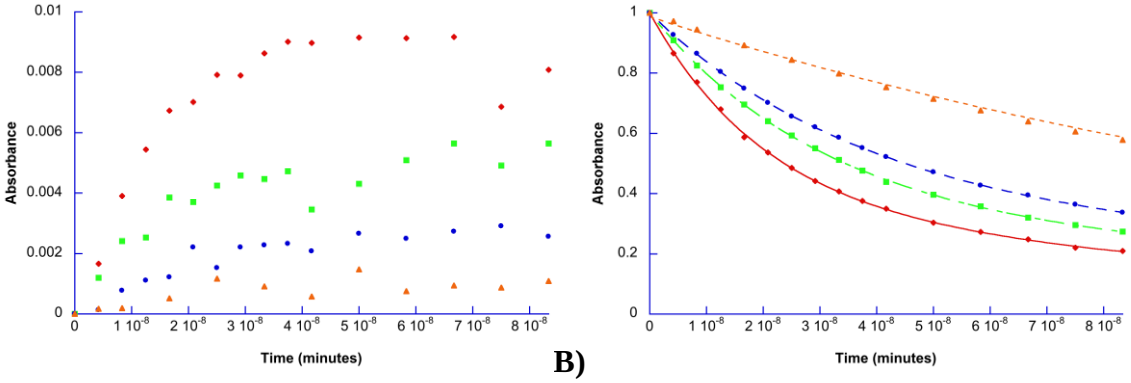

A) **B)**

Figure 3.23: A) The absorbance of mOrange at 631 nm with $K_3Fe(CN)_6$ (0.25 mM) while exposed to the pulsed laser for 1000 shots. Where the wavelengths of irradiation are 497 nm (red diamonds), 532 nm (green squares), 548 nm (blue circles), and 560 nm (orange triangles). B) The absorbance of mOrange at 548 nm with $K_3Fe(CN)_6$ (0.25 mM) while exposed to the pulsed laser for 1000 shots. Where the wavelengths of irradiation are 497 nm (red diamonds), 532 nm (green squares), 548 nm (blue circles), and 560 nm (orange triangles). The data were fitted such that 497 nm, 532 nm and 548 nm laser irradiations were modeled by equation 2.2a, while the 560 nm irradiation was modeled by equation 2.1. The fit analysis can be found in appendix A.

Table 3.2 The values from the overall decay as determined through the analysis of the maximum absorbance at 548 nm of mOrange during photobleaching at the indicated wavelengths.

Wavelength of Irradiation	*A*	k_1 (min^{-1})	*B*	k_2 (min^{-1})
497 nm	0.367 (±0.049)	7.40 X 10^6 (±1.57 X 10^6)	0.634 (±0.048)	5.01 X 10^7 (±3.5 X 10^6)
532 nm	0.324 (±0.064)	4.20 X 10^6 (±1.79 X 10^6)	0.674 (±0.063)	3.25 X 10^7 (±2.3 X 10^6)
548 nm	0.366 (±0.058)	3.67 X 10^6 (±1.24 X 10^6)	0.634 (±0.057)	2.67 X 10^7 (±1.6 X 10^6)
560 nm	0.988 (±0.006)	6.24 X 10^6 (±1 X 105)	-	-

Fascinatingly, when mOrange was irradiated in the presence of $K_3Fe(CN)_6$ with the 497 nm laser, the decay pattern follows a bi-exponential decay. When compared to the 497 nm induced decay pattern of mOrange alone (first order decay), the additional decay rate constant suggests a second decay pathway for the green immature mOrange. On the other hand, the observed decay of the mature mOrange remains a first order when excited at 560 nm, suggesting that the mature mOrange is acting in a similar manner to that seen in chapter two. Specifically, it was established through peak deconvolution and rate analysis in chapter two that only the mature mOrange is excited upon 560 nm laser irradiation. Thus, if the mature mOrange were to be undergoing a second decay pathway by interacting with $K_3Fe(CN)_6$ then the decay should follow a more complex pattern. Due to mOrange's first order decay upon 560 nm irradiation in the presence of $K_3Fe(CN)_6$, the link between the mature mOrange converting to the FR mOrange is not supported.

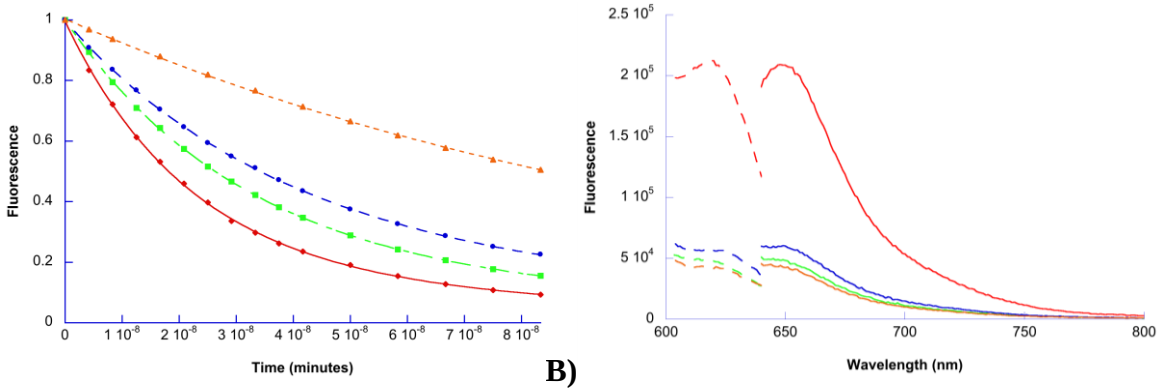

A) **B)**

Figure 3.24: A) The max normalized and corrected fluorescence of mOrange at 565 nm, when excited at 548 nm, while in the presence of $K_3Fe(CN)_6$ (0.25 mM) during exposure to the pulsed laser for 1000 shots. Where the wavelengths of irradiation are 497 nm (red diamonds), 532 nm (green squares), 548 nm (blue circles), and 560 nm (orange triangles). The data were fitted such that 497 nm, 532 nm and 548 nm laser irradiations were modeled by equation 2.2a, while the 560 nm irradiation was modeled by equation 2.1. The fit analysis can be found in appendix A. B) The excitation (661 nm emission, dashed traces) and emission (631 nm excitation, solid traces) spectra of mOrange in the presence of $K_3Fe(CN)_6$ (0.25 mM) after photobleaching with the 497 nm (red traces), 532 nm (green traces), 548 nm (blue traces) or 560 nm (orange traces) laser.

Upon inspection of the rates of decay for mOrange's fluorescence (figure 3.24A), the link between the green immature mOrange and the FR mOrange is given further weight. Indeed, where in chapter two it was seen that mOrange's fluorescence decays with a first order rate during photobleaching with the 497 nm laser, when in the presence of $K_3Fe(CN)_6$, mOrange's fluorescence follows now a bi-exponential decay. This confirms the trend seen in absorbance. Additionally, the lack of mature mOrange contribution to the production of the FR mOrange is confirmed with the fluorescence of mOrange during irradiation with the 560 nm laser. From figure 3.24A (orange trace), the mature mOrange follows the expected first order decay. Therefore, this data suggests that there exists some link between the peak appearing at 631 nm and the loss of the green immature mOrange. Hence, to ensure that the observed peak at 631 nm was the desired FR mOrange, each solution after irradiation was assessed for fluorescence through the excitation at 631 nm (figure 3.24B, solid traces). Additionally, the excitation spectra

were taken for emission at 661 nm (figure 3.24B, dashed traces). From the results, the presence of the FR mOrange is most prominent for the mOrange and $K_3Fe(CN)_6$ solution that was irradiated with the 497 nm laser, while it was the least apparent for the 560 nm laser irradiation, adding further evidence for the link between the FR mOrange and the decay of the green immature mOrange. However, it could be argued that the observed trend is due to the differences in relative bleaching of mOrange as well as the relative power for each wavelength of laser excitaiton. Ergo, to determine if the observed trend for FR mOrange production was a function of laser power and relative mOrange decay amount within 1000 shots, all the solutions were photobleached until an absorbance of about 0.1 (about 66% of the original 548 nm intensity) was reached. However, no change was observed in the relative amount of FR mOrange seen for each wavelength of excitation, indicating that the amount laser power was not a factor in FR mOrange development.

Therefore, from the data of the laser irradiation, it has been shown that the disappearance of the green immature mOrange has a link to the appearance of the FR mOrange species, due to the prominence of the 631 nm peak in the absorbance, the 661 nm peak in the fluorescence and the bi-exponential decay for the 497 nm laser irradiation. Yet to confirm this data, it will be of benefit to separate the green immature mOrange and the mature mOrange. Hence, to achieve the separation, the solution of mOrange and $K_3Fe(CN)_6$ will need to be heated to 82 °C, in order to removed the possibility of exciting the green immature mOrange altogether.

3.3.3 mOrange and $K_3Fe(CN)_6$ with Heat

Unique to the entirety of this work has been the photobleaching of FPs at elevated temperature. Made possible by the stable β-barrel of FPs, this new method of photobleaching has provided the ability to separate the photophysical properties of two physically inseparable FPs.

Thus to confirm the link between the green immature mOrange and the FR mOrange, the solution of mOrange and $K_3Fe(CN)_6$ needs to be heated. As was shown in chapter two, by heating mOrange to 82 °C the photophysical presence of the green immature mOrange will be removed from solution. Therefore, if the green immature mOrange cannot be excited, then the FR mOrange should not be able to be created. Before this experiment can be undertaken, however, it is necessary to first determine the effects of heat on both $K_3Fe(CN)_6$ and mOrange in the presence of $K_3Fe(CN)_6$ to ensure no other reactions are taken place at the high temperatures.

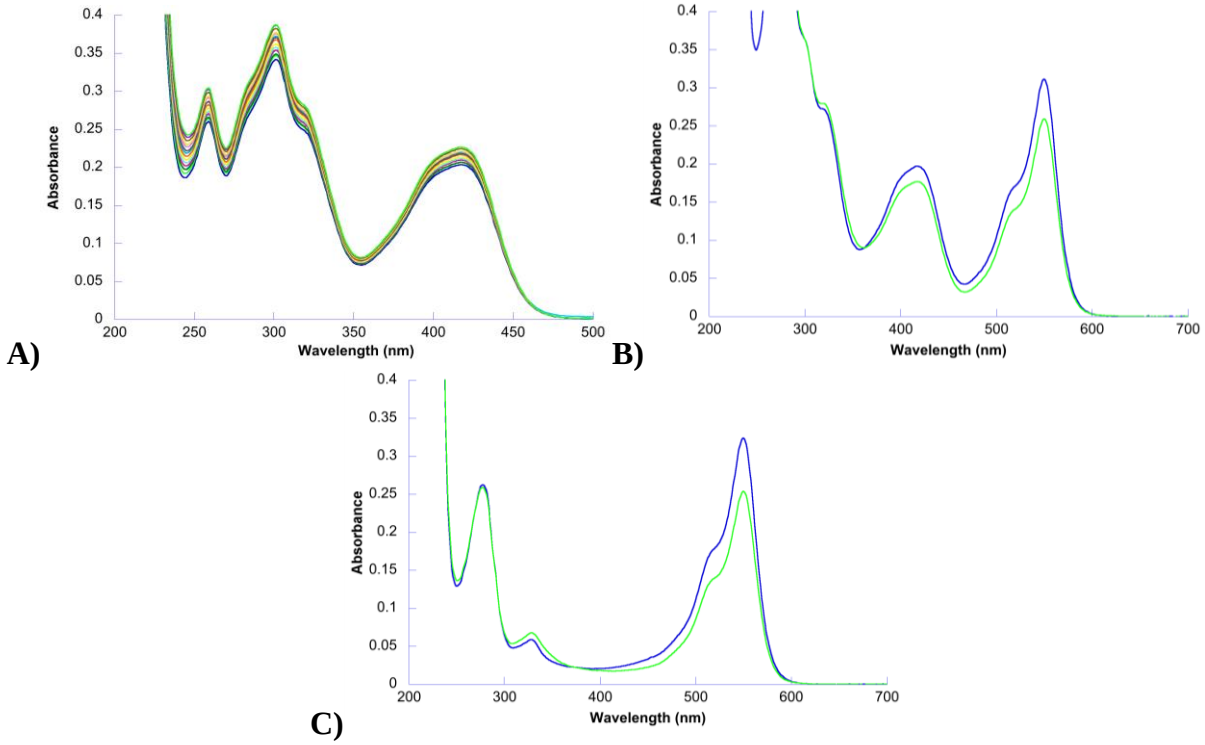

Figure 3.25: A) The absorbance of $K_3Fe(CN)_6$ (0.25 mM) while maintained at 82 °C for 2.5 hours. The increase in the absorbance spectra is due to evaporation. B) The absorbance of mOrange (5.21 X 10^{-6} M) and $K_3Fe(CN)_6$ (0.25 mM) while maintained at 82 °C for 2 hours. C) The absorbance of mOrange (5.40 X 10^{-6} M) while maintained at 82 °C for 2 hours. For B) and C), the initial absorbance at 82 °C is the blue trace while the 2 hour absorbance is the green trace.

From figure 3.25A, by maintaining $K_3Fe(CN)_6$ at 82 °C there in no decrease seen, instead a slight global increase occurs as the solution evaporates. This suggests that the $K_3Fe(CN)_6$ is

stable at the elevated temperature. Moving to the absorbance spectra of mOrange and $K_3Fe(CN)_6$ at 82 °C (figure 3.25B), it can be seen that the 550 nm main peak of mature mOrange decreases along with the $K_3Fe(CN)_6$ peak, indicating a possible interaction. However, from the absorbance spectra of mature mOrange alone at 82 °C, there is a similar decrease occurring, suggesting that although relatively stable compared to the green immature mOrange, the mature mOrange is slowly denaturing at 82 °C, leading to some loss of its absorbance. Based on these controls, it can be assumed that the mature mOrange and the $K_3Fe(CN)_6$ are not interacting at 82 °C.

Having established the non-reactivity of mature mOrange and $K_3Fe(CN)_6$ at high temperatures, the final step in the investigation of the FR mOrange was to irradiate mature mOrange in the presence of $K_3Fe(CN)_6$ at 82 °C. This experiment was carried out, with the results presented in figure 3.36A. Immediately apparent from these results, is the drastic increase of an absorbing by-product at 620 nm. With the apparent decrease of the 550 nm mature mOrange peak and the concurrent decrease of the 419 nm $K_3Fe(CN)_6$ peak, this suggests that the excitation of mature mOrange is actually linked to the appearance of this 620 nm species. This result was unexpected as it hypothesized in the previous section that FR mOrange was linked to the interaction of the excited immature mOrange and $K_3Fe(CN)_6$. To determine if the 620 nm species was the desired FR mOrange, the fluorescent excitation spectrum was taken (figure 3.26B). From the appearance of the correlating peak at 620 nm, the evidence is in support that the new absorbing species was indeed the FR mOrange. It should be noted that the blue-shift of the FR mOrange from 631 nm is unexpected, however if the β-barrel of the FR mOrange were to be less stabilizing for the chromophore at 82 °C this could lead to the observed blue shift. This is based on the results of Cody *et al.* where the chromophore of GFP is significantly blue-shifted without the β-barrel.[99]

Realizing the potential link of the mature mOrange to the FR mOrange, the main evidence that would help support this connection would be the rate of decay. Essentially, if the excited mOrange were to interact with the $K_3Fe(CN)_6$, then there would be at least two deactivation pathways for the excited mature mOrange. Considering that the decay was first order for mOrange when photobleached at 560 nm in the presence of $K_3Fe(CN)_6$, the logical result of the mature mOrange contributing to the FR mOrange at 82 °C would be an observed change in the decay pattern.

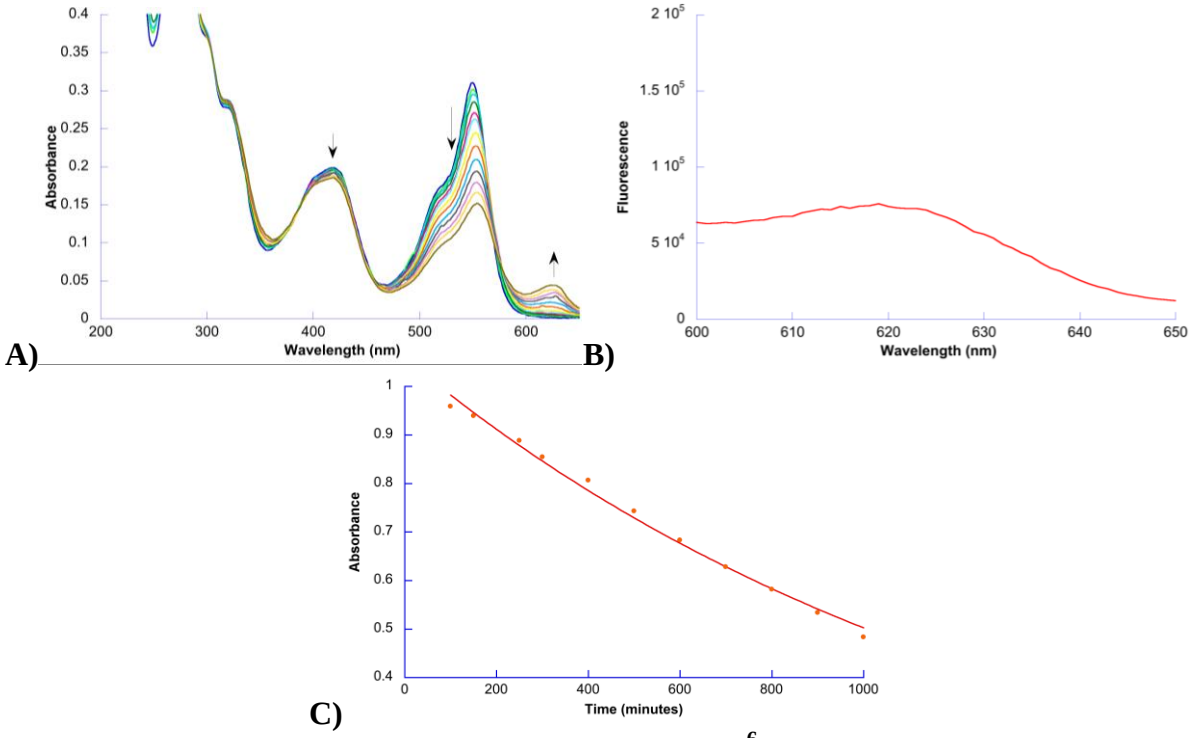

Figure 3.26: A) The absorbance of mOrange (5.12 X 10^{-6} M) and $K_3Fe(CN)_6$ (0.25 mM) 82 °C while irradiated with the pulse laser (532 nm, 5.073 ± 0.579 mJ, 10 Hz) for 1000 shots. The arrows indicate the direction of change. B) The excitation spectra of mOrange (for emission at 661 nm) while irradiated with the pulse laser (532 nm, 5.073 ± 0.579 mJ, 10 Hz) for 1000 shots in the presence of $K_3Fe(CN)_6$. C) The maximum normalized absorbance at 550 nm for A), modeled by equation 2.1.

Following the pattern of decay, figure 3.26C demonstrates a first order decay with a rate constant of 8.93 X 10^6 ± 2.59 X 10^5 min^{-1}, which is similar to the rate constant found in figure

3.23B (orange trace) during 560 nm laser excitation ($6.24 \times 10^6 \pm 1 \times 10^5$ min^{-1}). This indicates that the mature mOrange is decaying in a similar manner to that seen when no FR mOrange was created. Thus, the kinetics results seem to reject a link between the excitation of the mature mOrange and the production of a FR mOrange.

With the rate constant of the mature mOrange working against a link to the FR mOrange, there must be another reason for the appearance of the observed FR mOrange. Taking stock of the previous information presented in this chapter, the high power LED data has suggested that the FR mOrange is created when mOrange is excited, and not $K_3Fe(CN)_6$. From the room temperature laser excitation, it was shown that there exists a dependency of the FR mOrange on the excitation of the green immature mOrange, observed during the 497 nm laser excitation. However as was just shown in figure 3.26, when the green immature mOrange was prevented from becoming excited through the temperature selective denaturation, the FR mOrange still appeared without affecting the decay pattern of the mature mOrange. All of this data leads to the proposition that it is not the direct excitation of the mature mOrange that is leading to the FR mOrange. Strikingly, this observation is in direct contrast to the conclusion of Subach *et al*. who assumed that the mature mOrange was undergoing oxidative reddening through its excite state interaction with $K_3Fe(CN)_6$.[58]

Considering it is suggested that the FR mOrange is not a direct consequence of mOrange excitation, there exists only one other possibility. This last option comes from the fact that the photobleaching of mOrange leads to a protonated by-product. To expand on this idea, when mOrange undergoes photobleaching the presence of a protonated by-product appears at 420 nm. If the FR mOrange does not originate from the excited mOrange, and from the control experiments of mOrange and $K_3Fe(CN)_6$ in the dark (appendix B for room temperature and

figure 3.25B for 82 °C) where it was shown that the FR mOrange does not originate from the unphotobleached mOrange, then the only source of protein left to create the FR mOrange would be the pronated by-products of photobleaching. Therefore if this were true, then the FR mOrange should appear without excitation, given the presence of the protonated by-product. Following this logic, a solution of mOrange was irradiated with the 532 nm pulsed laser for 1000 shots at 82 °C then had $K_3Fe(CN)_6$ added without further irradiation. The results are displayed in figure 3.27.

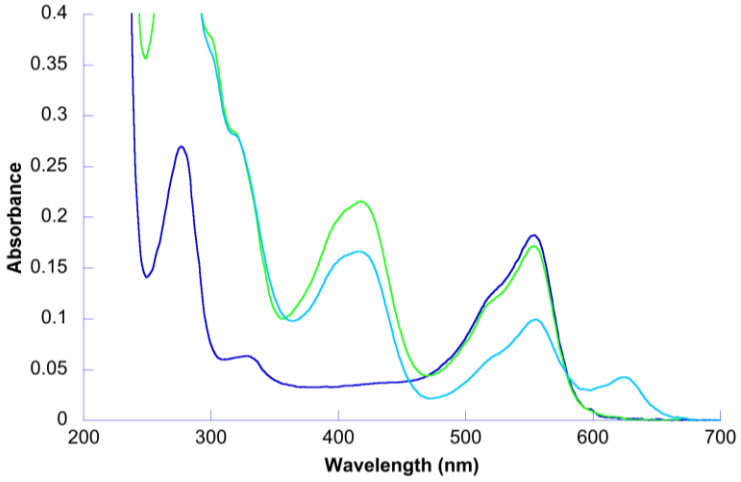

Figure 3.27: The absorbance of mOrange (5.41 X 10^{-6} M) at 82 °C after 1000 shots of the pulsed laser (532 nm, 7.196 ± 0.570 mJ, 10Hz) represented by the dark blue trace. After 1000 shots, $K_3Fe(CN)_6$ was added to a final concentration of 0.25 mM, shown as the green trace. The resulting solution was maintained at 82 °C for 2.5 hours (similar time frame for laser excitation experiment) which is shown as the light blue trace.

Remarkably, by first photobleaching mOrange then incubating the resultant products with $K_3Fe(CN)_6$ in the dark, there appears to be the presence of FR mOrange (figure 3.27, light blue trace). Additionally it can be seen that the 419 nm KFeCN peak and the 548 nm mOrange peak decrease. However this is expected, as the control experiment (figure 3.25B) of KFeCN and mOrange at 82 C displayed a similar behaviour. Conversely, this control experiment did not show the production of the FR mOrange. Therefore, the decrease observed at the 548 nm peak

cannot be link to the presence of the FR mOrange. Since the addition of $K_3Fe(CN)_6$ occurred without any further irradiation, the observed FR mOrange cannot be contributed to an excitation event. This leaves the denatured green immature mOrange and protonated by-product of mOrange as the sources of the FR mOrange. Where the proposed conversion of the protonated by-product to the FR mOrange can be thought of as the following:

$$mO_{Ma} + h\nu \rightarrow mO_{MaPB}, \text{ Scheme 3.1}$$

where mO_{Ma} is mature mOrange undergoing excitation when in the presence of light, $h\nu$, leading to the protonated by-product (mO_{MaPB}). With the creation of the protonated by-product, $K_3Fe(CN)_6$ can now interact with it, forming the FR mOrange according to the following reaction:

$$mO_{MaPB} + K_3Fe(CN)_6 \rightarrow FRmO + X, \text{ Scheme 3.2}$$

where *FRmO* represents the FR mOrange, and *X* is some by-product resulting from $K_3Fe(CN)_6$'s interaction with the mO_{PB}. Additionally, the denatured green immature mOrange can undergo an interaction with $K_3Fe(CN)_6$ to produce the FR mOrange according to a similar reaction:

$$mO_{GrDN} + K_3Fe(CN)_6 \rightarrow FRmO + X, \text{ Scheme 3.3}$$

where mO_{GrDN} is the denatured green immature mOrange.

A ramification of this process is that the FR mOrange should be able to appear upon addition of $K_3Fe(CN)_6$ to a previously photobleached solution of mOrange carried out at room temperature. Thus two separate solutions of mOrange were photobleached using either the 532 nm pulsed laser or the Green LED. Once irradiated, $K_3Fe(CN)_6$ was added to the solutions and they were maintained in the dark for and additional three hours. From the results in figure 3.28, the appearance of the FR mOrange couldn't be observed in both of these experiments. This

intriguing result is unexpected, yet an explanation for this lies in the ability to access the chromophore.

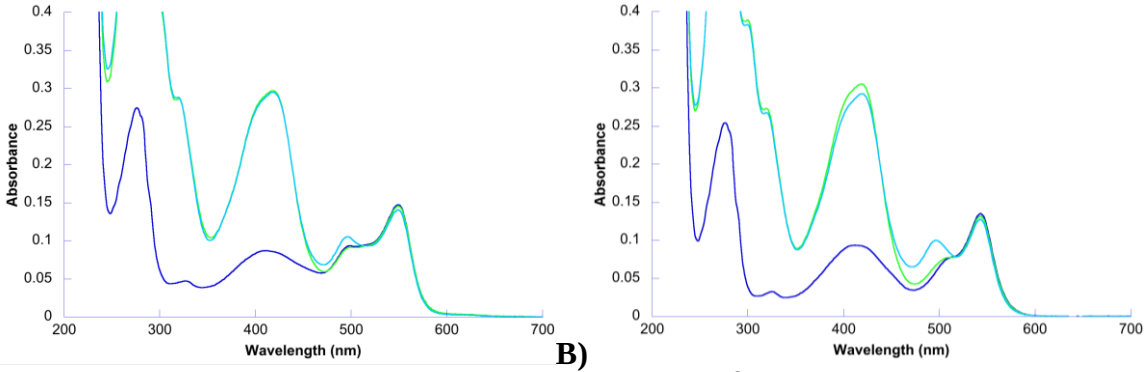

A) **B)**

Figure 3.28: A) The absorbance of mOrange (5.24 X 10^{-6} M) at room temperature after 1000 shots of the pulsed laser (532 nm, 4.572 ± 0.500 mJ, 10Hz) represented by the dark blue trace. After 1000 shots, $K_3Fe(CN)_6$ was added to a final concentration of 0.25 mM, shown as the green trace. The resulting solution was maintained in the dark for 3 hours, which is shown as the light blue trace. B) The absorbance of mOrange (5.24 X 10^{-6} M) at room temperature after 3 hours exposure to the Green LED, represented by the dark blue trace. After irradiation, $K_3Fe(CN)_6$ was added to a final concentration of 0.25 mM, shown as the green trace. The resulting solution was maintained in the dark for 3 hours, which is shown as the light blue trace.

Given that the portion of mOrange responsible for its absorbance is the chromophore,[67] in order to see a red shift in absorbance it stands to reason that the chromophore of mOrange must undergo an oxidation. However as previously discussed, the β-barrel of mOrange protects the chromophore from the external environment enabling its absorbance and fluorescence. Therefore, the chromophore is relatively protected against external factors influencing its characteristics. It was only until the work of Regmi *et al*. and Chapagain *et al*. that through theoretical models, it was shown that the β-barrel of mFruit FPs undergo fluctuations during an excitation event allowing solvent access to the chromophore.[74,75] Thus, in order to gain access to the chromophore, there needs to be an excitation event. Alternatively it was shown in chapter two that by heating the protein solution, both the green immature mOrange and the protonated by-products of photobleaching could be denatured. Assuming that the heat denaturation process

opens the chromophore to the solvent, when the protein solution is held at 82 °C, those proteins that have undergone denaturation would have allowed easy access to their chromophores. Essentially what is being proposed is that there are two methods in which $K_3Fe(CN)_6$ could interact with the photobleached protonated by-products of mOrange.

The first method is when there exists an excitation event, allowing the solvent to come into contact with the chromophore. Of the two mOrange species in solution, the most likely to undergo a β-barrel fluctuation during excitation is the green immature mOrange. Support for this idea stems from the fact that the green immature mOrange is less stable at 82 °C, which can be attributed to the relative strength of the β-barrel to resist the heat.[98] In addition to the less stable β-barrel, through the laser excitation results in section 3.3.2, it was shown that exciting the green immature mOrange results in the greatest amount of FR mOrange. This suggests that that when the green immature mOrange is excited, the chromophore is able to be exposed to the solvent, and once it becomes protonated, it can interact with the $K_3Fe(CN)_6$ resulting in the FR mOrange. Therefore, when the experiments were run at room temperature in figure 3.28, without the light induced β-barrel fluctuation, $K_3Fe(CN)_6$ could not interact with chromophores of the newly formed protonated by-products, preventing their conversion to the FR mOrange.

The second method for achieving the FR mOrange, is to expose the protonated by-products to the solvent through heat denaturation. As was shown in chapter two, the addition of heat to the photobleached solutions of mOrange results in their denaturation, marked by a global increase in absorbance due to Rayleigh scattering. With the abundant amount of protonated by-products from both the green immature and mature mOrange undergoing denaturation, there would be a large amount of chromophores exposed to the solvent. This suggests that there should be a greater increase in the observed FR mOrange at 82 °C compared to the same experiment carried

out a room temperature. Confirming this line of thought are the results of figure 3.27, suggesting that indeed the $K_3Fe(CN)_6$ is interacting not with the excited chromophore itself, rather it is interacting with mOrange's protonated by-products of photobleaching

Based on the results obtained from the addition of heat to the solution of mOrange and $K_3Fe(CN)_6$ it was demonstrated that increased temperature leads to greater FR mOrange production. Given the relatively unaltered rate of decay for the mature mOrange, this increased presence of FR mOrange could not be attributed to mature mOrange's decay. Instead it was shown that it is in fact the photobleached protonated by-product of mOrange that results in the formation of the FR mOrange.

3.4 Conclusion

The motivation for this work stemmed from the FR mOrange created by Subach *et al.* where mOrange was irradiated in the presence of $K_3Fe(CN)_6$. It was concluded that the excited mOrange chromophore was interacting with the $K_3Fe(CN)_6$, leading to the oxidative reddening of the chromophore. However, the method of conversion for mOrange was not clear as the photophysical properties of $K_3Fe(CN)_6$ were not addressed, leaving the possibility of excited $K_3Fe(CN)_6$ to be responsible for its conversion rather than the excited chromophore. Thus to elucidate the origins of the FR mOrange, solutions of mOrange and $K_3Fe(CN)_6$ were irradiated using high power LEDs, and investigated for FR mOrange using western blot protein analysis in addition to absorption and fluorescence spectroscopy. From these studies it was determined that it was indeed an excitation event of mOrange which lead to the formation of the FR mOrange rather than the excited $K_3Fe(CN)_6$.

Having previously demonstrated the presence of both green immature and mature mOrange in a solution of purified protein, it was essential to determine which species was

contributing to the formation of the FR mOrange. This study was carried out using the Opotek Inc. Vibrant 355 tunable NIR-Vis pulsed laser (10 Hz), where the use of 497, 532, 548 and 560 nm laser irradiation helped separate the contributions of each species in solution. The results indicated a potential correlation between the decay of the green immature mOrange and the growth of the FR mOrange. However, without being able to fit the growth of the FR mOrange, it was difficult assign this link. Therefore, the novel addition of heat was carried out to remove the ability of the green immature mOrange to become excited. This enabled only the mature mOrange to become excited, and the prediction was made that no FR mOrange would appear. Unfortunately this prediction was proven to be incorrect, as the greatest amount of FR mOrange was seen during the heating experiments. Through a careful review of the results it was deemed possible that the FR mOrange was actually linked to the presence of the photobleached protonated by-products, to which this link was proven to be correct.

Based on the data presented in this chapter, it can be concluded that contrary to the proposed conversion mechanism of Subach *et al*., the excited chromophore is not interacting with external oxidants to convert mOrange to the FR mOrange. Rather, the conversion results from the protonated by-products of photobleaching, which through light or heat induced β-barrel fluctuations, expose the chromophore to the solvent where an external oxidant may then interact with the chromophore. The ramification that results from this data is that although light is necessary in the process of FR mOrange production, it is not the direct cause. Therefore, conversion would also be dependent on the amount and type of oxidant present, suggesting that the FR mOrange conversion is not innate to the protein, and will depend on its external environment. Thus, this dependence of the photoconversion on the environment is a critical factor to consider when carrying out imagining experiments with mOrange.

Chapter Four: **Singlet oxygen production in mOrange**

4.1 Introduction

The utility that has developed from the initial discovery of Fluorescent Proteins (FPs) is undeniable and the pool of FP employment is ever expanding as further applications are being created for these molecular lanterns. Indeed, one of the recent applications of FPs has been in Chromophore Assisted Laser Inactivation (CALI) where chromophores capable of producing reactive oxygen species (ROS) are utilized for the application of oxidative stress on cellular components. Briefly, originally developed by Jay *et al.*, CALI enables the specific deactivation of a target (generally proteins), enabling their function to be determined.[100,101] CALI proceeds via the use of an antibody specific to a target of a cell, and attached to the antibody is a chromophore capable of producing ROS.[102,103] Upon activation of the chromophore through the use of a laser, the chromophore can photosensitize oxygen, leading to the production of ROS.[102] Given the short lifetime of most ROS (less than 1 μs in H_2O),[33,104] only the immediate area surrounding the ROS production will be damaged due to the ROS induced oxidative stress.[105] Thus, the target of the antibody will be oxidized and deactivated, allowing the subsequent loss of activity of a cell to elucidate the target's function.

How this relates to FPs is that several studies have been performed with the use of either enhanced Green Fluorescent Protein (EGFP) or KillerRed as the ROS producing chromophore.[33,103,105-107] The reason for the use of FPs, is that it has been shown that the free chromophore of GFP is capable of producing singlet oxygen ($^1O_2$), a ROS. Indeed, it has been shown that EGFP as a whole protein was able to produce $^1O_2$ with a modest quantum yield (Φ_{1O2}) of 8 X 10^{-6}, and more impressively it was shown that TagRFP produced $^1O_2$ with Φ_{1O2} = 0.004.[107] However, the production of $^1O_2$ from FPs is not immediately clear, and thus to

understand the production of $^1O_2$ from FPs, the method of photosensitization of the ground state molecular oxygen ($^3O_2$) will be examined.

The general process of $^1O_2$ production is known as Triplet-Triplet Annihilation (TTA), where a molecule (known as a photosensitizer) in its excited triplet state, can transfer its energy to $^3O_2$ when the two molecules come into contact with each other.[35,108,109] The result of this TTA process is that $^3O_2$ is converted to its singlet excited state and the photosensitizer is returned to its ground state. This process can be shown according to the following schemess:

$$^1PS + h\nu \longrightarrow {}^1PS^*, \text{ Scheme 4.1}$$

where ^1PS is the photosensitizer in its singlet ground state, and through the absorption of a photon of light of sufficient energy ($h\nu$), the photosensitizer will be excited to its excited singlet state ($^1PS^*$). Once the excited singlet state is achieved, the photosensitizer can undergo a process known as intersystem crossing (ISC), as shown:

$$^1PS^* \xrightarrow{k_{ISC}} {}^3PS^*, \text{ Scheme 4.2}$$

where the desired excited triplet state is achieved ($^3PS^*$) with a rate constant for ISC of k_{ISC}. From this triplet excited state, $^3O_2$ can interact with the photosensitizer forming $^1O_2$ via the following scheme:

$$^3PS^* + {}^3O_2 \longrightarrow {}^1PS + {}^1O_2. \text{ Scheme 4.3}$$

It is this excitation, ISC and eventual interaction of the chromophore of FPs with $^3O_2$, which enables $^1O_2$ production.

However, with the process of $^1O_2$ production explained, one final caveat remains for FPs. This is the ability of $^3O_2$ to actually encounter the excited chromophore, considering the chromophore of FPs is nestled within the centre of the β-barrel. Yet, this hurdle has been mitigated through the work of Regmi *et al.* and Chapagain *et al.*, who have shown that during

chromophore excitation of FPs, the β-barrel undergoes fluctuations enabling solvent access to the previously shielded chromophore.[36,74,75] Thus, with the excited chromophore exposed to the solvent during excitation, it is possible for $^3O_2$ to interact with the chromophore.

Still it should be noted, that not all FPs exhibit the production of ROS. With no literature precedence for mOrange's ability to generate ROS, the question of mOrange's ability to photosensitze $^3O_2$ remains. The only clue to the possible production of ROS from mOrange is the protective effect that a lack of oxygen has on its photobleaching characteristics.[31] However, in order to determine if mOrange does interact with $^3O_2$ under the photobleaching conditions established in chapters two and three, it will be prudent to repeat the removal of $^3O_2$. If this proves to have the same protective effect, the search for the production of $^1O_2$ can be carried out.

4.2 Methods

4.2.1 Materials

To carry out the investigation of $^1O_2$ production in mOrange, additional reagents were required on top of those already mentioned in chapters two and three. Specifically, 9,10-anthracenediyl-bis(methylene)dimalonate (ABDA) and D_2O were purchased from Sigma Aldrich Canada.

4.2.2 Experimental Setup

To determine if oxygen was an important variable in the observed photobleaching of mOrange, a solution of mOrange in PBS (pH 7.4) in a custom 1 cm width by 1 cm path length, long neck quartz cuvette, fabricated by the University of Calgary Scientific Glass Shop, was deoxygenated via nitrogen bubbling for 40 minutes. This solution was capped and irradiated with the Green LED, with the resulting absorption and fluorescence followed according to the previously established methods (chapters two and three).

Detection of $^1O_2$ occurred through the use of ABDA, where a solution of mOrange in PBS, had an addition of 10 μL of a 0.1 M stock solution of ABDA dissolved in MilliQ H_2O (18.2 MΩ.cm), to achieve a final ABDA concentration of 0.1 mM in 1 mL. The solution was irradiated with the Green LED in a 0.4 cm width by 1 cm path length quartz cuvette (International Crystal Laboratories) with the resultant absorption and fluorescence monitored following the previously established methods. The irradiations were carried out with the Green LED, or the pulsed laser.

4.2.3 Evaluating Singlet Oxygen Production

To determine the amount of $^1O_2$ produced, the spectra of mOrange and ABDA after irradiation, had the equivalent spectra of mOrange irradiated alone subtracted. This allowed the isolation of the spectra of ABDA and the resulting decay at 380 nm could be plotted as a function of time (or shots) in order to determine the rate of decay. This procedure for $^1O_2$ production is modified from Kuznetsova *et al.*[110] The data were fitted using the KaleidaGraph 4.1 software suite.

4.3 Results

4.3.1 Deoxygenated mOrange and the Green LED

Given the literature precedence of ROS production from FPs, the question of $^3O_2$'s role in the photobleaching of mOrange arose. Specifically, how susceptible to light is mOrange when $^3O_2$ is present? And if mOrange susceptibility depends significantly on $^3O_2$, then does mOrange sensitize $^3O_2$ to a ROS? To answer these questions, the first step in determining the extent of mOrange's light susceptibility to $^3O_2$, was to remove it. This was carried out through the continuous bubbling of inert nitrogen gas in a solution of mOrange in PBS for 40 minutes. Once the solution had been purged of $^3O_2$, the absorption and fluorescence were followed during exposure to the Green LED.

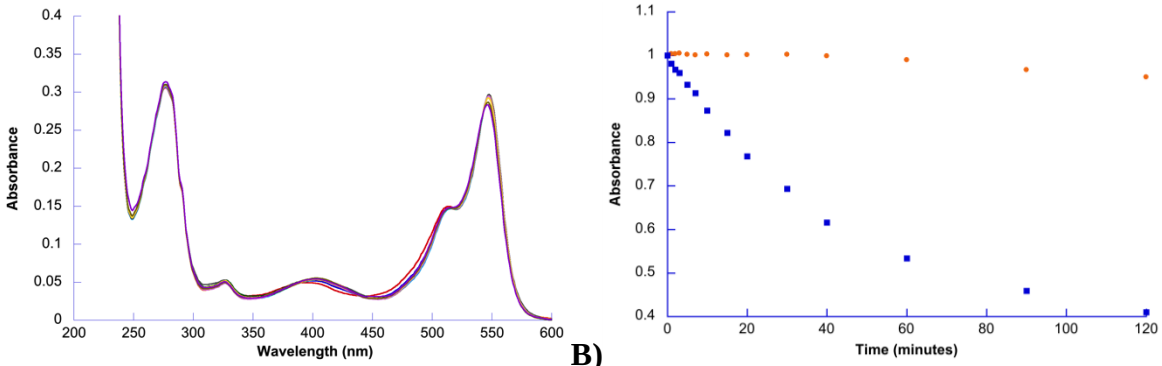

A) **B)**

Figure 4.1: A) The absorbance mOrange (4.16 X 10^{-6} M) in the absence of O_2 while exposed the Green LED for 2 hours. B) The decay of mOrange at 548 nm in the absence of O_2(orange circles) and in the presence of O_2 (blue squares) while exposed the Green LED for 2 hours.

From figure 4.1A it is immediately apparent that the lack of $^3O_2$ has a significant effect on mOrange's light susceptibility. With little change observed in the absorbance spectrum over two hours of irradiation, it can be assumed that $^3O_2$ plays a key role in mOrange's photobleaching. Indeed oxygen's role in photobleaching can be seen by plotting the 548 nm maxima of mOrange over the two hour irradiation (figure 4.1B, orange circles), resulting in very little decay seen during the two hour irradiation. Given the lack of significant decay at 548 nm, it was difficult to fit this data to either a first order or bi-exponential decay. This is in stark contrast to the observed bi-exponential decay for mOrange seen in chapter two, where nearly 40 % of the original intensity remains after two hours of irradiation with the Green LED in oxygenated solutions (figure 4.1B, blue squares). Thus, these results suggest a significant link between the observed photobleaching and the presence of $^3O_2$. Therefore, the next step was to determine if $^3O_2$ reacts with mOrange in a manner conducive to ROS production.

4.3.2 The interaction of 9,10-Anthracenediyl-bis(methylene)dimalonate (ABDA) and mOrange with the Green LED

4.3.2.1 The use of ABDA

Of the methods available to determine the presence of $^1O_2$, a majority of them require special equipment or conditions to carry out the experiments.[33,110] However, if mOrange did produce ROS such as $^1O_2$, it would be beneficial to quantify the amount produced using the same experimental conditions set out in chapters two and three. This would provide much more consistent data to draw conclusions about mOrange ROS production. Fortunately, the work of Kuznetsova *et al.* has provided the solution for this quandary. In their work, Kuznetsova *et al.* created a set of absorbing $^1O_2$ sensors that upon their favourable interaction with $^1O_2$, lead to a quantifiable decrease in their absorbance.[110] In addition to the observed decrease in absorbance, these sensors were water-soluble making them a highly suitable choice for $^1O_2$ detection in our experimental setups. The chosen compound was 9,10-anthracenediyl-bis(methylene)dimalonate (ABDA) which can be seen as compound **1** in figure 4.2A. Comprised of an electron rich anthracene core, the interaction of ABDA with electrophilic $^1O_2$ leads to the oxidation of ABDA, resulting in the endoperoxide of ABDA (compound **2**, figure 4.2A). From the absorbance spectrum of ABDA (figure 4.2B, red trace) it can be seen the characteristic absorbance of ABDA resides in the 300 – 425 nm range. As it interacts with $^1O_2$, the characteristic absorbance decreases, represented by the black trace in figure 4.2B. Conveniently, the absorbance spectra of ABDA does not overlap with the main absorbance peak of mOrange (figure 4.2C), suggesting that if mOrange were to be excited using the Green LED, only mOrange will undergo interactions with the Green light. Furthermore, to ensure no interaction of the Green LED with ABDA, a 488 nm shortwave cutoff filter was used (black vertical line, figure 4.2C). Thus, with the conditions previously outlined for the photobleaching of mOrange via the Green LED, ABDA stands out as a good choice for the detection of $^1O_2$.

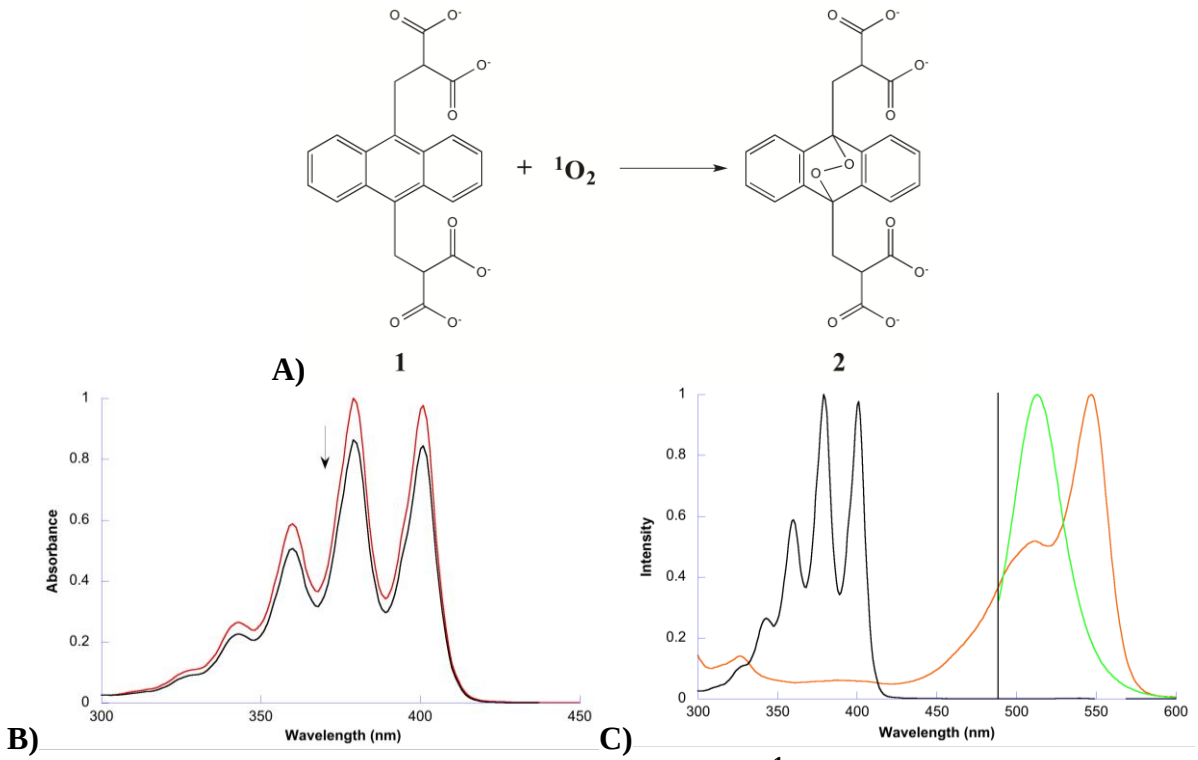

Figure 4.2: A) The reaction of ABDA (compound I) with $^1O_2$, to form the endoperoxide of ABDA, ABDA-O_2 (compound 2). The absorbance spectrum of ABDA before $^1O_2$ addition (red trace), the decrease in the absorbance spectrum of ABDA as $^1O_2$ interacts with ABDA (black trace). C) The absorbance spectra of mOrange (solid orange trace) and ABDA (black trace). The green trace represents the Green LED and the black vertical line represents the shortwave cutoff filter.

Before the analysis of mOrange could be carried out with ABDA, it is first necessary to understand the rates of interaction for ABDA with $^1O_2$ in order to be able to comprehend the results. As previously described, $^1O_2$ is produced through the interaction of an excited photosensitizer in the triplet excited state (in this case mOrange) with ground state $^3O_2$ through TTA.[35] Once formed, the excited $^1O_2$ can deactivate through several processes involving either solvent deactivation with a rate constant k_d, physical quenching with ABDA at some rate constant k_P, or direct chemical reaction with ABDA forming the endoperoxide of ABDA (ABDA-O_2), at some rate constant k_R. This results in three deactivation equations for $^1O_2$ where:

$$^1O_2 \xrightarrow{k_d} {}^3O_2, \text{ Eq 4.1}$$

$$^1O_2 + ABDA \xrightarrow{k_P} {}^3O_2 + ABDA, \text{ Eq 4.2}$$

$$^1O_2 + ABDA \xrightarrow{k_R} ABDA\text{-}O_2. \text{ Eq 4.3}$$

From these three equations it has been shown in the literature that the rate law for $^1O_2$ production of a photosensitizer can be solved.[110,111] However, the derivation of the rate law is based on a system which is inherently different from the one being studied within this work. Where in the work of Kuznetsova *et al.* the rate is derived based on a system that involves a $^1O_2$ photosensitizer (Rose Bengal) that is exposed to the solvent, enabling immediate escape of the produced $^1O_2$. Contrary to this situation, if mOrange is acting as a $^1O_2$ photosensitizer, then the produced $^1O_2$ has to escape the β-barrel of mOrange in order to be freely available in solution. This presents a problem, as there are now additional interactions for $^1O_2$ to take part in. Specifically, $^1O_2$ can undergo physical quenching with the amino acids of mOrange, enabling its decay via some rate constant k_{PAA}. Additionally as it was mentioned before, it is known that $^1O_2$ reacts chemically with amino acids such as histidine, tryptophan, methionine, tyrosine and cysteine.[35,53] Thus, it is possible for the produced $^1O_2$ to react chemically with several of the amino acids of mOrange with some rate constant k_{RAA}. Therefore, two additional equations must be included:

$$^1O_2 + mO \xrightarrow{k_{PAA}} {}^3O_2 + mO, \text{ Eq 4.4}$$

$$^1O_2 + mO \xrightarrow{k_{RAA}} mO\text{-}O_2, \text{ Eq 4.5}$$

where *mO* represents the constituent amino acids of mOrange and *mO-O₂* represents the oxidized amino acids of mOrange.

Based on this additional information, it is not possible to accurately predict the rate law for mOrange's $^1O_2$ production under these circumstances, given the unknown amount of $^1O_2$ that

will interact with the amino acids of mOrange. Fortunately all is not lost, such that even though the quantity of $^1O_2$ cannot be accurately determined, at least the presence of $^1O_2$ can be detected. Due to the selectivity of ABDA towards $^1O_2$,[110] the observed decay of ABDA at its peak absorbance intensity of 380 nm can be attributed to the sole interaction of ABDA and $^1O_2$. Hence, based on equation 4.3, the rate of ABDA decay can be expressed as the reaction:

$$\frac{d[ABDA]}{dt} = -k_R[ABDA][^1O_2], \text{ Eq 4.6}$$

where [*ABDA*] and [$^1O_2$] are the concentrations of ABDA and $^1O_2$ initially. However, given the aforementioned uncertainty in the concentration of $^1O_2$ in order to simplify this equation, a few assumptions have to be made. The first is that if mOrange produces $^1O_2$, then in order for ABDA to interact with $^1O_2$, it has to escape the β-barrel. The second assumption is the production of $^1O_2$ escaping the β-barrel of mOrange is constant. Applying these assumptions to equation 4.6, the [$^1O_2$] will be consider to be a constant and thus combined with k_R forming k'_R as seen in equation 4.7:

$$\frac{d[ABDA]}{dt} = -k'_R[ABDA]. \text{ Eq 4.7}$$

From here, equation 4.7 can be integrated to give the final first order rate of decay for ABDA when in the presence of mOrange:

$$[ABDA]_t = [ABDA]_0 e^{-k'_R t}. \text{ Eq 4.8}$$

Thus, if these assumptions prove to be correct, ABDA should decay with a first order rate when mOrange is irradiated with the Green LED.

4.3.2.2 ABDA and mOrange in PBS with the Green LED

Having established ADBA as a suitable sensor for the production of $^1O_2$ from mOrange, the next step in the investigation was to irradiate mOrange with the Green LED, and monitor the absorbance of ABDA over time. However, before the loss of absorbance for ABDA at 380 nm can be followed, it will be essential to follow the decay of the 548 nm absorbance and 565 nm fluorescence maxima over time. The reason for this is to ensure that excited mOrange is not interacting with ABDA. Additionally, the possibility exists for ABDA to exert a protective effect on mOrange. This is due to the favourable interaction of $^1O_2$ with ABDA, and by removing $^1O_2$ from solution; it is conceivable that less amino acids would be oxidized. Thus, if there were to be an interaction of the excited mOrange and ABDA, or a protective effect through the removal of $^1O_2$, then the result would be an alteration to the observed decay patterns for mOrange. Hence, a solution of mOrange and ABDA was irradiated with the Green LED for four hours, and the maxima for the absorbance and fluorescence were plotted. From figure 4.3A and B, it can be seen that mOrange still undergoes the characteristic bi-exponential decay seen in chapter two. Indeed, from the comparison of the rates for the absorbance decay in table 4.1 it can be seen that even with the presence of ABDA, the absorbance still follows the same pattern of decay. In agreement with this is the fluorescence (figure 4.3C and D), which also fits a bi-exponential decay and has similar rates to those seen in chapter two (table 4.1). Based on this data it can be assumed that when mOrange is in the presence of ABDA, it decays in a similar manner as seen when no ABDA was present. Ergo, this suggests that ABDA is not either reacting with the excited mOrange or exerting a protective effect on mOrange from $^1O_2$.

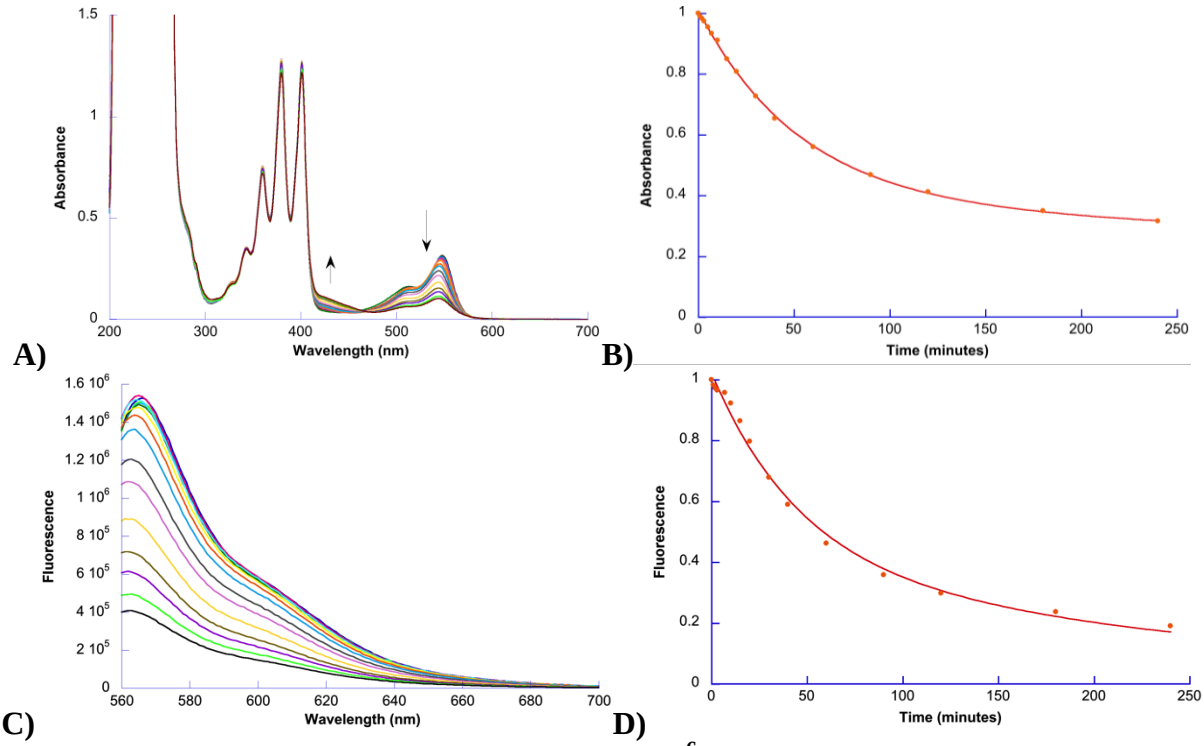

Figure 4.3: A) The absorbance mOrange (4.45 X 10^{-6} M) in the presence of ABDA (0.1 mM) while exposed the Green LED for 4 hours. B) The decay of mOrange (4.45 X 10^{-6} M) at 548 nm in the presence of ABDA (0.1 mM) while exposed the Green LED for 4 hours. C) The fluorescence of A). D) The maximum corrected and normalized fluorescence of C) at 565 nm. The arrows represent the direction of change. The data were modeled with equation 2.2a and the analysis is in appendix A.

Table 4.1: The comparison of the values for the rate constants of decay for mOrange with (+) and without (-) ABDA as determined through the analysis of the decay for the maximum absorbance at 548 nm and fluorescence at 565 nm of mOrange during photobleaching with the Green LED.

λ_{max} (ABDA)	A	k_1 (min^{-1})	B	k_2 (min^{-1})
548 nm (-)	0.404 (±0.019)	0.000907 (±0.000216)	0.598 (±0.018)	0.0216 (±0.0008)
548 nm (+)	0.375 (±0.038)	0.000785 (±0.000439)	0.633 (±0.368)	0.0187 (±0.0012)
565 nm (-)	0.262 (±0.038)	0.000804 (±0.000669)	0.744 (±0.037)	0.0215 (±0.0013)
565 nm (+)	0.418 (±0.227)	0.00378 (±0.00255)	0.603 (±0.223)	0.0221 (±0.0073)

With the lack of evidence for the interaction of mOrange and ABDA, it was now possible to determine if mOrange was producing $^1O_2$. In order to do this, it would be a simple matter of plotting the 380 nm maxima. Unfortunately, along with the observed bi-exponential decay in figure 4.3A, the appearance of the protonated by-product can be seen at about 420 nm (marked by the upward arrow). This suggests that there exists an overlap between the protonated by-product of mOrange and ABDA. Given that in chapter two it was shown that the protonated by-product appears as mOrange is irradiated, it can be assumed that if the absorbance spectra of ABDA were to decay, the apparent decay for ABDA will be masked by the overlapping protonated by-product. Thus, if the spectra of the photobleached mOrange could be removed, leaving the spectra of ABDA, it would be possible to plot ABDA's 380 nm maxima. Following this thought process, the spectra of mOrange photobleached with the Green LED alone was removed from the spectra of mOrange and ABDA photobleached with the Green LED.

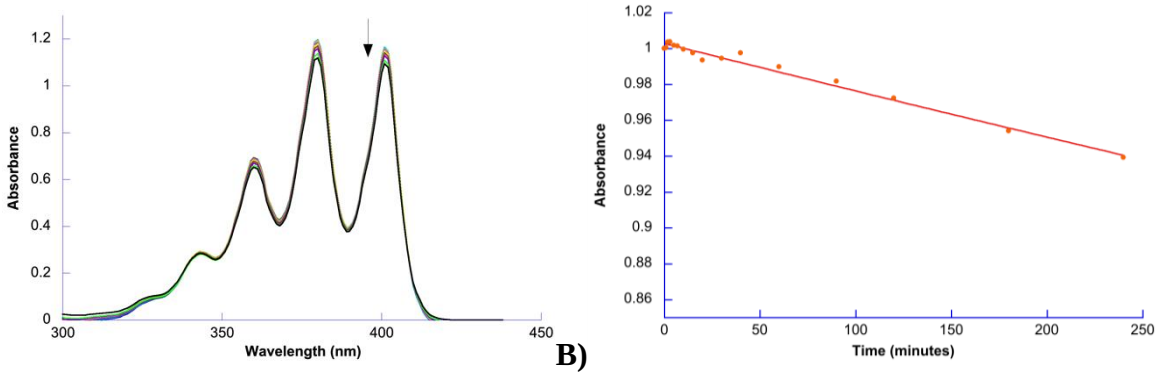

Figure 4.4: A) The absorbance of ABDA (0.1 mM) in the presence of mOrange during exposure to the Green LED for 4 hours with the spectra of mOrange removed. B) The decay of ABDA at 380 nm, from A). The data were modeled with equation 2.1 and the analysis is in appendix A.

By removing the spectra of photobleached mOrange, the resulting spectra of ABDA can be seen in figure 4.4A and displays a decrease over time. Plotting the 380 nm maxima as a function of time, figure 4.4B shows a definite decrease with the loss of 5 % of the original

intensity over the irradiation period. This suggests that $^1O_2$ is indeed produced from mOrange, with enough $^1O_2$ able to escape the β-barrel of mOrange and interact with the ABDA in solution. Additionally, given that ABDA is a $^1O_2$ specific sensor,[110,112] only the presence of $^1O_2$ can be confirmed but the presence of other ROS is not precluded, but is beyond the scope of this work. Moving to the analysis of the decay in figure 4.4B, the data were fit to a first order decay with a rate constant of $2.68 \times 10^{-4} \pm 9 \times 10^{-6}$ min^{-1} suggesting that the assumption of constant $^1O_2$ production for the first order decay rate of ABDA is valid within the given conditions. Ergo, with these results it is established that mOrange does indeed produce $^1O_2$ during excitation, but one of the characteristics of $^1O_2$ is its extended lifetime in D_2O due to less solvent deactivation.[35,113] Therefore in order to confirm the presence of $^1O_2$, it would be prudent to perform the previous experiments in D_2O and monitor the production of $^1O_2$.

4.3.2.3 With D_2O as the solvent

To expand on the idea of the use of D_2O, it was shown in equation 4.4 that one of the major deactivation pathways for $^1O_2$ is through solvent interactions. In fact for $^1O_2$, solvent deactivation is the most significant decay pathway.[110] Specifically for $^1O_2$ in aqueous buffers, this solvent deactivation occurs due to the high frequency vibrations of the O-H bond in H_2O. These high frequency vibrations are a good match for the electronic energy levels of $^1O_2$, enabling efficient deactivation through energy exchange with the vibration level of H_2O.[35] However, this efficient relaxation is mitigated when the heavier isotope deuterium replace the hydrogens of H_2O. Due to the heavier weight of deuterium atoms, the vibrational frequencies of the O-D bonds are lower than that of O-H, preventing a good overlap with the $^1O_2$ electronic energy levels.[113,114] The ramifications of this loss of energy overlap is that the lifetime of $^1O_2$ in

deuterated solution is increased by ten-fold, from 3.8 μs in H_2O to 62.0 μs in D_2O.[35,114] Therefore, if the $^1O_2$ experiments were to be repeated in D_2O, the end result should be that the $^1O_2$ which has escaped the β-barrel of mOrange will persist longer in solution. This would ultimately lead to an increased loss of ABDA as there would be more $^1O_2$ available to interact. Yet before this experiment can be carried out, it should be noted that by changing the solvent of mOrange, it is possible that the photobleaching characteristics will be altered. Thus, it is necessary to first determine the characteristics of photobleaching for mOrange in the presence of D_2O.

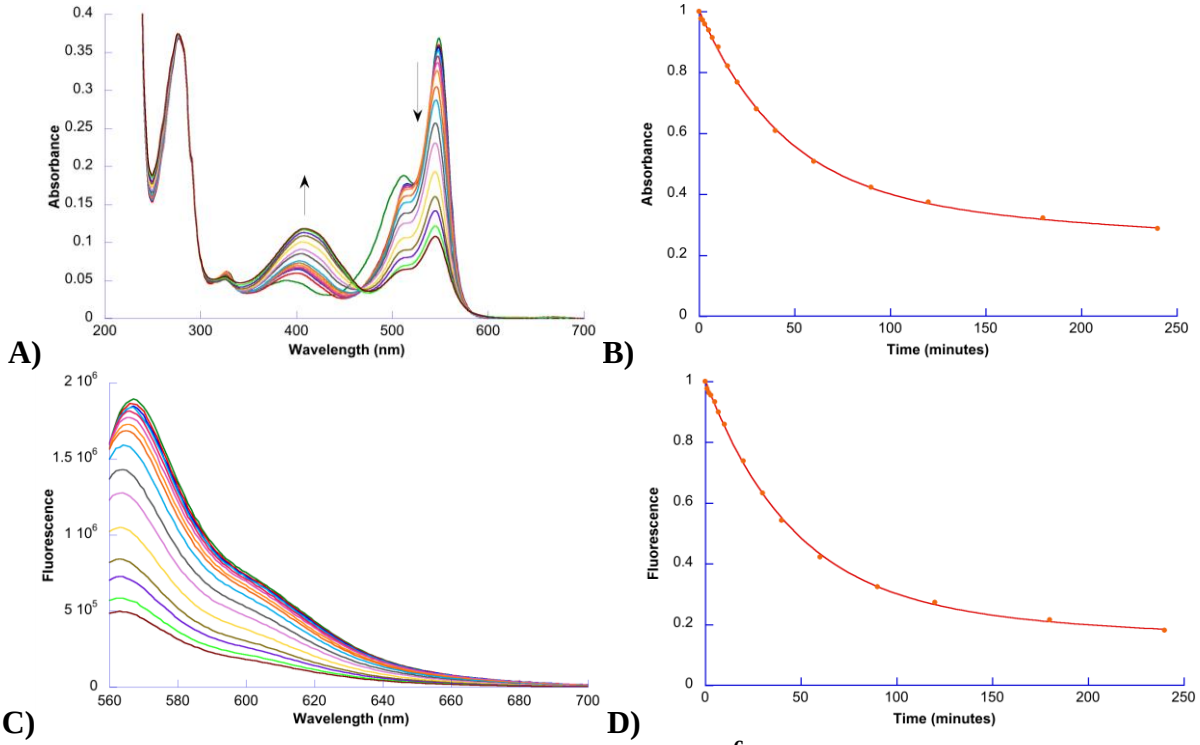

Figure 4.5: A) The absorbance of mOrange (5.18 X 10^{-6} M) in D_2O during exposure to the Green LED for 4 hours. B) The decay of mOrange at 548 nm, from A). C) The fluorescence of mOrange (5.18 X 10^{-6} M) in D_2O during exposure to the Green LED for 4 hours. D) The decay of mOrange at 565 nm, from C). For B) and D), the data were modeled with equation 2.2a and the analysis is in appendix A.

To investigate the effects of D_2O on mOrange, a solution of mOrange in D_2O was irradiated with the Green LED according to the previously established procedure. Upon inspection of the absorption spectra (figure 4.5A), it appears as if mOrange behaves in a similar manner to mOrange with PBS as the solvent, with the loss of the main 548 nm peak and appearance of the protonated by-product peak at 406 nm. Interestingly, the only noticeable difference is the immediate loss of the shoulder for mOrange (figure 4.5A, dark green trace). This observed loss of the shoulder will be addressed later in this chapter. Moving to the 548 nm maxima plotted as a function of time (figure 4.5B), the data were fit to a bi-exponential decay with rate constants very similar to those found in chapter two for mOrange in PBS (appendix A). This suggests that D_2O has no significant impact on the photobleaching of mOrange. Indeed, in agreement with this conclusion is the observed fluorescence of mOrange in D_2O (figures 4.5C – D), where the fluorescent decay follows a bi-exponential over the four hours irradiation with similar rate constants to those previously established (appendix A). Thus, it can be concluded that D_2O does not have any significant effects on the overall photobleaching of mOrange, enabling the study of $^1O_2$ production to proceed.

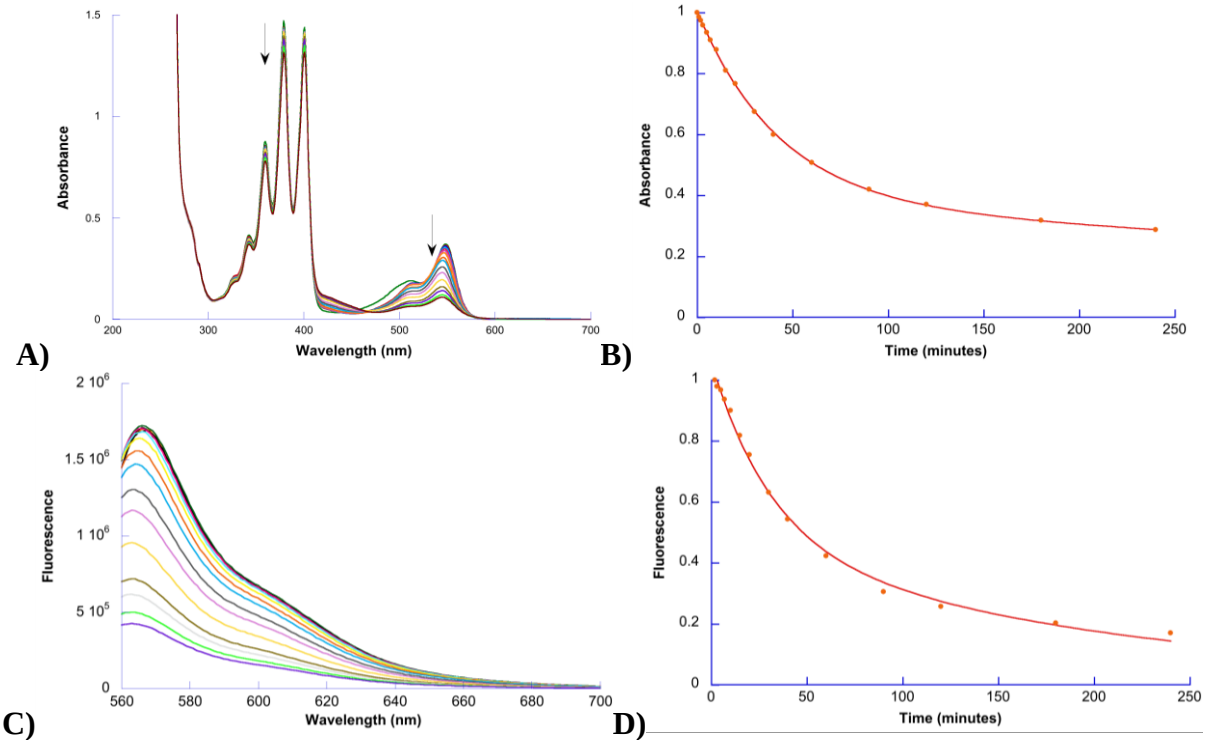

Figure 4.6: A) The absorbance mOrange (5.22 X 10^{-6} M) in the presence of ABDA (0.1 mM) in D_2O while exposed the Green LED for 4 hours. B) The decay of mOrange (5.22 X 10^{-6} M) at 548 nm in the presence of ABDA (0.1 mM) in D_2O while exposed the Green LED for 4 hours. C) The fluorescence of mOrange (5.22 X 10^{-6} M) in the presence of ABDA (0.1 mM) in D_2O while exposed the Green LED for 4 hours. D) The maximum corrected and normalized fluorescence of mOrange (5.22 X 10^{-6} M) at 565 nm while in the presence of ABDA (0.1 mM) in D_2O during exposure the Green LED for 4 hours. For B) and D) the data were modeled with equation 2.2a and the analysis is in appendix A.

Having established the characteristics of photobleaching for mOrange in D_2O, it was now possible to explore the production of $^1O_2$ through the addition of ABDA. Hence, a solution of mOrange and ABDA was irradiated with the Green LED for four hours in D_2O. Immediately, the effects of the D_2O on $^1O_2$ are apparent from figure 4.6A, as there is a noticeable decrease in the ABDA absorbance even with the overlapping appearance of the protonated by-product, indicating that more $^1O_2$ has interacted with ABDA than previously shown. In addition, it should be noted that the initial decrease of the shoulder of mOrange remains apparent (dark green trace of figure 4.6A), suggesting that this new phenomenon needs to be further understood. However,

this will be better explained below. To ensure that the observed decrease in the ABDA spectra is not a result of some new interaction of mOrange and ABDA in D_2O, the maxima at 548 nm was plotted. From figure 4.6B it can be seen that the decay of the 548 nm mOrange peak was found to fit the expected bi-exponential decay, having very similar rate constants to those seen before (appendix A, tables A.29, A.32 and A.34). Concurrently, the fluorescence decay follows the same bi-exponential decay with similar rate constants to those previously established (appendix A, tables A.30, A.33 and A.35), suggesting that the presence of D_2O has no effect on the overall photobleaching characteristics of mOrange in the presence of ADBA. Based on the lack of alteration to mOrange's photobleaching characteristics, the spectra of ABDA can now be examined.

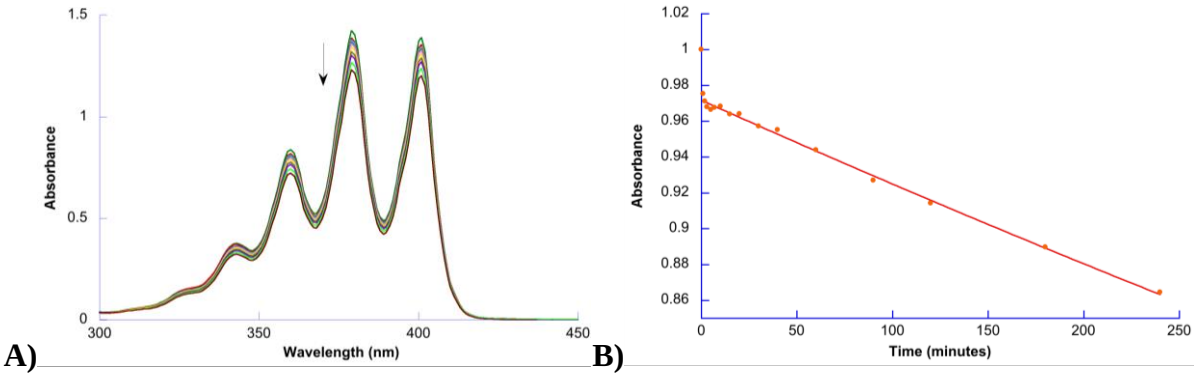

Figure 4.7: A) The absorbance of ABDA (0.1 mM) in the presence of mOrange during exposure to the Green LED for 4 hours with the spectra of mOrange removed. B) The decay of ABDA at 380 nm, from A). The data were modeled with equation 2.1 and the analysis are in appendix A.

Following the same spectral manipulation as before, the spectra of mOrange photobleached alone in D_2O was removed from the spectra of mOrange and ABDA in D_2O. This resulted in the spectra of ABDA alone, which can be seen in figure 4.7A and has a noticeable decrease over the four hours irradiation. By plotting the maxima at 380 nm, the decay for ABDA can be followed over time (figure 4.7B). Interestingly, there appears to be a significant initial

decay seen for ABDA after the first minute of irradiation with the Green LED. This initial loss suggests a link to the observed immediate loss in absorbance for the shoulder of mOrange when it was irradiated in D_2O (figure 4.5A, dark green trace). Briefly, when the results of mOrange and ABDA in PBS are examined, there is no initial decrease seen for the 380 nm maxima of ABDA (figures 4.4) and concurrently there is no initial loss seen for the shoulder of mOrange (figure 4.3A). On the other hand, this initial decrease is seen in the spectra of ABDA and in the spectra of mOrange when D_2O was used as the solvent, indicating a link between $^1O_2$ production and mOrange's decay. Specifically, since a loss in the absorbance of ABDA is only a result of $^1O_2$ interaction, then this initial decay must be due to the presence of a larger quantity of $^1O_2$ compared to what is seen for the subsequent periods of irradiation. This indicates that there appears to be a significant amount of $^1O_2$ being produced from the shoulder of mOrange upon initial irradiation.

To explain this, it is necessary to recall the results of chapter two where it was shown that the green immature mOrange was contributing to the observed shoulder at 515 nm. If the green immature mOrange were able to produce more $^1O_2$ than the mature mOrange, then considering the propensity of $^1O_2$ to interact with amino acids and oxidize them, it is possible that the extended lifetime of $^1O_2$ in D_2O is leading to an enhanced bleaching of the green immature mOrange. To expand on this idea, it was shown in chapter two and three that the green immature mOrange appears to be less resilient to heat denaturation than the mature mOrange, indicating a β-barrel for the green immature mOrange that is less 'stout' than the mature variant. Additionally, it was shown from the laser irradiation data in chapter three that the excitation of the green immature mOrange when in the presence of the external oxidant $K_3Fe(CN)_6$, leads to the formation of the Far Red mOrange. Based on this data, it was suggested that the large

$K_3Fe(CN)_6$ could interact with the chromophore of the green immature mOrange. This means that the β-barrel of the green immature mOrange would not be shielding the chromophore from the solution as well as the mature mOrange, allowing the $K_3Fe(CN)_6$ to interact with the chromophore. Thus, for the case of $^1O_2$ production, the lowered shielding ability of the green immature mOrange would allow greater access of dissolved $^3O_2$ to the chromophore, enabling greater amounts of $^1O_2$ to be produced. Therefore, with greater amounts of $^1O_2$ being produced and the lifetime of the $^1O_2$ enhanced due to D_2O, there would be a greater loss of the green immature mOrange. This would ultimately result in the loss of the shoulder of mOrange as seen in figures 4.4A and 4.6A and the greater amounts of $^1O_2$ from the green immature mOrange would lead to the observed initial decay for ABDA seen in figure 4.7B.

Having established a possible reason for the initial decay of the ABDA, it is now necessary to examine the resulting rate of decay seen for ABDA after the first minute of irradiation. From the results of mOrange and ABDA in PBS, it was shown that ABDA decayed with a rate constant of $2.68 \times 10^{-4} \pm 9 \times 10^{-6}$ min^{-1}, however, the first order decay of the data in figure 4.7B has a rate constant of $4.93 \times 10^{-4} \pm 8 \times 10^{-6}$ min^{-1}. With a greater rate constant, it can be assumed that ABDA is interacting with a larger number of $^1O_2$ molecules. However, since the only variable that was changed is the solvent, the enhanced interaction with $^1O_2$ cannot be attributed to a greater production of $^1O_2$, rather it is the result of the enhanced lifetime for $^1O_2$ in D_2O. Thus, with a greater amount of ABDA undergoing decay, the presence of $^1O_2$ is confirmed, suggesting its involvement in the photobleaching of mOrange.

The investigation of mOrange with ABDA and the Green LED for the production of $^1O_2$ has not only revealed the presence of $^1O_2$, but it has also demonstrated the greater propensity of the green immature mOrange to produce $^1O_2$. However, in order to confirm this link, it will be

necessary to further study mOrange and ABDA. As was shown in chapter two and three, one method to elucidate the effects of either the green immature or mature mOrange within a photobleaching experiment, is to use the tuneable laser to selectively excite one of the species in solution.

4.3.3 mOrange and the Laser

As seen in the previous chapters, the use of the Green LED leads to the excitation of both the green immature and mature mOrange. Given that previous section (4.3.2.3) demonstrated a link between the green immature mOrange and greater $^1O_2$ production, the use of the tuneable laser for the specific excitation of the green immature mOrange over the mature mOrange will enable this link to be supported or negated. Additionally, given that it has been shown that there is the presence of $^1O_2$ confirmed by the increased decay of ABDA in D_2O, it will be advisable to carry out the experiments in D_2O.

4.3.3.1 mOrange in D_2O during laser irradiation

For the thorough investigation of $^1O_2$ production from mOrange with pulsed laser excitation, it is essential to first determine how mOrange photobleaches in the presence of D_2O. Additionally, considering the link between $^1O_2$ production and the green immature mOrange was shown, the photobleaching experiment will be conducted with the use of the 497 nm pulsed laser to primarily excite the green immature mOrange as shown in chapter two and three. Thus, a solution of mOrange in D_2O was irradiated with the 497 nm pulsed laser for 1000 shots. From the results, it can be see that main 548 nm peak for mOrange is decaying (figure 4.8A), with an observed red shift. Concomitantly, the fluorescence of mOrange in figure 4.8B is decaying and red shifting. Although this red shift in the absorbance is expected due to the loss of the

comparatively blue shifted green immature mOrange (chapter two), the red shift in the fluorescence is unexpected as it was not observed in previous chapters where the experiments were conducted in PBS. To explain this observed red shift, it needs to be considered that D_2O could have an affect on the absorption spectra of mOrange. Specifically, the chromophore of mOrange has been shown to have at least five separate H_2O molecules interacting to help stabilize the chromophore through hydrogen bonding.[24] Concurrently, it has been shown in the literature and in chapter three that the excitation of FPs can lead to light induced β-barrel fluctuations, allowing solvent access to the chromophore.[36,74,75] Given that mOrange is matured in an environment containing H_2O (Lysogeny broth), the molecules involved in the stabilization of the chromophore will not be deuterated. Thus, it is possible that the light induced β-barrel fluctuations are allowing D_2O the chance to exchange with the H_2O interacting with the chromophore. This exchange could lead to slightly stronger stabilizing interactions on the chromophore due to the presence of the D_2O, resulting in the observed red shift. Indeed, the work of Hildebrandt *et al.* supports this hypothesis through the observed red shift of Bacteriorphodopsin's chromophore due to the exchange of H2O with D_2O, using resonance Raman spectroscopy.[115] Concurrently, it has been shown that for anionic fluorophores, an increase in solvent polarity leads to a red shift in absorbance and fluorescence.[116,117] Thus, given the fact that D_2O is slightly more polar than H_2O,[118] and that it is possible for D_2O to exchange with H_2O,[115] the observed red shift is understandable.

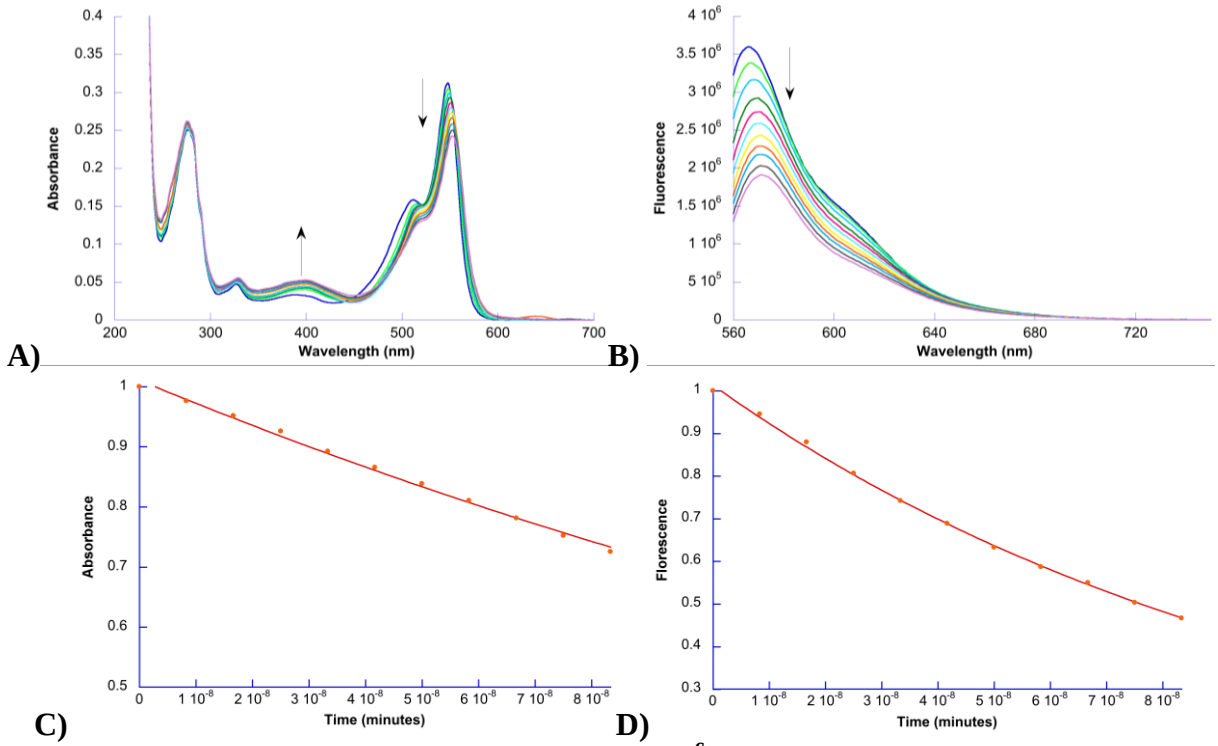

Figure 4.8: A) The absorbance mOrange (4.40 X 10^{-6} M) in D_2O while exposed to the pulsed laser (497 nm, 4.286 ± 0.657 mJ, 10 Hz) for 1000 shots. B) The fluorescence of mOrange (4.40 X 10^{-6} M) in D_2O while exposed to the pulsed laser (497 nm, 4.286 ± 0.657 mJ, 10 Hz) for 1000 shots. C) The decay of the absorbance for mOrange at 548 nm. D) The maximum corrected and normalized fluorescence of mOrange at 565 nm. For C) and D) the data were modeled with equation 2.1 and the analysis is in appendix A.

A ramification of this solvent exchange, is that the rate constants of reaction should be slowed due to the presence of the heavier deuterium isotope.[114] Indeed, looking at the rate constants of decay for mOrange in D_2O (figures 4.8C, table 4.2), it can be seen that the absorbance at 548 nm decays in a first order manner with a rate constant smaller than that seen for mOrange in PBS (table 4.2). Thus, the presence of D_2O is slowing the observed photobleaching of mOrange. However, it should be noted that the fluorescence appears to decay at a faster rate than that seen when in PBS, which it counter intuitive to what is expected. Yet, given that the mOrange is undergoing a solvent exchange, it could be that the stronger stabilizing interactions[119] are favouring the non-emissive decay for mOrange. Thus, although the D_2O has a

protective effect on the photobleaching of the protein, it ultimately leads to a loss of fluorescence. Realizing the effects of D_2O on the decay of mOrange, the question arose if other characteristics would be affected, such as the appearance of the protonated by-product. Despite the observed changes to the decay, it appears that mOrange is still photobleaching in a similar fashion to what was seen in chapter two, where a protonated by-product is created upon irradiation. This can be observed with the appearance of the expected protonated by-product at 406 nm in the absorbance spectra (figure 4.8A). Therefore, having established the manner of photobleaching for mOrange in D_2O when the 497 nm pulsed laser is used as the irradiation source, the next step in determining the $^1O_2$ production will be the addition of ABDA.

Table 4.2: The comparison of the values for the rate constants of decay for mOrange with D_2O or PBS as determined through the analysis of the decay for the maximum absorbance at 548 nm and fluorescence at 565 nm of mOrange during photobleaching with the 497 nm pulsed laser.

λ_{max} (D_2O / PBS)	*A*	*k* (min^{-1})
548 nm (PBS)	1.014 (±0.005)	1.22 X 10^7 (±2 X 10^5)
548 nm (D_2O)	1.011 (±0.004)	3.85 X 10^6 (±8 X 10^4)
565 nm (PBS)	1.048 (±0.013)	1.84 X 10^7 (±5 X 10^5)
565 nm (D_2O)	1.014 (±0.005)	9.27 X 10^6 (±1.2 X 10^5)

4.3.3.2 mOrange with ABDA in D_2O during laser irradiation

To reiterate, the use of the 497 nm laser was employed in order to determine if the primary excitation of the green immature mOrange was responsible for the production of a greater amount of $^1O_2$. Essentially, it can be argued that if the green immature mOrange did

produce more $^1O_2$ than the mature mOrange, then the primary excitation of the green immature mOrange should result in a greater decay for ABDA due to larger amounts of $^1O_2$ being produced. Ergo, a solution of mOrange and ABDA in D_2O was irradiated with the 497 nm laser for 1000 shots.

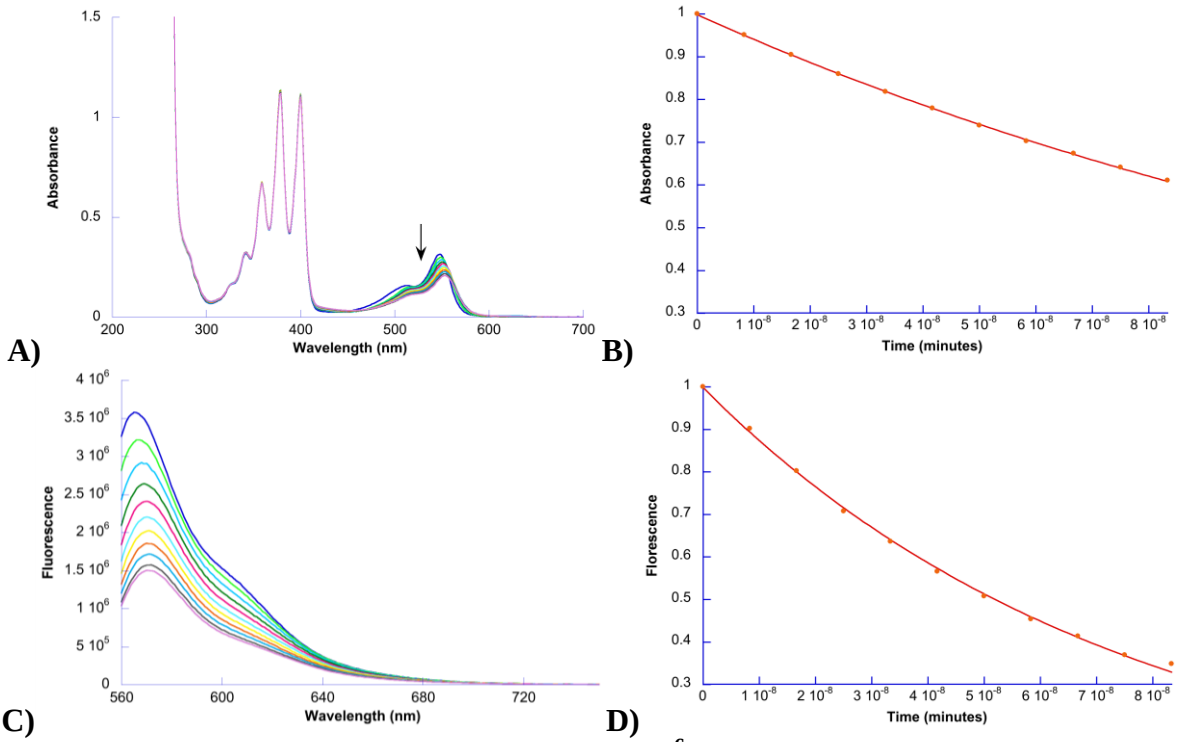

Figure 4.9: A) The absorbance mOrange (4.42 X 10^{-6} M) in the presence of ABDA (0.1 mM) in D_2O while exposed the pulsed laser (497 nm, 6.262 ± 0.914 mJ, 10 Hz) for 1000 shots. B) The decay of the absorbance for mOrange at 548 nm. C) The fluorescence of mOrange (5.22 X 10^{-6} M) in the presence of ABDA (0.1 mM) in D_2O while exposed the Green LED for 4 hours. D) The decay of the maximum corrected and normalized fluorescence for mOrange at 565 nm. For B) and D) the data were modeled with equation 2.1 and the analysis is in appendix A.

From the results in figure 4.9A, it can be seen that mOrange is decaying with the same red shift observed for mOrange and D_2O alone. In agreement with this is the analysis of the decay at 548 nm (figure 4.9B), which fits a first order rate similar to the one seen in figure 4.8C. Concurrently, the fluorescence of mOrange displays the same red shift and first order decay seen

for mOrange in figures 4.8B and D. This suggests that ABDA is not affecting the 497 nm pulsed laser photobleaching of mOrange, just as was seen for the Green LED. Thus, the spectral manipulation necessary to determine the amount of $^1O_2$ produced during irradiation could be undertaken.

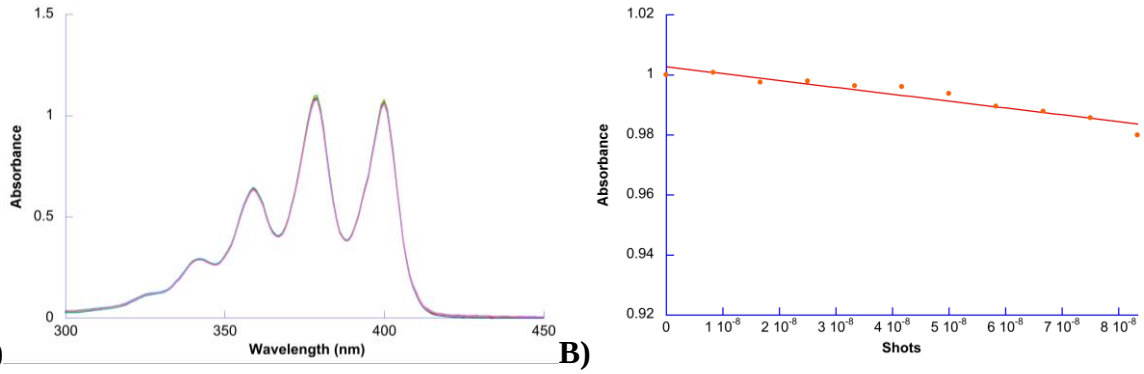

A) **B)**

Figure 4.10: A) The absorbance of ABDA (0.1 mM) in the presence of mOrange and D_2O during exposure to the pulsed laser (497 nm) for 1000 shots with the spectra of mOrange removed. B) The decay of ABDA at 380 nm. The data were modeled with equation 2.1 and the analysis is in appendix A.

The resulting spectra of ABDA can be seen in figure 4.10A, however, unlike the spectra of ABDA obtained in D_2O with the Green LED, no significant decrease can be immediately seen. Yet, by plotting the maxima at 380 nm for ABDA (figure 4.10B), a gradual decrease can be observed. This indicates that $^1O_2$ is being produced, but with only about 2% of the original intensity of ABDA being removed, the use of the 497 nm pulsed laser is not inducing $^1O_2$ production to the same extent as the Green LED, which had about a 10% loss. This perplexing result seems to suggest that the link between the green immature mOrange and $^1O_2$ is not as strong as was previously thought.

However, before this conclusion can be made there are a few factors to be considered. First of all, the amount of protein undergoing excitation is essential. Since it has been shown that 497 nm irradiation results in green immature mOrange excitation, it stands to reason that the $^1O_2$

produced will originate from the green immature mOrange. However, with estimates of the green immature mOrange being less than 20% of the total protein in solution,[24] there is considerably less protein available to produce $^1O_2$. Therefore, with less protein undergoing excitation to produce $^1O_2$, the observed decay for ABDA will be lower.

Additionally, it can be speculated that the solvent exchange would have an additional effect on the apparent amount of $^1O_2$ in solution. Specifically, it is possible to imagine a scenario in which the now extended lifetime of the newly created $^1O_2$ would lead to a greater interaction with the amino acids of mOrange's β-barrel. Therefore, if the interaction of $^1O_2$ with mOrange's amino acids were enhanced due to the D_2O solvent exchange, then there would be less $^1O_2$ able to escape the β-barrel of mOrange. The impetus for this comes from the microheterogeneity of biological environments, where $^1O_2$ was shown to spend a majority of its life within a lipid vesicle environment rather than in solution.[120,121] Ergo, the fact that $^1O_2$ spends a majority of its life not in the solvent phase, and that there exists a solvent exchange which would increase the lifetime of $^1O_2$ in the β-barrel, it is possible that $^1O_2$ would be more likely to stay within the β-barrel of mOrange. Thus, there would be greater opportunity for $^1O_2$ to interact with the amino acids of mOrange and therefore less $^1O_2$ available to interact with ABDA, decreasing the observed decay of ABDA. However, in order to confirm this enhanced amino acid oxidation, further experiments would need to be performed, such as mass spectroscopy.[122] Unfortunately without this data, the explanation of prolonged $^1O_2$ interactions with the β-barrel, can only be considered to be speculation.

Given these factors, the current application of the pulsed laser appears to be inadequate for the determination of $^1O_2$ production preference from either the green immature or the mature mOrange. Although the laser excitation data has demonstrated the red shift of fluorescence from

a fluorescent protein due to solvent exchange, this data has not been able to support the conclusions drawn from the Green LED induced mOrange $^1O_2$ production. This indicates that other methods will need to be employed, such as determining $^1O_2$ directly via its 1275 nm emission.[35] It should be noted that in chapters two and three, the use of heat was employed to remove the photophysical presence of the green immature mOrange from solution. Upon first glance, this technique presents itself as a viable option for the determination of $^1O_2$ from the mature mOrange. However, the use of ABDA would not be adequate, as it is known that the $^1O_2$ oxidized ABDA variants such as 3,3'-(1,4-naphthylidene)dipropionate, are thermal releasers of $^1O_2$.[123,124] Thus, it is possible that any loss of the ABDA spectra due to $^1O_2$ would be negated by the subsequent heat induced release of $^1O_2$ from ABDA-O_2, suggesting that the addition of heat would be counterproductive to $^1O_2$ detection.

4.4 Conclusion

In the investigation of the photobleaching characteristics of mOrange, $^3O_2$ has been shown to be a key factor, where in the absence of $^3O_2$ very little photobleaching was seen. Given the extent of fluorescent protein ROS producers known in literature, it was speculated that the excitation of mOrange could lead to the production of ROS. To determine if mOrange was producing ROS, it was essential to maintain the same conditions that have been previously established for the photobleaching of mOrange in order to limit variability in experimental parameters. Thus, the water-soluble $^1O_2$ (a species of ROS) specific sensor, ABDA, was employed to determine if mOrange was producing $^1O_2$ via monitoring the absorbance at 380 nm during the mOrange irradiation period. It was shown through absorption spectroscopy that $^1O_2$ was being produced upon mOrange excitation. Indeed, confirming the presence of $^1O_2$, was the enhance decay of ABDA when the solvent was changed to D_2O, which is known to prolong the

lifetime of $^1O_2$. In addition to the presence of $^1O_2$, unique to this study was the demonstration of a link between $^1O_2$ production and the green immature mOrange. This was determined through the correlation between the large initial decay of mOrange's shoulder and the concurrent large initial decay for ABDA, when mOrange was irradiated with the Green LED in D_2O.

Realizing the potential to further elucidate the link between the green immature mOrange and $^1O_2$ production, the pulsed laser was employed to selectively enhance the excitation of the green immature mOrange. Although the presence of $^1O_2$ was observed, the pulsed laser excitation resulted in significantly less $^1O_2$ production compared to the Green LED. However, these results do not negate the link between the green immature mOrange and $^1O_2$ production. This is because it was reasoned that the percent of $^1O_2$ producers was lower with the 497 nm laser irradiation, and the non-continuous type of irradiation along with the length of irradiation affected the ability to produce $^1O_2$ to the same extent as the Green LED. Unfortunately, these results indicate that the use of the pulsed laser is not effective for the determination of $^1O_2$ production in fluorescent proteins. This suggests that other methods need to be employed, such as detection of $^1O_2$ phosphorescence emission at 1275 nm[35] or the use of continuous wave lasers that could irradiate a whole sample simultaneously. Additionally, the use of known fluorescent protein $^1O_2$ producers such as TagRFP[107] could be employed in order to determine the Φ_{1O2} through comparative measurements.

Chapter Five: **Conclusions**

5.1 Summary of Findings

5.1.1 On the interaction of mOrange with light

The basis of the work presented within this thesis, rests on the idea of FP photobleaching. Although the topic is well studied, it is still not fully understood. Having reviewed the literature on the topic, there appears to be several means for photobleaching of FPs to occur, including photoisomerization and excited state proton transfer.[46,80,125,126] Indeed, of the vast body of knowledge on FP photobleaching, there still appears to be no general consensus on FP photobleaching. Hence, to garner a better picture of FP photobleaching, the use of a highly light susceptible protein was required. The ideal candidate was mOrange, a variant of DsRed, whose high fluorescent brightness and light susceptibility[25-27] provided the perfect combination for this study. With its strong initial absorbance (at 548 nm) and fluorescence (at 565 nm), the photobleaching characteristics could be easily followed while mOrange was irradiated.[25]

Therefore, having determined the ideal candidate for the photobleaching study, the first step in the investigation was to produce mOrange in order to obtain pure samples for photobleaching. The reason for this was that it is known that the cellular environment contains components that could interact with the photobleaching characteristics of FPs.[58] Thus, in an effort to produce the purified protein, it was discovered that the maturation of mOrange required warmer conditions to obtain the properly folded protein as compared to the Green Fluorescent Protein (GFP).[60] It was through the study of the maturation of mOrange that we showed the proposed branched chromophore pathway for variants of DsRed[67,68] also held true for mOrange. Thus, this indicated that a solution of purified mOrange would have both the properly folded

mature mOrange and the improperly folded green immature mOrange; suggesting a possible unforeseen effect on the photobleaching of mOrange.

Having produced the necessary purified protein to carry out the photobleaching experiments, the irradiation of mOrange with high power LEDs began. The three LEDs that were used were a UV LED (λ_{max} = 406 nm), Blue LED (λ_{max} = 447 nm) and a Green LED (λ_{max} = 513 nm). By overlapping the absorbance spectrum of mOrange and the spectral profiles of the LEDs, it was shown that the UV and Blue LED did not overlap significantly with the chromophore of mOrange between 460 nm – 570 nm. One the other hand, it was shown that the Green LED did have significant overlap. To determine the effects of these LEDs on mOrange, PBS solutions containing about 4 X 10^{-6} M mOrange were irradiated with each of the LEDs. It was shown that for both the UV and Blue LED the 548 nm absorbance and 565 nm fluorescence maxima followed a first order decay, which was linked to the alteration of the β-barrel due to photoinduced fluctuations of the β-barrel itself.[13,74,75] Given that neither the UV nor the Blue LEDs induced chromophore mediated photobleaching; the irradiation of the mOrange solutions was carried out with the Green LED. The results of this irradiation produced a bi-exponential decay of the 548 nm absorbance and 565 nm fluorescence maxima as well as the concomitant appearance of a protonated by-product, which was not seen in the previous Blue and UV LED irradiations.

To elucidate the nature of the observed bi-exponential decay, one of the possible hypotheses centred on the simultaneous excitation of the green immature and mature mOrange species in solution. It was reasoned that if the two species of mOrange were indeed contributing to the observed decay of mOrange, then the use of a tuneable laser would allow the separate excitation of the species in solution. Thus, the irradiation of mOrange using the 532 nm pulsed

laser was carried out, resulting in the expected bi-exponential decay for the characteristic peaks of mOrange. Surprisingly however, the presence of a peak at 495 nm was revealed, which was not seen before for the Green LED photobleaching sessions, suggesting that the green immature mOrange was present in solution. Therefore, to assess the extent of overlap between the green immature and mature mOrange, peak deconvolution was carried out on a non-photobleached sample of mOrange, supporting the presence of both the green immature and mature mOrange. Based on the deconvolution, additional wavelengths of pulsed laser excitation were chosen (497, 548 and 560 nm), to attempt to separate the photobleaching contributions of the green immature mOrange from the mature mOrange.

Fascinatingly, by carrying out the unique photobleaching study of mOrange using multiple laser excitation wavelengths, the rates of decay within the original bi-exponential decay could be attributed to either the green immature or the mature mOrange. This conclusion was drawn from the fact that the use of the 497 nm laser excitation, that primarily excited the green immature mOrange, produced a first order decay that was linked to the observed rate of the green immature mOrange. Whereas the 560 nm laser excitation, that primarily excited the mature mOrange, produced a first order decay which was linked to the mature mOrange. Not only did these results enable the correlation of the observed rates within the bi-exponential decay, they also demonstrated the mature mOrange's greater resilience to photobleaching when compared to the green immature mOrange. Although these results provided strong support of the bi-exponential decay being a product of both the green immature and the mature mOrange photobleaching, the only way to provide conclusive evidence for the correlation of the observed rates, was to remove one the photobleaching species from solution.

Without the ability to physically remove one of the species of mOrange from the solution, it could be argued that the presence of the two species would be affecting the manner of decay for mOrange as a whole. Thus, to provide the evidence needed to support the correlations described through the pulsed laser, it was reasoned that the application of heat to a solution of purified mOrange would be able to selectively denature the comparatively less 'stable' green immature mOrange. Therefore, by heating the solution of mOrange to 82 °C, the loss of the green immature mOrange was observed. Although this loss of the green immature mOrange was not a physical removal of the protein, the photophysical presence of the green immature mOrange was removed, enabling the mature mOrange to be photobleached on its own.

Having never been previously reported in the literature, the first demonstration of high temperature photobleaching was carried out on a FP. The results of the 532 nm laser photobleaching were that at 82 °C, mOrange decayed with a similar rate to that seen for the 560 nm laser excitation, confirming the rate correlations. Thus, by removing the photophysical presence of the green immature mOrange from solution with heat, it was shown that the mature mOrange decays in a first order manner, and that the green immature mOrange participates in the overall photophysical properties of mOrange. Considering that the immature variants of FPs have never been considered to play a role in the photophysics of FPs before, these results suggest that the presence of immature variants of FPs may contribute to observed phenomena and require attention in order assure conclusive data.

5.1.2 On the photoconversion of mOrange with Potassium Ferricyanide

The discovery of the role of the green immature mOrange in the overall photophysics of mOrange, prompted the examination of other observed FP phenomena. One such phenomenon that has been recently reported by Subach *et al.*, is the ability of mOrange to undergo a

photoinduced conversion to a far red mOrange (FR mOrange) variant when in the presence of the external oxidant potassium ferricyanide ($K_3Fe(CN)_6$).[58] Not only could the presence of the green immature mOrange have an effect on the production of FR mOrange, the ability of the $K_3Fe(CN)_6$ to undergo photoinduced excitation was not addressed, indicating that the excited $K_3Fe(CN)_6$ may be interacting with mOrange to produce the FR mOrange. Thus, to determine if the proposed excitation of the mature mOrange was actually producing the FR mOrange, several solutions of mOrange and $K_3Fe(CN)_6$ were examined under different photobleaching conditions.

The first conditions assessed were the light sources used to irradiate the solution of mOrange and $K_3Fe(CN)_6$. Considering that the $K_3Fe(CN)_6$ absorbs within the region of the UV and Blue LEDs, while it does not overlap with the Green LED, it was suggested that the use of the UV and Blue LEDs would enable the study of the presence of excited $K_3Fe(CN)_6$ on mOrange. Thus, solutions of mOrange and $K_3Fe(CN)_6$ were irradiated with the UV and Blue LEDs, resulting in their dramatic loss of fluorescence. It was determined through the use of the antioxidant, imidazole, and western blot analysis, that the presence of the excited $K_3Fe(CN)_6$ was the cause of the observed loss of fluorescence as the amino acids of the β-barrel were becoming oxidized. However, without the presence of any FR mOrange, the photoconversion of mOrange could not be contributed to the excited $K_3Fe(CN)_6$. This left the excitation of mOrange as the source of the FR mOrange.

Indeed, when mOrange was irradiated with the Green LED in the presence of $K_3Fe(CN)_6$, the appearance of the FR mOrange was observed, confirmed through absorption and fluorescence spectroscopy. However, realizing that the Green LED excited both the green immature and mature mOrange species, it was essential to separate the contribution of these two species to determine from which species (if not both) the FR mOrange was originating.

Therefore, the use of the tuneable laser was employed with the same 497, 532, 548 and 560 nm excitation wavelengths to elucidate the contributions to the growth of the FR mOrange. Interestingly, it was the excitation of the green immature mOrange using the 497 nm pulsed laser that induced the most significant amount of FR mOrange previously seen. This suggested that the green immature mOrange excitation was responsible for the FR mOrange, which was in contrast to the conclusions drawn by Subach *et al.*.[58] Although the size of the $K_3Fe(CN)_6$ is not conducive to interaction with the chromophore of FP, it was reasoned that the green immature mOrange, with its propensity to denature at a lower temperature than the mature mOrange, was more apt to undergo light induced β-barrel fluctuations,[36,74,75] that would expose the chromophore to the solution. This would ultimately allow the excited chromophore to interact with the $K_3Fe(CN)_6$ in solution, allowing it to become oxidized.

Based on the link presented between the green immature mOrange and the FR mOrange, it was concluded that if the excited green immature mOrange could be removed from the solution, then no FR mOrange should appear. To do this, a solution of mOrange and $K_3Fe(CN)_6$ was heated to 82 °C and the photophysical present of the green immature mOrange was removed. However, upon the 82 °C irradiation, it was shown that the most significant amount of FR mOrange was produced. Although perplexing, it was concluded that the FR mOrange was actually resulting from the interaction of the protonated by-products of mOrange photobleaching and $K_3Fe(CN)_6$. Indeed, no light was required in order to demonstrate the growth of the FR mOrange from a photobleached solution of mOrange, suggesting that the only requirement for the production of the FR mOrange was access to the chromophore. Given that the high temperature would expose the chromophores of the protonated by-product to the solution, the conversion by $K_3Fe(CN)_6$ is understandable. Therefore, based on the investigation into the

photoswitchable nature of mOrange, the FR mOrange results from an interaction of either the excited green immature mOrange, or the protonated by-products.

These results demonstrate that the conclusion drawn by Subach *et al.* is incorrect. The implications of this study indicate that the use of this method to achieve an orange to red colour change would not be practical, due to the inability of the mature mOrange protein itself to convert to the FR mOrange. To expand on this idea, if the imaging experiment is relying on the orange fluorescence of mOrange to change to red, then the results would be misleading as the red fluorescence would most likely result form the green immature mOrange or the protonated by-product of mOrange, not the expected mature mOrange.

5.1.3 Singlet Oxygen production in mOrange

One of the most prominent reactive oxygen species (ROS) that is known to induce oxidative stress is singlet oxygen ($^1O_2$).[35,127] Mainly created through a process known as triplet-triplet annihilation (TTA), the production of $^1O_2$ is dependent on the interaction of molecular oxygen ($^3O_2$) with a photosensitizer. Considering it has been shown that the photobleaching characteristics of mOrange are reliant on the presence of oxygen,[31] it was postulated that one pathway for photobleaching could be due to the production and subsequent interaction of $^1O_2$ with mOrange. Thus, confirming the significant dependence of mOrange's light susceptibility on $^3O_2$, a solution of mOrange was deoxygenated with inert nitrogen gas, and irradiated for two hours with the Green LED. This experiment demonstrated very little loss of the main mOrange peak whereas when $^3O_2$ is present, nearly 40% of the main mOrange peak is lost during photobleaching. These results suggest that $^3O_2$ is essential to the photobleaching process for mOrange, thus the use of the $^1O_2$ specific sensor, 9,10-anthracenediyl-bis(methylene)dimalonate (ABDA), was employed to see if $^1O_2$ was being created by mOrange.

Monitoring the main 380 nm peak of ABDA for decay due to $^1O_2$ interaction, the photobleaching experiments of mOrange were repeated with ABDA and $^3O_2$, and after four hours of irradiation it was shown that mOrange does indeed produce $^1O_2$. However, given the possible interactions of $^1O_2$ with ABDA and the amino acids of mOrange, the exact quantum yield could not be determined. To confirm the presence of $^1O_2$, the solvent was changed from PBS to D_2O, which would enhance the lifetime of the $^1O_2$ in solution, ultimately resulting in an enhanced decay of ABDA. After four hours of irradiation with the Green LED, there was a noticeable increase in the decay of ABDA at 380 nm, suggesting that $^1O_2$ was indeed being produced from the excitation of mOrange. It should be noted that although ABDA demonstrated the presence of $^1O_2$, since it is a $^1O_2$ specific sensor, the presence of other ROS could not be determined.

Unique to this study, was the link observed between the green immature mOrange and the production of $^1O_2$. This link was seen through the significant initial decay in the shoulder of mOrange when irradiated with the Green LED in D_2O and the corresponding significant initial decay of ABDA. These results reaffirm the conclusion drawn earlier, suggesting that the presence of immature variants of FPs may contribute to observed phenomena and require attention in order assure conclusive data.

Finally, in an attempt to assess the extent of the link between the green immature mOrange and $^1O_2$ production, the pulsed laser at 497 nm was used to photobleach mOrange in D_2O in the hopes of increasing the amount of $^1O_2$ produced. Unfortunately, the use of the higher power laser excitation lead to a novel solvent exchange with D_2O, altering the photobleaching characteristics of mOrange. Indeed, when ABDA was used to detect $^1O_2$ during laser irradiation, very little loss of the 380 nm was observed over the photobleaching session. Given the changes observed in the

characteristics of photobleaching for mOrange in D_2O, the results suggest that the use of the pulsed laser to elucidate the link between the green immature mOrange and $^1O_2$ production, was inadequate.

5.2 Future Perspectives

Based on the results of the photobleaching of mOrange, the significant contributions of the immature variant to the overall photobleaching characteristics, needs to be studied on a wider basis. The logic for this rests on the fact that most of the wide varieties of FPs based on DsRed also form their characteristic chromophores through the branched chromophore maturation mechanism proposed by Strack *et al.*.[67] Thus, it would be pertinent to determine the extent of interaction that other immature variants have on their mature counter parts. Other DsRed variants such as mApple, mCherry, or even mRFP[22,27] would provide ample starting ground. Were this study to prove successful, it would highlight the necessity of ensuring that FPs are not only properly folded, but their photobleaching characteristics are completely understood.

Additionally, the study of $^1O_2$ production needs to be expanded for mOrange. Indeed, one method that could be employed to elucidate the link between the green immature mOrange and $^1O_2$ production is the direct detection of $^1O_2$'s 1275 nm emission.[35] By using a tuneable laser to excite mOrange, either the mature or the immature mOrange would be primarily excited, and the subsequent relative intensities of 1275 nm emission could be monitored. This relative emission intensity would allow the correlation to be drawn between $^1O_2$ production amount and species being excited. Also, the direct direction of the 1275 nm emission would allow the comparison of Tag-RFP $^1O_2$ production to that of mOrange $^1O_2$ production, enabling the $^1O_2$ quantum yield for mOrange to be determined.[107] Finally, another possibility for $^1O_2$ production would be to follow the effects of $^1O_2$ on the β-barrel amino acids of mOrange, by monitoring them for oxidative

stress by mass spectroscopy.[122] This would allow the determination of the amino acids that are affected the most by $^1O_2$ oxidation, and the correlation between $^1O_2$ and photobleaching to be studied.

References

(1) Yuste, R. *Nature Methods* **2005**, *2*, 902

(2) König, K.; So, P. T. C.; Mantulin, W. W.; Tromberg, B. J.; Gratton, E. *Journal of Microscopy* **1996**, *183*, 197.

(3) Tsien, R. Y. *Ann. Rev. Neurosci* **1989**, *12*, 227

(4) Song, L.; Hennink, E. J.; Young, I. T.; Tanke, H. J. *Biophysical Journal* **1995**, *68*, 2588.

(5) Rizzo, M. A.; Davidson, M. W.; Piston, D. W. *Cold Spring Harb Protoc* **2009**, *4*.

(6) Chalfie, M.; Tu, Y.; Euskirchen, G.; Ward, W. W.; Prasher, D. C. *Science* **1994**, *263*, 802

(7) Shimomura, O.; Johnson, F. H.; Saiga, Y. *Journal of Cellular Physiology* **1962**, *59*, 223

(8) Remington, S. J. *Current Opinions in Structural Biology* **2006**, *16*, 714

(9) Zimmer, M. *Chem. Rev.* **2002**, *102*, 759

(10) Tsien, R. Y. *Annual Review of Biochemistry* **1998**, *67*, 509.

(11) Tolbert, L. M.; Baldridge, A.; Kowalik, J.; Solntsev, K. M. *Accounts of Chemical Research* **2012**, *45*, 171

(12) Dong, J.; Abulwerdi, F.; Baldridge, A.; Kowalki, J.; Solntsev, K. M.; Tolbert, L. M. *Journal of The American Chemical Society* **2008**, *130*, 14096

(13) Mizuno, H.; Mal, T. K.; Wälchli, M.; Kikuchi, A.; Fukano, T.; Ando, R.; Jeyakanthan, J.; Taka, J.; Shiro, Y.; Ikura, M.; Miyawaki, A. *Proceedings of the National Academy of Sciences* **2008**, *105*, 9227.

(14) Stoner-Ma, D.; Jaye, A. A.; Matousek, P.; Towrie, M.; Meech, S. R.; Tonge, P. J. *Journal of The American Chemical Society* **2005**, *127*, 2864

(15) Brejc, K.; Sixma, T. K.; Kitts, P. A.; Kain, S. R.; Tsien, R. Y.; Ormö, M.; Remington, S. J. *Proceedings of the National Academy of Sciences* **1997**, *94*, 2306

(16) Solntsev, K. M.; Poizat, O.; Dong, J.; Rehault, J.; Lou, Y.; Burda, C.; Tolbert, L. M. *The Journal of Physical Chemistry B* **2008**, *112*, 2700

(17) Gepshtein, R.; Huppert, D.; Agmon, N. *The Journal of Physical Chemistry B* **2006**, *110*, 4434

(18) Dong, J.; Solntsev, K. M.; Tolbert, L. M. *Journal of The American Chemical Society* **2009**, *131*, 662

(19) Usman, A.; Mohammed, O. F.; Nibbering, E. T. J.; Dong, J.; Solntsev, K. M.; Tolbert, L. M. *Journal of The American Chemical Society* **2005**, *127*, 11214

(20) Zhang, G.; Gurtu, V.; Kain, S. R. *Biochemical and Biophysical Research Communications* **1996**, *227*, 707

(21) Matz, M. V.; Fradkov, A. F.; Labas, Y. A.; Savitsky, A. P.; Zaraisky, A. G.; Markelov, M. L.; Lukyanov, S. A. *Nature Biotechnology* **1999**, *17*, 969

(22) Campbell, R. E.; Tour, O.; Palmer, A. E.; Steinbach, P. A.; Baird, G. S.; Zacharias, D. A.; Tsien, R. Y. *Proceedings of the National Academy of Sciences* **2002**, *99*, 7877

(23) Yarbrough, D.; Wachter, R. M.; Kallio, K.; Matz, M. V.; Remington, S. J. *Proceedings of the National Academy of Sciences* **2001**, *98*, 462

(24) Shu, X.; Shaner, N. C.; Yarbrough, C. A.; Tsien, R. Y.; Remington, S. J. *Biochemistry* **2006**, *45*, 9639

(25) Shaner, N. C.; Campbell, R. E.; Steinbach, P. A.; Giepmans, B. N. G.; Palmer, A. E.; Tsien, R. Y. *Nature Biotechnology* **2004**, *22*, 1567

(26) Shaner, N. C.; Lin, M. Z.; McKeown, M. R.; Steinbach, P. A.; Hazelwood, K. L.; Davidson, M. W.; Tsien, R. Y. *Nature Methods* **2008**, *5*, 545.

(27) Shaner, N. C.; Steinbach, P. A.; Tsien, R. Y. *Nature Methods* **2005**, *2*, 905.

(28) Henderson, J. N.; Ai, H. W.; Campbell, R. E.; Remington, S. J. *Proceedings of the National Academy of Sciences* **2007**, *104*, 6672

(29) Subach, F. V.; Malashkecih, V. N.; Zencheck, W. D.; Xiao, H.; Filonov, G. S.; Almo, S. C.; Verkhusha, V. V. *Proceedings of the National Academy of Sciences* **2009**, *106*, 21097

(30) Betzig, E.; Patterson, G. H.; Sougrat, R.; Lindwasser, O. W.; Olenych, S.; Bonifacino, J. S.; Davidson, M. W.; Lippincott-Schwartz, J.; Hess, H. F. *Science* **2006**, *313*, 1642.

(31) Xiao, J. In *Single-Molecule Imaging in Live Cells*; 1st ed.; Hinterdorfer, P., Van Oijen, A., Eds.; Springer: 2009.

(32) Chudakov, D. M.; Matz, M. V.; Lukyanov, S.; Lukyanov, K. A. *Physiological Reviews* **2010**, *90*, 1103

(33) Vegh, R. B.; Solntsev, K. M.; Kuimova, M. K.; Cho, S.; Liang, Y.; Loo, B. L. W.; Tolbert, L. M.; Bommarius, A. S. *ChemComm* **2011**, *47*, 4887.

(34) Imlay, J. A. *Nat Rev Micro* **2013**, *11*, 443.

(35) Ogilby, P. R. *Chemical Society Reviews* **2010**, *39*, 3181.

(36) Vegh, R. B.; Bravaya, K. B.; Bloch, D. A.; Bommarius, A. S.; Tolbert, L. M.; Verkhovsky, M.; Krylov, A. I.; Solntsev, K. M. *The Journal of Physical Chemistry B* **2014**.

(37) Kremers, G. J.; Piston, D. W. *Nature Methods* **2008**, *5*, 472

(38) Dean, K. M.; Lubbeck, J. L.; Binder, J. K.; Schwall, L. R.; Jimenez, R.; Palmer, A. E. *Biophysical Journal* **2011**, *101*, 961.

(39) Chen, M. C.; Lambert, C. R.; Urgitis, J. D.; Zimmer, M. *Chemical Physics letters* **2001**, *270*, 157

(40) Turro, N. J.; Ramamurthy, V.; Scaiano, J. C. In *Principles of molecular photochemistry an introduction*; University Science Books: Sausalito, 2009, p 169

(41) Lakowicz, J. R. In *Principles of Fluorescence Spectroscopy*; 3rd ed.; Springer: Baltimore, 2006, p 440.

(42) Wurth, C.; Grabolle, M.; Pauli, J.; Spieles, M.; Resch-Genger, U. *Nat Protoc* **2013**, *8*, 1535.

(43) Habuchi, S.; Ando, R.; Dedecker, P.; Verheijen, W.; Mizuno, H.; Miyawaki, A.; Hofkens, J. *Proceedings of the National Academy of Sciences* **2005**, *102*, 9511

(44) Tolbert, L. M.; Solntsev, K. M. *Accounts of Chemical Research* **2002**, *35*, 19

(45) Tonge, P. J.; Meech, S. R. *Journal of Photochemistry and Photobiology A: Chemistry* **2009**, *205*, 1

(46) Habuchi, S.; Dedecker, P.; Hotta, J.-i.; Flors, C.; Ando, R.; Mizuno, H.; Miyawaki, A.; Hofkens, J. *Photochemical & Photobiological Sciences* **2006**, *5*, 567.

(47) Quillin, M. L.; Anstrom, D. M.; Shu, X.; O'Leary, S.; Kallio, K.; Chudakov, D. M.; Remington, S. J. *Biochemistry* **2005**, *44*, 5774

(48) Andersen, M.; Wahl, M. C.; Stiel, A. C.; Gräter, F.; Schäfer, L. V.; Trowitzsch, S.; Weber, G.; Eggeling, C.; Grubmüller, H.; Hell, S. W.; Jakobs, S. *Proceedings of the National Academy of Sciences* **2005**, *102*, 13070

(49) He, X.; Bell, A. F.; Tonge, P. J. *FEBS Letters* **2003**, *549*, 35

(50) van Thor, J. J.; Ronayne, K. L.; Towrie, M.; Sage, J. T. *Biophysical Journal* **2008**, *95*, 1902

(51) Turro, N. J.; Ramamurthy, V.; Scaiano, J. C. In *Principles of molecular photochemistry and introduction*; University Science Books: Sausalito, 2009, p 1

(52) Tsien, R. Y.; Ernst, L.; Waggoner, A. In *Handbook of biological confocal micrscopy*; 3rd ed.; Pawley, J. B., Ed.; Springer: New York, 2006, p 338

(53) Valencia-Perez, A. Z.; Heyne, B. *ChemBioChem* **2010**, *11*, 2384.

(54) Nielsen, M. B.; Andersen, L. H.; Rocha-Rinza, T. *Monatshefte für Chemie Chemical Monthly* **2011**, *142*, 709

(55) Drobizhev, M.; Tillo, S.; Makarov, N. S.; Hughes, T. E.; Rebane, A. *The Journal of Physical Chemistry B* **2009**, *113*, 12860

(56) Pletnev, S.; Subach, F. V.; Dauter, Z.; Wlodawer, A.; Verkhusha, V. V. *Journal of Molecular Biology* **2012**, *417*, 144

(57) Subach, O. M.; Malashkecih, V. N.; Zencheck, W. D.; Morozova, K. S.; Piatkevich, K. D.; Almo, S. C.; Verkhusha, V. V. *Chemistry & Biology* **2010**, *17*, 333

(58) Subach, O. M.; Patterson, G. H.; Ting, L.-M.; Wang, Y.; Condeelis, J. S.; Verkhusha, V. V. *Nature Methods* **2011**, *8*, 771.

(59) McAnaney, T. B.; Zeng, W.; Doe, C. F. E.; Bhanji, N.; Wakelin, S.; Pearson, D. S.; Abbyad, P.; Shi, X.; Boxer, S. G.; Bagshaw, C. R. *Biochemistry* **2005**, *44*, 5510.

(60) Ormö, M.; Cubitt, A. B.; Kallio, K.; Gross, L. A.; Tsien, R. Y.; Remington, S. J. *Science* **1996**, *273*, 1392.

(61) Guzman, L. M.; Belin, D.; Carson, M. J.; Beckwith, J. *Journal of bacteriology* **1995**, *177*, 4121.

(62) Fery-Forgues, S.; Lavabre, D. *Journal of Chemical Education* **1999**, *76*, 1260.

(63) Xiao, J. In *Handbook of Single-Molecule Biophysics*; Hinterdorfer, P., Oijen, A., Eds.; Springer US: 2009, p 43.

(64) Wall, M. A.; Socolich, M.; Ranganathan, R. *Nat Struct Mol Biol* **2000**, *7*, 1133.

(65) Li, S.; Song, K. S.; Lisanti, M. P. *Journal of Biological Chemistry* **1996**, *271*, 568.

(66) Porterfield, J. Z.; Zlotnick, A. *Virology* **2010**, *407*, 281.

(67) Strack, R. L.; Strongin, D. E.; Mets, L.; Glick, B. S.; Keenan, R. J. *Journal of The American Chemical Society* **2010**, *132*, 8496

(68) Moore, M. M.; Oteng-Pabi, S. K.; Pandelieva, A. T.; Mayo, S. L.; Chica, R. A. *PLOS one* **2012**, *7*, e52463.

(69) Bravaya, K. B.; Subach, O. M.; Korovina, N.; Verkhusha, V. V.; Krylov, A. I. *Journal of the American Chemical Society* **2012**, *134*, 2807.

(70) Glickman, G.; Byrne, B.; Pineda, C.; Hauck, W. W.; Brainard, G. C. *Biological Psychiatry* **2006**, *59*, 502.

(71) Bogdanov, A. M.; Kudryavtseva, E. I.; Lukyanov, K. A. *PLoS One* **2012**, *7*, e53004.

(72) Donnert, G.; Eggeling, C.; Hell, S. W. *Nature Methods* **2007**, *4*, 81

(73) Sullivan, K. F. *Fluorescent Proteins*; Elsevier Science, 2007.

(74) Chapagain, P. P.; Regmi, C. K.; Castillo, W. *The Journal of Chemical Physics* **2011**, *135*, 235101.

(75) Regmi, C. K.; Bhandari, Y. R.; Gerstman, B. S.; Chapagain, P. P. *The Journal of Physical Chemistry B* **2013**, *117*, 2247.

(76) Saeed, I. A.; Ashraf, S. S. *International Journal of Biological Macromolecules* **2009**, *45*, 236.

(77) Alkaabi, K.; Yafea, A.; Ashraf, S. S. *Appl Biochem Biotechnol* **2005**, *126*, 149.

(78) Verkhusha, V. V.; Akovbian, N. A.; Efremenko, E. N.; Varfolomeyev, S. D.; Vrzheshch, P. V. *Biochemistry (Moscow)* **2001**, *66*, 1342.

(79) Jung, G.; Wiehler, J.; Zumbusch, A. *Biophysical Journal* **2005**, *88*, 1932

(80) Addison, K.; Heisler, I. A.; Conyard, J.; Dixon, T.; Bulman Page, P. C.; Meech, S. R. *Faraday Discussions* **2013**, *163*, 277.

(81) Persaud, V.; Song, S.; Hogstrom, L.; Zimmer, M.; American Chemical Society: 2009, p NERM.

(82) Shu, X.; Leiderman, P.; Gepshtein, R.; Smith, N. R.; Kallio, K.; Huppert, D.; Remington, S. J. *Protein Science* **2007**, *16*, 2703.

(83) Lounis, B.; Deich, J.; Rosell, F. I.; Boxer, S. G.; Moerner, W. E. *The Journal of Physical Chemistry B* **2001**, *105*, 5048.

(84) Pickering, J. W. *Journal of Photochemistry and Photobiology B: Biology* **1992**, *16*, 101.

(85) Fernandez-Suarez, M.; Ting, A. Y. *Nat. Rev. Mol. Cell Biol.* **2008**, *9*, 929.

(86) Kremers, G. J.; Hazelwood, K. L.; Murphy, C. S.; Davidson, M. W.; Piston, D. W. *Nature Methods* **2009**, *6*, 355.

(87) Moyá, M.; Rodríguez, A. *Transition Met Chem* **1991**, *16*, 230.

(88) Batsanov, S. S. *Inorganic Materials* **2001**, *37*, 871.

(89) Bogdanov, A. M.; Mishin, A. S.; Yampolsky, I. V.; Belousov, V. V.; Chudakov, D. M.; Subach, F. V.; Verkhusha, V. V.; Lukyanov, S.; Lukyanov, K. A. *Nature Chemical Biology* **2009**, *5*, 459.

(90) Arellano, C. A. P.; Martínez, S. S. *Solar Energy Materials and Solar Cells* **2010**, *94*, 327.

(91) Woodbury, W.; Spencer, A. K.; Stahmann, M. A. *Analytical Biochemistry* **1971**, *44*, 301.

(92) De, A. K. *A Text Book of Inorganic Chemistry*; New Age International (P) Limited, 2007.

(93) Wade, A. M.; Tucker, H. N. *The Journal of Nutritional Biochemistry* **1998**, *9*, 308.

(94) Laloo, D.; Mahanti, M. K. *Journal of the Chemical Society, Dalton Transactions* **1990**, 311.

(95) Kremers, G. J.; Gilbert, S. G.; Cranfill, P. J.; Davidson, M. W.; Piston, D. W. *Journal of Cell Science* **2011**, *124*, 157.

(96) Jung, G.; Wiehler, J.; Zumbusch, A. *Biophysical journal* **2005**, *88*, 1932.

(97) Albani, J. R. *Structure and Dynamics of Macromolecules : Absorption and Fluorescence Studies*; Elsevier Science & Technology: Amsterdam, NLD, 2004.

(98) Stepanenko, O. V.; Stepanenko, O. V.; Kuznetsova, I. M.; Verkhusha, V. V.; Turoverov, K. K. In *International Review of Cell and Molecular Biology*; Kwang, W. J., Ed.; Academic Press: 2013; Vol. Volume 302, p 221.

(99) Cody, C. W.; Prasher, D. C.; Westler, W. M.; Prendergast, F. G.; Ward, W. W. *Biochemistry* **1993**, *32*, 1212.

(100) Jay, D. G. *Proceedings of the National Academy of Sciences* **1988**, *85*, 5454.

(101) Linden, K. G.; Liao, J. C.; Jay, D. G. *Biophysical Journal* **1992**, *61*, 956.

(102) Liao, J. C.; Roider, J.; Jay, D. G. *Proceedings of the National Academy of Sciences* **1994**, *91*, 2659.

(103) Tanabe, T.; Oyamada, M.; Fujita, K.; Dai, P.; Tanaka, H.; Takamatsu, T. *Nat Meth* **2005**, *2*, 503.

(104) Pryor, W. A. *Annual Review of Physiology* **1986**, *48*, 657.

(105) Jacobson, K.; Rajfur, Z.; Vitriol, E.; Hahn, K. *Trends in Cell Biology* **2008**, *18*, 443.

(106) Ruiz-González, R.; White, J. H.; Cortajarena, A. L.; Agut, M.; Nonell, S.; Flors, C. 2013; Vol. 8596, p 859609.

(107) Ragàs, X.; Cooper, L. P.; White, J. H.; Nonell, S.; Flors, C. *ChemPhysChem* **2011**, *12*, 161.

(108) Adarsh, N.; Shanmugasundaram, M.; Avirah, R. R.; Ramaiah, D. *Chemistry-a European Journal* **2012**, *18*, 12655.

(109) Turro, N. J.; Ramamurthy, V.; Scaiano, J. C. In *Principles of molecular photochemistry an introduction*; University Science Books: Sausalito, 2009, p 414.

(110) Kuznetsova, N. A.; Gretsova, N. S.; Yuzhakova, O. A.; Negrimovskii, V. M.; Kaliya, O. L.; Luk'yanets, E. A. *Russian Journal of General Chemistry* **2001**, *71*, 36.

(111) Lindig, B. A.; Rodgers, M. A. J.; Schaap, A. P. *Journal of the American Chemical Society* **1980**, *102*, 5590.

(112) Wang , J.; Hou, Y.; Lei, W.; Zhou, Q.; Li, C.; Zhang, B.; Wang, X. *ChemPhysChem* **2012**, *13*, 2739.

(113) Ogilby, P. R.; Foote, C. S. *Journal of the American Chemical Society* **1983**, *105*, 3423.

(114) Anslyn, E. V.; Dougherty, D. A. *Modern Physical Organic Chemistry*; University Science, 2006.

(115) Hildebrandt, P.; Stockburger, M. *Biochemistry* **1984**, *23*, 5539.

(116) Dong, J.; Solntsev, K. M.; Tolbert, L. M. *Journal of the American Chemical Society* **2006**, *128*, 12038.

(117) Eisinger, J.; Navon, G. *The Journal of Chemical Physics* **1969**, *50*, 2069.

(118) Lopez-Barron, C. R.; Wagner, N. J. *Soft Matter* **2011**, *7*, 10856.

(119) Chaplin, M. *Los Alamos Natl. Lab., Prepr. Arch., Condens. Matter* **2007**, 1.

(120) Hoebeke, M.; Piette, J.; van de Vorst, A. *Journal of Photochemistry and Photobiology B: Biology* **1991**, *9*, 281.

(121) Ramamurthy, V.; Schanze, K. S. *Understanding and Manipulating Excited-State Processes*; Taylor & Francis, 2001.

(122) Vivekanadan-Giri, A.; Wang, J.; Byun, J.; Pennathur, S. *Rev Endocr Metab Disord* **2008**, *9*, 275.

(123) Di Mascio, P.; Sies, H. *Journal of The American Chemical Society* **1989**, *111*, 2909.

(124) Aubry, J. M. *Journal of Organic Chemistry* **1989**, *54*, 726.

(125) Di, D. M.; van, W. L. J. G. W.; Van, S. I. H. M.; Stuart, T. C.; Kennis, J. T. M.; Hellingwerf, K. J.; van, G. R.; Groot, M. L. *Phys. Chem. Chem. Phys.* **2011**, *13*, 16295.

(126) Addison, K.; Conyard, J.; Dixon, T.; Bulman Page, P. C.; Solntsev, K. M.; Meech, S. R. *The Journal of Physical Chemistry Letters* **2012**, *3*, 2298.

(127) Ragàs, X.; He, X.; Agut, M.; Roxo-Rosa, M.; Gonsalves, A. R.; Serra, A. C.; Nonell, S. *Molecules* **2013**, *18*, 2712.

APPENDIX A: FITMENT OF DATA

To understand the kinetics of interaction between light and mOrange, for the decays seen in the absorbance and fluorescence, the respective maxima were plotted as a function of time (for LED irradiation) or shots (for laser irradiation). These data were fitted using the KaleidaGraph 4.1 software. Listed below are the results of the fitment, where the equation used to fit the data is described in each table. For each table, the values of the equation used are displayed along with their associated error, as well as the Chi squared (Chi Sq) and R values to determine the 'goodness of fit'.

Briefly, the 'Chi Sq' value calculated within KaleidaGraph, is used to determine if the null hypothesis can be rejected. For each data set, the null hypothesis is that for each fitment, the equation used describes the given data well. In order to determine if the null hypothesis is false, the degrees of freedom have to be determined. Since the KaleidaGraph 4.1 software uses 100 curve fit points to determine the fit of the data, the degrees of freedom is n-1 or 99 degrees of freedom. From a Chi squared critical value table, the value obtained in order to reject the null hypothesis with a 99.9 % certainty, has to be greater than 61.137. Thus, for the data not to fit a given equation, the Chi Sq value has to be greater than 61.137. For the R^2 values, the closer the value is to 1, the better the predicted trend fits the given data.

Finally, the errors listed in the tables are not standard deviations. Rather, they represent the range at which the values for a given parameter could be realistically be, as calculated from one trial. Thus, the smaller the error calculated, the greater the certainty in the given value.

Table A.1: The analysis of the decay for mOrange's max normalized absorbance at 548 nm after exposure to the UV LED for 4 hours. The equation used for fit was: $y = Ae^{(-k_1 x)}$. From figure 2.10A

	Value	Error
k_1	0.0023926	0.000025915
A	0.99532	0.0016075
Chi Sq	0.00033541	
R^2	0.99876	

Table A.2: The analysis of the decay of mOrange normalized and corrected fluorescence at 565 nm after exposure to the UV LED for 4 hours. The equation used for fit was: $y = Ae^{(-k_1 x)}$. From figure 2.10B

	Value	Error
k_1	0.002573	0.000015464
A	0.99687	0.00093778
Chi Sq	0.00011326	
R^2	0.99963	

Table A.3: The analysis of the decay of mOrange normalized absorbance at 548 nm after exposure to the Blue LED for 4 hours. The equation used for fit was: $y = Ae^{(-k_1 x)}$. From figure 2.12A

	Value	Error
k_1	0.0018158	0.000022132
A	1.0026	0.001495
Chi Sq	0.00029757	
R^2	0.99833	

Table A.4: The analysis of the decay for mOrange normalized and corrected fluorescence at 565 nm after exposure to the Blue LED for 4 hours. The equation used for fit was: $y = Ae^{(-k_1 x)}$. From figure 2.12B

	Value	Error
k_1	0.0022375	0.000040264
A	1.0048	0.0025745
Chi Sq	0.00086617	
R^2	0.99656	

Table A.5: The analysis of the decay for mOrange normalized absorbance at 420 nm after exposure to the Green LED for 4 hours. This was repeated three times. The equation used for fit was: $y = Ae^{(-k_1 x)} + Be^{(-k_2 x)}$. From figure 2.15B

	Value	Error
k_1	0.016601	0.0011188
A	0.065695	0.0014652
k_2	2.0011	1.6065
B	0.0086705	0.00098113
Chi Sq	0.002566	
R^2	0.9931	

Table A.6: The analysis of the decay for mOrange absorbance at 548 nm after exposure to the Green LED for 4 hours. This experiment was performed four times. The equation used for fit was: $y = Ae^{(-k_1 x)} + Be^{(-k_2 x)}$. From figure 2.16A

	Value	Error
k_1	0.00090661	0.00021552
A	0.4039	0.018716
k_2	0.021559	0.00080332
B	0.59809	0.018079
Chi Sq	0.00019909	
R^2	0.99978	

Table A.7: The analysis of the decay for mOrange's max normalized and corrected fluorescence at 565 nm after exposure to the Green LED for 4 hours. This experiment was repeated three times. The equation used for fit was: $y = Ae^{(-k_1 x)} + Be^{(-k_2 x)}$. From figure 2.16B

	Value	Error
k_1	0.00080447	0.00066854
A	0.26248	0.037813
k_2	0.02146	0.0013097
B	0.74397	0.036513
Chi Sq	0.00083435	
R^2	0.99933	

Table A.8: The analysis of the fit for the peak deconvolution, as determined using three Gaussian peaks with the Origin 8.5 Software Suite.

	Value
Number of data points	230
Degrees of freedom	223
Chi Sq	0.00000349801
R^2	0.999664

Table A.9: The analysis of the decay for mOrange absorbance at 548 nm after 1000 shots of the 497 nm pulsed laser. The equation used for fit was: $y = Ae^{(-k_1 x)}$. From figure 2.19D (Red Trace)

	Value	Error
k_1	1.2199 X 10^7	1.4991 X 10^5
A	1.0138	0.0046001
Chi Sq	0.0010395	
R^2	0.99828	

Table A.10: The analysis of the decay for mOrange normalized absorbance at 548 nm after 1000 shots of the 532 nm laser. The equation used for fit was: $y = Ae^{(-k_1 x)} + Be^{(-k_2 x)}$. From figure 2.19D (Green Trace)

	Value	Error
k_1	5.2667 X 10^6	1.5186 X 10^6
A	0.50071	0.074043
k_2	3.9963 X 10^7	4.8964 X 10^6
B	0.49824	0.072177
Chi Sq	0.00033707	
R^2	0.99944	

Table A.11: The analysis of the decay for mOrange max normalized absorbance at 548 nm after 1000 shots of the 548 nm laser. The equation used for fit was: $y = Ae^{(-k_1 x)} + Be^{(-k_2 x)}$. From figure 2.19D (Blue Trace)

	Value	Error
k_1	2.9903 X 10^6	5.9404 X 10^5
A	0.52025	0.03514
k_2	3.0292 X 10^7	1.6884 X 10^6
B	0.48188	0.034554
Chi Sq	0.000028778	
R^2	0.99993	

Table A.12: The analysis of the decay for mOrange max normalized absorbance at 548 nm after 1000 shots of the 560 nm laser. The equation used for fit was: $y = Ae^{(-k_1 x)}$. From Figure 2.19D (Orange Trace)

	Value	Error
k_1	5.3318 X 10^6	4.7026 X 10^4
A	0.99789	0.0017378
Chi Sq	0.00018498	
R^2	0.99899	

Table A.13: The analysis of the decay for mOrange normalized and corrected fluorescence at 565 nm after 1000 shots of the 497 nm laser. The equation used for fit was: $y = Ae^{(-k_1 x)}$. From figure 2.20B (Red Trace)

	Value	Error
k_1	1.8366 X 10^7	4.7435 X 10^5
A	1.0475	0.012578
Chi Sq	0.0065466	
R^2	0.99353	

Table A.14: The analysis of the decay for mOrange max normalized and corrected fluorescence at 565 nm after 1000 shots of the 532 nm laser. The equation used for fit was: $y = Ae^{(-k_1 x)} + Be^{(-k_2 x)}$. From figure 2.20B (Green Trace)

	Value	Error
k_1	9.4088 X 10^6	1.8402 X 10^6
A	0.35378	0.076325
k_2	3.4703 X 10^7	2.3675 X 10^6
B	0.64608	0.075524
Chi Sq	0.000053396	
R^2	0.99994	

Table A.15: The analysis of the decay for mOrange max normalized and corrected fluorescence at 565 nm after 1000 shots of the 548 nm laser. The equation used for fit was: $y = Ae^{(-k_1 x)} + Be^{(-k_2 x)}$. From figure 2.20B (Blue Trace)

	Value	Error
k_1	5.5458 X 10^6	2.6593 X 10^6
A	0.33842	0.11931
k_2	2.703 X 10^7	2.9229 X 10^6
B	0.66125	0.11831
Chi Sq	0.000078558	
R^2	0.99989	

Table A.16: The analysis of the decay for mOrange normalized and corrected fluorescence at 565 nm decay after 1000 shots of the 560 nm laser. The equation used for fit was: $y = Ae^{(-k_1 x)}$. From figure 2.20B (Orange Trace)

	Value	Error
k_1	7.339 X 10^6	5.6813 X 10^4
A	1.006	0.0019963
Chi Sq	0.00022811	
R^2	0.99925	

Table A.17: The analysis of the decay for mOrange normalized absorbance at 550 nm after 1000 shots of the 532 nm laser at 82 °C. The equation used for fit was: $y = Ae^{(-k_1 x)}$. From figure 2.22

	Value	Error
k_1	4.5743 X 10^6	9.9876 X 10^4
A	1.0132	0.0041867
Chi Sq	0.00061639	
R^2	0.99544	

Table A.18: The analysis of the decay for the absorbance of mOrange (4.57 X 10^{-6} M) at 548 nm, in the presence of $K_3Fe(CN)_6$ (0.25 mM) while exposed to the UV LED for 4 hours. The equation used for fit was: $y = Ae^{(-k_1 x)}$. From figure 3.5A

	Value	Error
k_1	0.0022017	0.000050951
A	0.98995	0.0032249
Chi Sq	0.0013612	
R^2	0.99421	

Table A.19: The analysis of the decay for the absorbance of mOrange at 548 nm, in the presence of $K_3Fe(CN)_6$ (0.25 mM) while exposed to the Green LED for 4 hours. This experiment was repeated three times. The equation used for fit was: $y = Ae^{(-k_1x)} + Be^{(-k_2x)}$. From figure 3.17A

	Value	Error
k_1	0.0025895	0.0010366
A	0.39672	0.10366
k_2	0.016716	0.0023119
B	0.60685	0.10209
Chi Sq	0.00086743	
R^2	0.99922	

Table A.20: The analysis of the decay for the normalized and corrected fluorescence of mOrange at 565 nm, in the presence of $K_3Fe(CN)_6$ (0.25 mM) while exposed to the Green LED for 4 hours. This experiment was repeated three times. The equation used for fit was: $y = Ae^{(-k_1x)} + Be^{(-k_2x)}$. From figure 3.17B

	Value	Error
k_1	0.0053809	0.0020246
A	0.5754	0.22596
k_2	0.025554	0.010946
B	0.44045	0.2214
Chi Sq	0.0084348	
R^2	0.99394	

Table A.21: The analysis of the decay for mOrange normalized absorbance at 548 nm after 1000 shots of the 497 nm laser, in the presence of $K_3Fe(CN)_6$ (0.25 mM). The equation used for fit was:$y = Ae^{(-k_1x)} + Be^{(-k_2x)}$. From figure 3.23B (Red Trace)

	Value	Error
k_1	7.4041 X 10^6	1.5726 X 10^6
A	0.3668	0.049406
k_2	5.0113 X 10^7	3.5212 X 10^6
B	0.63353	0.047752
Chi Sq	0.00032442	
R^2	0.99962	

Table A.22: The analysis of the decay for mOrange max normalized absorbance at 548 nm decay after 1000 shots of the 532 nm laser, in the presence of $K_3Fe(CN)_6$ (0.25 mM). The equation used for fit was:$y = Ae^{(-k_1x)} + Be^{(-k_2x)}$. From figure 3.23B (Green Trace)

	Value	Error
k_1	4.1964 X 10^6	1.7866 X 10^6
A	0.32426	0.064109
k_2	3.2518 X 10^7	2.308 X 10^6
B	0.67488	0.063008
Chi Sq	0.00010361	
R^2	0.99986	

Table A.23: The analysis of the decay for mOrange normalized absorbance at 548 nm after 1000 shots of the 548 nm laser, in the presence of $K_3Fe(CN)_6$ (0.25 mM). The equation used for fit was:$y = Ae^{(-k_1 x)} + Be^{(-k_2 x)}$. From figure 3.23B (Blue Trace)

	Value	Error
k_1	3.672 X 10^6	1.2438 X 10^6
A	0.36605	0.057723
k_2	2.6748 X 10^7	1.643 X 10^6
B	0.63445	0.057093
Chi Sq	0.000031262	
R^2	0.99995	

Table A.24: The analysis of the decay for mOrange normalized absorbance at 548 nm after 1000 shots of the 560 nm laser, in the presence of $K_3Fe(CN)_6$ (0.25 mM). The equation used for fit was: $y = Ae^{(-k_1 x)}$. From figure 3.23B (Orange Trace)

	Value	Error
k_1	6.2353 X 10^6	9.9743 X 10^4
A	0.98771	0.0055904
Chi Sq	0.0020314	
R^2	0.99693	

Table A.25: The analysis of the decay for mOrange normalized and corrected fluorescence at 565 nm after 1000 shots of the 497 nm laser, in the presence of $K_3Fe(CN)_6$ (0.25 mM). The equation used for fit was: $y = Ae^{(-k_1 x)} + Be^{(-k_2 x)}$. From figure 3.24A (Red Trace)

	Value	Error
k_1	4.6331 X 10^7	3.0905 X 10^6
A	0.81991	0.072277
k_2	9.969 X 10^6	4.5375 X 10^6
B	0.17554	0.073932
Chi Sq	0.00028004	
R^2	0.99975	

Table A.26: The analysis of the decay for mOrange normalized and corrected fluorescence at 565 nm after 1000 shots of the 532 nm laser, in the presence of $K_3Fe(CN)_6$ (0.25 mM). The equation used for fit was: $y = Ae^{(-k_1 x)} + Be^{(-k_2 x)}$. From figure 3.24A (Green Trace)

	Value	Error
k_1	3.152 X 10^7	1.3246 X 10^6
A	0.84834	0.053126
k_2	5.8139 X 10^6	3.0253 X 10^6
B	0.15174	0.053816
Chi Sq	0.000039169	
R^2	0.99996	

Table A.27: The analysis of the decay for mOrange normalized and corrected fluorescence at 565 nm after 1000 shots of the 548 nm laser, in the presence of $K_3Fe(CN)_6$ (0.25 mM). The equation used for fit was: $y = Ae^{(-k_1x)} + Be^{(-k_2x)}$. From figure 3.24A (Blue Trace)

	Value	Error
k_1	2.581 X 10^7	2.0804 X 10^6
A	0.78426	0.10935
k_2	5.6642 X 10^6	3.7265 X 10^6
B	0.21317	0.11014
Chi Sq	0.000047442	
R^2	0.99994	

Table A.28: The analysis of the decay for mOrange normalized and corrected fluorescence at 565 nm after 1000 shots of the 560 nm laser, in the presence of $K_3Fe(CN)_6$ (0.25 mM). The equation used for fit was: $y = Ae^{(-k_1x)}$. From figure 3.24A (Orange Trace)

	Value	Error
k_1	8.2424 X 10^6	4.2378 X 10^4
A	1.0041	0.0015656
Chi Sq	0.000078529	
R^2	0.99976	

Table A.29: Analysis of the decay for mOrange max normalized absorbance at 552 nm after 1000 shots of the 532 nm laser, in the presence of $K_3Fe(CN)_6$ (0.25 mM) at 82 °C. The equation used for fit was: $y = Ae^{(-k_1 x)}$. From figure 3.26C

	Value	Error
k_1	8.9348 X 10^6	2.5861 X 10^5
A	1.0582	0.01096
Chi Sq	0.001861	
R^2	0.99327	

Table A.30: The analysis of the decay for the absorbance of mOrange at 548 nm in the presence of ABDA while exposed to the Green LED for 4 hours. The equation used for fit was:$y = Ae^{(-k_1 x)} + Be^{(-k_2 x)}$. From figure 4.3B

	Value	Error
k_1	0.00078456	0.00043856
A	0.37537	0.037895
k_2	0.018693	0.0012287
B	0.63336	0.36825
Chi Sq	0.00049002	
R^2	0.99947	

Table A.31: The analysis of the decay for the maximum normalized and corrected fluorescence of mOrange at 565 nm in the presence of ABDA while exposed to the Green LED for 4 hours. The equation used for fit was:$y = Ae^{(-k_1 x)} + Be^{(-k_2 x)}$. From figure 4.3D

	Value	Error
k_1	0.0037821	0.002552
A	0.41821	0.2274
k_2	0.022144	0.0073402
B	0.60349	0.2227
Chi Sq	0.0083236	
R^2	0.99352	

Table A.32: Analysis of the decay for ABDA at 380 nm in the presence of mOrange during 4 hours irradiation with the Green LED. The equation used for fit was: $y = Ae^{(-k_1 x)}$. From figure 4.4B

	Value	Error
k_1	0.00026763	0.0000094024
A	1.003	0.00078541
Chi Sq	0.000088085	
R^2	0.998352	

Table A.33: The analysis of the decay for the absorbance of mOrange at 548 nm in D_2O while exposed to the Green LED for 4 hours. The equation used for fit was: $y = Ae^{(-k_1 x)} + Be^{(-k_2 x)}$. From figure 4.5B

	Value	Error
k_1	0.0010721	0.00035316
A	0.37274	0.026828
k_2	0.022396	0.0011853
B	0.62982	0.26828
Chi Sq	0.00047256	
R^2	0.99953	

Table A.34: The analysis of the decay for the maximum normalized and corrected fluorescence of mOrange at 565 nm in D_2O while exposed to the Green LED for 4 hours. The equation used for fit was: $y = Ae^{(-k_1 x)} + Be^{(-k_2 x)}$. From figure 4.5D

	Value	Error
k_1	0.0012395	0.00074996
A	0.24384	0.039348
k_2	0.021678	0.0013085
B	0.75891	0.38152
Chi Sq	0.00068487	
R^2	0.99949	

Table A.35: The analysis of the decay for the absorbance of mOrange at 548 nm in the presence of ABDA and D_2O while exposed to the Green LED for 4 hours. The equation used for fit was:$y = Ae^{(-k_1 x)} + Be^{(-k_2 x)}$. From figure 4.6B

	Value	Error
k_1	0.0012192	0.00023573
A	0.38429	0.018691
k_2	0.023507	0.00086468
B	0.61954	0.018691
Chi Sq	0.00024047	
R^2	0.99976	

Table A.36: The analysis of the decay for the maximum normalized and corrected fluorescence of mOrange at 565 nm in the presence of ABDA and D_2O while exposed to the Green LED for 4 hours. The equation used for fit was:$y = Ae^{(-k_1 x)} + Be^{(-k_2 x)}$. From figure 4.6D

	Value	Error
k_1	0.0050106	0.0013138
A	0.48056	0.1063
k_2	0.032519	0.0066674
B	0.57906	0.10045
Chi Sq	0.0044448	
R^2	0.99653	

Table A.37: Analysis of the decay for ABDA at 380 nm in the presence of mOrange during 4 hours irradiation with the Green LED. The equation used for fit was: $y = Ae^{(-k_1 x)}$. From figure 4.7B

	Value	Error
k_1	0.00049328	0.0000083369
A	0.97179	0.00067678
Chi Sq	0.000054147	
R^2	0.99649	

Table A.38: The analysis of the decay for the absorbance of mOrange at 548 nm in D_2O while irradiated with the pulsed laser for 1000 shots. The equation used for fit was:$y = Ae^{(-k_1 x)}$. From figure 4.8C

	Value	Error
k_1	3.8538×10^6	8.3752×10^4
A	1.011	0.0037857
Chi Sq	0.00035586	
R^2	0.99584	

Table A.39: The analysis of the decay for the maximum normalized and corrected fluorescence of mOrange at 565 nm in D_2O while irradiated with the pulsed laser for 1000 shots. The equation used for fit was: $y = Ae^{(-k_1 x)}$. From figure 4.8D

	Value	Error
k_1	9.273×10^6	1.1624×10^5
A	1.0135	0.0045111
Chi Sq	0.00043034	
R^2	0.99869	

Table A.40: The analysis of the decay for the absorbance of mOrange at 548 nm in the presence of ABDA in D_2O while exposed to the 497 nm pulsed laser. The equation used for fit was: $y = Ae^{(-k_1 x)}$. From figure 4.9B

	Value	Error
k_1	5.9384×10^6	2.7427×10^4
A	0.99844	0.001156
Chi Sq	0.000031102	
R^2	0.99981	

Table A.41: The analysis of the decay for the maximum normalized and corrected fluorescence of mOrange at 565 nm in the presence of ABDA in D_2O while exposed to the 497 nm pulsed laser. The equation used for fit was: $y = Ae^{(-k_1 x)}$. From figure 4.9D

	Value	Error
k_1	1.3308 X 10^7	1.7363 X 10^5
A	0.99857	0.0058579
Chi Sq	0.00065359	
R^2	0.99866	

Table A.42: Analysis of the decay for ABDA at 380 nm in the presence of mOrange and D_2O while exposed to the 497 nm pulsed laser. The equation used for fit was: $y = Ae^{(-k_1 x)}$. From figure 4.10B

	Value	Error
k_1	2.2978 X 10^5	2.4321 X 10^4
A	1.0027	0.0011957
Chi Sq	0.000040113	
R^2	0.90853	

APPENDIX B: EXTRA DATA

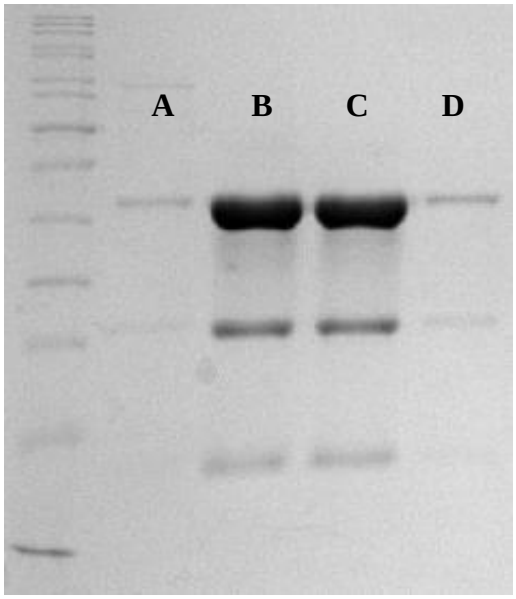

Figure B.1: The coomassie stain of mOrange after purification on the Ni+ affinity column. Where A is the initial elution, with minor inpurities and B – D is the collected fractions of mOrange. The lower weight bands in B-D were not removed after additional rounds of purification through sepadex and anion exchange columns, suggesting the lower weight band are apart of mOrange and appear from the staining process.

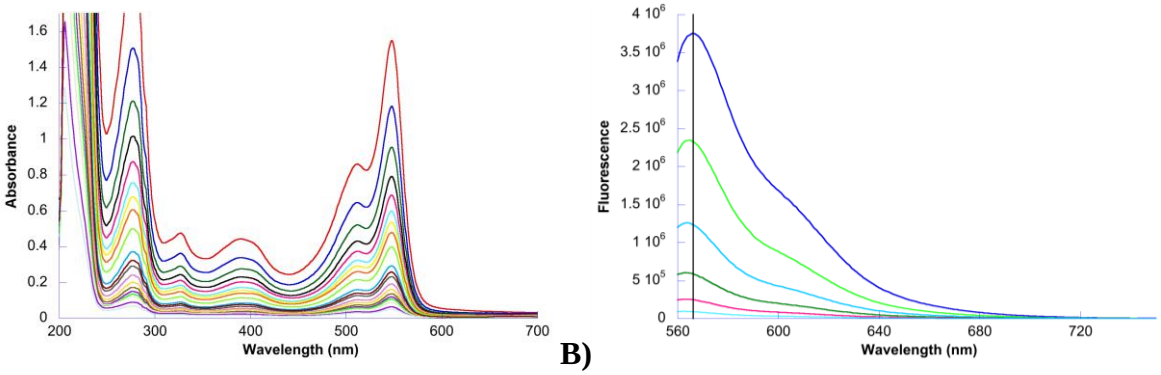

A) **B)**

Figure B.2: A) The serial dilution absorbance spectra of mOrange. B) The serial dilution fluorescent emission spectra of mOrange. The black line demonstrated the blue shift due to the loss of the inner filter effect as the concentration of mOrange is decreased.

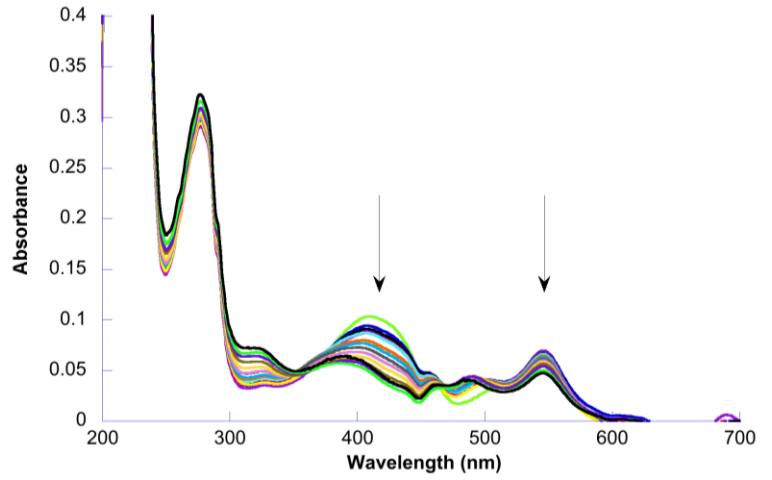

Figure B.3: The absorbance spectra of mOrange (4.65 X 10^{-6} M) after exposure to the Green LED for 4 hours, followed by the UV LED for 2 hours. The arrows indicate the direction of change.

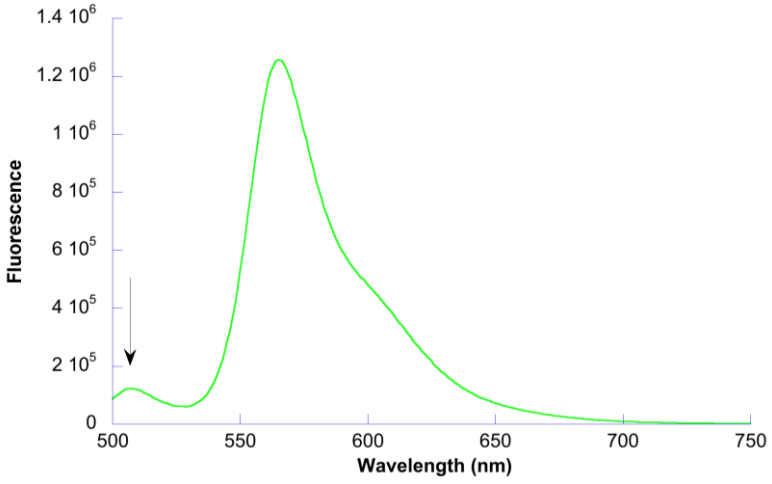

Figure B.4: The fluorescent emission spectra of mOrange when excited at 495 nm. The arrow indicates the emission of the green immature mOrange at 510 nm. The presence of the mature mOrange emission suggests a slight excitation of mOrange at 495 nm.

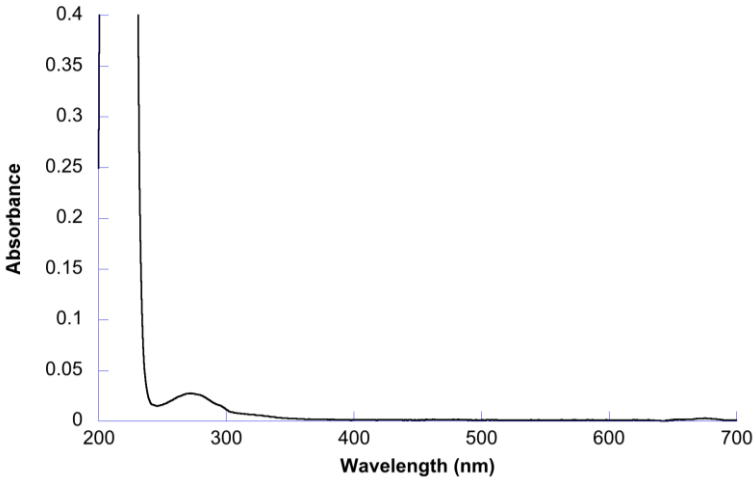

Figure B.5: The absorbance spectra of Imidazole (10 mM).

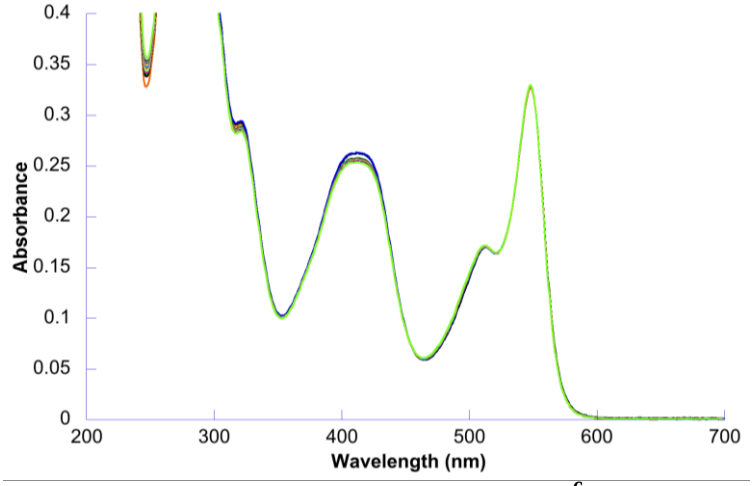

Figure B.6: The absorbance spectra of mOrange (4.61×10^{-6} M) and $K_3Fe(CN)_6$ (0.25 mM) while incubated at room temperature in the dark overnight.

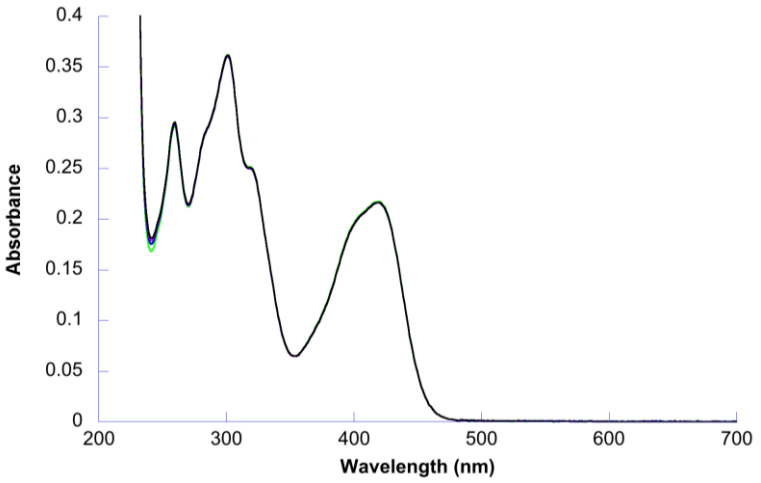

Figure B.7: The absorbance spectra of $K_3Fe(CN)_6$ (0.25 mM) and Imidazole (10 mM) incubated at room temperature in the dark overnight.